

**Bangor University**

**DOCTOR OF PHILOSOPHY**

**Glacial sculpting and post-glacial drowning of the Celtic Sea**

Lockhart, Edward Alan

*Award date:*  
2020

*Awarding institution:*  
Bangor University

[Link to publication](#)

#### **General rights**

Copyright and moral rights for the publications made accessible in the public portal are retained by the authors and/or other copyright owners and it is a condition of accessing publications that users recognise and abide by the legal requirements associated with these rights.

- Users may download and print one copy of any publication from the public portal for the purpose of private study or research.
- You may not further distribute the material or use it for any profit-making activity or commercial gain
- You may freely distribute the URL identifying the publication in the public portal ?

#### **Take down policy**

If you believe that this document breaches copyright please contact us providing details, and we will remove access to the work immediately and investigate your claim.

Download date: 26. Apr. 2024

**Bangor University**

**DOCTOR OF PHILOSOPHY**

**Glacial sculpting and post-glacial drowning of the Celtic Sea**

Lockhart, Edward Alan

*Award date:*  
2020

[Link to publication](#)

#### **General rights**

Copyright and moral rights for the publications made accessible in the public portal are retained by the authors and/or other copyright owners and it is a condition of accessing publications that users recognise and abide by the legal requirements associated with these rights.

- Users may download and print one copy of any publication from the public portal for the purpose of private study or research.
- You may not further distribute the material or use it for any profit-making activity or commercial gain
- You may freely distribute the URL identifying the publication in the public portal ?

#### **Take down policy**

If you believe that this document breaches copyright please contact us providing details, and we will remove access to the work immediately and investigate your claim.

Download date: 10. Feb. 2020

# **Glacial sculpting and post-glacial drowning of the Celtic Sea**

A thesis submitted in accordance with the requirements of  
Bangor University for the degree of Doctor of Philosophy

**By**  
**Edward Alan Lockhart**



PRIFYSGOL  
**BANGOR**  
UNIVERSITY

School of Ocean Sciences  
Bangor University, Wales  
August 2019

## Acknowledgements

After nearly a decade spent in full-time education, I have a lot of people to thank who have helped me on my journey to where I am now.

I thank my undergraduate thesis supervisor, Rory Quinn, who first introduced me to seafloor mapping. I never knew that I could be so fascinated by a subject, something that my curiosity and passion for would shape the next few years of my life and my future career.

I wish to thank my supervisors (my PhD family) for their hard work, perseverance, encouragement and advice throughout this journey. Their input has helped make me into the curious, enthusiastic and confident scientist that I am now. I thank James Scourse for his guidance and encouragement, and his ability to continue to juggle commitments to me with those that come with being based at a different university. I am indebted to Katrien Van Landeghem for her guidance and encouragement throughout my MSc which led me to pursue this PhD. She has given me valuable advice and has driven me onwards with constant reassurance and encouragement when I needed it the most. I express thanks to Claire Mellett for helping me when I had to move to Edinburgh, she was so welcoming and kind, always there if I needed to talk to someone. Daniel Praeg has played a crucial role in the development of this PhD. I thank him greatly for many stimulating discussions about the mysteries of the Celtic Sea shelf and for his attention to detail which has greatly improved the rigor of my work.

I thank my friends and volunteer colleagues from the North Wales Cave Rescue Organisation and neighbouring teams for introducing me to my new passion in life, and for providing a much-needed underground break from my PhD. Nothing focuses the mind on what is important in life better than when you are abseiling down a 60 m collapsing mineshaft or crawling through water-filled passages to rescue a casualty from the deepest cave in Britain.

I am eternally grateful to my family, especially my mum and dad, for their endless support throughout my education. You have always spurred me on to be the best version of myself that I can be. My family have kept me sane throughout this PhD with its many ups and downs, and I am really glad that you encouraged me to take breaks away with you all to Donegal, Venice, the Lake District and Dorset, or to visit you all back home in Northern Ireland. These breaks really helped keep me focused on what is important during some of the most stressful times of my PhD. Thank you.

To those who may be reading this PhD thesis during the writing of their own, I know what you are going through. The best advice that I was given at the start of this journey is “always remember that a PhD is a marathon, not a sprint.” Pace yourself.



## Abstract

Concerns as to the stability of present-day ice sheets and their future contribution to sea-level rise have prompted the investigation of palaeo ice sheets in order to study ice dynamics and evolution through deglaciation. Such observations of ice sheet behaviour are essential in the process of constraining and validating numerical ice sheet models in order to forecast the future response of Greenland and Antarctic ice sheets to warming and sea level rise which can rapidly destabilise marine-terminating margins and contribute to global sea-level rise. Therefore, a palaeo ice sheet of similar characteristics to Greenland and Antarctica is required in order to accurately capture the occurrence of marine ice sheet instability. A suitable analogue is the last British-Irish Ice sheet, which was drained by numerous marine-terminating ice streams. The largest of these was the Irish Sea Ice Stream (ISIS), which terminated on the continental shelf of the Celtic Sea. New modern geophysical and sediment core data collected during numerous scientific cruises of the Celtic Sea provide a unique opportunity to determine the stratigraphic position of glacial sediments and the origin of the ridges from which these sediments were recovered, and to investigate the imprint of glaciation and thus reconstruct deglacial dynamics.

Seismic data of the mid- and outer-shelf show that the largest shelf ridges in the west comprise two vertically stacked units which are draped by superficial deposits. The upper sandy bulk of these megaridges is correlative to the Melville Formation (MFm), comprising truncated and dipping bedding planes, which overlies mounds of the Upper Little Sole Formation (ULSFm) comprising Last Glacial Maximum glacial sediments that are exposed on the lower megaridge flanks. Stiff and deformed glacial sediments comprising the ULSFm record their overriding by the ice margin during its oscillatory retreat across the shelf before being partially eroded during marine transgression by megatidal conditions which fuelled the development of overlying sand ridges comprising the MFm. This updated stratigraphy suggests the presence of a glacial core under the MFm on the western shelf. In the east, channels of the ULSFm contain undisturbed seismic facies of unknown lithology, with implications for the ice margin extent in the French sector. Multi-beam bathymetric data reveal a large assemblage of seafloor glacial features preserved on the inner-shelf, including terminal and ribbed moraines, streamlined bedrock, iceberg grounding pits, meltwater channels and tunnel valleys. These features record the southwest advance of a grounded warm-based ice lobe and its northeast marine deglaciation in response to rising relative sea level into St. George's Channel and towards the southern coastline of Ireland.

These findings provide new palaeo observations of ice stream instability, whereby the ISIS rapidly broke up through calving in response to fracturing and thinning due to instability induced by ice margin flotation and deformable proglacial sediments in a rising relative sea level environment. Such factors need to be considered in the stability of present-day marine-terminating ice sheets. The maximum extent and subsequent northwest retreat of the ice margin across the mid- and outer-shelf, followed by more-complex retreat patterns on the inner-shelf, provide a framework against which numerical whole ice sheet models can be tested. Combined, these observations have implications for the study of ice stream stability and the validation of numerical ice sheet models.

## **Thesis Structure**

**Chapter 1** contains the relevant background information and scientific literature which highlights the importance of this work. Specific scientific literature pertaining to the Quaternary history of the Celtic Sea are discussed to identify knowledge gaps which will be investigated in this thesis using modern data and methods.

**Chapter 2** details the geophysical datasets and physical samples used in the investigation of the knowledge gaps identified in Chapter 1, and the methodologies deployed to produce the data which are described in Chapter 3.

**Chapter 3** reports the results by shelf region. The location and morphology of glacial features on the seafloor of the inner-shelf are described. The morphology of sediment ridges on the mid- and outer-shelf is described along with the sub-surface shallow stratigraphy and the results of geotechnical testing.

**Chapter 4** interprets the results in Chapter 3 in terms of the palaeo-environmental significance of the observed seafloor features, sub-surface stratigraphy and geotechnical test results. These details are compared to and integrated with previous observations discussed in Chapter 1 to produce an updated catalogue of palaeo-environmental observations by shelf region.

**Chapter 5** discusses the implications of the new observations and their palaeo-environmental significance by shelf region before integrating this information to produce regional reconstructions of the palaeo environment.

**Chapter 6** synthesises the findings to elucidate the glacial and post-glacial evolution of the Celtic Sea. The implications of this final reconstruction are then discussed.

The **References** section contains a list of all sources which are cited in the text.

The **Appendix** contains two manuscripts and supplementary information of published papers which this work contributed to, Lockhart et al. (2018) and Scourse et al. (2019).

## Table of Contents

|                              |       |
|------------------------------|-------|
| Declaration and Consent..... | i     |
| Acknowledgements .....       | iv    |
| Abstract .....               | v     |
| Thesis Structure .....       | vi    |
| Table of Contents .....      | vii   |
| List of Figures.....         | x     |
| List of Tables .....         | xviii |

|  |            |
|--|------------|
| <b>Chapter 1 - Literature Review .....</b>                             | <b>1-1</b> |
| 1.1 Concern and Background .....                                       | 1-1        |
| 1.1.1 Marine-terminating Ice Sheet Instability .....                   | 1-1        |
| 1.1.2 Glacial Processes and Deposits .....                             | 1-5        |
| 1.2 The Deposits and Quaternary History of the Celtic Sea .....        | 1-8        |
| 1.2.1 Celtic Sea Shelf Bathymetry .....                                | 1-8        |
| 1.2.2 Superficial Deposits of the Celtic Sea Shelf.....                | 1-9        |
| 1.2.3 Shallow Stratigraphy of the Mid- and Outer-shelf .....           | 1-10       |
| 1.2.4 Sub-Quaternary Geology of the Celtic Sea Shelf .....             | 1-12       |
| 1.2.5 The Glaciation of the Celtic Sea Shelf .....                     | 1-13       |
| 1.2.6 Post-glacial Evolution.....                                      | 1-18       |
| 1.2.7 Glacial vs Tidal Origin of the Shelf Ridges.....                 | 1-24       |
| 1.3 Seafloor Bathymetry for Environmental Reconstruction .....         | 1-26       |
| 1.3.1 Seafloor Geomorphology .....                                     | 1-26       |
| 1.3.2 Seafloor Features of the Celtic Sea Shelf.....                   | 1-27       |
| 1.4 Sub-seafloor Stratigraphy for Environmental Reconstruction.....    | 1-28       |
| 1.4.1 Seafloor Stratigraphy .....                                      | 1-28       |
| 1.4.2 Seismic Facies .....   | 1-29       |
| 1.4.3 Stratigraphic Investigations of the Celtic Sea Shelf .....       | 1-30       |
| 1.4.4 Seismic-stratigraphic Framework of the Mid- and Outer-shelf..... | 1-32       |
| 1.4.5 Litho-stratigraphic Framework of the Mid -and Outer-shelf .....  | 1-35       |
| 1.5 Sediment Geotechnics for Environmental Reconstruction .....        | 1-37       |
| 1.5.1 Effective Stress and Consolidation .....                         | 1-37       |
| 1.5.2 Stiff Deglacial Sediments of the Celtic Sea Shelf .....          | 1-38       |
| 1.6 Aims and Objectives .....  | 1-41       |

|  |      |
|--|------|
| <b>Chapter 2 - Data and Methods</b>                    | 2-1  |
| 2.1 Seafloor Geomorphology                             | 2-1  |
| 2.1.1 Regional Bathymetric Data                        | 2-1  |
| 2.1.2 Multi-beam Bathymetric Data                      | 2-1  |
| 2.1.3 Data Visualisation and Geomorphological Analyses | 2-3  |
| 2.2 Sub-seafloor Stratigraphy                          | 2-5  |
| 2.2.1 Seismic Reflection Data                          | 2-5  |
| 2.2.2 Physical Samples                                 | 2-6  |
| 2.2.3 Data Visualisation and Correlation               | 2-7  |
| 2.3 Sediment Geotechnics                               | 2-9  |
| 2.3.1 Sediment Core Data                               | 2-9  |
| 2.3.2 Geotechnical Analyses                            | 2-10 |
| <br><b>Chapter 3 - Results</b>                         | 3-1  |
| 3.1 Seafloor Geomorphology                             | 3-1  |
| 3.1.1 Large-scale Ridges                               | 3-1  |
| 3.1.2 Inner-shelf Features                             | 3-6  |
| 3.2 Sub-seafloor Stratigraphy                          | 3-20 |
| 3.2.1 Seismic Sections and Seismic Facies              | 3-20 |
| 3.2.2 Seismic Facies Summary                           | 3-45 |
| 3.2.3 Lithofacies Summary                              | 3-47 |
| 3.3 Sediment Geotechnics                               | 3-51 |
| 3.3.1 Undrained Shear Strength                         | 3-51 |
| 3.3.2 Effective Stress                                 | 3-51 |
| 3.3.3 Atterberg Limits                                 | 3-52 |
| 3.3.4 Over-consolidation Ratio                         | 3-55 |
| 3.3.5 Predicted Yield Stress                           | 3-56 |
| 3.3.6 Deformation                                      | 3-56 |
| 3.3.7 Summary of Findings                              | 3-57 |

|   |                |
|---|----------------|
| <b>Chapter 4 - Interpretation .....</b>                       | <b>4-1</b>     |
| 4.1 Seafloor Geomorphology .....                              | 4-1            |
| 4.1.1 Large-scale Ridges .....                                | 4-1            |
| 4.1.2 Glacially-related Features .....                        | 4-3            |
| 4.2 Sub-seafloor Stratigraphy .....                           | 4-9            |
| 4.2.1 Seismic Facies Interpretation.....                      | 4-9            |
| 4.2.2 Lithofacies Integration .....                           | 4-13           |
| 4.2.3 Stratigraphic Correlation to Other Investigations ..... | 4-15           |
| 4.3 Sediment Geotechnics .....                                | 4-27           |
| 4.3.1 Burial and Erosion.....                                 | 4-27           |
| 4.3.2 Glacial Loading .....                                   | 4-29           |
| <br><b>Chapter 5 - Discussion .....</b>                       | <br><b>5-1</b> |
| 5.1 Inner-shelf .....   | 5-1            |
| 5.1.1 Ice flow Pathways and Extent .....                      | 5-1            |
| 5.1.2 Retreat Configuration and Style .....                   | 5-6            |
| 5.1.3 Regional Reconstruction .....                           | 5-14           |
| 5.2 Mid- and Outer-shelf .....                                | 5-17           |
| 5.2.1 The Megaridges .....                                    | 5-17           |
| 5.2.2 Reconstruction of Palaeo-glacial Dynamics.....          | 5-26           |
| 5.2.3 Regional Reconstruction .....                           | 5-33           |
| <br><b>Chapter 6 - Synthesis .....</b>                        | <br><b>6-1</b> |
| 6.1 Glaciation of the Celtic Sea Shelf .....                  | 6-1            |
| 6.2 Post-glacial Evolution of the Celtic Sea Shelf .....      | 6-6            |
| 6.3 Future Work .....   | 6-8            |
| <br><b>References .....</b>                                   | <br><b>7-1</b> |
| <br><b>Appendix .....</b>                                     | <br><b>8-1</b> |

## List of Figures

**Figure 1.1** - Predictions of change in average surface temperature from 1986-2005 to 2081-2100 for Representative Concentration Pathway (RCP) RCP2.6 (left) and RCP8.5 (right). From IPCC (2014).

.....1-1

**Figure 1.2** - Mapped glacial features of the British Isles and surrounding offshore areas. Note the lack of features and deposits in the Celtic Sea region south of Ireland. From Clark et al. (2018). ....1-4

**Figure 1.3** - The interpreted glacial feature assemblage associated with the offshore advance of a marine-terminative ice lobe. From Ottesen et al. (2017). ....1-7

**Figure 1.4** - EMODnet bathymetry map of the Celtic Sea shelf showing place names and areas mentioned in this thesis. Regions of the shelf are separated by boundaries defined here (black lines) Triangles denote the recovery locations of subglacial sediments at the shelf edge by Praeg et al. (2015b; green) and Scourse et al. (2019; yellow), and on the mid-shelf in BGS core 49/-09/44 (red; Scourse et al., 1990). ....1-9

**Figure 1.5** - Map showing superficial sediment coverage by grainsize of the Celtic Sea shelf (BGS, 2011). ....1-10

**Figure 1.6** - Map showing the primary sub-Quaternary geology of the Celtic Sea shelf (BGS, 2013, 1979). ....1-13

**Figure 1.7** - Overview of the ice catchment feeding the Irish Sea Ice Stream in the northern Irish Sea during its southwest flow through St. GC into the Celtic Sea. From Roberts et al. (2007). ....1-15

**Figure 1.8** - Relative sea-level (black; Bradley et al., 2011) predictions with simulated tidal amplitudes (red; Ward et al., 2016) from 21 ka BP to the present-day for St. GC (dashed) and the outer-shelf of the Celtic Sea (solid). From Scourse et al. (2019). ....1-19

**Figure 1.9** - Palaeotidal model reconstruction of the Celtic Sea showing bed stress intensity (colour ramp) and dominant tidal current direction (arrows) for various time slices. From Ward et al. (2016). ....1-21

**Figure 1.10** - Seismic section and interpretation of the flank of a French ridge suggesting a marine transgressive surface (Melville Formation base), tidal deposits (Melville Formation) and an overlying wave erosion surface and late transgressive deposits. From Reynaud et al. (1999a). ....1-23

**Figure 1.11** - Schematic seismic section showing commonly used terms for describing reflection character. ....1-30

|  |      |
|--|------|
| <b>Figure 1.12</b> - Example reflector configurations and terminations. Edited from Mitchum et al. (1977).<br>.....  | 1-30 |
| <b>Figure 1.13</b> - Stratigraphic units of the Celtic Sea shelf. From Pantin and Evans (1984). ....   | 1-32 |
| <b>Figure 1.14</b> - Seismic sections from the outer-shelf of the UK sector showing the Melville Formation (M) and Upper Little Sole Formation (uLS). From Pantin and Evans (1984). ....   | 1-33 |
| <b>Figure 1.15</b> - Seismic section from the outer-shelf of the UK sector showing the interpreted boundary between the Melville Formation (M) and the Upper Little Sole Formation (uLS). From Pantin and Evans (1984). ....   | 1-33 |
| <b>Figure 1.16</b> - EMODnet bathymetry and slope map showing the northern limit of the Upper Little Sole Formation (red) by Pantin and Evans (1984) and channel thalwegs (black) by Bouysse et al. (1976).<br>.....   | 1-34 |
| <b>Figure 1.17</b> - Seismic section and interpretation showing the reflection geometry and stacking of seismic-stratigraphic units of the Celtic Sea shelf. From Evans (1990). ....   | 1-35 |
| <b>Figure 2.1</b> - EMODnet bathymetry and slope map showing the extent of multi-beam bathymetric datasets from the United Kingdom Hydrographic Office (UKHO) and the Integrated Mapping For the Sustainable Development of Ireland's Marine Resource (INFOMAR) project. The extent of INFORMAR (red) and UKHO (blue) datasets on the inner-shelf of the Celtic Sea are marked. .... | 2-2  |
| <b>Figure 2.2</b> - Example data visualisations showing the bias induced by uni-directional hillshades of linear bedrock compared to multi-directional shading and slope maps. ....  | 2-3  |
| <b>Figure 2.3</b> - Example cross-sectional profile of a ridge feature showing how vertical and horizontal measurements were derived manually. ....  | 2-4  |
| <b>Figure 2.4</b> - EMODnet bathymetry and slope map showing the coverage of JC-106 (red) and IPY GLAMAR and CV14007 (black) seismic reflection data in the Celtic Sea. ....   | 2-6  |
| <b>Figure 2.5</b> - Schematic diagram of a marine core sample defining the saturated sediment stresses ( $\sigma_{\text{sed}}$ ) produced from discrete density measurements ( $\rho_n$ ) with pore pressures ( $\mu Z$ ) used, referenced to a defined measurement depth ( $Z_n$ ). ....  | 2-12 |
| <b>Figure 2.6</b> - Schematic diagram of the cone penetration equipment setup. Edited from ISO (2018).<br>.....  | 2-13 |

|  |      |
|--|------|
| <b>Figure 3.1</b> - EMODnet bathymetry and slope map of the ridge field on the mid- and outer-shelf showing three populations of ridges, separated by the marked boundaries, with ridge numbers. Dark and light areas denote steep and flat areas respectively.....  | 3-2  |
| <b>Figure 3.2</b> - Height, width and length measurements per ridge. See Figure 3.1 for ridge number locations. ....   | 3-2  |
| <b>Figure 3.3</b> - Ridge height (red), width (yellow) and length (blue) histograms as generated from data in Figure 3.2. ....   | 3-3  |
| <b>Figure 3.4</b> - EMODnet bathymetry and slope map of ridges on the mid-shelf showing rotated ends (black arrows) and the axial transition into transverse ridges. Dark and light areas denote steep and flat areas respectively. See Figure 3.1 for ridge number locations.....   | 3-4  |
| <b>Figure 3.5</b> - EMODnet bathymetry and slope map of ridges on the outer shelf. Dark and light areas denote steep and flat areas respectively. See Figure 3.1 for ridge number locations. ....  | 3-5  |
| <b>Figure 3.6</b> - EMODnet bathymetry and slope map of ridges and neighbouring incision termini (black arrows) in the southeast of the shelf. Dark and light areas denote steep and flat areas respectively. See Figure 3.1 for ridge number locations. ....  | 3-6  |
| <b>Figure 3.7</b> - Thematic map of inner-shelf seafloor features and image and figure locations. A wide variety of seafloor features are observed on the inner-shelf, including arcuate ridges, streamlined features and over-deepened channels. The long-axis orientation of similar lineations and streamlined bedrock from Clark et al. (2018) is shown in red for southern Ireland. The limit of this feature assemblage to the east is marked by a dashed line. .... | 3-7  |
| <b>Figure 3.8</b> - INFOMAR (left) and UKHO (right) bathymetry and hillshaded relief (240° illumination for clarity) image of parallel ridges (red areas) in the Irish (left) and UK (right) sectors of St. George's Channel. For image location, see Area 1 in Figure 3.7. ....   | 3-14 |
| <b>Figure 3.9</b> - INFOMAR bathymetry and hillshaded relief (240° illumination for clarity) image of sinuous ridges (black arrows) south of the southern Irish coastline. For image location, see Area 2 in Figure 3.7. ....  | 3-16 |
| <b>Figure 3.10</b> - EMODnet bathymetry and slope map of prominent overdeepened channels (black arrows) on the Nymphe Bank Platform (left) and on the southern boundary of the Celtic Deep (right) adjacent to deep troughs. Dark and light areas denote steep and flat areas respectively. For image location, see Area 3 in Figure 3.7.....  | 3-17 |



|  |      |
|--|------|
| <b>Figure 3.11</b> - INFOMAR bathymetry and hillshaded relief (240° illumination for clarity) image of arcuate ridges (black arrows) and neighbouring features southwest of the southern Irish coastline. For image location, see Area 4 in Figure 3.7. .... | 3-18 |
| <b>Figure 3.12</b> - UKHO bathymetry and hillshaded relief (140° illumination for clarity) image of southwest oriented (black arrows) smooth elongate mounds with satellite imagery. For image location, see Area 5 in Figure 3.7. ....                      | 3-19 |
| <b>Figure 3.13</b> - EMODnet bathymetry and slope map showing the location of seismic lines referred to in this chapter. ....  | 3-20 |
| <b>Figure 3.14</b> - JC-106 chirp seismic reflection data with selected physical sample locations and interpretation with seismic facies. See Line 1 in Figure 3.13 for location. ....   | 3-21 |
| <b>Figure 3.15</b> - JC-106 chirp seismic reflection data and interpretation with seismic facies. See Line 2 in Figure 3.13 for location. ....   | 3-22 |
| <b>Figure 3.16</b> - JC-106 chirp seismic reflection data and interpretation with seismic facies. See Line 3 in Figure 3.13 for location. ....   | 3-23 |
| <b>Figure 3.17</b> - JC-106 chirp seismic reflection data and interpretation with seismic facies. See Line 4 in Figure 3.13 for location. ....   | 3-24 |
| <b>Figure 3.18</b> - JC-106 chirp seismic reflection data and interpretation with seismic facies. See Line 5 in Figure 3.13 for location. ....   | 3-24 |
| <b>Figure 3.19</b> - JC-106 chirp seismic reflection data with selected physical sample locations and interpretation with seismic facies. See Line 6 in Figure 3.13 for location. ....   | 3-25 |
| <b>Figure 3.20</b> - JC-106 chirp seismic reflection data with selected physical sample locations and interpretation with seismic facies. See Line 7 in Figure 3.13 for location. ....   | 3-26 |
| <b>Figure 3.21</b> - JC-106 chirp seismic reflection data and interpretation with seismic facies. See Line 8 in Figure 3.13 for location. ....   | 3-27 |
| <b>Figure 3.22</b> - CV14007 sparker seismic reflection data and interpretation with seismic facies. See Line 9 in Figure 3.13 for location. ....  | 3-28 |
| <b>Figure 3.23</b> - JC-106 chirp seismic reflection data with selected physical sample locations and interpretation with seismic facies. See Line 10 in Figure 3.13 for location. ....  | 3-29 |

|   |      |
|---|------|
| <b>Figure 3.24</b> - JC-106 chirp seismic reflection data with selected physical sample locations along the same line as Figure 3.25 and interpretation with seismic facies. See Line 11 in Figure 3.13 for location.<br>.....  | 3-31 |
| <b>Figure 3.25</b> - CV14007 sparker seismic reflection data along the same line as Figure 3.24 and interpretation with seismic facies. See Line 12 in Figure 3.13 for location. ....   | 3-31 |
| <b>Figure 3.26</b> - JC-106 chirp seismic reflection data and interpretation with seismic facies. See Line 13 in Figure 3.13 for location.....  | 3-32 |
| <b>Figure 3.27</b> - JC-106 chirp seismic reflection data and interpretation with seismic facies. See Line 14 in Figure 3.13 for location.....  | 3-33 |
| <b>Figure 3.28</b> - JC-106 chirp seismic reflection data and interpretation with seismic facies. See Line 15 in Figure 3.13 for location.....  | 3-34 |
| <b>Figure 3.29</b> - IPY GLAMAR sparker seismic reflection data and interpretation with seismic facies. The yellow box indicates chirp data of Figure 3.30 with red showing the corresponding reflection depth. The green line indicates a tie point with Figure 3.33 and Figure 3.34. The magenta line indicates a tie point with the seismic section in Figure 3.30 and Figure 3.31. See Line 16 in Figure 3.13 for location..... | 3-35 |
| <b>Figure 3.30</b> - IPY GLAMAR chirp seismic reflection data and interpretation with seismic facies. The magenta line indicates a tie point with the seismic section in Figure 3.29 and Figure 3.31. See Line 17 in Figure 3.13 for location.....  | 3-35 |
| <b>Figure 3.31</b> - JC-106 chirp seismic reflection data with selected physical sample locations and interpretation with seismic facies. The magenta line indicates a tie point with the seismic section in Figure 3.29 and Figure 3.30. See Line 18 in Figure 3.13 for location. ....   | 3-36 |
| <b>Figure 3.32</b> - IPY GLAMAR sparker seismic reflection data and interpretation with seismic facies. The blue line indicates a tie point with the seismic section in Figure 3.33 and Figure 3.34. See Line 21 in Figure 3.13 for location. ....  | 3-37 |
| <b>Figure 3.33</b> - JC-106 chirp seismic reflection data along the same line as Figure 3.34 with selected physical sample locations and interpretation with seismic facies. The green line indicates a tie point with the seismic section in Figure 3.29 and Figure 3.34. The blue line indicates a tie point with the seismic section in Figure 3.34 and Figure 3.32. See Line 19 in Figure 3.13 for location. ....               | 3-38 |

|   |      |
|---|------|
| <b>Figure 3.34</b> - IPY GLAMAR sparker seismic reflection data along the same line as Figure 3.33 and interpretation with seismic facies. The green line indicates a tie point with the seismic section in Figure 3.29 and Figure 3.33. The blue line indicates a tie point with the seismic section in Figure 3.33 and Figure 3.32. See Line 20 in Figure 3.13 for location. .... | 3-38 |
| <b>Figure 3.35</b> - JC-106 chirp seismic reflection data along the same line as Figure 3.36 with selected physical sample locations and interpretation with seismic facies. The red line indicates a tie point with the seismic section in Figure 3.36 and Figure 3.37. See Line 22 in Figure 3.13 for location. ....  | 3-39 |
| <b>Figure 3.36</b> - IPY GLAMAR sparker seismic reflection data along the same line as Figure 3.35 and interpretation with seismic facies. The red line indicates a tie point with the seismic section in Figure 3.35 and Figure 3.37. See Line 23 in Figure 3.13 for location. ....  | 3-40 |
| <b>Figure 3.37</b> - IPY GLAMAR sparker seismic reflection data and interpretation with seismic facies. The red line indicates a tie point with the seismic section in Figure 3.35 and Figure 3.36. See Line 24 in Figure 3.13 for location. ....   | 3-41 |
| <b>Figure 3.38</b> - JC-106 chirp seismic reflection data with selected physical sample locations and interpretation with seismic facies. See Line 25 in Figure 3.13 for location. ....   | 3-42 |
| <b>Figure 3.39</b> - JC-106 chirp seismic reflection data and interpretation with seismic facies. See Line 26 in Figure 3.13 for location. ....   | 3-43 |
| <b>Figure 3.40</b> - JC-106 chirp seismic reflection data and interpretation with seismic facies. See Line 27 in Figure 3.13 for location. ....   | 3-44 |
| <b>Figure 3.41</b> - Scatter plot showing undrained shear strength measurements for Vibrocore (VC) and Piston Core (PC) samples. ....   | 3-51 |
| <b>Figure 3.42</b> - Line graph showing effective stress with increasing depth for Vibrocores (VC) and Piston Cores (PC). ....  | 3-52 |
| <b>Figure 3.43</b> - Scatter plot showing OCR values at measurement depths for Vibrocore (VC) and Piston Core (PC) samples. ....  | 3-55 |
| <b>Figure 3.44</b> - Line graph showing OCR variability for Celtic Sea shelf Vibrocore (VC) samples. ....   | 3-56 |
| <b>Figure 3.45</b> - Scatter plot showing the predicted yield stress with depth for Vibrocore (VC) and Piston Core (PC) samples. ....   | 3-56 |

|  |      |
|--|------|
| <b>Figure 3.46</b> - Visible deformation structures (solid black) and fractures (solid red) with x-ray equivalent features (dashed) observed in Vibrocores (VC) containing Lithofacies (LF) LF8 (blue).....  | 3-57 |
| <b>Figure 4.1</b> - Cartoon showing a summary of the stratigraphic relationships between the observed Seismic Facies (SF). Vertical red lines indicate different sections. Not to scale. ....  | 4-12 |
| <b>Figure 4.2</b> - Correlation between cored lithofacies and imaged Seismic Facies (SF). Lithofacies colours for each core correspond to those in Table 3.2. ....   | 4-15 |
| <b>Figure 4.3</b> - Schematic cross-section of a megaridge showing stratigraphic units and Erosion Events (EE) as indicated by cored physical samples and the truncation of reflections on seismic profiles across the mid- and outer-shelf. EE1 (red) is regionally extensive over the Upper Little Sole Formation (ULSFm) while EE2 (blue) is localised to the Melville Formation (MFm). The formation of the superficial drape (SF1) is associated with a regionally-extensive but minor EE3 (yellow). ....   | 4-19 |
| <b>Figure 4.4</b> - Adjacent pinger data (right) collected by Praeg et al. (2015b) and JC-106 chirp data (left) with core locations, Seismic Facies (SF) and interpreted reflection configurations. A common channel feature is marked (green dot) to aid correlation along with the base of the Upper Little Sole Formation (ULSFm) in purple, and an overlying weak reflection in green interpreted as the Melville Formation (MFm)-ULSFm boundary reflection by Praeg et al. (2015b). The left interpretation is preferred due to improved data resolution, penetration and coverage..... | 4-21 |
| <b>Figure 4.5</b> - Column chart showing one-dimensional thicknesses of glacial ice ( $916.7 \text{ kg}\cdot\text{m}^{-3}$ ) and glaciaqueous sediment ( $1900 \text{ kg}\cdot\text{m}^{-3}$ ) required to result in the maximum predicted yield stresses for each Vibrocore (VC) and Piston Core (PC), not accounting for the observed overburden. ....   | 4-28 |
| <b>Figure 5.1</b> - UKHO bathymetry and slope map of the seafloor surrounding the Isles of Scilly showing a deeper and flatter northwest seafloor and a shallower and irregular southeast seafloor with satellite imagery. Dark and light areas denote steep and flat areas respectively. ....   | 5-3  |
| <b>Figure 5.2</b> - UKHO bathymetry and slope map of the area immediately offshore of the coastline of Cornwall. Dark and light areas denote steep and flat areas respectively. See Area 1 in Figure 5.3. ...  | 5-5  |
| <b>Figure 5.3</b> - Map showing the limit of glacial features on the eastern inner-shelf at the present-day 70 m isobath (dashed). ....  | 5-6  |
| <b>Figure 5.4</b> - INFOMAR bathymetry and slope map showing the southwestern moraine overprinted by pits (black arrows) produced by the grounding of icebergs. Dark and light areas denote steep and flat areas respectively. See Area 6 in Figure 3.7. ....  | 5-8  |

**Figure 5.5** - Map showing the primary sub-Quaternary geology of the Celtic Sea shelf (BGS, 2013, 1979) with glacial channel locations. ....5-9

**Figure 5.6** - The two primary advance and retreat pathways of the Irish Sea Ice Stream on the inner-shelf. White arrows denote the generalised ice flow pathways as evidenced by regional bathymetry and mapped features, with thicker arrows indicating the main ice stream. The eastern margin is marked as a solid white line and generalised ice margin retreat positions are indicated with white dashed lines. The general orientation of features aligned parallel to ice flow direction (red), parallel to ice retreat direction (black) and parallel to the ice margin (green) are marked along with the banks bounding major troughs through which ice would have flowed (dashed). Onshore features are from Clark et al. (2018). ....5-15

**Figure 5.7** - Cartoon showing stages of the tidal formation model showing areas of erosion (red) and deposition (blue) due to post-glacial tidal currents (red lines). A glacial topography (A) is then exposed to a regional erosion event (B) where a sand bank nucleates on a seafloor irregularity (C) which grows (D) until tidal currents diminish and the seafloor is draped (E). ....5-21

**Figure 5.8** - Cartoon showing stages of the esker formation model showing areas of erosion (red arrows) due to post-glacial tidal currents (red lines). Glaciation (A) results in the deposition of an esker (B) which is exposed to a regional erosion event (C) which sculpts the ridge (D) until tidal currents diminish and the seafloor is draped (E). ....5-23

**Figure 5.9** - Cartoon showing the stages of an ice margin oscillation during deglaciation. A marine-terminating ice margin (A) experiences relative sea-level rise which imparts stress on the margin due to flotation (B). This flotation results in a reduction in basal friction and an unstable advance to override deformable proglacial sediments along with the production of even more stress (C). Due to intense fracturing and over-extension, the ice margin subsequently breaks up through calving (D). ....5-32

**Figure 5.10** - The advance and retreat pathways of the Irish Sea Ice Stream on the mid- and outer-shelf based on ice flow direction reconstructed on the inner-shelf (Figure 5.6). White arrows denote generalised ice flow pathways while generalised ice margin retreat positions are indicated with white dashed lines. The extent of the Upper Little Sole Formation (ULSFm), comprising cored subglacial sediments (red triangles), within the megaridges (red lines) is marked on the western shelf. Cored undisturbed glaciaqueous sediments (blue triangle) are marked with ULSFm channels (blue lines) which are imaged to contain undisturbed seismic facies (blue square). ....5-34

**Figure 6.1** - The inferred advance and retreat pathways of the Irish Sea Ice Stream on the Celtic Sea shelf. White arrows denote generalised ice flow pathways while generalised ice margin retreat positions are indicated with white dashed lines, solid white represents the eastern margin limit north of the Isles of Scilly. ....6-1

## List of Tables

|  |      |
|--|------|
| <b>Table 2.1</b> - Multi-beam bathymetric datasets by area obtained from the United Kingdom Hydrographic Office (UKHO) and the Integrated Mapping For the Sustainable Development of Ireland's Marine Resource (INFOMAR) project. ....   | 2-2  |
| <b>Table 2.2</b> - Recent scientific cruises having collected extensive sub-bottom data in the Celtic Sea. .   | 2-5  |
| <b>Table 2.3</b> - Selected JC-106 Vibrocore (VC) and Piston Core (PC) recovery details. ....  | 2-7  |
| <b>Table 2.4</b> - Selected Vibrocore (VC) and Piston Core (PC) recovery details from JC-106 which were subjected to sampling and geotechnical testing. Annotated visual core logs are published in Lockhart et al. (2018), with the exception of 36VC and 39VC which are published in Scourse et al. (2019), while the visual log for 53VC is unpublished. .... | 2-9  |
| <b>Table 3.1</b> - Feature classes and morphological descriptions with example images existing as either hillshades or slope maps. Some measurements were obtained numerous times per individual feature and these are marked with an asterisk. For image locations see Figure 3.7. ....   | 3-8  |
| <b>Table 3.2</b> - Lithofacies (LF) present per selected Vibrocore (VC) and Piston Core (PC) recovered during JC-106 with approximate thicknesses in metres, and converted into ms using a sound velocity of 1600 m·s <sup>-1</sup> to aid correlation between seismic profiles and cored lithofacies. ....  | 3-48 |
| <b>Table 3.3</b> - Plasticity Index (I <sub>p</sub> ) and $\alpha$ values for selected Vibrocore (VC) and Piston Core (PC) samples as derived from data in Table 3.4 and Table 3.5. ....   | 3-52 |
| <b>Table 3.4</b> - Liquid limit (w <sub>L</sub> ) mass and Moisture Content (MC) results for various Penetration (P) measurements for Vibrocore (VC) and Piston Core (PC) samples. ....  | 3-53 |
| <b>Table 3.5</b> - Plastic limit (w <sub>P</sub> ) mass and Moisture Content (MC) results for Vibrocore (VC) and Piston Core (PC) samples. ....  | 3-55 |
| <b>Table 4.1</b> - Feature classes with example images existing as either hillshade or slope maps. For example image locations see Figure 3.7. ....  | 4-3  |

|   |      |
|---|------|
| <b>Table 4.2</b> - Correlation of Seismic Facies (SF; Figure 4.1) and Lithofacies (LF; Table 3.2) to the Celtic Sea stratigraphic units of Layers A and B, the Melville Formation (MFm), Upper Little Sole Formation (ULSFm) and the Cockburn Formation (CbFm) by Pantin and Evans (1984), incorporating evidence from Scourse et al. (2002) <sup>1</sup> , Furze et al. (2014) <sup>2</sup> , Praeg et al. (2015b) <sup>3</sup> , Scourse et al. (2019) <sup>4</sup> , Pantin and Evans (1984) <sup>5</sup> , Bouysse et al. (1976) <sup>6</sup> , Marsset et al. (1999) <sup>7</sup> , Reynaud et al. (1999b) <sup>8</sup> , Scourse et al. (1990) <sup>9</sup> and Evans and Hughes (1984) <sup>10</sup> . Associated Erosion Events (EE) are noted from Figure 4.3. | 4-24 |
|---|------|

## Chapter 1 - Literature Review

### 1.1 Concern and Background

#### 1.1.1 Marine-terminating Ice Sheet Instability

Global mean temperature is likely to rise in the future (Figure 1.1), threatening to increase the rate of global sea-level rise by amplifying the thermal expansion of seawater and increasing the rate of melting of terrestrially-based ice sheets and glaciers (IPCC, 2014). Major ice sheets such as the Greenland Ice Sheet and Antarctic Ice Sheet represent significant stores of freshwater which are currently being released into the ocean due to net negative mass balances (Harig and Simons, 2015; IMBIE, 2018; Mohajerani et al., 2018; Seo et al., 2015). The Greenland Ice Sheet and Antarctic Ice Sheet contain enough freshwater to result in global sea-level rise of 7 m (IPCC, 2014) and 58 m (Fretwell et al., 2013) respectively, with the West Antarctic Ice Sheet representing 3 m (Bamber et al., 2009). Catastrophic and irreversible collapse of these marine-terminating ice sheets is of great concern due to the wide-ranging impacts of global sea-level rise (IPCC, 2018). Of immediate concern is the West Antarctic Ice Sheet, as it is grounded below sea level with a reverse slope inland (Fretwell et al., 2013) which makes this region of the Antarctic Ice Sheet vulnerable to collapse in response to increasing temperatures and sea-level rise. This can occur due to positive feedback dynamic instability whereby the melting and thinning of an ice lobe can result in increased ice flow velocities and mass-wasting through calving at the marine margin (Benn et al., 2007) or through unstable grounding line retreat due to adverse bed slopes (Schoof, 2007). Both scenarios highlight that marine-terminating ice sheets can be unstable and deglacier rapidly. Therefore, rising temperatures and sea level would result in the destabilisation of marine-terminating ice sheets and the significant contribution of meltwater to short- and long-term global sea-level rise.

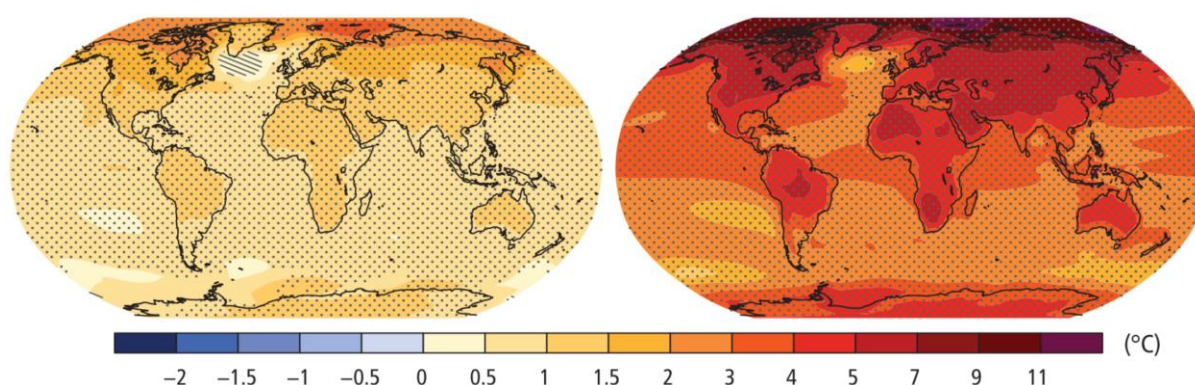


Figure 1.1 - Predictions of change in average surface temperature from 1986-2005 to 2081-2100 for Representative Concentration Pathway (RCP) RCP2.6 (left) and RCP8.5 (right). From IPCC (2014).

Currently, and in the near-future, natural and human systems in low-lying coastal areas are, and will be, profoundly affected by sea-level rise. Rising sea level can directly increase the intensity of storm events and associated flooding which could penetrate further inland, putting pressure on infrastructure and resources with profound implications for low-lying areas in developing countries (IPCC, 2018,



2014). Additionally, the Atlantic Meridional Overturning Circulation, which is responsible for ocean-atmosphere heat transfer and low- to high-latitude heat transport in the Atlantic Ocean, is likely to weaken into the future due to ice sheet melting (Caesar et al., 2018; IPCC, 2014) with implications for the Earth's climate. This weakening is possibly due to the accumulation of freshwater produced from the melting of the nearby Greenland Ice Sheet (Rahmstorf et al., 2015). Therefore, if the release of significant quantities of freshwater stored in the Greenland Ice Sheet and Antarctic Ice Sheet continues, this can profoundly alter the global coastline and severely affect ocean circulation and the Earth's climate. Due to the wide-ranging negative impacts of sea-level rise in the near- and far-future as a consequence of ice sheet collapse, the accurate forecasting of future global sea-level rise is essential to devise effective mitigation measures.

As the catastrophic collapse of an entire ice sheet has never been directly observed, there is significant concern as to the accuracy and intensity of future sea-level predictions if the Greenland Ice Sheet or Antarctic Ice Sheet deglaciates rapidly due to dynamic instability. This is because future predictions of sea-level rise are currently based on the melting of glaciers and the thermal expansion of seawater, with an uncertain ice sheet melt component (IPCC, 2014). This component of sea-level rise is undetermined due to the difficulty of replicating complex ice sheet behaviour for use in numerical model forecasts (IPCC, 2014). Previous numerical ice sheet models have been unable to predict dramatic present-day changes in contemporary ice sheets (e.g. Bamber et al., 2007) or large uncertainties exist in forecasted mass loss (e.g. Feldmann and Levermann, 2015; Ritz et al., 2015) due to complex and undetermined ice dynamics. Simply put, the accurate long-term forecasting of mass loss from ice sheets undergoing deglaciation due to dynamic instability requires long-term observations of ice sheets undergoing deglaciation due to dynamic instability. Observations of which are required to constrain, validate and improve numerical models of ice sheet behaviour, addressing the issues of reconstructing ice sheet behaviour (Stokes et al., 2015). These observations cannot be provided by contemporary instrumental records as they only represent a snapshot in the temporal scale over which ice sheet dynamics operate, and thus they do not record or represent long-term dynamic instability in response to environmental forcing. Therefore, the accurate forecasting of ice mass loss, and thus meltwater contribution to sea-level rise, needs to be based upon numerical models which simulate the long-term deglacial dynamics of an entire ice sheet. Such simulated dynamics should be rigorously tested against and informed by observations of ice sheet behaviour in the form of preserved sediments and glacial features. Such essential observations can only be provided through the investigation of palaeo-ice sheets which have undergone dynamic instability during their collapse, providing an indication of various styles and configurations of deglaciation over long timescales which may not be apparent in contemporary observations.

To accurately reconstruct the long-term dynamics of an ice sheet, it needs to be studied at the spatial and temporal scales over which such a complex system operates. This can only be accomplished by studying palaeo-ice sheets, where the evolution and deglaciation of the ice sheet is recorded by preserved evidence within its bed which can be used to reconstruct past dynamics (Clark, 1997; Kleman

and Borgström, 1996). Despite the fact that no complete deglacial chronology of an entire ice sheet yet exists, extensive geomorphological mapping of glacial features pertaining to the last ice sheet to cover Britain and Ireland (Clark et al., 2018) has provided a foundation for such a reconstruction pending further geochronological constraints (Figure 1.2). The resultant spatial and temporal reconstruction could then prove vital to constrain, validate and provide context for whole-ice sheet numerical models to increasing our understanding of deglacial dynamics. In such palaeo-ice sheet reconstructions, it is important to unravel the contributions of various forcings to ice dynamics and deglacial mechanisms, to both underpin and independently validate the numerical models. Such a rigorously tested ice sheet numerical model could then be applied to the Greenland Ice Sheet and West Antarctic Ice Sheet to forecast their dynamics and meltwater contribution to global sea-level rise in response to environmental change. When using palaeo-ice sheets for ice sheet behavioural studies, the palaeo-glacial environment needs to be reconstructed spatially and temporally as accurately as possible to represent the complex dynamic changes which occur during deglaciation. Such an accurate reconstruction can only be achieved through the thorough investigation of glacial signatures that are preserved in the present-day environment and are diagnostic of certain palaeo-glacial conditions.

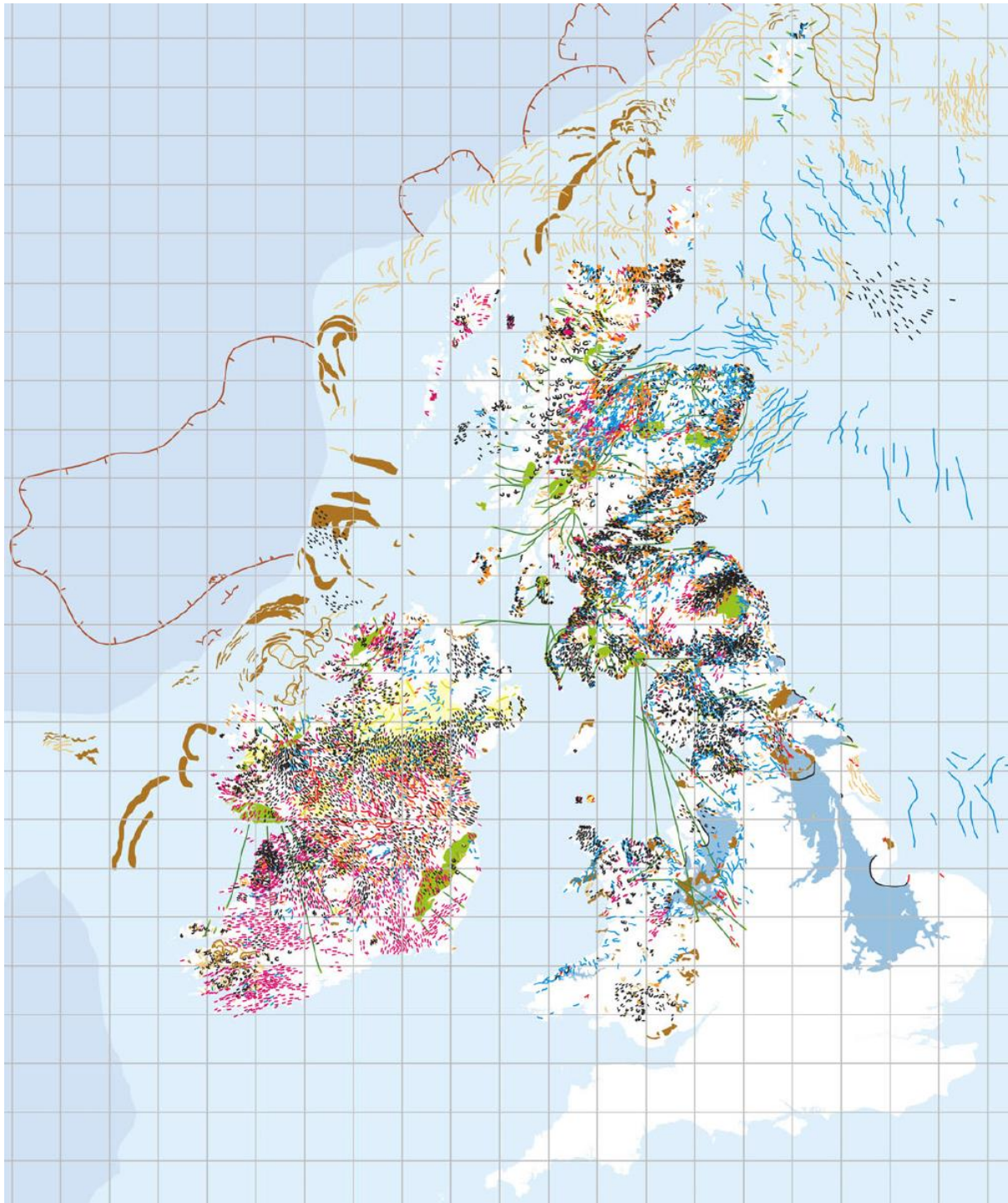


*Figure 1.2 - Mapped glacial features of the British Isles and surrounding offshore areas. Note the lack of features and deposits in the Celtic Sea region south of Ireland. From Clark et al. (2018).*

### 1.1.2 Glacial Processes and Deposits

In order to understand the palaeo-environmental significance of palaeo-glacial deposits, a knowledge of contemporary glacial processes and deposits is required. Such knowledge allows the correlation of contemporary and ancient glacial deposits and processes, where similar depositional environments can be inferred.

Given typical conditions, the vertical upward sequence of glacial deposits left by the deglaciation of a marine-terminating ice lobe on a continental shelf would comprise subglacial, proximal glacimarine and distal glacimarine which are then overlain by post-glacial transgressive deposits (Syvitski, 1991). Comprising the base of this sequence, subglacial sediments can consist of a variety of deposits (Evans et al., 2006). Any non-lithified substrate that is overridden by an ice stream will be actively deformed subglacially, permitting additional glacial motion along with that produced by basal sliding at the ice-sediment interface. In such instances, the deformable substrate generally displays visible deformation due to the sliding glacial sole and is stiff due to vertical loading by the ice mass (Boulton et al., 2001; Evans et al., 2006; McCarroll and Rijdsdijk, 2003). Such loaded and deformed sediments can transition from undisturbed material at the base to heavily deformed material directly under the glacial sole (Evans et al., 2006; Hiemstra et al., 2007) representing the upward increase in stress imparted by the sliding glacial sole. Abrasion and quarrying of lithified substrate can also result in the formation of diamict (Hiemstra et al., 2007), a stiff fine-grained matrix which supports larger clasts, commonly existing as gravel. However, it is also possible that grounded and floating icebergs can result in the deposition of diamict-like material of similar appearance to subglacial sediments through melt-out and turbation due to reworking by the grounded keels of icebergs (Dowdeswell et al., 1994). The primary methods by which a lithified substrate is altered by a flowing warm-based ice stream are through abrasion, quarrying and meltwater erosion (Glasser and Bennett, 2004). Abrasion occurs due to subglacial debris at the base of a sliding warm-based ice mass which results in the polishing and scoring of the substrate to produce a smooth bed (Hallet, 1981). Alternatively, quarrying results from the plucking and fracturing of the substrate by ice, generally by freeze-on, resulting in the production of angular debris and a rough bed (Hallet, 1996). These processes can combine during relegation, a mechanism where ice flows around a solid obstacle. This occurs through pressure melting on the up-flow side of an object where abrasion dominates while re-freezing occurs on the down-flow side to result in quarrying and plucking of solid material. During the withdrawal of this ice mass in contact with a marine environment, the ejection of debris from the margin into an aqueous environment results in horizontally-laminated proximal glacimarine sands, with coarser layers representing distinct subglacial meltwater debris ejections (Ó Cofaigh and Dowdeswell, 2001). As the ice margin retreats from the site of observation, this glacimarine sequence becomes finer and more distal, eventually comprising massive mud deposits (Ó Cofaigh and Dowdeswell, 2001). As these sediments occur through suspension settling in the water column, they are typically soft, horizontally-laminated and undeformed. Undisturbed glacimarine sediments are described as normally-consolidated unless they have been consolidated to a degree not achievable through the pressure applied by any present overlying material. In such instances, these sediments are described as being over-consolidated and such situations occur due to temporary vertical

loading, for example by an overriding ice margin to result in vertical loading and shear deformation or by erosion of the overlying material.

Warm-based ice actively slides at its bed, resulting in abrasion, quarrying, meltwater scouring and deformation which allows the production of various glacial features indicative of certain palaeo-glacial conditions. Streamlined and smoothed features which are elongated in the direction of ice flow are abundant in areas of past glaciation (Bradwell et al., 2008; C. D. Clark et al., 2009; Ottesen et al., 2017). Arcuate ridges represent distinct ice margin positions during standstill deposition (Howe et al., 2012; Ottesen et al., 2017; Shaw, 2003), while smaller ridges are oriented perpendicular to ice flow direction and record the transition between warm- and cold-based ice (Dunlop and Clark, 2006; Hättestrand, 1997; Hättestrand and Kleman, 1999). Subglacial meltwater laden with debris can scour and incise the solid substrate to form channels, the primary characteristic of which is a highly variable depth profile along their thalweg (Greenwood et al., 2007). If the substrate is resistant to incision, subglacial meltwater conduits can form up into the ice at the bed, producing sinuous ridges during deglaciation (Storrar et al., 2014; Van Landeghem et al., 2009). These features combine to produce a feature assemblage associated with the advance of an ice lobe (Figure 1.3), thus allowing the reconstruction of similar events where a similar assemblage is observed.

Therefore, basic physical glacial processes combine with other glacial conditions such as flow velocity, substrate saturation and composition, basal temperature and subglacial hydrology to result in the production of a wide assemblage of sediments and glacial features from which to reconstruct the palaeo-glacial environment (Clark, 1997; Kleman and Borgström, 1996; Stokes and Clark, 1999).

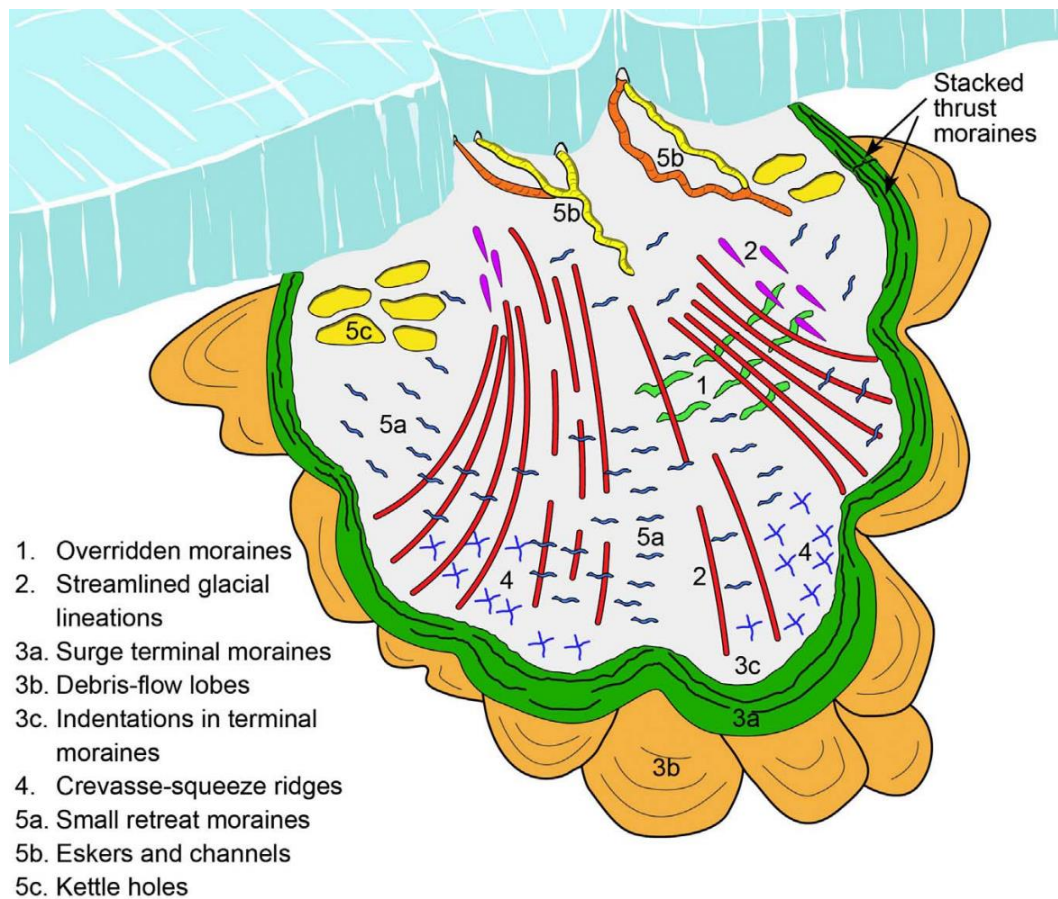


*Figure 1.3 - The interpreted glacial feature assemblage associated with the offshore advance of a marine-terminative ice lobe. From Ottesen et al. (2017).*

## **1.2 The Deposits and Quaternary History of the Celtic Sea**

### **1.2.1 Celtic Sea Shelf Bathymetry**

The Celtic Sea extends out to the continental shelf edge at 200 m water depth and towards the coastlines of Ireland, the UK and France (Figure 1.4). The inner-shelf of the Celtic Sea consists of the Nymphe Bank, Haig Fras and Lundy platforms which surround the Celtic Deep (CD) to the west, south and east respectively (Tappin et al., 1994). The Nymphe Bank Platform exists to the south of the Irish coastline and contains water depths of up to 100 m. This platform is gently sloping at  $0.02^\circ$  to the south and contains several isolated channels, one of which is very prominent to the south of the platform. The CD comprises an isolated basin which is elongated towards the south and contains water depths of up to 140 m. St. George's Channel (St. GC) exists as a trough between the coastlines of Ireland and Wales which extends south into the CD. The CD exists as a single trough which widens and deepens to the south where several deep channels are found on its southern boundary. To the west of the Bristol Channel and to the east of the CD is the Lundy Platform which slopes towards the Haig Fras Platform to the west at  $0.03^\circ$  and contains water depths up to 100 m. This northwest sloping seafloor exists along the coast of Cornwall towards the Isles of Scilly to the southwest. South of the CD, the seabed rises towards water depths of 90 m at the northern boundary of the Haig Fras Platform, before increasing in water depth at a slope of  $0.02^\circ$  towards the mid-shelf and Haig Fras, a large granite intrusion similar to that forming the Isles of Scilly to the southeast (BGS, 2013, 1979). To the southwest of the Haig Fras Platform, the shelf gently slopes towards the shelf edge where it is populated by linear ridges.



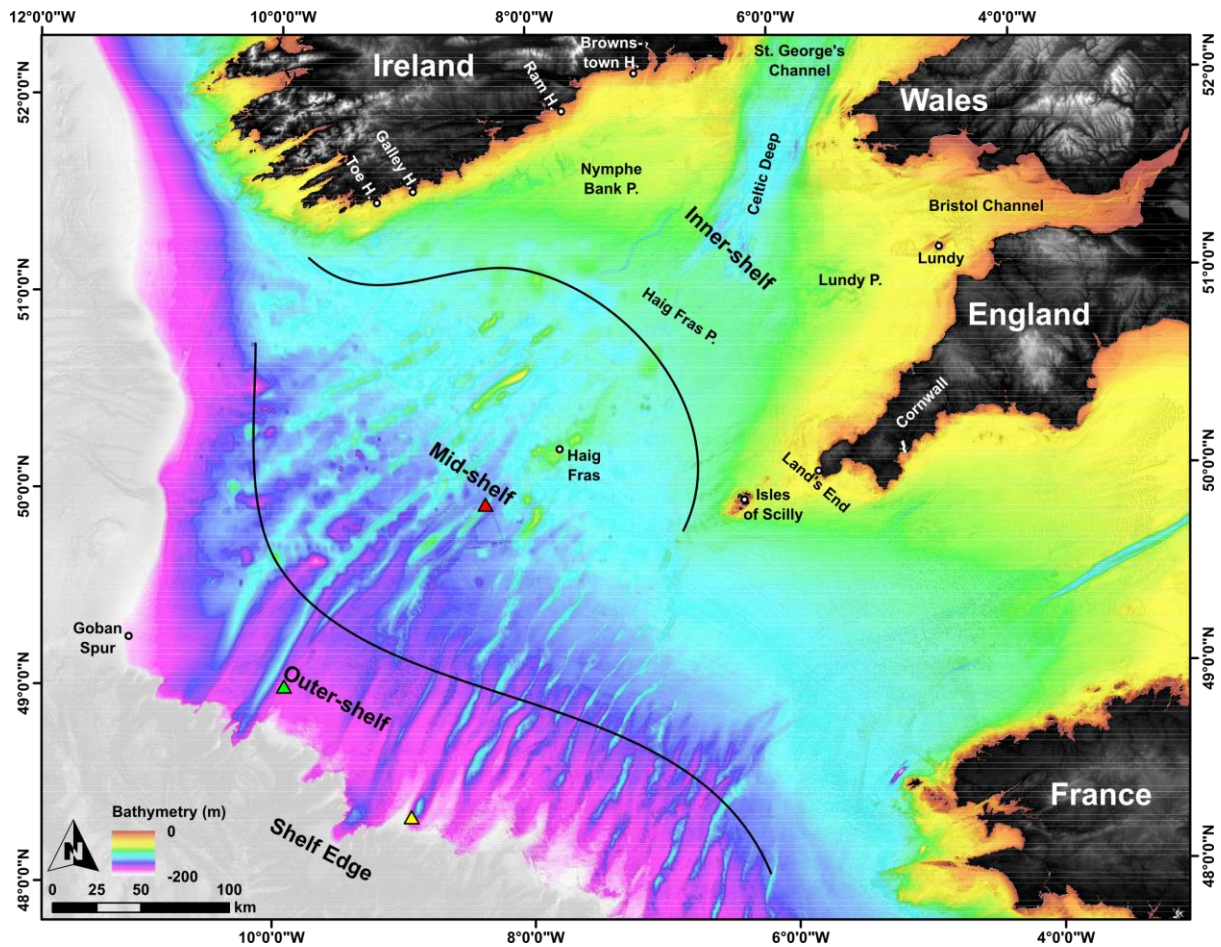


Figure 1.4 - EMODnet bathymetry map of the Celtic Sea shelf showing place names and areas mentioned in this thesis. Regions of the shelf are separated by boundaries defined here (black lines) Triangles denote the recovery locations of subglacial sediments at the shelf edge by Praeg et al. (2015b; green) and Scourse et al. (2019; yellow), and on the mid-shelf in BGS core 49/-09/44 (red; Scourse et al., 1990).

### 1.2.2 Superficial Deposits of the Celtic Sea Shelf

The Celtic Sea shelf contains a wide assemblage of superficial sediment types (Figure 1.5) ranging from mud to exposed bedrock, the spatial distribution of which is available for UK waters and part of Irish waters, obtained from grab and dredge samples and sediment cores collected by the British Geological Survey (BGS) in the 1970s (BGS, 2011; Evans, 1990; Tappin et al., 1994). Outcropping bedrock exists primarily along the southern coast of Ireland, west of the coast of Cornwall and in the Bristol Channel, with sporadic areas occurring around the contemporary UK coastline, providing the only rugged seafloor topography of the shelf (Evans, 1990). Sand and mud dominate across the shelf in various ratios. The CD is one of the few areas of the shelf to contain pure mud, sandy mud and muddy sand. Elsewhere, sand is the primary constituent of the seabed, which is punctuated with areas of gravel. The most significant areas of superficial gravel are within St. GC, the Bristol Channel and to the west of the coast of Cornwall towards the mid-shelf. On the inner-shelf, this superficial sediment



coverage is thin, apart from in the CD basin where Quaternary sediments can be over 375 m thick, comprising up to six stratigraphic units (Evans, 1990; Tappin et al., 1994). The mid- and outer-shelf contains a large assemblage of northeast-southwest trending linear ridges which consist of sand and gravel which can exist up to 50 m thick (Evans, 1990; Pantin and Evans, 1984). These ridges represent some of the thickest (5-50 m) Quaternary deposits found on the shelf, with exception to the CD and St. GC in the north (>50 m), as across the mid-shelf and to the west of the coast of Cornwall the Quaternary deposit thickness decreases below 5 m (BGS, 2014).

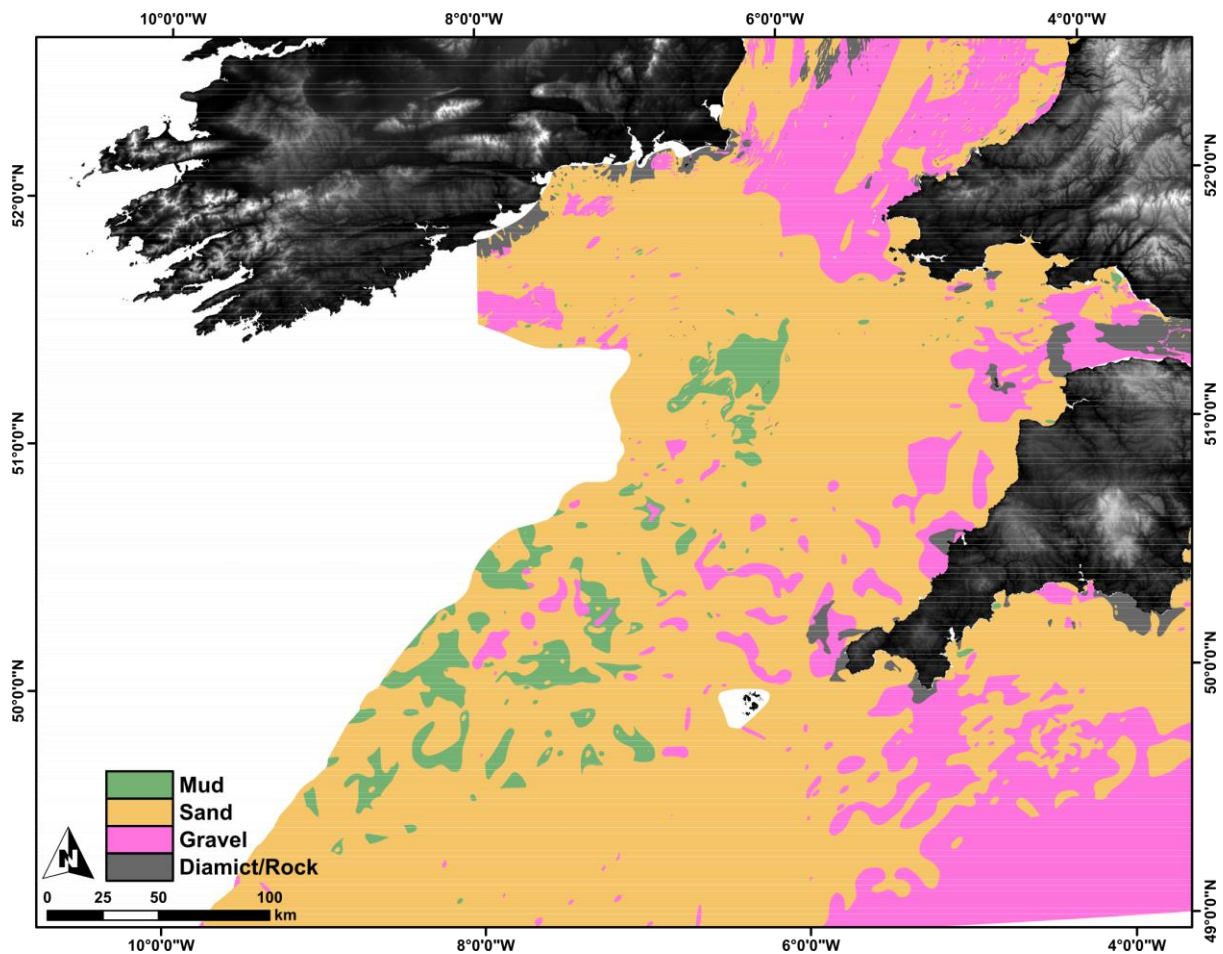


*Figure 1.5 - Map showing superficial sediment coverage by grainsize for the Celtic Sea shelf (BGS, 2011).*

### 1.2.3 Shallow Stratigraphy of the Mid- and Outer-shelf

The Celtic Sea shelf has been studied extensively using geophysical data correlated to physical samples collected in the 1970s by the BGS to investigate its stratigraphy and infer its evolution during the Quaternary (Evans, 1990; Pantin and Evans, 1984; Tappin et al., 1994). The investigations by Pantin and Evans (1984) identified the following regional shelf units that comprise the consensus shallow stratigraphy of the mid- and outer-shelf:

## **Layers A and B**

The superficial sediment coverage consists of Layer A, a discontinuous and sometimes fining-upwards drape up to 2 m thick which overlies Layer B, a distinct coarse layer 10s of centimetres thick containing shell fragments, pebbles and occasionally boulders above an unconformity (Furze et al., 2014; Pantin and Evans, 1984). These superficial layers were primarily reconstructed from physical samples, as seismic resolution was not sufficient enough to resolve them (Pantin and Evans, 1984). On the inner-shelf, these superficial sediments have maximum ages of 14 ka BP (Furze et al., 2014; Scourse et al., 2002) with a wide spread of dates obtained from Layer B, suggestive of extensive reworking at the commencement of its formation at 14 ka BP (Furze et al., 2014). These superficial deposits have been interpreted as representing the vertical transition from an underlying erosion surface and deposits of a high-energy shallow water environment (Layer B) to sedimentation during rising Holocene sea level (Layer A; Furze et al., 2014). Alternatively, Layer B has also been suggested to be glacial in origin, representing deposits from ice rafting during deglaciation (Pantin and Evans, 1984). Similar deposits to Layers A and B exist on the inner-shelf where they correlate to Sedimentary Layer 1 and 2 members respectively of the Surface Sands Formation (Tappin et al., 1994). This formation is predominantly sandy and found spatially over a large portion of the inner-shelf where it generally is less than 2 m thick and has a basal unconformity (Tappin et al., 1994).

## **Melville Formation**

Below Layers A and B exist laminated silty clays interpreted to represent glacialaqueous deposition across the inner- and mid-shelf (Furze et al., 2014), and stiff diamict, interpreted as subglacial (Scourse et al., 1990). BGS core 49/-09/44, retrieved from a ridge flank (Figure 1.4; Pantin and Evans, 1984), contains both glacial facies, representing a vertical subglacial to deglacial sequence of the last glaciation of the shelf (Scourse et al., 1990). While recent data confirm that these glacial facies are recovered from the ridges (Praeg et al., 2015a), an exact stratigraphic link is yet to be determined. This resulted in these glacial facies being correlated to the Melville Formation (MFm; Pantin and Evans, 1984). In the absence of additional geochronological information, the recovery of glacial facies sediments from the upper ridge flanks suggests that the ridges pre-date deglaciation of the shelf (Evans, 1990). Sands and gravels exhibiting occasional cross-bedding predominantly comprise the MFm, representing the internal bulk of the linear ridges, which is overlain by Layers A and B (Pantin and Evans, 1984). These ridge features can be up to 55 m high, 25 km wide and 200 km long (Stride et al., 1982), extending across the mid- and outer-shelf creating an extensive ridge field in the Irish, UK and French sectors of the Celtic Sea (Bouysse et al., 1976; Pantin and Evans, 1984). The consensus view is that these ridges are tidal in origin (Belderson et al., 1986; Scourse et al., 2009b; Stride, 1963; Stride et al., 1982). However, a tidal origin has been disputed based upon recent data that suggest a glacial origin of the ridges due to the confirmation that glacial facies sediments have been recovered from the ridges and have been correlated to internal units (Praeg et al., 2015b, 2015a). As the MFm is discontinuous between ridges, this results in Layers A and B directly overlying pre-Quaternary deposits. Where this occurs, boulders have been recovered from Layer B in places (Pantin and Evans, 1984).

### **Upper Little Sole Formation**

Below the MFm exists a sand, gravel and mud unit comprising the Upper Little Sole Formation (ULSFm) which begins at approximately 49°N, -8°E and extends southwest, expanding in thickness towards the shelf edge where it can be up to 50 m thick (Pantin and Evans, 1984). Both units are separated by a distinct reflection interpreted to exist as a coarse layer while the lower boundary of the ULSFm displays channelling (Pantin and Evans, 1984). This channelling is also found in the French sector (Bouysse et al., 1976), but becomes more discontinuous to the west (Pantin and Evans, 1984). The ULSFm is inferred to be fluvial in origin with a Late Pliocene or Early Pleistocene age across its entirety based upon the foraminiferal assemblage in the only core to penetrate this unit on the outer-shelf and the observation of basal channelling (Evans and Hughes, 1984; Pantin and Evans, 1984). Due to the similar grain size and constituent material with the above MFm, the boundary between the MFm and ULSFm can be acoustically transparent, making their differentiation difficult in places (Pantin and Evans, 1984). To the north of the ULSFm where it thins, the MFm overlies Neogene strata which exist under a regional angular unconformity (Evans, 1990; Pantin and Evans, 1984).

#### **1.2.4 Sub-Quaternary Geology of the Celtic Sea Shelf**

The spatial distribution of the underlying rock type and its structure are essential information in areas of past glaciation, as this produces a spatial distribution of varying rock mass properties which may have an influence on glacial dynamics and the expression of glaciation in the geological record. Regional reports (Evans, 1990; Tappin et al., 1994) and maps (BGS, 2013, 1979) of the offshore geology of the Celtic Sea produced by the BGS provide an overview of the sub-Quaternary geology across the shelf. The inner-shelf contains the most varied geology while the mid- and outer-shelf comprise Miocene mudstone and siltstone below Pleistocene deposits (Figure 1.6). Devonian-Carboniferous sandstone, mudstone and limestone are found around the contemporary coastlines of Ireland, Wales and Cornwall. The Isles of Scilly are formed from intrusive granite, of which a similar outcrop is found to the west of the islands, forming Haig Fras. Both of which are surrounded by Devonian-Carboniferous deposits. Towards the centre of the inner-shelf, various Palaeogene and Upper Cretaceous deposits exist. Palaeogene siliciclastic, argillaceous and sandstone deposits dominate in the central southeast, while Upper Cretaceous chalk is found between Haig Fras and the Isles of Scilly, and in the central northwest. However, throughout this area are smaller regions where Palaeogene and Upper Cretaceous deposits outcrop with northeast-southwest orientations, similar in orientation to the main geological boundaries. South of the Irish coastline, numerous northwest-southeast trending faults occur through Palaeogene deposits. West of Lundy exists an area of Jurassic deposits of mudstone and limestone which are interlaced with areas of Upper Cretaceous chalk, both of which are faulted northwest-southeast.

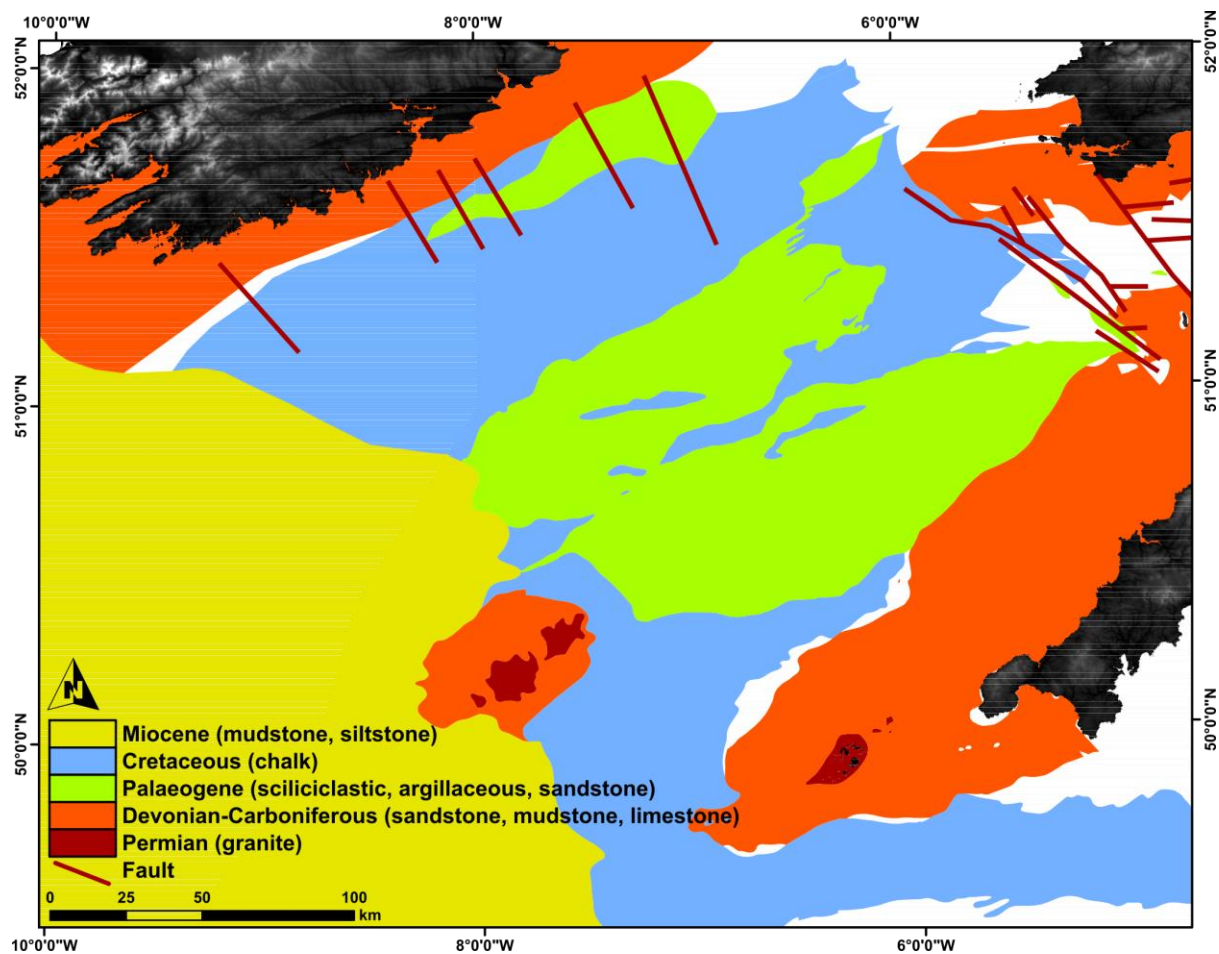


Figure 1.6 - Map showing the primary sub-Quaternary geology of the Celtic Sea shelf (BGS, 2013, 1979).

### 1.2.5 The Glaciation of the Celtic Sea Shelf

During the global Last Glacial Maximum (LGM), 26.5-19 ka BP (P. U. Clark et al., 2009; Peltier and Fairbanks, 2006), several major terrestrially based ice sheets existed which resulted in a glacio-eustatic sea level 130 m lower than that of the present-day (Lambeck et al., 2002). The Late Pleistocene glaciation of the British Isles has been found to have been more extensive than previously thought, mostly due to the increased availability of remotely sensed data in terrestrial and marine settings which permitted the identification of glacial features (e.g. Clark et al., 2018; Dove et al., 2015; Dunlop et al., 2010). The last British-Irish Ice Sheet (BIIS) has been reconstructed as reaching the northwest European continental shelf edge (Dunlop et al., 2010; Peters et al., 2015; Praeg et al., 2015b), resulting in an ice sheet that was dominantly marine-terminating and drained by several ice streams (C. D. Clark et al., 2012). This characteristic, and the position of the BIIS in the North Atlantic, made the BIIS sensitive to changes in climate conditions such as warming and sea-level rise which heavily influenced its behaviour (J. Clark et al., 2012; McCabe et al., 2005; Ó Cofaigh and Evans, 2007; Scourse et al., 2009a; Wilson et al., 2002). Due to convergent ice flows, underlying topography and subglacial geology, several ice streams occurred in various sectors, draining the ice sheet interior towards marine-

terminating lobes (C. D. Clark et al., 2012). These characteristics make the BIIS an ideal candidate from which to reconstruct glacial dynamics to study ice sheet behaviour over glacial timescales in response to many environmental variables such as tides, oceanic and atmospheric temperature, bed slope and bed substrate etc. In order for the BIIS to be used as a template for ice sheet behaviour studies, the palaeo-glacial environment needs to be reconstructed spatially and temporally as accurately as possible. One such key area of the BIIS reconstruction is the Celtic Sea shelf, which was glaciated by the largest marine-terminating lobe of the ice sheet, the Irish Sea Ice Stream (ISIS). The ISIS existed as a marine-terminating lobe of the BIIS (C. D. Clark et al., 2012; Praeg et al., 2015b; Scourse et al., 2019, 1990), and as such its advance into and retreat from the Celtic Sea shelf imprinted various glacial signatures in the geological record indicative of certain glacial conditions and processes.

The ISIS was the largest ice stream to drain the interior of the BIIS, fuelled by ice flow convergence in the northern Irish Sea (Figure 1.7). It extended from the Irish Sea through St George's Channel, and formed the maximum extent of the BIIS within the Celtic Sea (Figure 1.4; Praeg et al., 2015b; Scourse et al., 2019). This southern advance into the Celtic Sea occurred after 25-24 ka BP (Ó Cofaigh and Evans, 2007), and is suggested to have been a short-lived surge (Ó Cofaigh et al., 2012) as deglaciation had commenced by 25 ka BP at the shelf edge (Praeg et al., 2015b; Scourse et al., 2019) and ice had evacuated the shelf by 24.2 ka BP (Small et al., 2018). It was previously inferred that the presence of deformable sediment reduced subglacial friction and increased ice flow velocities, resulting in an interpreted thin and over-extended ice lobe reaching the mid-shelf (Scourse et al., 1990). Therefore, recent observations suggest that the ISIS reached the shelf edge based on the recovery of subglacial deposits in sediment cores (Figure 1.4; Praeg et al., 2015b; Scourse et al., 2019), implying a much larger ice extent than previously envisioned for this short-lived surge. Such an advancing mid-latitude ice lobe would have been warm-based and flowed mainly due to sliding and deformation of the underlying substrate, both combining to result in increased ice flow velocities. This increase in ice flow velocity can result in enhanced mass-wasting rates at the terminus through calving (Benn et al., 2007). As porewater pressures increase in the subglacial environment due to increasing saturation and being vertically loaded by the ice above, this reduces the effective stress and thus overall strength of the substrate (Terzaghi, 1943) which can facilitate enhanced sliding (Benn and Evans, 1996). This results in subglacial deformation of the substrate down to a depth of several metres over which deformation is more pronounced directly beneath the glacial sole, decreasing towards undisturbed substrate at depth (Boulton et al., 2001; Evans et al., 2006). Therefore, the overridden substrate can heavily influence the dynamics of an ice stream, and may have had a role in inducing ISIS margin instability (Ó Cofaigh and Evans, 2007, 2001), especially fine-grained deposits which would be inherently deformable. The sliding ice lobe would result in the transport of ice mass and debris towards its terminus while being fed from the main catchment to the north. Therefore, a point of extension is reached where ice mass being supplied to the ice lobe is in equilibrium with that being lost at the terminus and bed through melting and mass-wasting. If the ice lobe extends beyond this point, it is over-extended and cannot be sustained, resulting in thinning and fracturing which can precondition the ice lobe for later rapid retreat. Simultaneously, this thinning near the margin may result in dynamic instability through increased ice

flow velocities and calving rates at the marine margin if the lobe is close to flotation (Benn et al., 2007). This scenario is likely if ice margin retreat is eustatically driven, considering that the ice lobe is already over-extended and thin, and therefore flotation is more likely. Ice margin retreat from the Celtic Sea shelf edge had commenced by 25 ka BP (Praeg et al., 2015b; Scourse et al., 2019) due to rising relative sea level caused by glacial-isostatic depression in the southern regions of the BIIS (Scourse et al., 2019). Deglaciation coincided with the timing of Heinrich Event 2 (H2), characterised by a pulse of rapid sea-level rise which may have initiated or contributed to the initial rapid retreat of the marine sectors of the BIIS (Haapaniemi et al., 2010). Therefore, the initial retreat of the ice margin from the shelf break appears forced by relative sea-level rise (Scourse et al., 2019), while later retreat was forced by atmospheric and oceanic warming during Greenland Interstadial 2 (Rasmussen et al., 2014; Smedley et al., 2017).

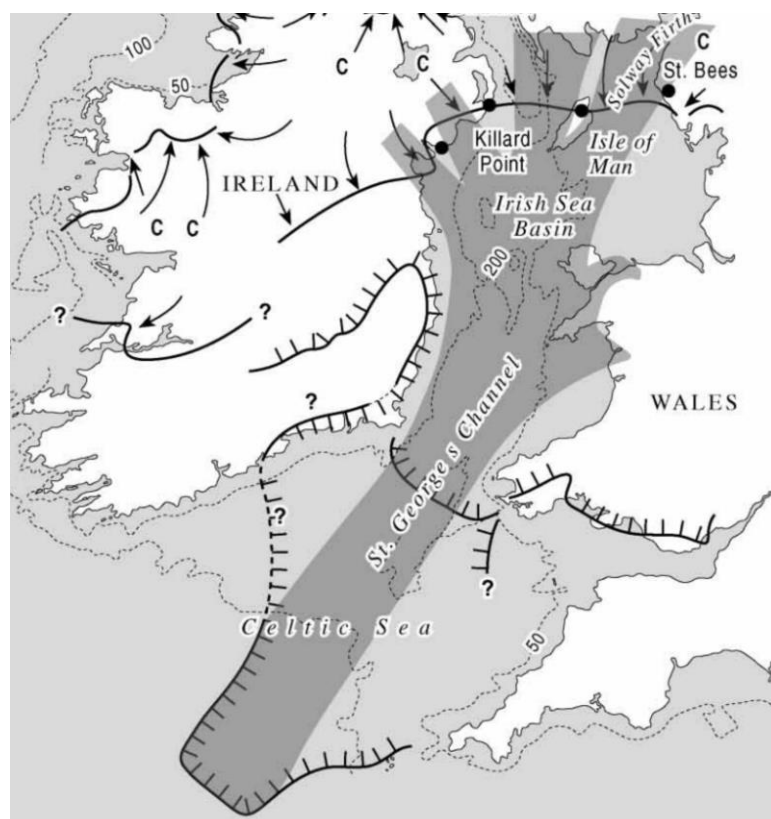


*Figure 1.7 - Overview of the ice catchment feeding the Irish Sea Ice Stream in the northern Irish Sea during its southwest flow through St. GC into the Celtic Sea. From Roberts et al. (2007).*

The preserved glacial landform record on southern Ireland records the last ice flows of the region where a dominant southeast flow of ice originated from the Irish coastline into the Celtic Sea (Greenwood and Clark, 2009). This Irish ice was subsequently warped by the surge of the ISIS from St. GC directed southwest towards the shelf edge (Greenwood and Clark, 2009; Ó Cofaigh and Evans, 2001). There are few studies on preserved landform assemblages of the Celtic Sea (e.g. Tóth et al., 2016), and larger spatial distributions of preserved features are needed to help reconstruct ice flow direction, ice extent

and deglacial dynamics as has been done for the rest of the BIIS (C. D. Clark et al., 2012; Clark et al., 2018; Greenwood and Clark, 2009). In this regard, the Celtic Sea has been neglected (Figure 1.2), representing a large gap in the reconstruction of the BIIS. In the east of the Celtic Sea, observations from the Isles of Scilly suggest that the eastern ice margin impinged on the north coast of the islands at 25.5 ka BP (Scourse, 1991; Smedley et al., 2017) but did not overtop them. North and south of the Isles of Scilly, the extent of ice to the east towards Cornwall and onto the eastern shelf is undetermined (Scourse et al., 1990). The previous grounded extent of the ice lobe in the Celtic Sea was proposed based on the southern limit of cored over-consolidated diamict, Melville Till (MT), at a boundary -135 m Ordnance Datum at the recovery site of core 49/-09/44 (Figure 1.4), south of which only Melville Laminated Clay (MLC) was found (Scourse et al., 1990). This spatial distribution of glacial facies across the shelf suggests that the ISIS was grounded out to this boundary on the mid-shelf, before terminating in a tidewater setting beyond which glacial marine deposition occurred (Scourse et al., 1990). The provenance of clasts within the MT was suggested to have been as a result of the southwest flow of grounded ice across the shelf, eroding the corresponding clast lithology which exists as bedrock to the northeast of the core locations (Scourse et al., 1990; Scourse and Furze, 2001). However, an alternative ice flow direction has been suggested adjacent to the Isles of Scilly which contradicts this southwest flow direction. John (2018) suggests that the Isles of Scilly were in contact with a terminal limit of the ISIS as opposed to a lateral limit, as suggested by Scourse et al. (1990), inferring that ice flow was from the northwest to the southeast adjacent to the Isles of Scilly. Both MT and MLC facies were retrieved in core 49/-09/44 which was collected in the 1970s by the BGS from the flank of a mid-shelf sediment ridge (Pantin and Evans, 1984) and correlated to the MFm (Evans, 1990; Pantin and Evans, 1984). As the basal MT was not totally penetrated, the glacial sequence of MT and MLC was correlated either to the unit comprising large linear ridge features which exist on the mid- and outer-shelf or to an eroded glacial layer draping these features (Evans, 1990; Pantin and Evans, 1984; Praeg et al., 2015b). This undetermined stratigraphic relationship has resulted in the suggestion that the ridges pre-date deglaciation of the shelf (Evans, 1990). More-recently recovered cores from the shelf edge were interpreted to contain subglacially deformed and proximal glacial marine sediments based on high undrained shear strengths suggesting over-consolidation in addition to visible deformation, suggesting further extension of the ISIS to the shelf edge (Praeg et al., 2015b). Similar sediments have been recovered across the mid- and outer-shelf which also record the presence of a grounded tidewater ice margin reaching the shelf edge (Scourse et al., 2019). This evidence suggests that the ISIS was grounded to the continental shelf edge, with the possibility of the existence of a continuous sheet of subglacial sediment extending across the shelf, buried by overlying deposits (Sejrup et al., 2005). Similar to glacial sediments in core 49/-09/44, glacial sequences on the mid- and outer-shelf have been recovered from the flanks of the Celtic Sea ridges (Praeg et al., 2015b; Scourse et al., 2019), bringing their origin as tidal features into question (Praeg et al., 2015a).

Marine deglaciation had commenced at 25 ka BP across the outer- and mid-shelf as recorded by radiocarbon dates from deglacial muds (Praeg et al., 2015b; Scourse et al., 2019), likely as a result of rising relative sea level due to glacial-isostatic depression caused by increased ice extent in the southern regions of the BIIIS (Scourse et al., 2019). During this time, a large-scale calving event took place which resulted in the formation of distinct sedimentary Ice Rafted Debris (IRD) layers on the seafloor of the North Atlantic, produced by deposited material from the melting of icebergs (Scourse et al., 2009a). These layers consist of material which was subglacially eroded and transported, thus they comprise various geologies and provenances based upon the local ice catchment being eroded. The OMEX-2K core, retrieved west of the Celtic Sea shelf, contains such IRD layers, some of which contain detrital carbonate sourced from the Laurentide Ice Sheet and an additional Cretaceous chalk signature (Haapaniemi et al., 2010). This chalk IRD signature can be interpreted to represent ISIS calving activity for two reasons (Scourse et al., 2009a); 1) Cretaceous chalk is found in the geology of the Celtic Sea shelf (Scourse and Furze, 2001) which would have been glacially eroded, entrained and transported offshore via icebergs for deposition as IRD; and 2) the close proximity of the core location to the catchment of the ISIS increases the likelihood that any chalk signature has a Celtic Sea provenance. Within the IRD signature is a detrital carbonate peak associated with the main calving event of H2 in the North Atlantic, occurring at 24 ka BP, which also coincides with a spike in the chalk signature (Haapaniemi et al., 2010). The occurrence of this chalk IRD signature suggests that the ISIS deglaciated in a tidewater setting coincident with H2. Subsequent decreasing intensity of this chalk signature most likely represents the withdrawal of the ice margin progressively northward towards the northern Irish Sea, possibly even disconnecting from the marine environment during ice margin retreat. However, several factors including the extent of the tidewater ice margin, the rate and debris content of calving along with melting rate and regional currents can influence the amount of IRD deposited at a location (Peck et al., 2007).

Laminated silty clays identified across the inner- and mid-shelf have been suggested to possibly represent glaciolacustrine deposition during deglaciation due to the lack of marine fossils, making them distinct from the glaciomarine MLC found on the outer-shelf (Furze et al., 2014). The ambiguous depositional environment across the inner- and mid-shelf has led to the formation of two competing hypotheses, both of which can explain the occurrence of deglacial muds lacking a diagnostic fossil assemblage (Furze et al., 2014). The glaciolacustrine hypothesis requires the deglaciation of a terrestrially based ISIS in contact with a freshwater proglacial waterbody on a subaerial shelf during lower sea-level conditions. The competing glaciomarine hypothesis requires tidewater deglaciation during higher sea-level conditions with high sedimentation rates to result in high-turbidity water to prevent marine phytoplankton production. As the retreat of the ISIS was rapid (Chiverrell et al., 2013), evacuating the shelf by 24.2 ka BP towards St. GC (Small et al., 2018), a subaerial shelf could have existed whereby the ice margin retreated faster than sea-level rise across the shelf. This exposed shelf could then have hosted isolated proglacial water bodies in which glaciolacustrine deposition took place. However, the glaciolacustrine model requires the presence of isolated water bodies dammed by glacial geomorphology (Furze et al., 2014), of which no evidence has been observed on the shelf. Prior to the



offshore advance of the main ice lobe across the shelf, lacustrine conditions occurred along the southern Irish coastline due to the inland advance of Irish ice from offshore, producing lacustrine embayments damned against the coastline (Ó Cofaigh et al., 2012). During evacuation of the shelf, the ice margin retreat rate of the ISIS reduced in St. GC, resulting in ice margin stabilisation, possibly due to the confining topography (Small et al., 2018), a fall in relative sea level and reduced palaeotidal amplitudes (Scourse et al., 2019).

The short-lived advance and retreat of the ISIS in the Celtic Sea make it an ideal candidate for the study of ice stream stability and behaviour in response to environmental forcing such as warming, sea-level rise and tidal conditions. As such conditions can drive ice sheet instability, their reconstruction is crucial to provide environmental context to any palaeo-glacial reconstruction of the Celtic Sea.

#### **Specific Questions:**

- Did the ISIS advance southwest across the shelf as suggested by the provenance of clasts within the MT?
- What was the maximum extent of the ISIS on the outer-shelf?
- Did the ISIS deglaciate in a marine or lacustrine setting on the mid- and inner-shelf?

#### **1.2.6 Post-glacial Evolution**

At the LGM, glacio-eustatic sea level was 130 m lower than present (Lambeck et al., 2002). Therefore, during the subsequent sea-level rise associated with deglaciation, the majority of the Celtic Sea shelf experienced marine transgression and megatidal conditions as suggested by palaeotidal model outputs (Scourse et al., 2018). In the Celtic Sea, relative sea level lowered to at least -110 m at 21 ka BP on the outer-shelf before rising at various rates towards the present-day position (Figure 1.8).

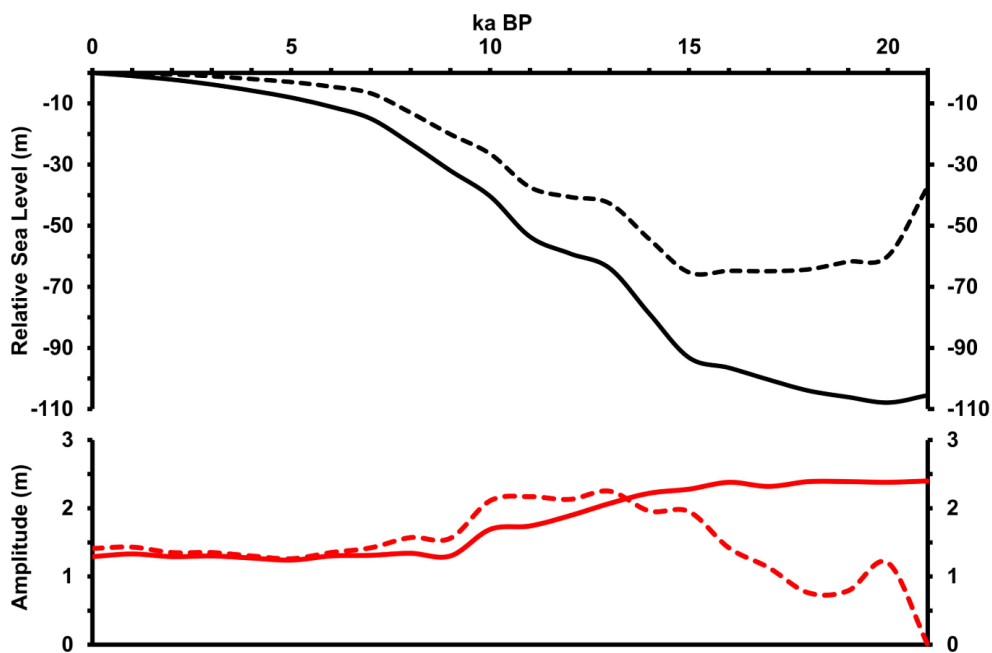


Figure 1.8 - Relative sea-level (black; Bradley et al., 2011) predictions with simulated tidal amplitudes (red; Ward et al., 2016) from 21 ka BP to the present-day for St. GC (dashed) and the outer-shelf of the Celtic Sea (solid). From Scourse et al. (2019).

Palaeo relative sea levels in the Celtic Sea have been primarily investigated as a method to determine the origin of a large assemblage of linear sediment ridges that exist across the mid- to outer-shelf. A low sea-level origin of the ridges was first investigated by Belderson et al. (1986), who, through numerical modelling of tides, identified that such conditions would produce tidal currents significantly more powerful than experienced at present. This work was subsequently developed by Scourse et al. (2009b) who used numerical modelling to show tidal current evolution from 21 ka BP towards the present, taking Glacial-Isostatic Adjustment (GIA) into account in the model (Uehara et al., 2006). Scourse et al. (2009b) suggest that the Celtic Sea experienced energetic tidal currents during lowered sea level, but also showed that such conditions persisted for several thousand years (Scourse et al., 2009b) as the North Atlantic was resonant with the principal lunar semi-diurnal tide (Wilmes and Green, 2014). Such conditions continued until 12 ka BP when resonance decreased due to continued sea-level rise (Wilmes and Green, 2014). Further developments in palaeotidal modelling with a more realistic GIA input, generated by Bradley et al. (2011), continue to confirm that such conditions had commenced by 21 ka BP and persisted until 16 ka BP (Figure 1.9) which had the energy to entrain coarse sand during this period (Ward et al., 2016, 2015). During this time period, palaeotidal models suggest that tidal amplitudes were in the order of several metres for the Celtic Sea shelf and, combined with sea-level rise, these conditions provided significant forcing for deglaciation of the ISIS (Scourse et al., 2018). When integrated with sea level, palaeotidal model outputs show that megatidal conditions persisted in the southern Celtic Sea, while the northern area experienced less energetic conditions (Scourse et al., 2018; Ward et al., 2016).

Palaeotidal modelling requires a GIA component to produce accurate sea-level evolution reconstructions from which to study temporal and spatial changes in tides. GIA modelling itself requires an earth crust model, a eustatic sea-level model, and an ice sheet model, see Whitehouse (2018) for a review. These two latter components have to be constrained by observations such as sea level index points and chronologically-constrained ice sheet reconstructions, some of which are unevenly distributed or are lacking in areas which induces ambiguity as various loading intensities, durations and timings can fit the underpinning observations (Whitehouse, 2018). Therefore, as palaeotidal model outputs heavily rely upon the palaeo topographies generated by GIA models (Ward et al., 2016), their outputs are therefore dependent upon observations of the past environment which may be incorrect or unevenly distributed. Great variability in tidal current intensity and duration exists in palaeotidal amplitude predictions for various sectors surrounding the British Isles depending on which model is used (Scourse et al., 2018; Ward et al., 2016), highlighting the underlying variability. The Bradley et al. (2011) GIA model is used in recent palaeotidal models (Ward et al., 2016), incorporating the available observations at the time which suggested a less-extensive ISIS. Therefore, the ice sheet model used in the Bradley et al. (2011) GIA model does not include recent observations of a more extensive Celtic Sea glaciation by Praeg et al. (2015b) and Scourse et al. (2019). Therefore, the Bradley et al. (2011) GIA model will underpredict the intensity, duration and timing of loading which will affect palaeotidal model outputs and as such they will not represent an accurate sea-level history of the Celtic Sea. Despite this, it is unknown to what degree the ISIS would have influenced crustal loading, as the current chronology suggests that glaciation of the shelf was short-lived (Ó Cofaigh et al., 2012). The initial advance onto the shelf occurred after 25-24 ka BP (Ó Cofaigh and Evans, 2007) and the ice margin had evacuated the shelf by 24.2 ka BP (Small et al., 2018), resulting in a short residence time. Therefore, the crustal loading, and thus subsequent crustal rebound, may not have been significant due to the brevity of the loading event and its reduced intensity due to the interpretation that the ISIS was thin. Despite the inherent inaccuracies, palaeotidal models consistently show that the Celtic Sea experienced megatidal conditions during marine transgression (Ward et al., 2016), increasing the confidence that such an event occurred.

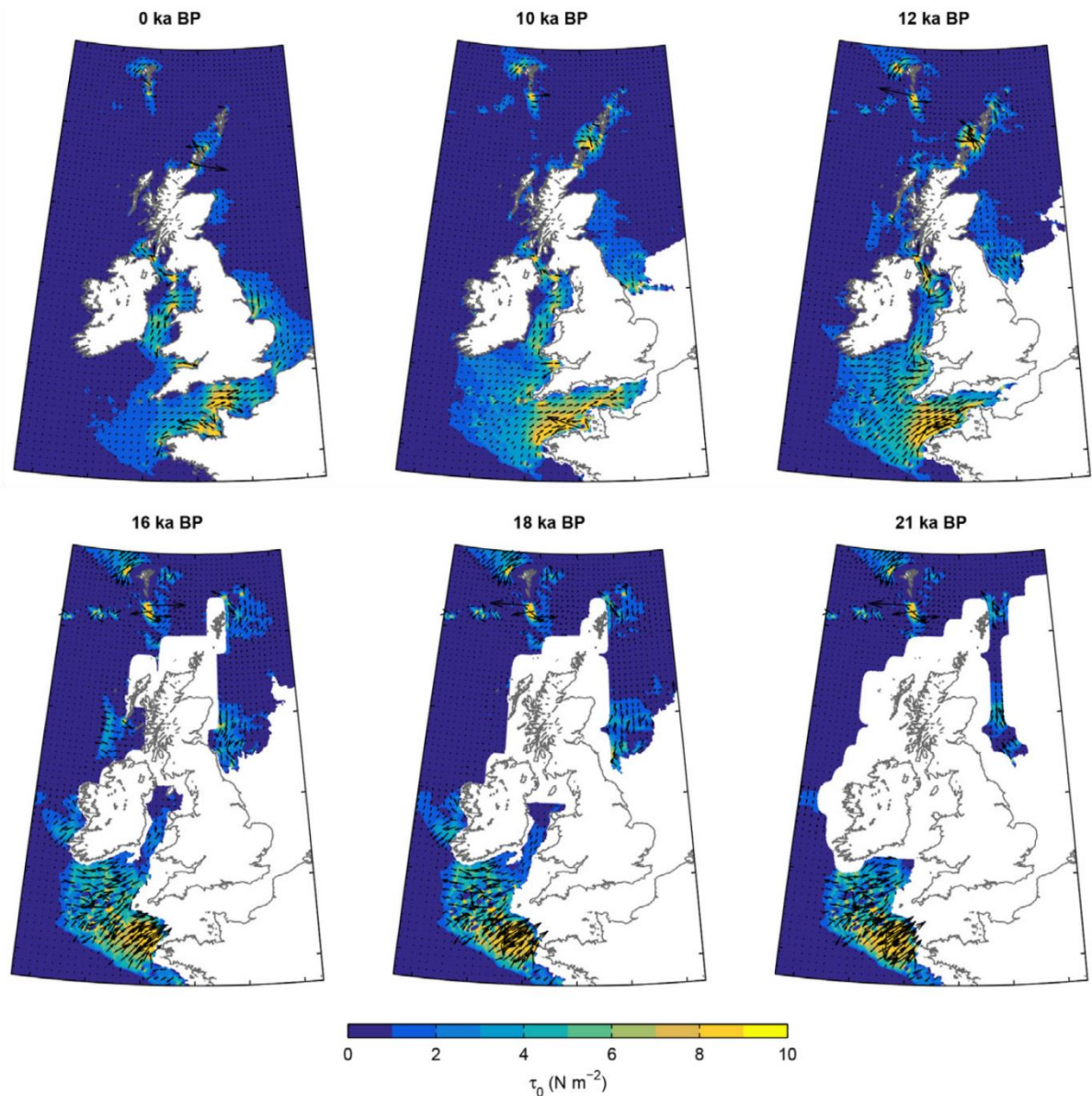


Figure 1.9 - Palaeotidal model reconstruction of the Celtic Sea showing bed stress intensity (colour ramp) and dominant tidal current direction (arrows) for various time slices. From Ward et al. (2016).

Prolonged and energetic tidal conditions (Figure 1.9) are inferred to have produced the large sediment ridges which extend across the mid- and outer-shelf of the Celtic Sea (Scourse et al., 2009b). Such ridges form according to the Huthnance (1982a, 1982b) mechanism, whereby tidal currents interact with seabed irregularities such as mounds to result in net deposition on the crest of the feature, resulting in ridge generation. During transgression, palaeotidal model outputs suggest that a bedload parting zone formed parallel to the shelf edge which migrated northeast across the shelf as relative sea level rose (Scourse et al., 2009b). A zone of high tidal bed stress then formed behind this bedload parting zone as it continued to migrate across the shelf (Uehara et al., 2006). This energetic zone resulted in the transport of shelf sediment offshore and the initial growth of the ridges, representing post-glacial tidal sand banks (Scourse et al., 2009b). On the western shelf, these features can be up to 55 m high,

25 km wide and 200 km long (Stride et al., 1982). This contrasts with ridges on the eastern shelf which can be up to 50 m high, 7.5 km wide and 70 km long (Bouysse et al., 1976). Therefore, there appears to be a transition from larger ridges to the west in the Irish-UK sectors and smaller ridges to the east in the French sector. However, these ridge morphology measurements were obtained from individual seismic lines and single-beam echo-sounder data, therefore a more detailed analysis of ridge morphology may yield information as to how and why their morphology changes west to east across the ridge field. The observation that larger ridges exist on the western shelf conflicts with palaeotidal observations that show that the eastern shelf experienced more intense tidal current conditions for a longer duration compared to the western shelf (Ward et al., 2016). This suggests that sediment supply was a dominant factor in ridge formation on the eastern shelf (Scourse et al., 2009b), where the French sector was sediment starved and the Irish-UK sectors had a large sediment supply due to glaciation. As transgression continued, bed stresses weakened as sea level rose, resulting in the ridges becoming stagnant with no additional growth (Scourse et al., 2009b). An alternative hypothesis of ridge development in the French sector is that the features are erosional in origin, as opposed to being depositional, where tidal currents have sculpted low-stand shelf deposits into the observed ridge features (Berné et al., 1998). This is based on the observation that the upper bulk of the investigated French ridge contains transverse channels incised into its upper bulk which are interpreted as being fluvial, estuarine or deltaic in origin (Berné et al., 1998). These channels appear to have once extended beyond the upper surface of the ridge. In addition to these channels, the upper surface truncates reflections in the underlying units, suggesting that it is erosional in origin (Berné et al., 1998). This interpretation that the bulk of the ridge comprises tidally sculpted low-stand deposits was challenged by Reynaud et al. (1999b) who provide new data to suggest that the ridge bulk was deposited in a marine environment and that the channels which incise the upper surface are a product of cross-ridge tidal currents. Additionally, these ridges overlie a basal surface which has been interpreted as being transgressive in origin (Reynaud et al., 1999a), representing the onset of an erosion event before the start of ridge formation. Therefore, the internal stratigraphy of the ridge and the incision of channels can be explained by a constructional tidal mechanism (Figure 1.10). Berné et al. (1998) also identified neighbouring ridges to the east that appear transgressive in origin, which consist of dipping clinoforms resting over an erosion surface also interpreted as being transgressive. These observations and new interpretations suggest that the ridges in the French sector are tidal in origin. In the Irish-UK sectors, Pantin and Evans (1984) identified that the ridges comprise the MFm, which predominantly exists as sand and gravel overlying a coarse layer as interpreted from seismic reflection data. Across the Celtic Sea, the MFm contains truncated and dipping reflections (Pantin and Evans, 1984; Reynaud et al., 1999b). It has also been noted however that the MFm appears to mantle earlier deposits (Marsset et al., 1999; Pantin and Evans, 1984; Reynaud et al., 1999b), suggesting that underlying seafloor irregularities presented a nucleus for ridge development. Offshore ridges comprising bedded sands are commonly interpreted as tidal sand banks (Davis and Balson, 1992) which overlie a lag deposit (Houbolt, 1968) most likely representing an erosion surface. This erosion event is most likely associated with the predicted energetic tidal currents which existed across the Celtic Sea during transgression. Additionally, the coarse grainsize of the MFm can be explained by energetic conditions during

transgression, where strong tidal currents, as indicated by palaeotidal model outputs (Scourse et al., 2009b; Ward et al., 2016), achieved the energy to entrain coarse sediment (Ward et al., 2015). This resulted in fine-grainsize material being transported off the shelf while coarse grainsize material remained to form the ridges. However, it must be remembered that glacial sediments have been correlated to the MFm due to being recovered from ridge flanks (Pantin and Evans, 1984; Praeg et al., 2015b, 2015a), suggesting that a simple constructional tidal origin for the ridges is not the case in the Irish-UK sectors. These observations have been accommodated previously through the interpretation that the northern ridges have been overridden by the ISIS (Scourse et al., 1990) or formed during deglaciation (Scourse et al., 2009b). However, since glacial sediments have been recovered from a ridge flank at the shelf edge, a glacial origin of the ridges has been proposed where they represent glacialfluvial features (Praeg et al., 2015a), as it is unlikely that the ridge field would have survived being overridden by the ISIS during its advance to the shelf edge. Therefore, a thorough investigation of the internal geometry and composition of these ridges can yield information as to their age and stratigraphic relationship to glacial sediments. Such pieces of information are crucial in order to explain how these ridge features developed and if they do comprise glacial features or tidal sand banks. This would provide essential data from which to study how the Celtic Sea shelf evolved and if such ridges provide a pathway from which to study the glaciation and deglaciation of the shelf.

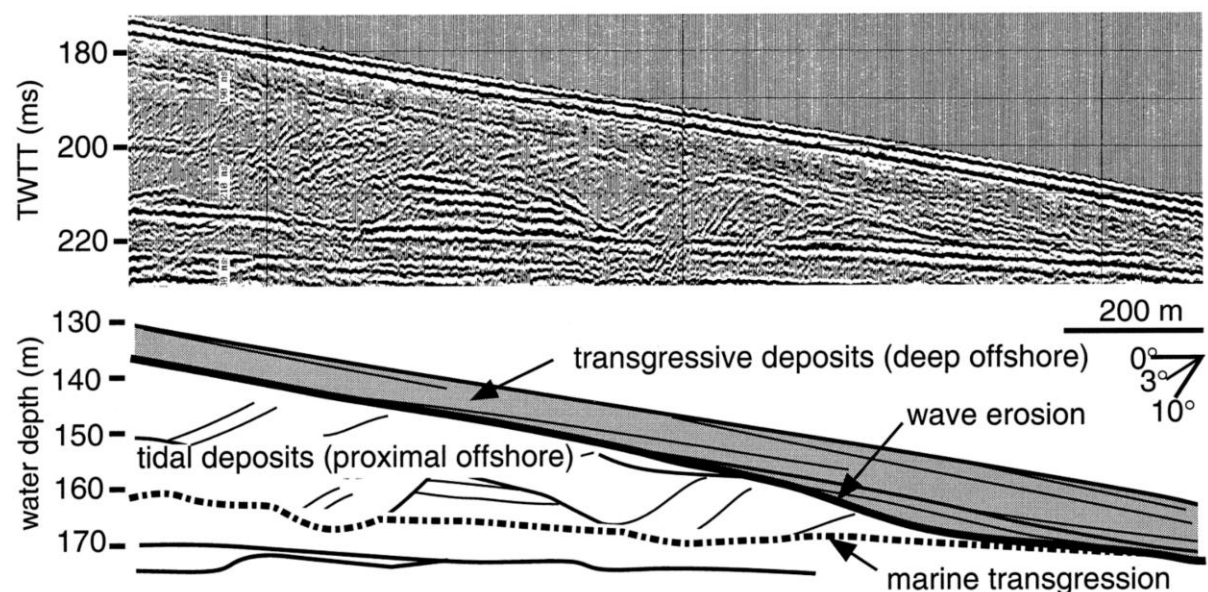


Figure 1.10 - Seismic section and interpretation of the flank of a French ridge suggesting a marine transgressive surface (Melville Formation base), tidal deposits (Melville Formation) and an overlying wave erosion surface and late transgressive deposits. From Reynaud et al. (1999a).

Palaeotidal model outputs suggest that energetic tidal currents began to reduce in intensity after 16 ka BP (Scourse et al., 2018; Ward et al., 2016) due to a loss of resonance because of sea-level rise (Wilmes and Green, 2014). As tidal currents diminished, wave reworking became the dominant process during continued transgression (Reynaud et al., 1999b). In the French sector, the ridges are capped by

a coarse lag (Reynaud et al., 1999a), similar to Layer B found in the Irish-UK sectors (Pantin and Evans, 1984) which was interpreted to have formed during energetic conditions where it overlies an extensive erosion surface (Furze et al., 2014). This coarse lag which overlies the ridges was interpreted to have been produced by the combination of tidal and wave reworking, where the latter dominates in present-day water depths shallower than 145 m as evidenced by the presence of wave-related bedforms (Reynaud et al., 1999a). On the inner-shelf, beyond the ridge field extent, Layer B had started to form at 14 ka BP (Furze et al., 2014), during the period when tidal currents were reducing across the shelf. As sea level continued to rise, Layer A was deposited as a conformable sequence as seen in the CD (Scourse et al., 2002).

#### **Specific Questions:**

- How can the deposition of easily-erodible deglacial muds occur in the context of energetic marine conditions?

#### **1.2.7 Glacial vs Tidal Origin of the Shelf Ridges**

Tidal models of the Celtic Sea megaridges, the larger western ridges, have been based on observations of their morphology and internal character, and the modelling of shelf conditions during lower sea levels. Seismic profiles across the Celtic Sea ridges reveal dipping and truncated internal reflection surfaces (Pantin and Evans, 1984; Reynaud et al., 1999b), while short (mainly <5 m) sediment cores obtained from the megaridges across the Irish-UK sectors show that the primary unit comprising the ridges, the MFm, mainly consists of medium to coarse sand and gravel (Evans, 1990; Pantin and Evans, 1984). Huthnance (1982a, 1982b) proposed a mechanism for ridge growth based upon the interaction between bottom friction over a mound and tidal currents, resulting in ridge growth through deposition on the crest and lateral migration. This is different to the mechanism of Houbolt (1968), who suggested that longitudinal helical vortices either side of a mound can result in axial ridge growth with little lateral migration. Tidal ridges generally consist of medium sand with some bedding planes (Davis and Balson, 1992) which transition to an underlying lag deposit at the base of the ridge (Houbolt, 1968), similar to observations of the MFm by Pantin and Evans (1984). Palaeotidal modelling investigations support the interpretation that the Celtic Sea ridges are constructional features formed during rising sea level by strong tidal currents which commenced at, or before, 21 ka BP following deglaciation (Belderson et al., 1986; Scourse et al., 2009b; Uehara et al., 2006; Ward et al., 2016), with the energy required to transport coarse sand (Ward et al., 2015). Palaeotidal model results presented in Scourse et al. (2009b) suggest that the northern limit of the ridge field could represent the boundary where bed stresses weakened at 10 ka BP, resulting in the features becoming moribund with no additional axial growth.

However, a post-glacial tidal formation of the megaridges conflicts with the presence of glacialic sediments on their flanks, including laminated and/or stiff fine-grained sediment, from the mid- and outer-shelf (Praeg et al., 2015b; Scourse et al., 2019, 1990). Additionally, gravel and boulders have been recovered from the flanks of ridges across the Irish-UK sectors, with the presence of the former

being suggested to represent a mantle of ice-rafted debris (Pantin and Evans, 1984). The presence of glacial sediments overlying the ridges and the recovery of MT and MLC in core 49/-09/44 on a megaridge flank, was interpreted to indicate that the MFm existed prior to deglaciation (Evans, 1990; Pantin and Evans, 1984). The observation that glacial sediments appear to drape the megaridge flanks in the Irish-UK sectors has been attributed to either partial glacial overriding of the mid-shelf ridges (Scourse et al., 1990) or to tidal ridges forming syngenetically with deglaciation (Scourse et al., 2009b). Alternatively, the entire internal bulk of the megaridges could represent large glacial features or giant eskers (Praeg et al., 2015a). The large-scale internal cross-bedding and sandy composition of the MFm, as well as the presence of stiff glacial sediments, could be consistent with the characteristics of eskers (Praeg et al., 2015a). Eskers may also be hundreds of kilometres long and up to 80 m high, but commonly have widths <150 m that are consistent with a single subglacial meltwater conduits (e.g. Banerjee and McDonald, 1975; Rust and Romanelli, 1975; Storrar et al., 2015). However, eskerine ridges with widths of kilometres also occur (e.g. Banerjee and McDonald, 1975; Mäkinen, 2003; Rust and Romanelli, 1975), including features up to 10 km wide (Noormets and Flodén, 2002; Veillette, 1986). Large ridges have been attributed to deposition from multiple conduits supplying sediment to over- and back-lapping outwash fans from a receding ice margin (Rust and Romanelli, 1975). A time-transgressive origin can account for esker networks >100 km long within a receding ice-marginal zone, producing linear ridge segments with spacings of up to 19 km (Storrar et al., 2014). Eskers are highly variable in structure and lithology, but generally contain several metres of plane- and cross-bedded sand and gravels (Banerjee and McDonald, 1975; Brennand and Shaw, 1996; Gorrell and Shaw, 1991; Hebrand and Åmark, 1989; Mäkinen, 2003). Additionally, eskers may contain a core of boulders and cobbles which fine upward and outward from the centre, representing the deposition of finer grained material due to decreasing meltwater pressures in the final stages of development (Gorrell and Shaw, 1991). As eskers develop in ice marginal zones that may also be subaqueous, glaciofluvial sands and gravels may be interlayered with subglacial diamict and both give way laterally to lacustrine or marine muds (Rust and Romanelli, 1975).

Therefore, if the Celtic Sea ridges do correspond to glacial features, they provide evidence of an extremely extensive glaciation of the majority of the Celtic Sea shelf which has implications for GIA modelling for the reconstruction of palaeo sea level, and for palaeo-glacial dynamics. Such a significant extension of the ISIS needs to be reconciled with the over-extended nature of the ISIS and its rapid advance and retreat in the Celtic Sea.

#### **Specific Questions:**

- Does the MFm mantle earlier deposits as suggested by initial observations?
- Does the MFm have characteristics consistent with either a tidal or glacial origin?
- When did the MFm form?



### **1.3 Seafloor Bathymetry for Environmental Reconstruction**

#### **1.3.1 Seafloor Geomorphology**

The high-resolution and high-spatial precision mapping of large swaths of the seafloor has a variety of uses and has been important for various discoveries pertaining to geological and oceanographic processes (Wöelfl et al., 2019). Surrounding Britain and Ireland, multi-beam echo-sounders have revealed a diverse and dynamic environment comprising relict glacial terrain, rocky outcrops, large migrating bedform fields and in places a featureless seabed. The spatial distribution of such features provides a unique insight into how present and past processes have influenced and are influencing the evolution of the seafloor. Therefore, seafloor morphology provides a method through which to reconstruct and study the evolution of the seafloor. Examples include a qualitative assessment of bedload sediment transport in response to present hydrodynamic forcing through the repeat surveying of migratory bedform fields (Knaapen, 2005; Van Landeghem et al., 2012), the identification of features indicative of past glaciation (Dowdeswell et al., 2016) or the reconstruction of past landscapes drowned by sea-level rise (Westley et al., 2011).

The usage of remote sensing and direct sampling in terrestrial and marine environments has been key to the identification of glacial features for use in the glacial inversion approach to ice sheet reconstruction (Clark et al., 2018; Dowdeswell et al., 2016). In essence, where features exist that are indicative of certain glacial processes and condition, such as ice flow direction and speed, margin extent and deglacial setting, they can be used to infer the presence of similar situations in the past (Dowdeswell et al., 2016). Therefore, such features provide direct observations from which to reconstruct past glacial dynamics at the spatial scales at which major ice sheet dynamics operate, thus allowing the reconstruction of entire ice sheets (Clark et al., 2018; Kleman and Borgström, 1996). The preserved glacial feature assemblage can be used to infer the configuration and direction of ice margin retreat, but its referencing to a robust geochronological framework then provides information on rates of ice margin retreat, forming a complete deglacial ice sheet reconstruction. Such reconstructions then provide essential observations against which numerical ice sheet models can be tested. Such an exercise has been conducted for the Eurasian ice sheet complex, where modelled ice flow pathways generally agree with ice flow observations, however the timing and pace of ice margin retreat remains an issue (Patton et al., 2017). Where deglaciation is reconstructed as a large-scale chronology, glacial features can provide essential context and constraints in precise locations, enhancing our knowledge of when, how and where deglaciation occurred which a chronology alone cannot provide. Geomorphological data are however not homogeneously available, especially in the present marine environment, either due to the difficulty and cost of surveying the offshore environment, the removal of glacial signatures by contemporary processes or that no signatures were produced. This results in areas where the palaeo-glacial environment is not accurately understood or reconstructed due to a lack of glacial geomorphology such as the Celtic Sea (Figure 1.2).

### **1.3.2 Seafloor Features of the Celtic Sea Shelf**

Bathymetric measurements in the Celtic Sea were first extensively produced during investigations of the shelf in the 1970s from seismic lines and single-beam echo-sounders. Despite having inadequate spatial density to permit the detailed mapping of shelf features, these datasets allowed the study of the shelf bathymetry and large-scale seafloor morphology. A large assemblage of linear ridges exist on the mid- to outer-shelf which comprise some of the world's largest linear shelf sediment ridges (Stride, 1963; Stride et al., 1982), with reported dimensions of up to 60 m in height and 200 km in length (Pantin and Evans, 1984). The dimensions of these features were first based on seismic profiles of a few individual ridges, and they suggest a change in morphology through the ridge field from larger ridges in the northwest to smaller ridges in the southeast. Ridges in the northwest can be up to 55 m high, 25 km wide and 200 km long (Stride et al., 1982), while ridges to the southeast can be up to 50 m high, 7.5 km wide and 70 km long (Bouysse et al., 1976). Since these measurements were reported, the morphology of the ridges has not been studied across the ridge field using modern bathymetric datasets. Therefore, a more-detailed assessment and description of ridge morphology may yield information on how these features developed, especially in relation to glaciation, as such sediments have been recovered from their flanks in the northwest (Pantin and Evans, 1984). Such observations provide useful information to reconstruct how glaciation may have influenced the evolution of the shelf.

The Celtic Sea has not been sufficiently investigated in terms of the possible presence of glacial features preserved on the seafloor, as all previous evidence of shelf glaciation has originated from sediment core observations (Praeg et al., 2015b; Scourse et al., 2019, 1990). However, some glacial geomorphology may be preserved on the seafloor of the inner-shelf, as glacial features have been identified on seismic reflection data collected south of Ireland (Eyles and McCabe, 1989; Tappin et al., 1994; Tóth et al., 2016) and from remotely sensed data onshore (Clark et al., 2018; Greenwood and Clark, 2009). Therefore, there is potential for modern bathymetric data to shed new light on the glaciation of the Celtic Sea shelf by the ISIS and study the configuration of its advance and final retreat.

#### **Specific Questions:**

- How do the ridges change in morphology from west to east?
- Is this change related to glaciation of the western shelf?
- Do glacial features exist on the seafloor of the inner-shelf?
- If glacial features are observed, what was the advance and retreat configuration of the ISIS?

## **1.4 Sub-seafloor Stratigraphy for Environmental Reconstruction**

### **1.4.1 Seafloor Stratigraphy**

While seafloor bathymetric data provide an essential tool from which reconstruct seafloor evolution and glacial history based on the spatial mapping of geomorphology, sub-surface investigations using seismic reflection data provide information on the relative chronology of deposits, allowing a depositional history to be inferred. Additionally, seismic reflection data may provide an indication as to the composition and depositional environment of a layer based upon its acoustic character, but this is purely speculative when based on acoustic data alone. Therefore, such acoustic data need to be referenced to physical samples that penetrate the observed acoustic stratigraphy to define their composition. This approach allows acoustic data to provide large-scale information while detail is provided by correlation to physical samples from strategically picked coring sites. Such an approach has been used to study the glaciation of continental shelves, which produce a typical ordered stratigraphy of deposits based upon the retreat of the ice margin and a change in the environment during deglaciation (Syvitski, 1991). Another example of the evolution of the seafloor as reconstructed from seismic data is the growth of sand banks, the internal character of which can reveal various stages of growth (Reynaud et al., 1999b).

The depth of the acoustic phenomenon under investigation largely dictates the acoustic equipment to be used, as the sub-surface can be imaged down to significant depths depending upon the deployed system. However, at significant depths the resolution of the acoustic data is reduced; this is due to the trade-off between seismic penetration and resolution which is dictated by the frequency of the system. Where a thin medium exists between two much thicker media above and below, the seismic reflections from the upper and lower surface of the thin layer can interfere, resulting in a single observed reflection. If the vertical resolution of the data was increased by using a higher frequency system, the upper and lower returns from this thin layer would eventually be distinguishable. A higher frequency system will provide higher resolution but shallower penetration, contrasting with a lower frequency system which will achieve the opposite. In addition, significantly deep investigations require dedicated vessels to deploy complex drilling and coring equipment to obtain physical samples for ground truthing of the acoustic stratigraphy, which is generally beyond the capacity of common scientific research ships. Therefore, scientific sub-surface investigations generally focus within the top few decametres of the seafloor depending on their objective.

Seismic reflection data comprise numerous individual traces which are stacked laterally to produce a vertical section containing reflections representing boundaries in the sub-surface. By first delineating seismic packets based upon major reflections to form a seismic-stratigraphy, this framework is then integrated with physical samples comprising a litho-stratigraphy to produce a full stratigraphic framework. Such a framework permits the reconstruction of the temporal and spatial evolution of the offshore environment based upon the composition of the units and their relative stacking to produce a depositional chronology. Therefore, such a product provides a powerful tool from which to reconstruct the evolution of the offshore environment over significant areas. This has been commonly used to study

offshore sedimentary units to reconstruct palaeo-environments, ranging from the study of palaeo relative sea-level change (Kelley et al., 2006; Plets et al., 2015) to the evolution of bedforms (Berné et al., 1994; Liu et al., 2007; Marsset et al., 1999), and continental shelf glaciation (Callard et al., 2018; Roberts et al., 2018).

#### **1.4.2 Seismic Facies**

Seismic sections provide similar information to geological sections, but they are acoustic in origin with the vertical scale representing two-way-time; see Keary et al., (2002) for an overview of reflection seismology. These seismic sections contain reflections which are produced through the simultaneous upward reflection and downward transmission of an acoustic pulse at a physical interface in the sub-surface. These reflections are commonly described in terms of their amplitude, continuity and geometry (Figure 1.11 and Figure 1.12) and can be used to reconstruct the deposition environment and its evolution.

Reflection amplitude describes the intensity of the reflection which is directly related to the acoustic impedance contrast between two media. The acoustic impedance of a medium is the product of its density and sound velocity. The larger the impedance contrast, the higher the amplitude of the return at the boundary, meaning that amplitude can provide an approximate indication of lithology contrast. Reflection continuity can be used to infer the energy of the depositional environment, where low-energy conditions can produce continuous reflections that can be traced throughout a seismic section and reworking can result in disturbed and discontinuous reflections. Reflector geometry and continuity comprise the acoustic character of a unique seismic packet which provides clues as to the depositional environment in which that acoustic packet formed. Continuous horizontal and parallel reflections can represent the acoustic expression of the sequential deposition of layers in a low-energy environment, for example in an aqueous setting (Callard et al., 2018; Syvitski, 1991). This contrasts with chaotic and discontinuous reflections which suggest that reworking occurred to disrupt the boundaries, for example due to subglacial deformation (Callard et al., 2018; Lønne and Syvitski, 1997; O'Regan et al., 2010). Seismic facies represent acoustic packets of distinct reflection geometries which are delineated by upper and lower bounding reflections, and the layering of these facies represents deposition in chronostratigraphic order where younger facies overlie older facies. Within this chronostratigraphic framework exist instances of deposition, non-deposition and erosion to produce the observed stratigraphy, and therefore the observed seismic section and its acoustic facies. Uninterrupted deposition will produce a conformable time-transgressive record, contrasting with periods of non-deposition and erosion which will produce an unconformity, representing a break of 'missing time' in the stratigraphic record. Periods of non-deposition and horizontal erosion may be difficult to identify without additional geochronological data to identify the time gap, as the seismic reflection character alone may not be diagnostic of either event. Where seismic facies contain inclined reflections which terminate at an angle against an upper surface, they are said to be truncated (Figure 1.11) which is diagnostic of an erosion event having occurred which resulted in partial removal of the underlying material and the

observed abrupt reflection termination against the upper contact. Such an erosion event might have occurred due to subglacial reworking or high-energy shallow marine conditions.

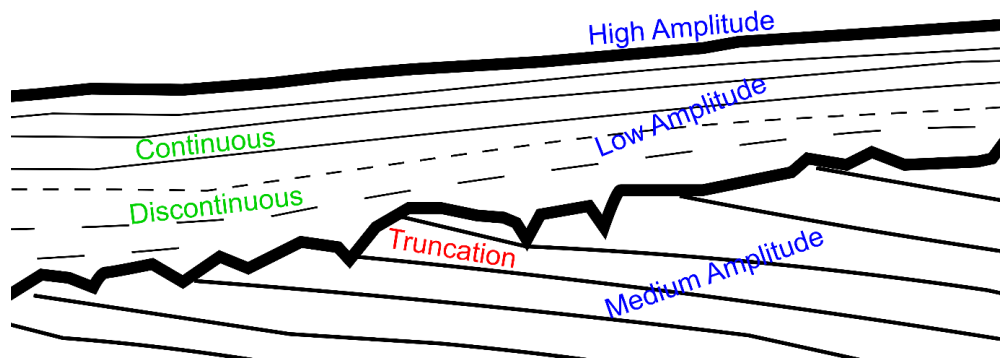


Figure 1.11 - Schematic seismic section showing commonly used terms for describing reflection character.

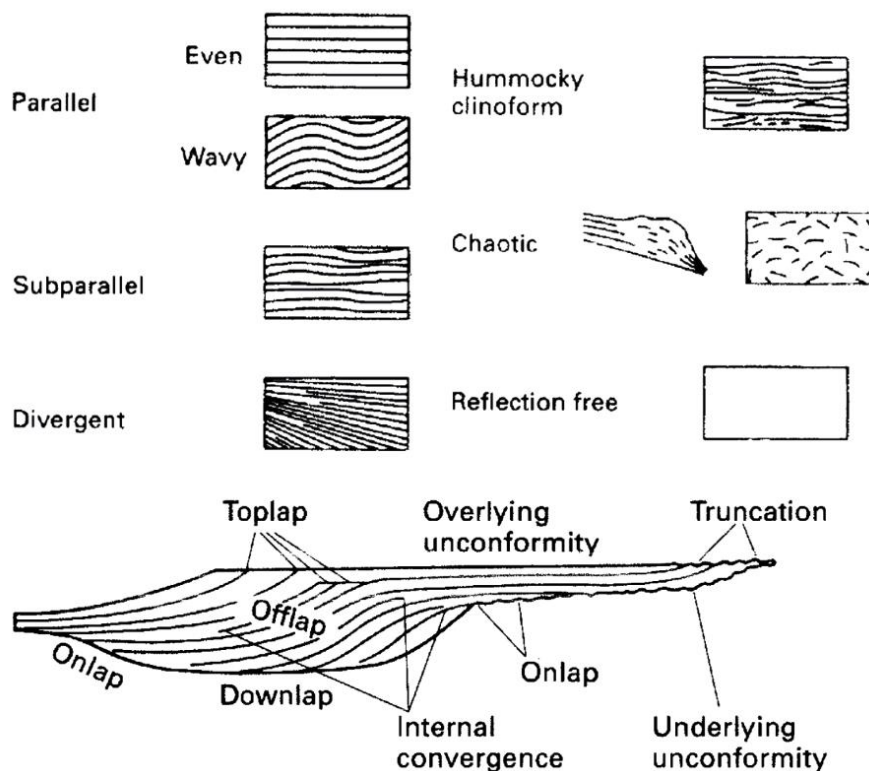


Figure 1.12 - Example reflector configurations and terminations. Edited from Mitchum et al. (1977).

### 1.4.3 Stratigraphic Investigations of the Celtic Sea Shelf

The Celtic Sea shelf has been thoroughly investigated using seismic reflection data since the 1970s by the BGS to study the offshore geology of the British Isles (Evans, 1990; Pantin and Evans, 1984; Tappin et al., 1994). As these investigations had broad objectives with no defined target depth, deep and

shallow seismic data were collected using airguns, sparkers, boomers and pingers which decrease in penetration but increase in resolution from the former to the latter. The acoustic data produced by these systems was then referenced to physical samples obtained from boreholes, shallow sediment cores and grab samples. Shallow vibrocores were positioned based on the vessel remaining stationary relative to a single acoustic transponder attached to the coring equipment (Fannin, 1989). However, only high-resolution seismic data provided sufficient clarity to permit direct correlation between seismic packets and physical samples, and such data were not collected extensively across the shelf. Seismic data and physical samples were generally positioned using the Decca Mark 21 and Decca Pulse 8 systems (Pantin and Evans, 1984), which have a spatial accuracy of up to several hundred metres, which increases with distance from the coastal signal transmitters. The spatial precision of this method was the best available at the time and adequate given the broad scale of the Celtic Sea shelf investigation. During this operation, some areas of the Celtic Sea shelf were surveyed using a deep-tow boomer, providing significantly higher resolution data than that acquired by a sparker, allowing better correlation with physical samples. Therefore, the confident integration of physical samples with seismic data was not achievable in many instances, resulting in some aspects of the shelf stratigraphy being not accurately determined. For example, the exact stratigraphic relationship between glacial sediments recovered from the mid- and outer-shelf and the MFm comprising the ridges is unknown. It was suggested that glacial sediments overlie the MFm, based on the observation that they were in places recovered from ridge flanks (Pantin and Evans, 1984), complicating the interpretation that the ridges are post-glacial in age (Evans, 1990). This was further complicated due to the fact that the base of the MFm was not imaged in places, meaning that observations suggesting that the MFm overlies earlier deposits (Marsset et al., 1999; Pantin and Evans, 1984) were unable to be effectively investigated. Additionally, various units linked to the ridges were not delineated and were poorly sampled, in places resulting in the amalgamation of various large units, some of which were only approximately correlated to at least a one physical core sample to provide age and environmental information. Such issues can be addressed through the strategic high-precision acoustic surveying and physical sampling of previously identified units in combination with more recent technological advancements to facilitate such an endeavour. The technology involved in the collection of seismic reflection data has progressed since the 1970s, permitting the collection of digital seismic data of a high spatial precision using the Global Positioning System (GPS) and through the compensation of vessel motion. In addition, submarine sampling equipment has become more easily deployable and is able to achieve greater penetration in a variety of sediment types, increasing the chances of acquiring samples from deeper units. This sampling equipment can also be accurately located underwater using acoustic positioning, allowing the determination of the precise seafloor position of the coring equipment at the time of sampling, and thus the recovered physical sample. These advancements allow the accurate positioning of both seismic data and physical samples, allowing their correlation to determine the composition of seismic units of interest. Therefore, a modern investigation of the shallow stratigraphy of the Celtic Sea shelf from a scientific focus using purposefully selected equipment can provide new insight into the shelf stratigraphy that was previously unobservable.

#### 1.4.4 Seismic-stratigraphic Framework of the Mid- and Outer-shelf

Pantin and Evans (1984), Evans and Hughes (1984) and Evans (1990) provided the first seismic-stratigraphic framework for the Celtic Sea shelf based upon extensive geophysical data collected primarily in the 1970s by the BGS. They identified and described the following major seismic units of the mid- and outer-shelf, the relationships of which are shown in Figure 1.13. This stratigraphy provides a framework from which to put new observations into context, the integration with which leads towards a more complete and realistic stratigraphy which permits a more accurate environmental reconstruction.

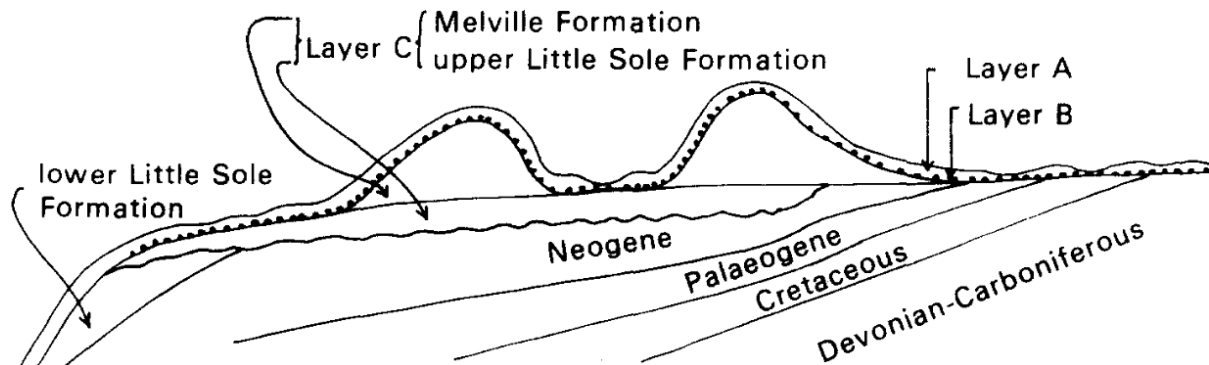


Figure 1.13 - Stratigraphic units of the Celtic Sea shelf. From Pantin and Evans (1984).

#### Melville Formation

The MFm comprises the first consistently identifiable and upper regional seismic unit which forms positive features on the seafloor, correlative to the ridges (Figure 1.14). No direct geochronological data exist to provide an age for the MFm, complicating its interpretation. This unit contains various complex and cross-bedded internal reflections (Pantin and Evans, 1984), some of which exist as truncated dipping reflections also seen in the French sector (Reynaud et al., 1999b). Based upon this seismic character, the MFm was suggested to comprise mainly of sand. In places the “flattish” basal reflection of the MFm is distinct on the lower ridge flanks (Figure 1.15), however towards the centre of the ridge and in other instances it is not imaged (Pantin and Evans, 1984). A similar base reflection has been identified below the MFm in the French sector (Reynaud et al., 1999b). One explanation for the variability in basal reflection continuity is that the MFm and its underlying unit have a similar lithology, and thus the boundary is acoustically transparent in places. This basal reflection is suggested to exist as a thin lag deposit representing a gravel layer, as opposed to a boundary between two units, which merges with the seafloor reflection on the lower ridge flanks (Pantin and Evans, 1984). This characteristic is also observed in the French sector (Reynaud et al., 1999b). The MFm was inferred to mantle earlier deposits based on observations from the Irish and UK sectors (Pantin and Evans, 1984) and the French sector (Marsset et al., 1999), however the inability to delineate between the MFm and any underlying core in places meant that this was unable to be investigated with confidence. The MFm thins between the ridges, resulting in underlying units being directly overlain by superficial deposits which are commonly not resolvable on seismic data.

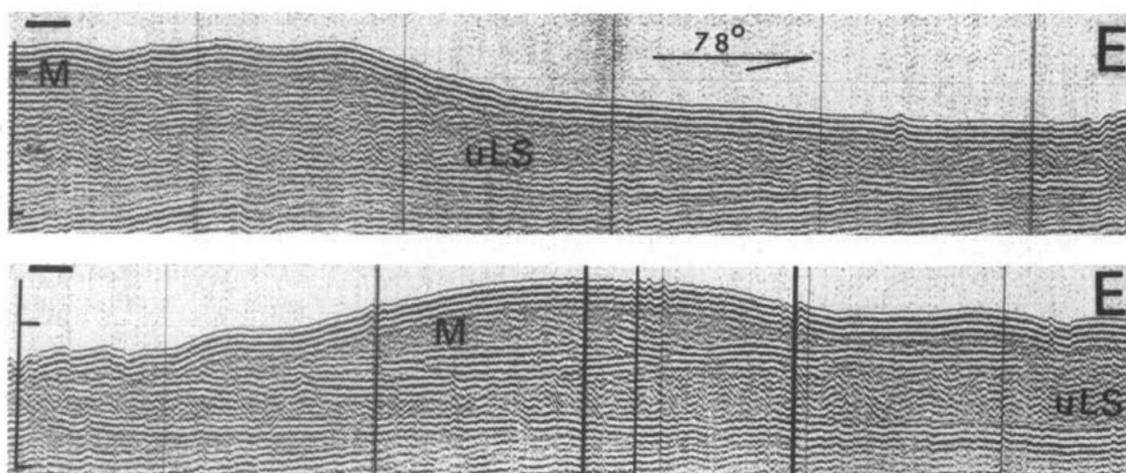


Figure 1.14 - Seismic sections from the outer-shelf of the UK sector showing the Melville Formation (M) and Upper Little Sole Formation (uLS). From Pantin and Evans (1984).

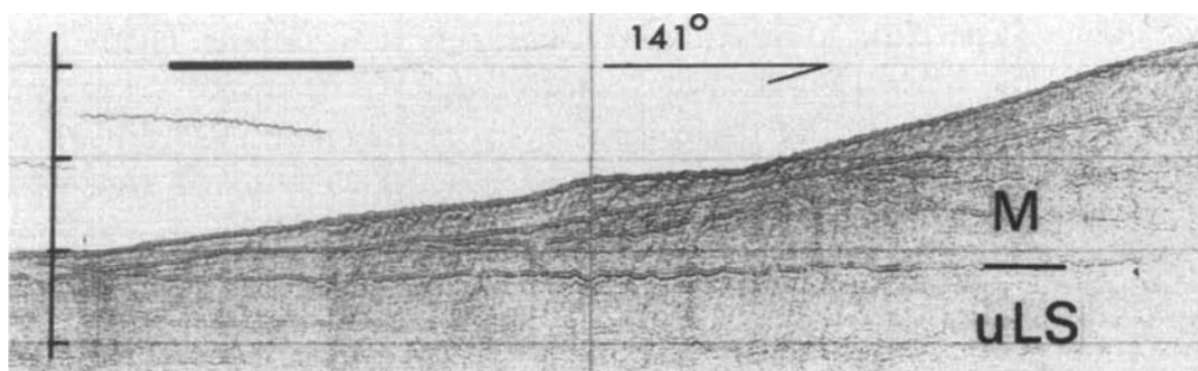


Figure 1.15 - Seismic section from the outer-shelf of the UK sector showing the interpreted boundary between the Melville Formation (M) and the Upper Little Sole Formation (uLS). From Pantin and Evans (1984).

### Upper Little Sole Formation

The ULFSm was identified to exist under the MFm on the outer-shelf, forming a wedge in the UK sector which terminates parallel to the shelf edge (Figure 1.16). In the French sector, a seismic unit correlated to the ULFSm is observed to comprise parallel channels under the MFm (Figure 1.16). This observation of channelling is consistent across the shelf, as in the Irish and UK sectors the base of the ULFSm exists as a channelled surface (Pantin and Evans, 1984). In the Irish and UK sectors, this unit is described as containing sporadic hyperbolic reflections, suggesting that gravel comprises part of the unit which is interpreted to consist mainly of sand, in addition to discontinuous and chaotic internal reflections (Pantin and Evans, 1984). Underlying this unit exists a generally horizontal erosion platform which truncates underlying units, including Neogene strata across the shelf and the Lower Little Sole Formation at the shelf edge (Evans, 1990).



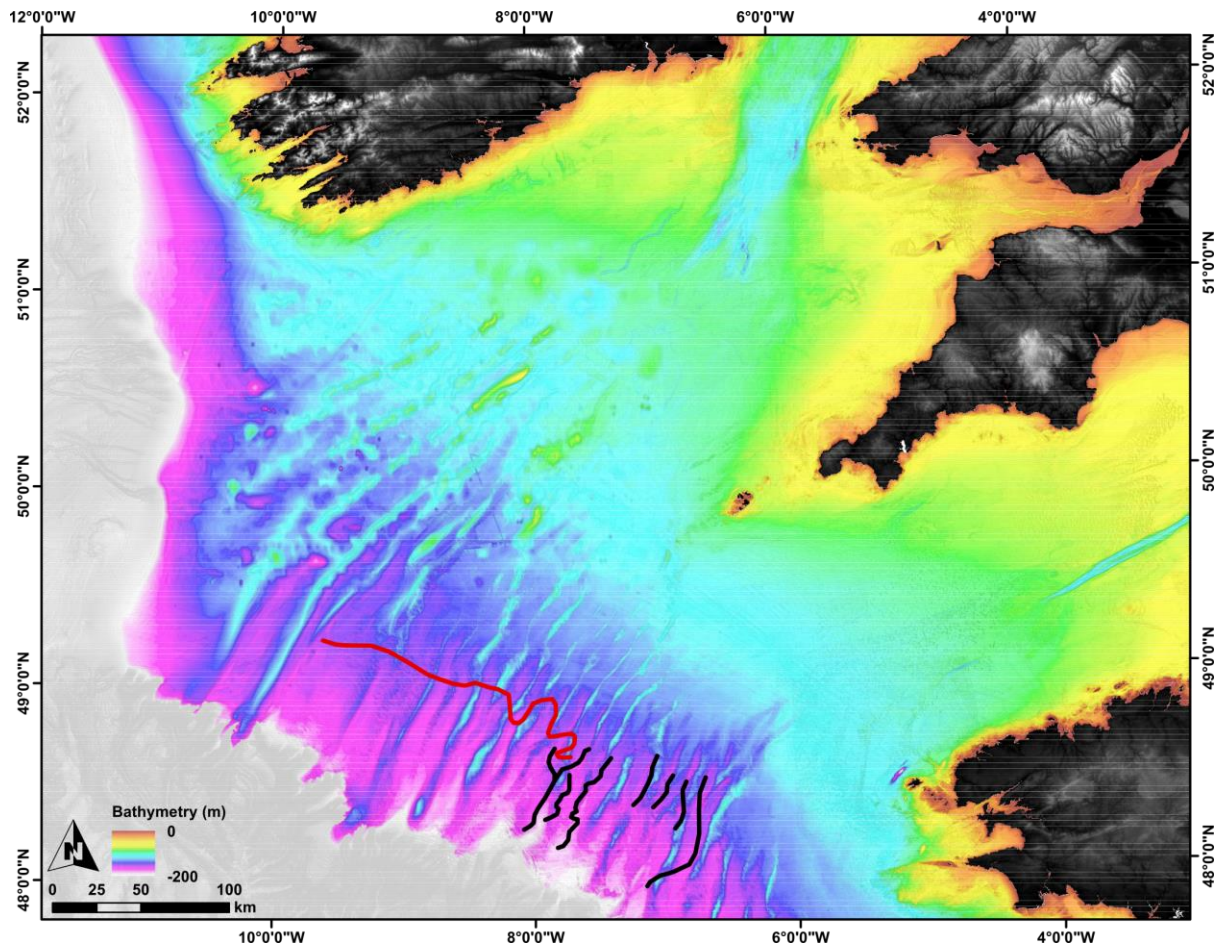


Figure 1.16 - EMODnet bathymetry and slope map showing the northern limit of the Upper Little Sole Formation (red) by Pantin and Evans (1984) and channel thalwegs (black) by Bouysse et al. (1976).

### Cockburn Formation

Evans and Hughes (1984) show this unit comprises continuous dipping parallel reflections which can be overlain by either the ULSFm on the outer-shelf or the MFm on the mid-shelf (Figure 1.17). The base of this unit truncates the underlying Jones Formation.

### Jones Formation

Evans and Hughes (1984) show this unit consists of continuous parallel horizontal reflections which grade downward into gently dipping southwest reflections at the base of the unit (Figure 1.17).

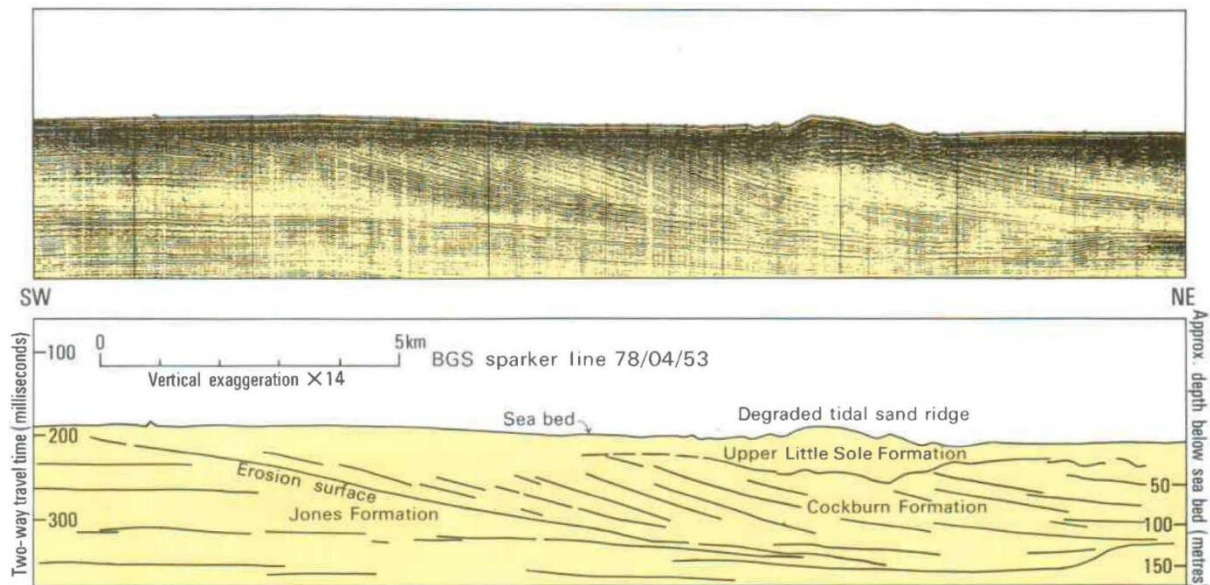


Figure 1.17 - Seismic section and interpretation showing the reflection geometry and stacking of seismic-stratigraphic units of the Celtic Sea shelf. From Evans (1990).

#### Specific Questions:

- What is the stratigraphic relationship of glacial sediments to the ridges from which they have been recovered?
- Do the MT and MLC correlate to the MFm?
- Can the MFm and the ULFSm be delineated using more modern seismic data?
- Is the ULFSm fluvial in origin and of a Late Pliocene to Early Pleistocene age?

#### 1.4.5 Litho-stratigraphic Framework of the Mid- and Outer-shelf

Based on physical samples obtained through grab samples and shallow sediment cores, the following litho-stratigraphy was proposed by Pantin and Evans (1984):

##### Layers A and B

Shallow sediment cores consistently show that the seafloor consists of fining upward deposits of sand and mud which were named Layer A (Furze et al., 2014; Pantin and Evans, 1984). Layer A can be up to several metres thick and it overlies a much thinner Layer B which can contain gravel and shell fragments and occasional boulders, overlying an erosional surface (Furze et al., 2014; Pantin and Evans, 1984). In places, Layer A thins which results in Layer B comprising the seafloor. However, the inverse also occurs, where Layer B is absent most notably between the ridges across the shelf. These superficial deposits are consistently found across the Celtic Sea from the outer-shelf to the inner-shelf (Evans, 1990; Furze et al., 2014; Tappin et al., 1994). Only Layer A is resolvable on seismic data when it exists in significant thicknesses, generally when it forms bedforms, and therefore Layer A and Layer

B have not been linked to seismic-stratigraphic units. As these layers were consistently recovered at the seafloor, they are suggested to overlie the MFm and other deposits.

### **Layer C**

Physical samples containing bedded sands and gravel, including instances of mud and glacigenic sediments, were amalgamated into Layer C as seismic resolution was insufficient to result in their consistent correlation to the seismic units comprising the MFm or the ULSFm (Pantin and Evans, 1984). In places, shallow physical samples were correlated to either the MFm or the ULSFm with varying degrees of confidence. Where shallow cores were recovered from the upper surfaces of the ridges, the sediments underlying Layers A and B were thus assumed to correspond to the MFm. Whereas on the lower flanks of the ridges and in the inter-ridge areas where the MFm thins, shallow cores may have penetrated either the thinning MFm or the ULSFm where they are directly overlain by Layers A and B. In one instance on the outer-shelf a shallow core was recovered a significant distance away from the ridges and interpreted to have been recovered from the ULSFm, containing mud (Evans and Hughes, 1984).

### **Specific Questions:**

- What sediments from Layer C correlate to the MFm and ULSFm?

## **1.5 Sediment Geotechnics for Environmental Reconstruction**

### **1.5.1 Effective Stress and Consolidation**

Due to complex processes such as glaciation and post-glacial transgression, a variety of deposits with varying physical characteristics exist across the shelf. The physical characteristics of a sediment can provide clues as to its depositional environment and any post-depositional reworking. A primary process through which depositional setting and post-depositional changes are recorded is in the stress history of a sediment which results in a change of physical characteristics when it has been loaded or deformed. Therefore, the understanding of the physical properties of shelf sediments provides a tool from which to understand their palaeo-environmental significance.

Terzaghi (1943) proposed the idea of effective stress ( ) in soils, which is the pressure that the solid grains comprising a sediment exert on one another at points of contact that can cause volumetric strain if excess hydrostatic pressure (pore pressure) is allowed to dissipate through draining. The degree of effective stress comes about due to changes in total stress ( ) and pore pressure ( $\mu$ ) which combine in Equation 1.1.

*Equation 1.1* 
$$\sigma' = \sigma - \mu$$

This shows that as pore pressure increases, there will be a reduction in the effective stress of a saturated material. To calculate the effective stress experienced at a specific depth in a marine sediment, the total stress (sediment overburden and pore pressure) is subtracted from the pore pressure (hydrostatic head), resulting in the effective stress being produced solely by the pressure exerted by the overburden. As the overburden thickness increases, the effective stress increases, which can be calculated if the overlying sediment densities are known. As a saturated sediment consolidates in response to loading, it reduces in volume due to the removal of porewater at a rate dictated by the sediment's permeability, which can be in the order of thousands of years for low-permeability sediments to dissipate pore pressure (Boulton and Hindmarsh, 1987). If the sediment is loaded beyond its capacity to dissipate pore pressure, this excess pore pressure results in a dramatic reduction of effective stress and thus strength of the sediment as the solid grains are forced apart. Below this critical loading stress, the sediment will still consolidate but at a reduced rate and with higher effective stresses. The behaviour of low-permeability sediments is heavily determined by moisture content, which can be described in terms of Atterberg Limits. These limits represent critical moisture content boundaries that affect how a fine-grained sediment behaves due to changes in moisture content, which would occur during various states of consolidation. This can allow the material to easily experience a variety of styles of subglacial deformation (Benn and Evans, 1996) and exert a strong influence on glacial dynamics as part of a deforming bed, increasing ice flow velocities. Such a scenario is suggested to have resulted in the over-extension of the ISIS on the Celtic Sea shelf (Scourse et al., 1990).

A sediment is described as normally-consolidated if it is consolidated to a degree which can be produced by the effective stress imparted by the present-day overburden, while an over-consolidated sediment has experienced a yield stress larger than that which can be currently produced by the present-day effective stress. The degree of over-consolidation can be expressed as a ratio of the yield stress to the present-day effective stress at a point within the stratigraphy. As a sediment undergoes consolidation, its density increases due to a decrease in void volume through the reorganisation of the solid structure. This results in increased intergranular friction which increases the undrained shear strength of the material. This increase in undrained shear strength is an important observation, as it can represent the stress-history of a sediment and may indicate glacial loading, as such sediments have undrained shear strengths >100 kPa (Bell, 2002; Clarke, 2018; Clarke et al., 2008) compared to sediments which have not been loaded that have much lower undrained shear strengths (Bartetzko and Kopf, 2007). When a load is applied to a saturated uniform-grainsize sediment, the upper contact surface is the first area to expel porewater and consolidate. As loading continues, the consolidating zone advances downward through the stratigraphy as porewater travels to the upper surface to dissipate the pore pressure. This would theoretically produce a trend of increasing consolidation state upward toward a maximum consolidation state at the contact surface. However, any change in grainsize will result in a change in permeability, even producing conduits through which excess pore pressure can dissipate, and this would contribute to vertically-varying states of consolidation. When a uniform grainsize sediment consolidates due to gravity, progressive burial generally results in increasing consolidation, and thus increasing undrained shear strength, with increasing depth (Bartetzko and Kopf, 2007). However, a similar trend can also be seen in glacially loaded sediments, although with greater variability in undrained shear strength (Clarke, 2018). In terms of palaeo-environmental significance, it is possible for a sediment to achieve high undrained shear strengths through gravitational consolidation, where significant overburden thicknesses during continued deposition existed to normally-consolidate the underlying sediment, but this overburden was then removed through erosion to result in the underlying sediment being over-consolidated without a glacial influence. Therefore, high undrained shear strengths alone are not diagnostic of glacial loading, especially in scenarios where an energetic post-glacial erosion event may have occurred and removed significant overburden thicknesses such as suggested for the Celtic Sea (Scourse et al., 2009b). Undrained shear strength values therefore need to be studied and be combined with other observations to present a case for glacial loading. Such an observation has important implications for any reconstruction, as this could signify the product of a major readvance or minor oscillation of an ice margin during deglaciation which would represent a significant change in glacial dynamics.

### **1.5.2 Stiff Deglacial Sediments of the Celtic Sea Shelf**

The deglacial drape found across the Celtic Sea shelf consists of fine-grained and laminated sediments deposited during the last glaciation of the shelf (Furze et al., 2014; Praeg et al., 2015b; Scourse et al., 2019, 1990). Such sediments represent suspension-settling deposits in an quiet aqueous environment which are typically horizontally laminated, fine-grained and have low undrained shear strengths (Ó Cofaigh and Dowdeswell, 2001). At the shelf edge however, laminated sediments were first interpreted

as overridden glacimarine deposits based on visible deformation and high undrained shear strengths which were then partially eroded during the subsequent post-glacial transgression (Praeg et al., 2015b). Similar glacial deposits collectively called Lithofacies (LF) LF8 were recovered across the shelf from shallow vibrocores during the JC-106 BRITICE-CHRONO cruise (Ó Cofaigh, 2014), and were interpreted as being glacimarine in origin which had been overridden by the ISIS (Scourse et al., 2019), based largely on recorded undrained shear strengths >110 kPa. The high undrained shear strengths in LF8 could be due to glacial loading, as some deformation structures do exist. However, deformation structures do not exist with every instance of high undrained shear strength, and they are not as pronounced as those seen in other instances of subglacial deformation, and do not appear to show a trend of increasing deformation upwards as is expected in a typical subglacially deforming bed (Boulton et al., 2001; Evans et al., 2006). In addition, LF8 exists under an erosion surface at the base of Layers A and B which most likely represents the expression of the energetic post-glacial transgression that the Celtic Sea experienced as suggested by palaeotidal model outputs (Scourse et al., 2009b; Ward et al., 2016). This event most likely removed any upper overburden if it did exist. Therefore, the high undrained shear strengths could be due to burial under significant thicknesses of glacial and/or marine overburden which consolidated the underlying stratigraphy. The overburden was then eroded during transgression, as evidenced by the overlying erosion surface, to result in over-consolidated sediments with high undrained shear strengths.

LF8, recovered across the shelf, contrasts with LF3 and LF4 which were recovered in the CD. LF3 and LF4 are also deglacial muds, with sporadic sand laminations in LF4, similar to LF8, but have much lower undrained shear strengths, typically <40 kPa, and have no visible deformation (Scourse et al., 2019). A previous investigation of deglacial muds from across the shelf commented on their uniformity in terms of their litho- and biostratigraphy over large distances, suggesting that their deposition occurred during rapid ice margin retreat to result in such uniformity (Furze et al., 2014). This agrees with other studies which suggest that ice margin retreat of the ISIS was rapid, as retreat had commenced at 25 ka BP at the shelf edge (Praeg et al., 2015b; Scourse et al., 2019) and ice had reached St. GC by 24.2 ka BP (Small et al., 2018). Therefore, the indication of rapid deglaciation by the available chronology and grain size similarities between LF8 on the shelf and LF4 and LF3 in the CD provide an opportunity to test how different post-depositional processes may have affected the geotechnical properties of these deglacial sediments. A working hypothesis is that LF8 has been overridden by the ISIS, while LF3 and LF4 have not, and thus the latter have only consolidated due to gravity. Geotechnical investigations may aid in the identification of either a glacial loading scenario or a progressive burial and subsequent erosion scenario, providing essential context for the interpretation of high undrained shear strengths in glacial sediments and their significance for the palaeo-environmental reconstruction of the Celtic Sea shelf. Such an observation has profound implications for the deglaciation of the Celtic Sea shelf, as the reworking of deglacial muds suggests that oscillations of the retreating ice margin occurred, implying that even during rapid withdrawal, offshore readvances did occur. Such a scenario needs to be explained in the context of eustatically driven ice margin retreat from the shelf edge.

**Specific Questions:**

- Can burial and later erosion explain the observed undrained shear strengths of LF8?
- Does LF8 display characteristics consistent with subglacial reworking?
- In what context did the subglacial reworking event occur?

## **1.6 Aims and Objectives**

The Celtic Sea shelf was extensively investigated in the 1970s using geophysical methods and physical sampling of the seafloor and shallow sub-surface to produce a consensus stratigraphic framework. These data provided the first observations of glaciation of the shelf as recorded from sediment cores (Scourse et al., 1990), while subsequent studies have built upon this data to suggest a more extensive glaciation of the shelf at 25 ka BP (Praeg et al., 2015b; Scourse et al., 2019). Subsequent advances in GIA modelling and the production of broad ice sheet thickness and chronology models have permitted palaeo sea levels to be reconstructed for the Celtic Sea region from 21 ka BP to the present-day (Scourse et al., 2009b; Ward et al., 2016). These studies suggest that during post-glacial sea-level rise, energetic tidal conditions existed which may have helped produce the large ridge features that exist across the shelf (Scourse et al., 2009b). The combination of these glacial and palaeo sea-level studies represent a broad reconstruction of the Celtic Sea from the LGM.

The accurate reconstruction of the advance and retreat of the ISIS in the Celtic Sea will provide essential observations for the study of ice stream stability in response to changing palaeo-environmental conditions, such as sea-level rise, megatidal conditions and warming, in addition to providing a framework against which whole ice sheet numerical models can be tested. Once validated against palaeo observations of glaciation, these numerical models will be used to forecast the behaviour of contemporary ice sheets that are threatened by changing environmental conditions to estimate their future contribution to global sea-level rise. Therefore, such an underpinning reconstruction needs to be constructed as accurately as possible based on the available evidence. Several specific questions remain unanswered that have implications for the palaeo-environmental reconstruction of the Celtic Sea. These can be distilled into fundamental issues which will be the focus of this investigation.

Fundamental issues:

- The stratigraphic position of glacial sediments – by determining the stratigraphic position of glacial sediments in the shallow sub-surface, this can provide essential information to allow the confident correlation between other glacial sediments recovered elsewhere across the shelf to produce a more-accurate stratigraphic framework of glaciation.
- The origin of the mid- to outer-shelf ridges – the recovery of glacial sediments of unknown stratigraphic position from the flanks of the ridges has implications for the origin of the features as either tidal or glacial features and for the evolution of the shelf.
- Direct observations of palaeo glacial dynamics recorded by preserved features – the glaciation of the shelf is heavily based on the spatial extent of glacial sediments recovered in sediment cores and in coastal regions of the inner-shelf, therefore the identification of glacial features preserved on the seafloor can allow the spatial reconstruction of palaeo glacial dynamics.



Specific questions:

- Did the ISIS advance southwest across the shelf as suggested by the provenance of clasts within the MT?
- What was the maximum extent of the ISIS on the outer-shelf?
- Did the ISIS deglaciate in a marine or lacustrine setting on the mid- and inner-shelf?
- How can the deposition of easily-erodible deglacial muds occur in the context of energetic marine conditions?
- Does the MFm mantle earlier deposits as suggested by initial observations?
- Does the MFm have characteristics consistent with either a tidal or glacial origin?
- When did the MFm form?
- How do the ridges change in morphology from west to east?
- Is this change related to glaciation of the western shelf?
- Do glacial features exist on the seafloor of the inner-shelf?
- If glacial features are observed, what was the advance and retreat configuration of the ISIS?
- What is the stratigraphic relationship of glacial sediments to the ridges from which they have been recovered?
- Do the MT and MLC correlate to the MFm?
- Can the MFm and the ULFSm be delineated using more modern seismic data?
- Is the ULFSm fluvial in origin and of a Late Pliocene to Early Pleistocene age?
- What sediments correlate to the MFm and ULFSm?
- Can burial and later erosion explain the observed undrained shear strengths of LF8?
- Does LF8 display characteristics consistent with subglacial reworking?
- In what context did the subglacial reworking event occur?

The majority of these questions stem from the undetermined shallow stratigraphy of the shelf, which is problematic as this is a key foundation used to determine the relative depositional order of deposits, thus elucidating the temporal evolution of the shelf spatially. If accurately determined, the composition and relative stacking of deposits can provide essential information on the extent of glaciation and the origin of the large ridge features on the mid- to outer-shelf while also providing a stratigraphic framework to aid future work in this region. The identification of new glacial features and deposits from seafloor bathymetric data and the integration of new geophysical and physical samples will represent essential observations of glaciation from which to most-accurately reconstruct the advance, maximum extent and retreat of the ISIS. The extent and nature of glacial seafloor features and sub-seafloor deposits across the shelf will help spatially constrain the maximum extent of glaciation and ice flow advance and retreat directions while the nature of the deposits can provide information on the deglacial setting. Only after the previously mentioned issues have been investigated and answered will the palaeo environment of the Celtic Sea be satisfactorily elucidated, permitting the creation of a more accurate temporal and spatial reconstruction of the evolution of the Celtic Sea from the LGM to the present-day.

## **Chapter 2 - Data and Methods**

The integration of various datasets is key to providing a solid foundation from which to confidently identify palaeo-environmental signatures, enabling a reconstruction of the evolution of the shelf. Bathymetric data produce information on the features comprising the seafloor across a large area, providing clues as to how the shelf may have evolved spatially to influence their size, shape and distribution. Sub-seafloor data allow the creation of a temporal reconstruction based on the stratigraphic order of deposits while correlation with physical samples allows their composition to be determined. Finally, the physical characteristics of the cored deposits provides a means from which to study the depositional environment in detail. The scalability offered by the integration of these data sources provides as much information as possible to allow for a more accurate evolutionary reconstruction of the Celtic Sea shelf.

### **2.1 Seafloor Geomorphology**

#### **2.1.1 Regional Bathymetric Data**

Open access European Marine Observation and Data Network (EMODnet) bathymetric data (2018) have been used as a regional dataset from which to resolve the morphology of large seabed features and the regional changes in bathymetry. These bathymetric data were downloaded from the EMODnet-bathymetry portal (EMODnet, n.d.). The EMODnet bathymetric dataset is comprised of reduced resolution multi-beam echo-sounder data which were submitted to the EMODnet project for interpolation with the lower-resolution (~1 km) General Bathymetry Chart of the Oceans (GEBCO) bathymetric data (2014) dataset. The final dataset is gridded at ~100 m cell size.

#### **2.1.2 Multi-beam Bathymetric Data**

Open access multi-beam bathymetric data have been collated from the United Kingdom Hydrographic Office (UKHO) and the Integrated Mapping For the Sustainable Development of Ireland's Marine Resource (INFOMAR) project (Table 2.1 and Figure 2.1). UKHO data were obtained through the Admiralty Marine Data Portal (UKHO, n.d.), while INFOMAR data were obtained through the Geological Survey Ireland (GSI) Interactive Web Data Delivery System (GSI, n.d.). The average grid cell size of the multi-beam datasets is 4 m, ranging between 2-8 m.

*Table 2.1 - Multi-beam bathymetric datasets by area obtained from the United Kingdom Hydrographic Office (UKHO) and the Integrated Mapping For the Sustainable Development of Ireland's Marine Resource (INFOMAR) project.*

| Area                               | Dataset ID  |
|------------------------------------|---|
| St. George's Channel               | UKHO: 2013 2015-178837 North Celtic Deep; 2016 HI1471 Off Smalls<br>INFOMAR: CV1202; CV0903   |
| Southern Irish Coastline (INFOMAR) | CV0903; CV1002; CV1605; CV0702; CV130; CV1604East; CV1602; CV1003; CV1203; CV1601; CV0802; CV1302; CV1604West; CV1403   |
| Cornwall Coastline (UKHO)          | 2011 HI1157 Hartland Point to Lands End Blk 3; 2011 HI1157 Hartland Point to Lands End Blk 2; 2011 HI1157 Hartland Point to Lands End Blk 1   |
| Isles of Scilly (UKHO)             | 2016 HI1470 Eastern Approaches to Isles of Scilly; 2017 HI1505 West Scillies; 2017 HI1504 South Scillies; 2013 HI1415 Lands End Blk 1; 2013 HI1415 Lands End Blk 2; 2013 HI1415 Lands End Blk 3 |

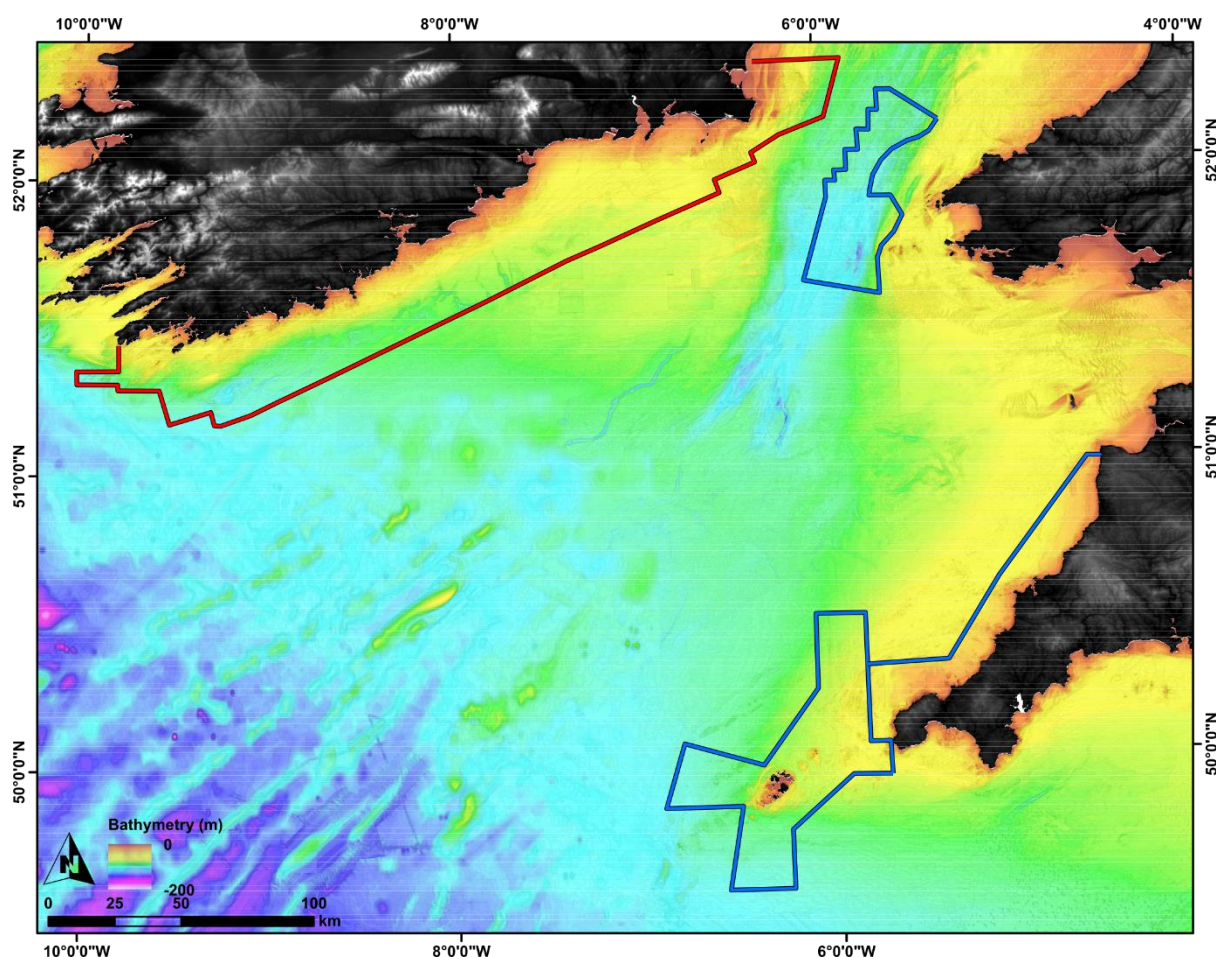


*Figure 2.1 - EMODnet bathymetry and slope map showing the extent of multi-beam bathymetric datasets from the United Kingdom Hydrographic Office (UKHO) and the Integrated Mapping For the*

*Sustainable Development of Ireland's Marine Resource (INFOMAR) project. The extent of INFORMAR (red) and UKHO (blue) datasets on the inner-shelf of the Celtic Sea are marked.*

### 2.1.3 Data Visualisation and Geomorphological Analyses

Where individual multi-beam bathymetric datasets neighboured each other, these datasets were mosaiced into one bathymetric dataset to allow seamless visualisations and mapping for each area. Using Environmental Systems Research Institute ArcMap (v10.3.1) software, slope and multi-directional oblique-weighted hillshade visualisations were generated from bathymetric data with no vertical exaggeration using the Terrain Tools script (Field & Beale, 2016). Such visualisations reduce bias for feature mapping (Figure 2.2), unlike uni-directional hillshade visualisations which can exaggerate or diminish features based upon the orientation of hillshading (Chandler et al., 2018; Smith & Clark, 2005).

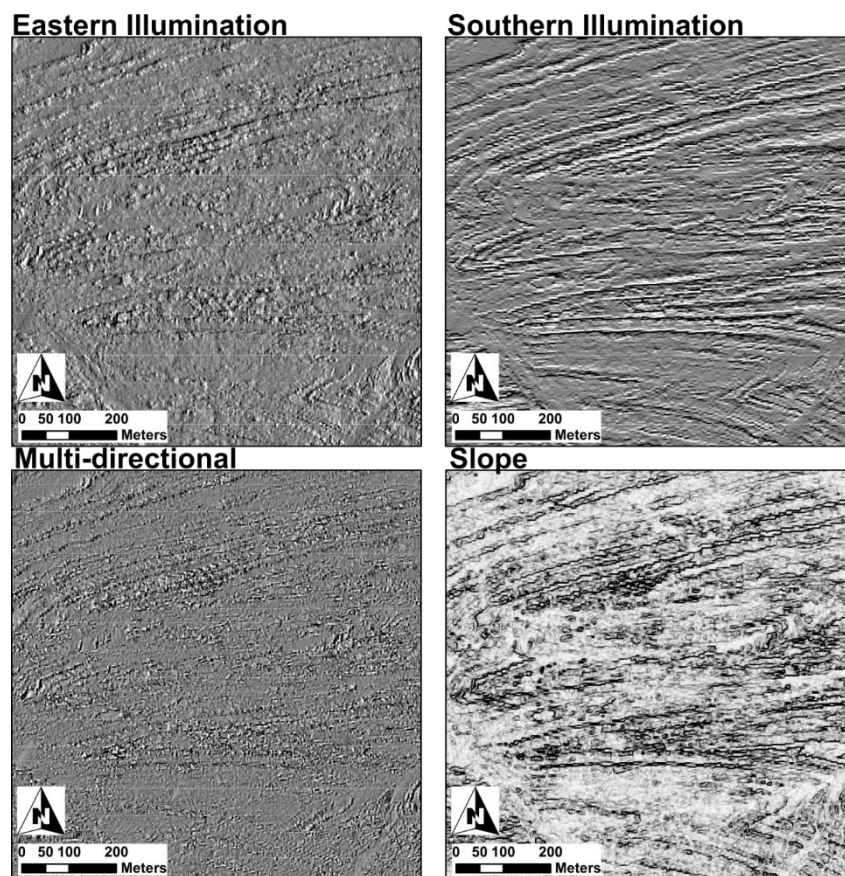


*Figure 2.2 - Example data visualisations showing the bias induced by uni-directional hillshades of linear bedrock compared to multi-directional shading and slope maps.*

Dove et al. (2016) provide a two-part methodology to classify seafloor features based on bathymetric data. Firstly, the identified features are described objectively in terms of their morphology (size, shape and appearance) and then they are interpreted to yield their geomorphology in terms of the process of

their formation and their origin. A similar methodology is deployed here where seafloor features comparable in morphology to glacially-related features described by Clark et al. (2018) are identified, objectively described and then interpreted in terms of their glacial origins. Where ambiguous seafloor features could not be explained by marine processes they were interpreted to be glacial in origin, such as features which did not have similar orientations, did not deviate due to topography or did not have sharp and prominent crests.

Large ridges which exist on the mid- to outer-shelf were digitised along their long-axis, representing their crestline, as identified from a combined slope-bathymetry visualisation. These polylines were analysed in ArcMap to produce length measurements for each individual feature using the Calculate Geometry tool. Heights and widths of these features were measured manually from cross-sectional profiles which were produced perpendicular to the digitised crestline every 10 km along the main trunk of each feature, avoiding the axial ends of the features where they thin. Therefore, longer ridges were sampled more frequently than shorter ridges. In the western mid- to outer-shelf, EMODnet bathymetric data consist of resampled 1 km resolution GEBCO data. Where the morphology of large seafloor features appeared ambiguous due to this reduced data resolution, the features were assumed to have similar morphological characteristics to neighbouring features in areas of higher resolution data.

Glacially-related features up to 10s of kilometres in scale were studied using visualisations of slope and multi-directional oblique-weighted hillshade. These features were delineated along their bounding break-of-slope as polygon shapefiles or as polylines along their mid-point. Feature shapefiles which were dominantly rectilinear were then analysed using the Bounding Container script (Patterson, 2015) to generate the long- and short-axis length measurements for simple features based upon the short- and long-axis measurements of the smallest rectangle able to surround each individual feature. The orientation of the long-axis of this bounding rectangle was used to calculate the orientation of the individual features. The dimensions of complex nonrectilinear features were measured manually from cross-sectional profiles. Heights and depths of features were measured manually from cross-sectional profiles based on the minimum vertical height change of the feature from the bounding break-of-slope (Figure 2.3). The bounding break-of-slope is defined as the first distinct change in slope which occurs moving away from the crest of a feature.

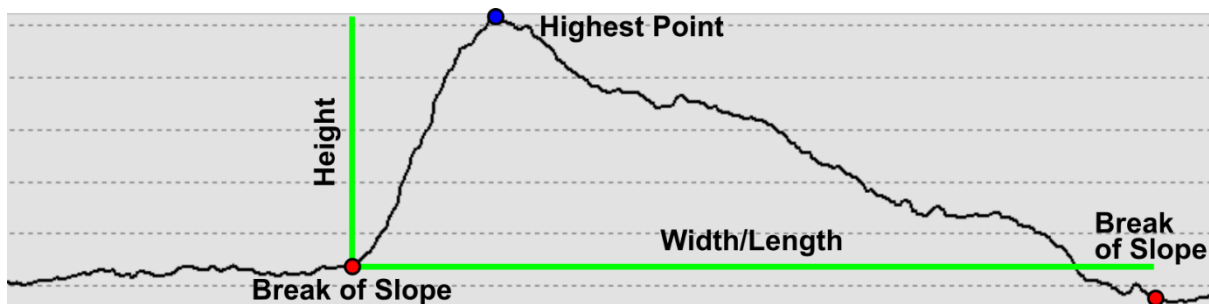


*Figure 2.3 - Example cross-sectional profile of a ridge feature showing how vertical and horizontal measurements were derived manually.*

## **2.2 Sub-seafloor Stratigraphy**

### **2.2.1 Seismic Reflection Data**

Since the first sub-bottom profiling of the Celtic Sea shelf by the BGS in the 1970s, more recent seismic surveys have been conducted. These datasets have been made available for this study (Table 2.2), the most extensive being BRITICE-CHRONO cruise JC-106 which comprises the primary dataset used, followed by the IPY GLAMAR and CV14007 cruises in decreasing data extent (Figure 2.4). The primary objective of these projects was to study the Late Pleistocene glaciation of the Celtic Sea, and thus they focused on acoustic data collection within the top few decametres of the seafloor primarily across the western shelf. See O' Cofaigh (2014) for a detailed cruise report of all activities conducted during JC-106. The frequencies of the deployed geophysical systems during these investigations generally resulted in decimetric vertical resolution. These data were spatially located using differential GPS corrections and were referenced against the motion of the vessel, resulting in decimeter to metre spatial accuracy. The seismic data achieved a vertical resolution of up to 0.1 ms, equating to 16 cm in a medium with a sound velocity of  $1600 \text{ m}\cdot\text{s}^{-1}$  as measured from the seafloor return on seismic sections.

*Table 2.2 - Recent scientific cruises having collected extensive sub-bottom data in the Celtic Sea.*

| Cruise ID  | Vessel                   | Year        | Sub-bottom Profiling Equipment (Frequency)                              |
|------------|--------------------------|-------------|---|
| JC-106     | RRS <i>James Cook</i>    | August 2014 | Kongsberg SBP-120 chirp (2.5-6.5 kHz)                                   |
| CV14007    | RV <i>Celtic Voyager</i> | May 2014    | Geo-Source 200-400 tip sparker (0.5-4 kHz)                              |
| IPY GLAMAR | RV OGS <i>Explora</i>    | 2009        | Benthos CAP6600 chirp (2-7 kHz), Geo-Source 800 tip sparker (0.5-4 kHz) |



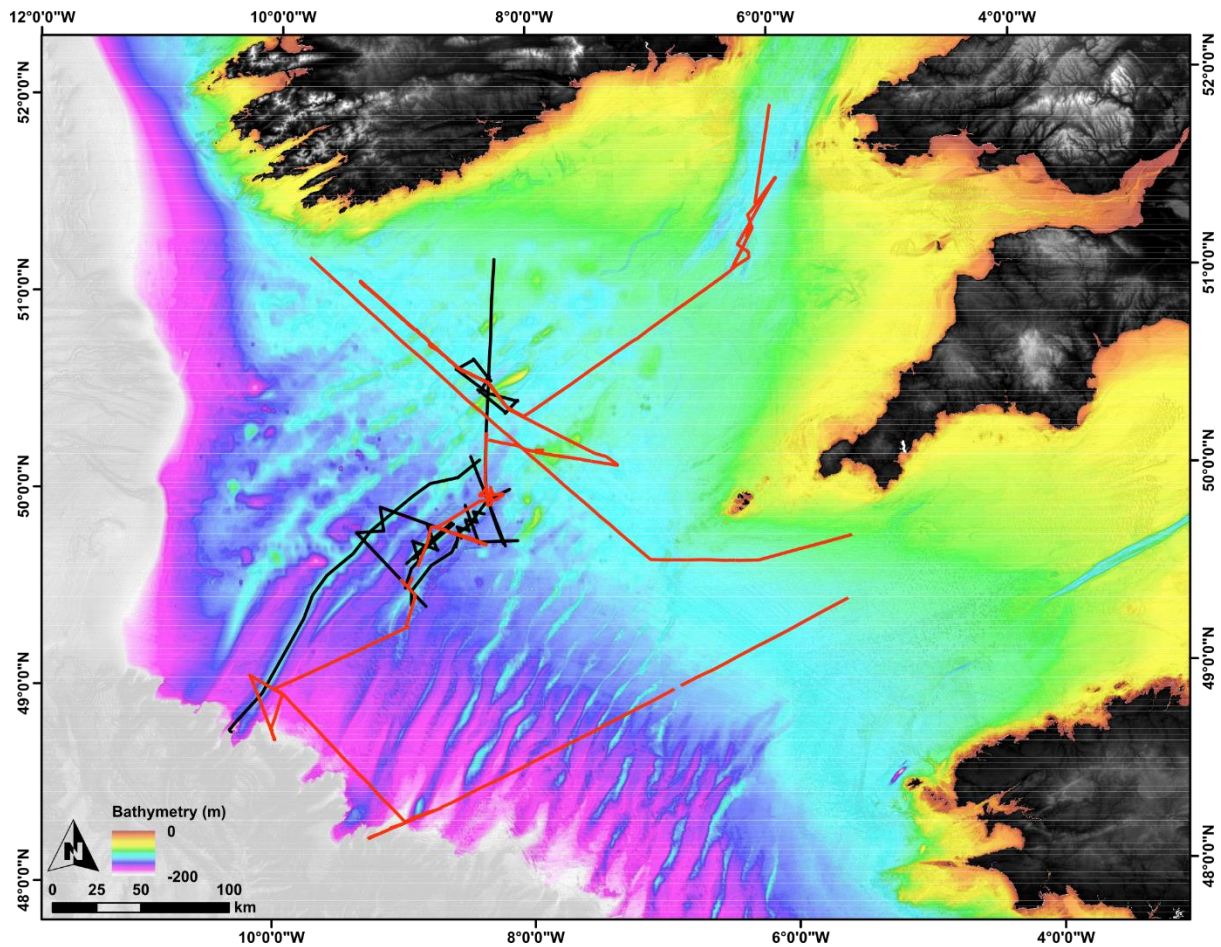


Figure 2.4 - EMODnet bathymetry and slope map showing the coverage of JC-106 (red) and IPY GLAMAR and CV14007 (black) seismic reflection data in the Celtic Sea.

### 2.2.2 Physical Samples

Sediment cores were collected across the Celtic Sea shelf during JC-106 using a 6 m Vibrocorer (VC) and 12 m Piston Corer (PC). Only a selection of these cores which had sufficient seafloor penetration, sediment recovery and were located on seismic sections which had resolution sufficient for correlation were used (Table 2.3). The seismic reflection data allowed coring sites to be picked strategically. The submerged coring equipment was located using a Sonardyne Ranger acoustic transponder array which provides decimeter to metre spatial accuracy on the seafloor. Cores were recovered, cut into 1 m long sections, split along their length and logged according to grainsize, sedimentary structures, texture, density and colour. One half of the split core length was used as a working half, available for sampling and testing, while the other half was sealed and stored as an archive copy. A handheld shear-vane was used to provide additional data on the undrained shear strength of fine-grained sediments. This instrument works through the selection of a vane head appropriate for the stiffness of the sediment which is then inserted and turned at a constant rate until failure of the sediment occurs through shearing. The torque value at which this occurs indicates the undrained shear strength of the sediment. Cores were processed onboard by teams lead by Margot Saher and Louise Callard, with final interpretation

and the creation of visual core logs by Margot Saher. Core logs can be found in Lockhart et al. (2018) and Scourse et al. (2019) in the Appendix.

*Table 2.3 - Selected JC-106 Vibrocore (VC) and Piston Core (PC) recovery details.*

| Core | Latitude<br>(DD WGS84) | Longitude<br>(DD WGS84) | Water<br>Depth (m) | Recovery (m) |
|------|------------------------|-------------------------|--------------------|--------------|
| 15VC | 48.99202               | -9.98281                | 165                | 2.17         |
| 16VC | 48.99945               | -10.00358               | 160                | 1.68         |
| 18VC | 49.54034               | -8.99374                | 146                | 1.86         |
| 19VC | 49.53904               | -8.99170                | 145                | 1.62         |
| 20VC | 49.53232               | -8.98568                | 143                | 1.52         |
| 21VC | 49.52230               | -8.96623                | 137                | 1.40         |
| 22VC | 49.79488               | -8.60675                | 142                | 1.28         |
| 28VC | 49.96353               | -8.31164                | 125                | 1.42         |
| 29VC | 49.96330               | -8.31675                | 122                | 1.40         |
| 30VC | 49.96230               | -8.33875                | 124                | 1.78         |
| 31VC | 49.96244               | -8.33887                | 125                | 1.74         |
| 32VC | 49.96216               | -8.34106                | 125                | 1.94         |
| 33VC | 50.27430               | -8.34522                | 132                | 1.82         |
| 34VC | 50.18612               | -8.35045                | 118                | 1.90         |
| 35VC | 50.27119               | -8.34521                | 130                | 2.63         |
| 36VC | 50.87645               | -8.98768                | 116                | 0.58         |
| 39VC | 50.76978               | -8.79774                | 119                | 0.79         |
| 44VC | 50.56035               | -8.32173                | 125                | 2.02         |
| 45VC | 50.56020               | -8.32172                | 125                | 2.17         |
| 51PC | 51.34570               | -6.18433                | 116                | 6.29         |
| 52PC | 51.36627               | -6.16656                | 116                | 7.58         |
| 53VC | 51.42468               | -6.14456                | 108                | 4.47         |

### **2.2.3 Data Visualisation and Correlation**

The seismic reflection datasets were not tidally corrected, and thus depths on seismic sections represent instantaneous depth below the vessel at the time of surveying. Additionally, the data were generally processed live during data acquisition, resulting in changes in reflection amplitude between sections. Amplitude gain was also adjusted when viewing sections in Information Handling Services Kingdom (2018) software to obtain the best data clarity for interpretation. Post-collection, the seismic reflection data were not frequency filtered or processed beyond changes in amplitude gain.



Seismic facies were identified on individual seismic sections based on bounding reflections delineating distinct changes in acoustic character and reflection geometry. These seismic facies were then correlated between sections based on similar acoustic character, reflection geometry and stratigraphic position. Based on the original seismic descriptions and core data produced in the 1970s, regionally extensive seismic facies identified from recent surveys were correlated to regional BGS units (Pantin & Evans, 1984) where descriptions of acoustic character, reflection geometry and stratigraphic position were similar. Lithofacies were identified in individual cores based on grainsize trends, bounding surfaces and the relative stratigraphic position of similar deposits. A sound velocity of  $1600 \text{ m}\cdot\text{s}^{-1}$ , determined from bulk average Geotek Multi-Sensor Core Logger (MSCL) measurements of the selected cores (Table 2.3), was used to approximately convert two-way-time on seismic profiles into depth. This aided the correlation of seismic facies to lithofacies where the depth of core penetration was significant and comparable in thickness to the cored seismic facies. However, this was not always possible and therefore the relative order of similar lithofacies below the seafloor was compared to the vertical stacking of seismic facies existing below the seafloor at the core site. Superficial lithofacies were assumed to be correlative to the seismic facies comprising the seafloor, and any subsequent lithofacies were correlated to seismic facies based upon their relative thicknesses, depths of occurrence and any dramatic changes in lithology which would correlate to a seismic facies character change. This resulted in a progression of confidence in correlation with depth from the seafloor.

## 2.3 Sediment Geotechnics

### 2.3.1 Sediment Core Data

After core retrieval during JC-106, the cores were split into metre long sections and were left horizontally for at least six hours to equilibrate with ambient temperatures. A Geotek MSCL was used to produce geophysical measures of gamma-ray density, sound velocity, magnetic susceptibility and electromagnetic resistivity in one- to two-centimetre resolution for each section with regular calibrations. Where density data gaps existed at the top of the geophysical properties log, the first valid value recorded was used to complete these overlying gaps, while a linear interpolation was used for internal data gaps. From the inventory of JC-106 sediment cores, only cores which recovered LF4 and LF8 were used (Table 2.4).

*Table 2.4 - Selected Vibrocore (VC) and Piston Core (PC) recovery details from JC-106 which were subjected to sampling and geotechnical testing. Annotated visual core logs are published in Lockhart et al. (2018), with the exception of 36VC and 39VC which are published in Scourse et al. (2019), while the visual log for 53VC is unpublished.*

| Core | Latitude<br>(DD WGS84) | Longitude<br>(DD WGS84) | Depth (m) | Recovery<br>(m) | Max<br>Undrained<br>Shear<br>Strength<br>(kPa) | Lithofacies<br>(LF)<br>Sampled | Sample<br>Depth<br>(m) |
|------|------------------------|-------------------------|-----------|-----------------|--|--------------------------------|------------------------|
| 18VC | 49.54034               | -8.99374                | 146       | 1.86            | 125  | LF8                            | 0.87-<br>0.93          |
| 19VC | 49.53904               | -8.99170                | 145       | 1.62            | 115  | LF8                            | N/A                    |
| 33VC | 50.27430               | -8.34522                | 132       | 1.82            | 133  | LF8                            | 1.37-<br>1.43          |
| 35VC | 50.27119               | -8.34521                | 130       | 2.63            | 148  | LF8                            | 1.83-<br>1.89          |
| 44VC | 50.56035               | -8.32173                | 125       | 2.02            | 165  | LF8                            | 0.96-<br>1.02          |
| 45VC | 50.56020               | -8.32172                | 125       | 2.17            | 145  | LF8                            | 1.26-<br>1.32          |
| 51PC | 51.34570               | -6.18433                | 116       | 6.29            | 35   | LF4                            | 4.97-<br>5.03          |
| 52PC | 51.36627               | -6.16656                | 116       | 7.58            | 30   | LF4                            | 6.02-<br>6.08          |
| 53VC | 51.42468               | -6.14456                | 108       | 4.47            | 25   | LF4                            | 3.90-<br>3.96          |

### 2.3.2 Geotechnical Analyses

Initially, one-dimensional oedometer tests were planned to be conducted on undisturbed sediment samples comprising the entire split core volume between the sample depths in Table 2.4. This would allow the calculation of the maximum yield stress that the sediments had been subjected to in the past to result in their consolidated state. However, the size of the sample available in the split core section and the size of sample accepted by the oedometer cell were too similar. This resulted in an inadequate fit where the sample was not sufficiently large enough to ensure that the cell was completely filled while remaining undisturbed. Without sufficiently smaller oedometer cells being available, and the fact that some samples were disturbed during excavation from the core barrel, this resulted in the tests being discontinued. As samples of adequate grainsize were limited in each core and each test resulted in the destruction of any sedimentary structures in the sample, a new methodology had to be developed to calculate the maximum yield stress of the sediments based upon the available data and without the destruction of additional samples. This new methodology is described as follows:

Samples (<30 g) of sediment were selected from laminated mud and fine sand deposits comprising Lithofacies (LF) LF8 and LF4, with clean mud or silt being preferentially sampled to result in a consistent grainsize between samples. However, in places these deposits are noticeably coarser with increased sand content due to laminations. Therefore, samples were recovered from the most fine-grained sections available, leaving the sandy 19VC unsampled (Table 2.4). The selected physical samples were recovered from depths at which shear-vane measurements were taken during JC-106 in order to represent the physical properties of the sediment tested by the shear-vane.

#### Effective Stress

The degree of effective stress ( $\sigma'$ ) imparted by a sediment mass comes about due to changes in total stress ( $\sigma$ ) and pore pressure ( $\mu$ ) which combine in Equation 2.1 (Terzaghi, 1943).

*Equation 2.1* 
$$\sigma' = \sigma - \mu$$

At any measurement depth, a marine core sample experiences total stress in the sub-surface as a result of the overlying water column pore pressure and the total saturated sediment stress (Figure 2.5). The saturated sediment stress can be determined using MSCL-derived gamma-ray density logs for each core. This resulted in discrete density measurements for packets of sediment with a thickness of the resolution of the MSCL data, producing a centimetric-resolution density stratigraphy for each core. The subsequent equations are based on the standard equation to calculate the vertical one-dimensional pressure ( $P$ ) imparted by a mass, knowing the density of the mass ( $\rho$ ), its height ( $h$ ), and acceleration due to gravity ( $g$ ), Equation 2.2.

*Equation 2.2* 
$$P = \rho gh$$

At the bottom of each depth interval ( $Z_n$ ) in the core, individual density measurements ( $\rho$ ) were used to calculate the saturated sediment contribution to total stress ( $\sigma_{n_{sed}}$ ) for each individual packet thickness ( $h$ ) using Equation 2.3 (Figure 2.5), with acceleration due to gravity ( $g$ ) as  $9.81 \text{ m}\cdot\text{s}^{-2}$ .

Equation 2.3 
$$\sigma_{n_{sed}} = \rho gh$$

The total pore pressure ( $\mu_{Z_{sea+core}}$ ) at any core depth interval ( $Z_n$ ) was calculated using Equation 2.4. This uses an assumed seawater density ( $\rho_w$ ) of  $1025 \text{ kg}\cdot\text{m}^{-3}$  and the height of water ( $Z_{sea+core}$ ) measured from the core depth of the measurement point to the height of the sea surface (Figure 2.5) from water depth measurements (Table 2.4). This assumes that a connected pore network exists from within the cored sediments to the water column. The water column pore pressure ( $\mu_{Z_{sea}}$ ) was calculated using Equation 2.4 and the height of water ( $Z_{sea}$ ) in the water column above the sediment (Figure 2.5), equivalent to the absolute water depth (Table 2.4).

Equation 2.4 
$$\mu_z = \rho_w g Z$$

The total stress ( $\sigma$ ) was obtained by adding the sum the saturated sediment contribution to total stress ( $\sigma_{n_{sed}}$ ) for each packet overlying a defined measurement depth ( $Z_n$ ) to the water column pore pressure ( $\mu_{Z_{sea}}$ ). Combining this with the total pore pressure ( $\mu_{Z_{sea+core}}$ ) at the same defined measurement depth ( $Z_n$ ), the effective stress ( $\sigma'$ ) experienced at each shear-vane measurement depth was calculated using Equation 2.1.

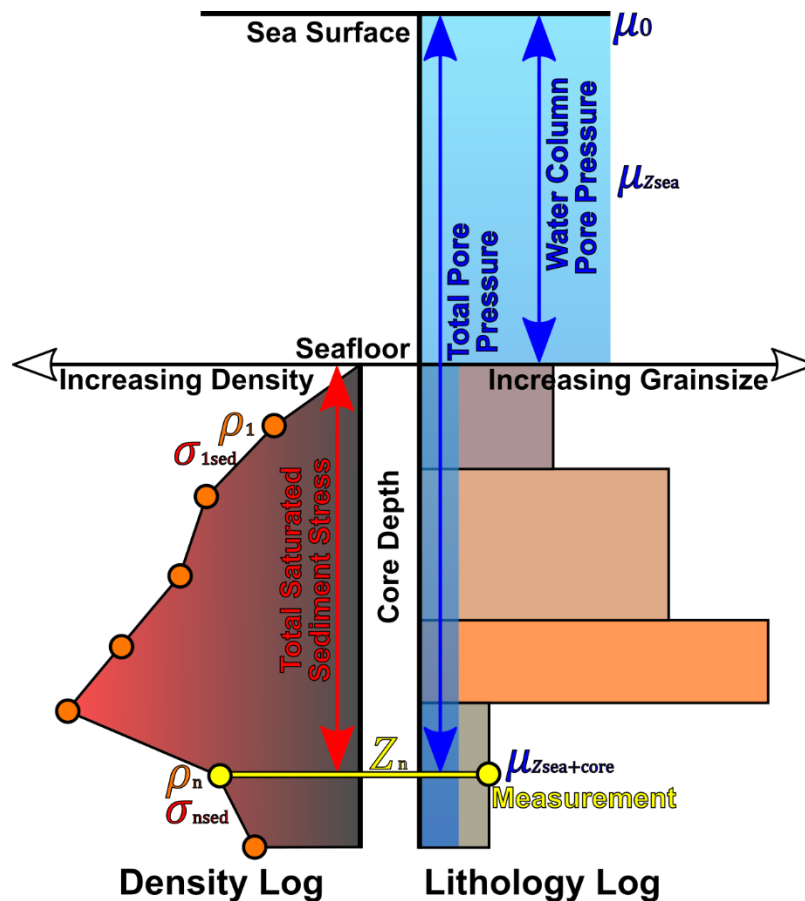


Figure 2.5 - Schematic diagram of a marine core sample defining the saturated sediment stresses ( $\sigma_{n_{sed}}$ ) produced from discrete density measurements ( $\rho_n$ ) with pore pressures ( $\mu_z$ ) used, referenced to a defined measurement depth ( $Z_n$ ).

### Atterberg Limits

Both liquid limit ( $w_L$ ) and plastic limit ( $w_P$ ) moisture content values were calculated for physical samples obtained within the depths over which shear-vane data were collected. These individual samples were separately reconstituted manually until they became homogeneous and without structure. The liquid and plastic limits, which define the plastic behaviour of a sediment, were measured using methods specified in ISO17892 Part 12 (ISO, 2018). These tests can only be conducted on sediments of a fine grainsize, leaving the sandy 19VC unprocessed.

A standard 80 g and 30° cone was used to determine the liquid limit by sample penetration. During this test, the cone was allowed to freefall into a cell 5 cm in diameter and 5 cm in height which was filled with the sample with a smoothed upper surface (Figure 2.6). The depth to which the cone penetrates the sample is read by a gauge attached to the equipment. The liquid limit is defined as the moisture content of the reconstituted sample at which 20 mm cone penetration occurs. This was achieved through the linear interpolation of at least three penetration measurements with varying moisture contents that resulted in between 15 mm and 25 mm cone penetration. At least two consistent penetration measurements were taken and averaged to produce a single penetration reading from

which to interpolate. Between each penetration test, the sample was hydrated and reconstituted before having its upper surface smoothed in preparation for the next penetration measurement. Once a satisfactory penetration measurement was made, a portion of the sample was used to determine the moisture content resulting in that penetration value. The moisture content of each sample was calculated through drying the pre-weighed wet samples in weighed tins at 100 °C for at least eight hours before being transferred to a desiccating chamber to cool prior to final weighing. The weight of salt in each dried sample was corrected for by assuming 3.5% salinity based upon the mass of water lost during drying to produce a pure dry sample mass.

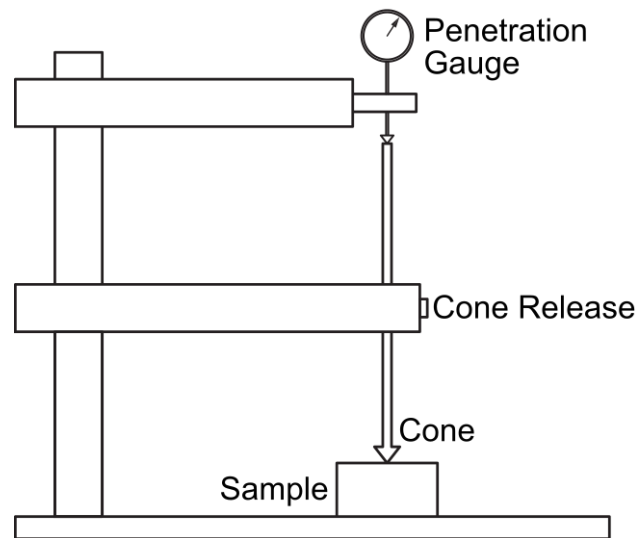


Figure 2.6 - Schematic diagram of the cone penetration equipment setup. Edited from ISO (2018).

The plastic limit was calculated through determination of the moisture content at the limit of plastic behaviour. This was done by rolling sub-samples into 6 mm diameter cylinders on a glass plate before being sub-divided further and rolled to a diameter of 3 mm within 15 hand strokes using an even pressure. If the samples cracked and crumbled before reaching a diameter of 3 mm, the samples were hydrated and the test was restarted. If the samples were too wet, they were dried by rolling between a pair of hands before retesting. When superficial cracking of the sample was observed in these 3 mm diameter rolls, the plastic limit had been reached. The moisture content of these samples was calculated through drying the pre-weighed wet samples in weighed tins at 100 °C for at least eight hours before being transferred to a desiccating chamber to cool prior to final weighing. The weight of salt in each dried sample was corrected for by assuming 3.5% salinity based upon the mass of water lost during drying to produce a pure dry sample mass.

Equation 2.5 describes the moisture content range over which the sediment behaves in a plastic manner, known as the plasticity index ( $I_p$ ).

Equation 2.5 
$$I_p = W_L - W_P$$

### Over-Consolidation Ratio & Yield Stress

The Over-Consolidation Ratio (OCR) is a ratio of the yield stress ( $\sigma_{yield}$ ) resulting in consolidation compared to the present-day effective stress ( $\sigma'$ ) described in Equation 2.6. If a sediment has been subjected to a greater yield stress compared to present-day effective stress, then it will have an OCR value greater than one and be described as over-consolidated. If the yield stress of a sediment is equal to the present-day effective stress, then it will have an OCR value of one and be described as normally-consolidated.

Equation 2.6 
$$OCR = \frac{\sigma_{yield}}{\sigma'}$$

Yield stress is commonly determined through oedometer testing where samples of undisturbed sediment are progressively consolidated in the laboratory under controlled conditions. Mayne and Mitchell (1988) provide a method for the calculation of OCR based on global measurements of undrained shear strength ( $C_u$ ), effective stress ( $\sigma'$ ) and OCR from various sediments in various geological settings reported in the literature. These data were used to study the best-fit relationship between OCR and undrained shear strength measurements to produce an equation describing the global relationship. The fit of this relationship is increased if the plasticity index of the investigated sediment is taken into account to produce an  $\alpha$  value in Equation 2.7 which is then used in Equation 2.8 to calculate OCR. This method therefore allows the back calculation of yield stress by incorporating Equation 2.6 and Equation 2.8 to give Equation 2.9 which uses the shear vane measurements obtained onboard during JC-106.

Equation 2.7 
$$\alpha = 22(I_p)^{-0.48}$$

Equation 2.8 
$$OCR = \alpha \left( \frac{C_u}{\sigma'} \right)$$

Equation 2.9 
$$\sigma_{yield} = \alpha C_u$$

## **Chapter 3 - Results**

### **3.1 Seafloor Geomorphology**

Regional and high-resolution multi-beam bathymetric data provide the opportunity to document the morphology of the main features which characterise the shelf and allow the identification of new features which have been missed due to the lack of data during legacy seafloor mapping. The morphology and characteristics of these features is important, as they dictate the interpretation of these features which is essential to the extraction of information about the environment during which they formed.

#### **3.1.1 Large-scale Ridges**

The mid- to outer-shelf of the Celtic Sea is characterised by a field of approximately 57 sub-parallel ridges that are generally aligned northeast-southwest and exist between water depths of 100-200 m (Figure 3.1). Based on the broad morphological characteristics of the ridges from bathymetric data (Figure 3.1), general trends in ridge morphology are observed based on ridge continuity, sinuosity and the presence of transverse ridges, as ridge measurement data alone show great variability (Figure 3.2) and do not reveal different ridge populations from the chosen measurements (Figure 3.3). The ridges exist either as individual features with one continuous crestline along their length or as beaded ridges with numerous crests which transition axially into elongated fields of much smaller transverse ridges between main ridge fragments. Ridges in the northwest appear to be some of the widest and axially uniform ridges with single crests, while ridges in the southeast are sinuous, fragmented and connected by transverse ridges. The ridges in the northwest appear to be some of the longest (Figure 3.1), extending up to 176 km long (Figure 3.2), although it is unknown to what degree the ridges are continuous due to low-resolution data on the western shelf, suggesting that they might be even longer. Across the ridge field, width and height measurements also show great variability up to maximums of 18 km and 64 m respectively. Ridges 24-28 display a reduction in height compared to the neighbouring ridge populations (Figure 3.1 and Figure 3.2) as this entire area is dominated by transverse ridges and low, long ridges. These general trends in ridge morphology from bathymetric data across the shelf can delineate three populations of ridges with distinct morphological characteristics (Figure 3.1), each of these populations will be discussed in turn.



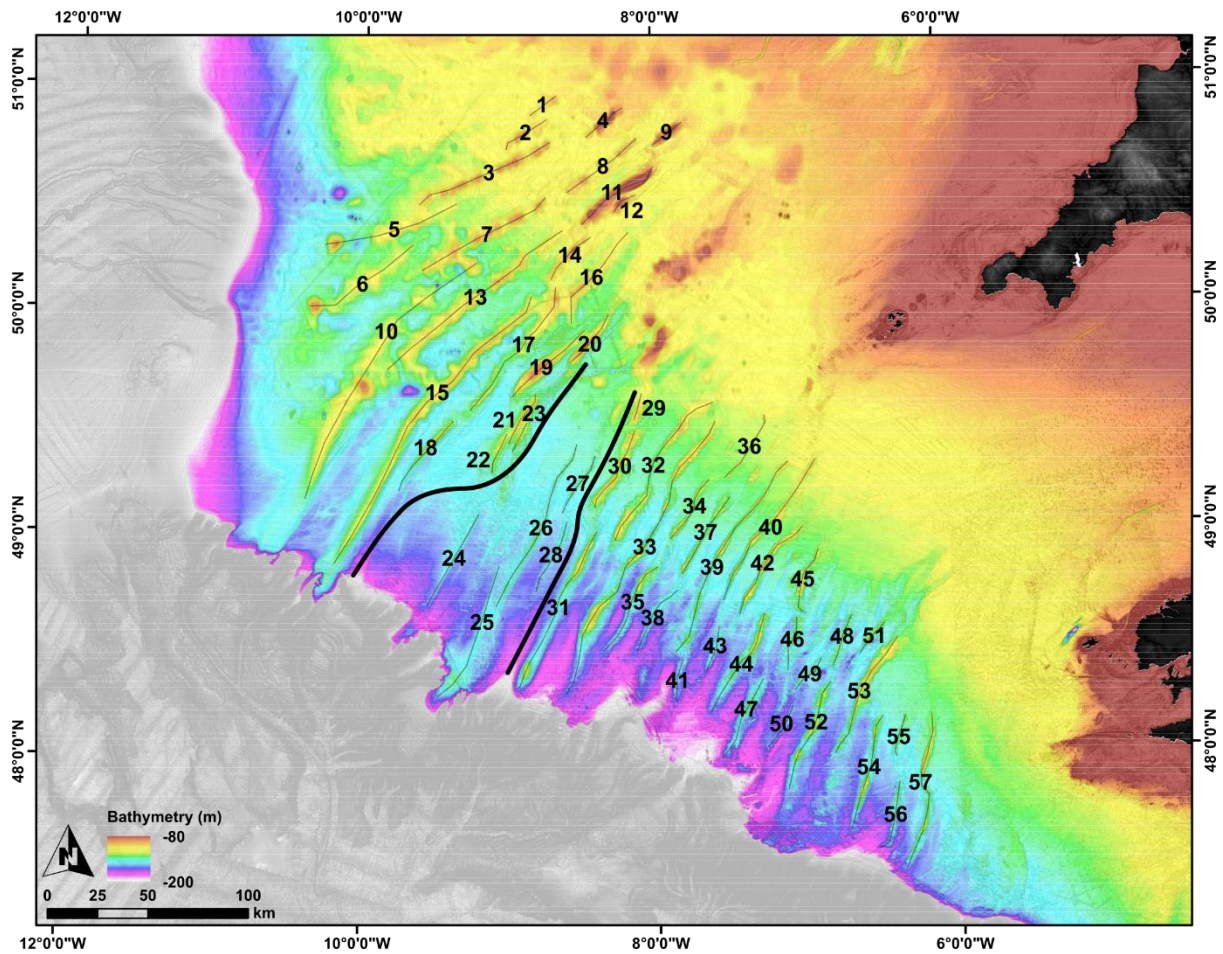


Figure 3.1 - EMODnet bathymetry and slope map of the ridge field on the mid- and outer-shelf showing three populations of ridges, separated by the marked boundaries, with ridge numbers. Dark and light areas denote steep and flat areas respectively.

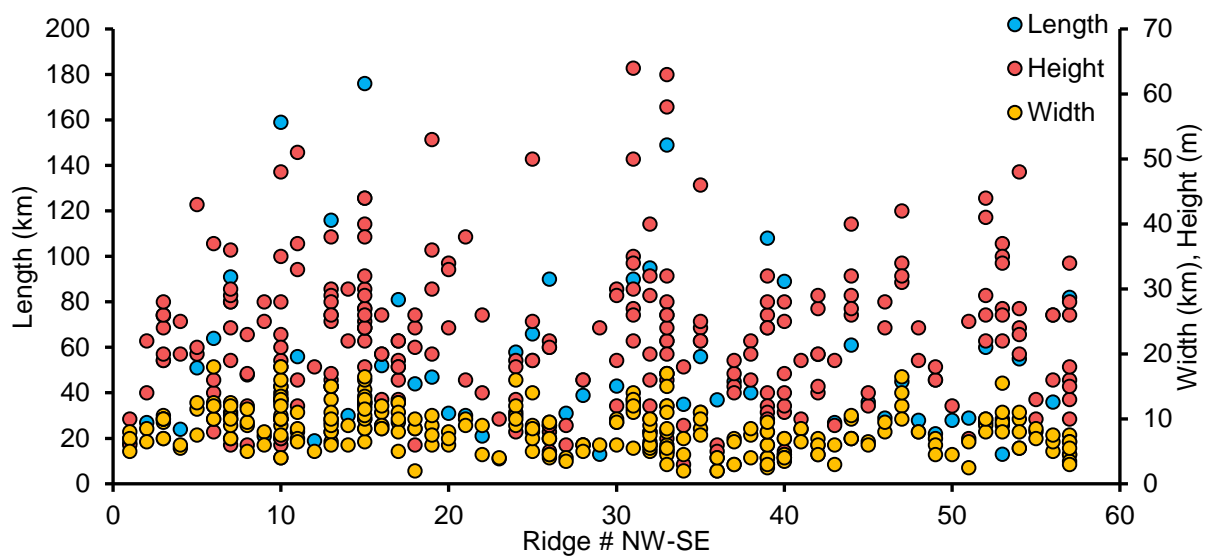


Figure 3.2 - Height, width and length measurements per ridge. See Figure 3.1 for ridge number locations.

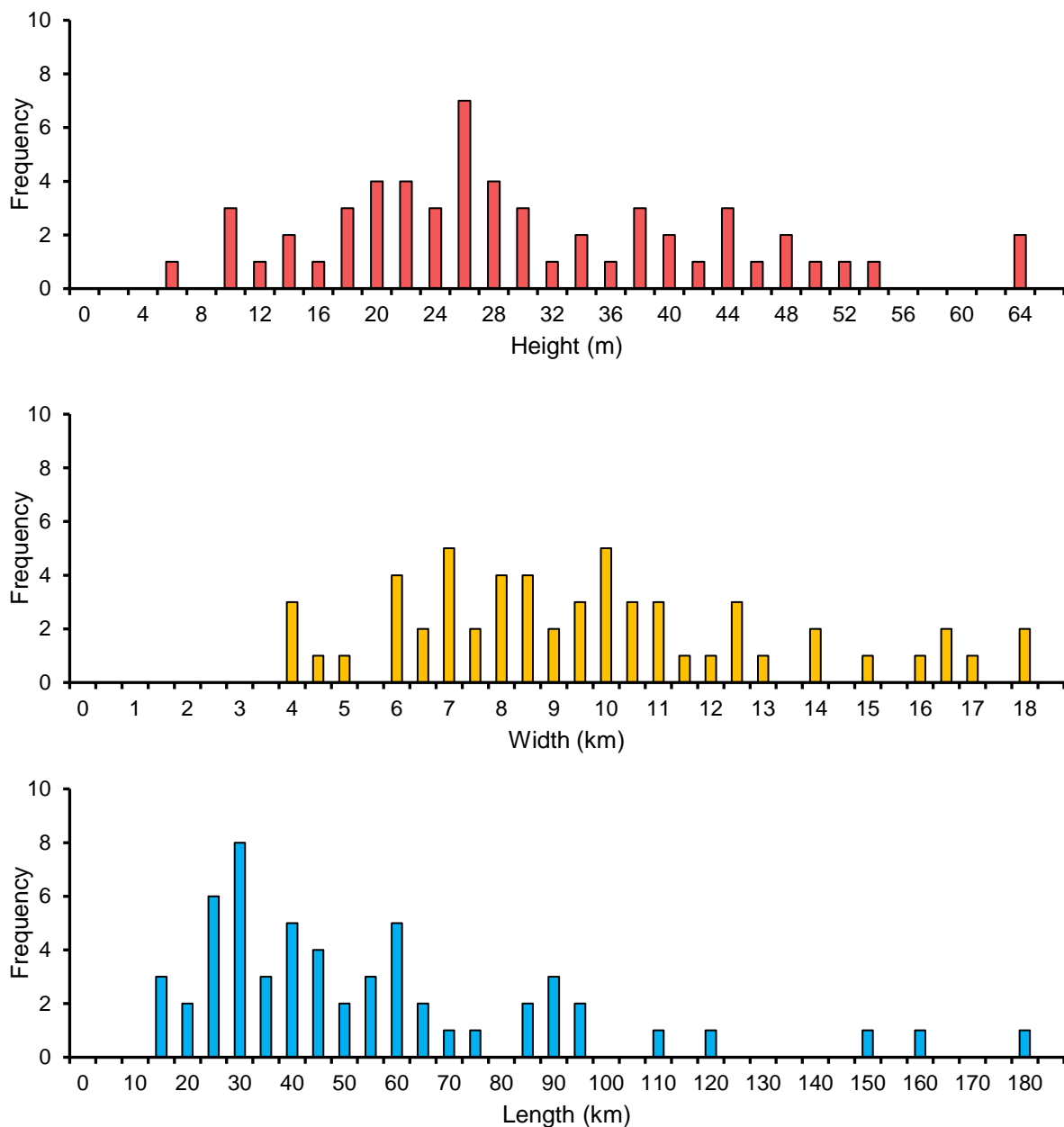
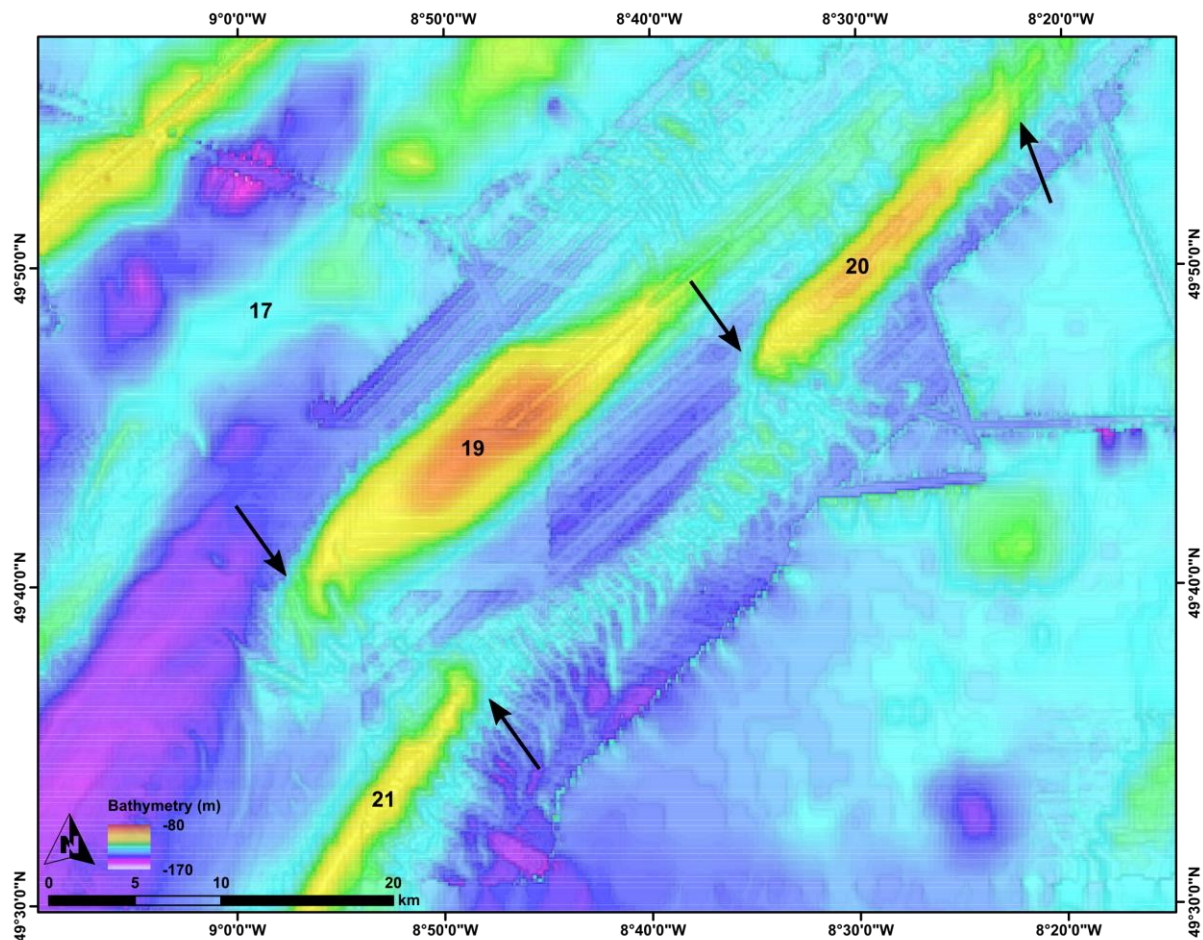


Figure 3.3 - Ridge height (red), width (yellow) and length (blue) histograms as generated from data in Figure 3.2.

Based on regional bathymetric data, the northwest area of the ridge field contains the longest, widest and most axially-uniform ridges, comprising ridge numbers 1-23, which are oriented northeast-southwest. Despite the reduced-quality bathymetric data in this region, these northwest ridges exist from the shelf edge towards the inner-shelf, representing the furthest inland extent of the ridge field (Figure 3.1). The largest and longest ridges appear regularly spaced at up to 22 km intervals and have uniform widths along their length, some of which can be up to 176 km long (Figure 3.2). However, in places where much smaller linear ridges exist, these can form tight groups of ridges of similar orientation where ridge spacing can be up to a few km. The heights and widths of these ridges can be up to 53 m and 18 km respectively (Figure 3.2). In places where multi-beam echo-sounder surveys are available,

some of the smaller ridges can appear slightly curved at their axial termini (Figure 3.4). In every case where curvature is observed around a prominent single ridge crest, the northern end of the ridge is curved to the northwest while the southern end is curved to the southeast. This results in the ridge ends being curved counter-clockwise around the highest point on the ridge crest. These ridges consistently have one crestline along their length and axially give way to small ridges which are oriented transverse the main ridge where it thins (Figure 3.4).



*Figure 3.4 - EMODnet bathymetry and slope map of ridges on the mid-shelf showing rotated ends (black arrows) and the axial transition into transverse ridges. Dark and light areas denote steep and flat areas respectively. See Figure 3.1 for ridge number locations.*

In the middle of the outer-shelf is an area of seafloor that extends to the shelf edge which lacks large ridges comparable to those found in the northwest or to the southeast. The ridges, numbered 24-28, that do exist in this area are smaller in terms of vertical extent compared to neighbouring ridges outside of this area (Figure 3.1) and are spaced 10-20 km apart. This region is dominated by the largest area of small transverse bedforms which here exist laterally between, or overprint, the main ridges (Figure 3.5). The main ridges themselves are up to 90 km long, 16 km wide and 50 m high, although heights are generally less than 22 m (Figure 3.2).



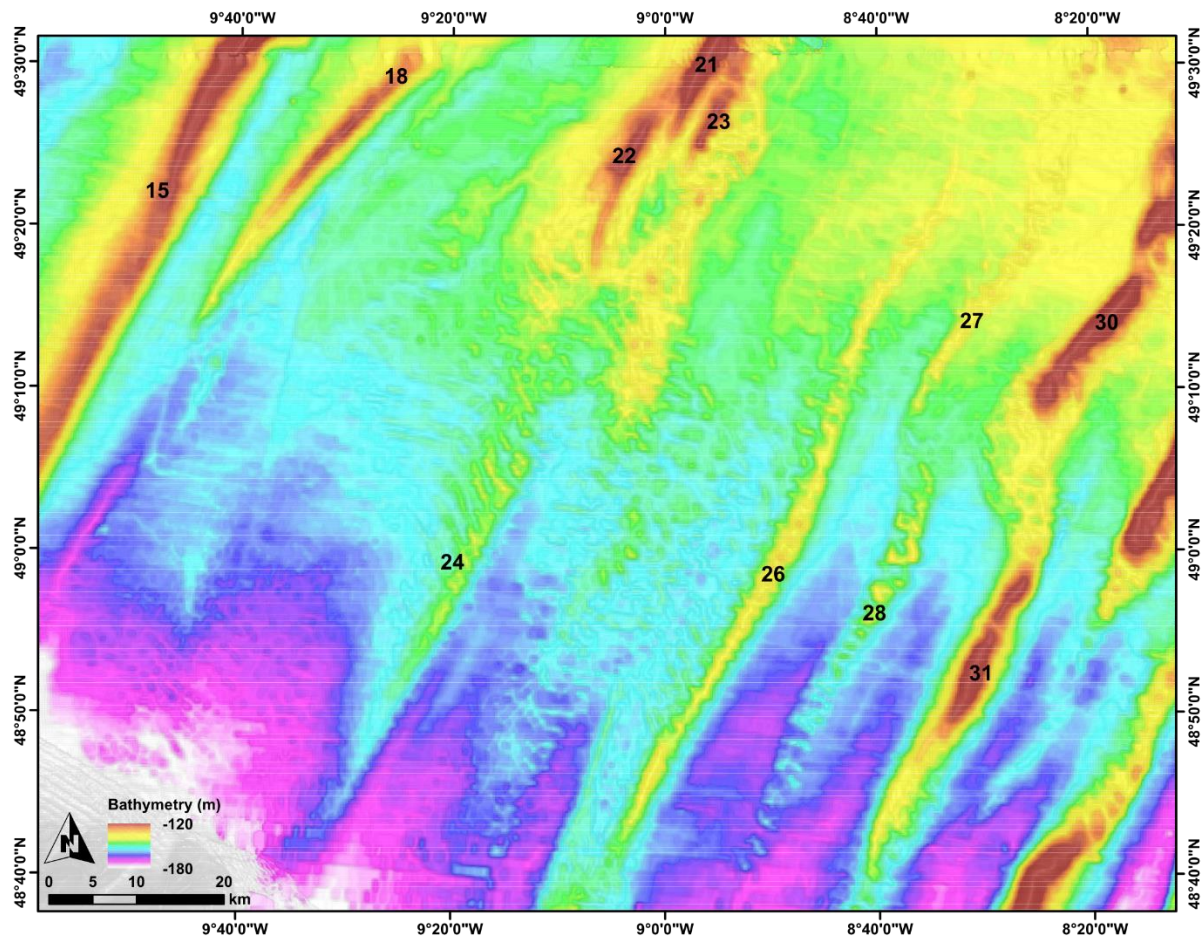


*Figure 3.5 - EMODnet bathymetry and slope map of ridges on the outer shelf. Dark and light areas denote steep and flat areas respectively. See Figure 3.1 for ridge number locations.*

To the southeast, ridges numbered 29-57 appear sinuous and long, extending from the mid-shelf to the shelf edge, and transition from being northeast-southwest oriented in the west to becoming more north-south aligned in the east (Figure 3.1). Their width is not uniform along their length, as they are fragmented with multiple crests along their length. These crestlines are in places connected by a path of smaller transverse ridges, similar to those observed in the northwest (Figure 3.4). This overall morphology results in main ridge fragments which are slightly offset in orientation from the main ridge, but generally aligned to form one prominent and sinuous ridge feature (see ridges 30 and 31 in Figure 3.5). These composite ridges have ends which are curved in opposite directions, giving the appearance of the ridge being rotated around its centre, similarly observed in the northwest (Figure 3.4). In this southeast region, ridges to the northwest exist as positive features while towards the southeast some ridges appear to exist as areas of seafloor which are bounded by incisions into the shelf on the northeast boundary of the ridge field adjacent to the English Channel (Figure 3.6). To the south of these ridges, typical positive ridges exist. It is possible that, at this northern boundary, positive ridges overlie areas of channelled seafloor such as those in Figure 3.6. Throughout this area the ridges are spaced by 10-15 km and can be up to 149 km long, 17 km wide and 64 m high (Figure 3.2).

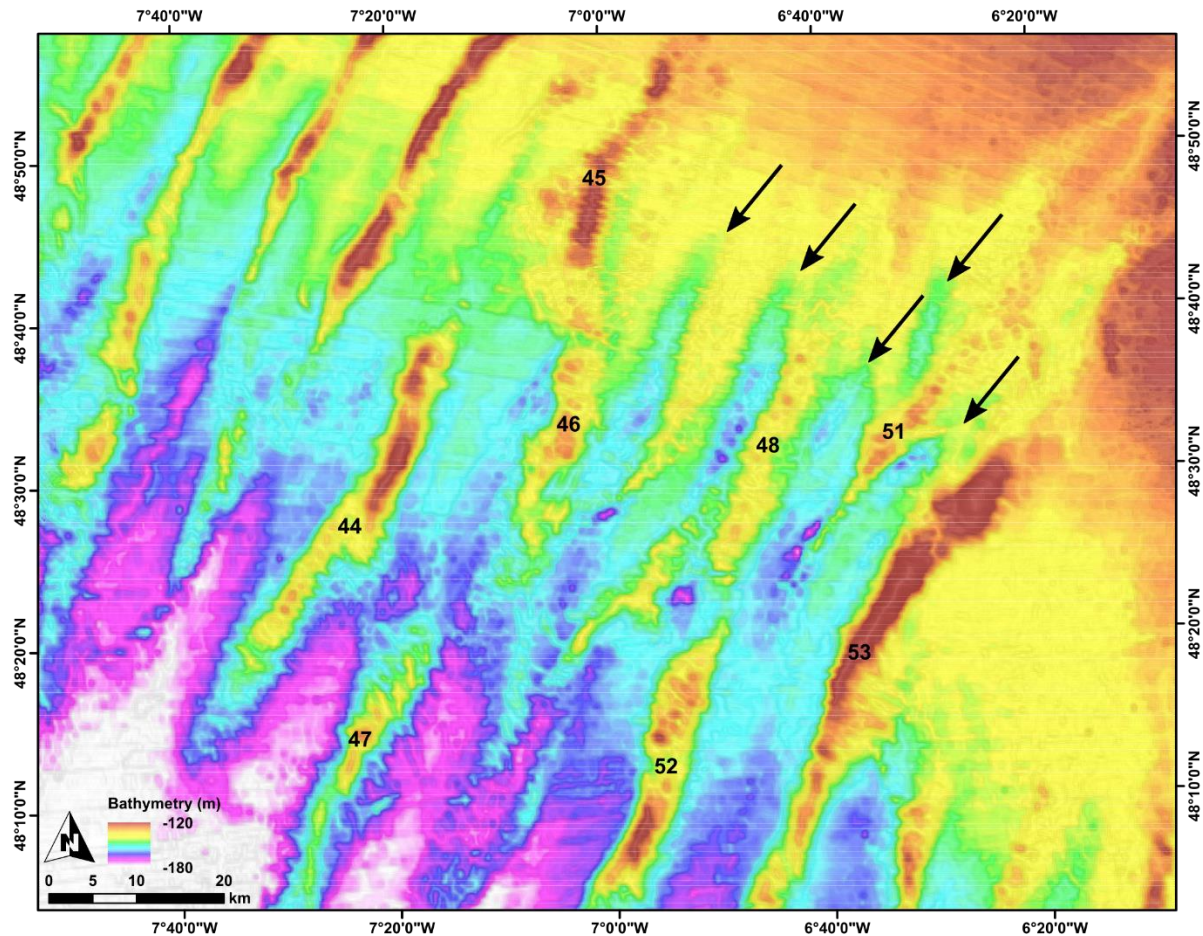


Figure 3.6 - EMODnet bathymetry and slope map of ridges and neighbouring incision termini (black arrows) in the southeast of the shelf. Dark and light areas denote steep and flat areas respectively. See Figure 3.1 for ridge number locations.

Therefore, these analyses allow the delineation of three populations of ridges; two populations of larger ridges to the northwest and southeast which are separated by a band of much smaller ridges (Figure 3.1). The ridges in the northwest are the longest and most axially-uniform ridges, contrasting to those in the southeast which are fragmented, sinuous and taller.

### 3.1.2 Inner-shelf Features

Disregarding the previously described large linear ridges, over 2000 distinct seafloor bedforms have been identified across the inner Celtic Sea shelf (Figure 3.7) and categorised according to broad morphological similarities when compared to glacial bedforms reported in the scientific literature. See Table 3.1 for morphological measurements, characteristics and example images based on the collective observations of each feature type.



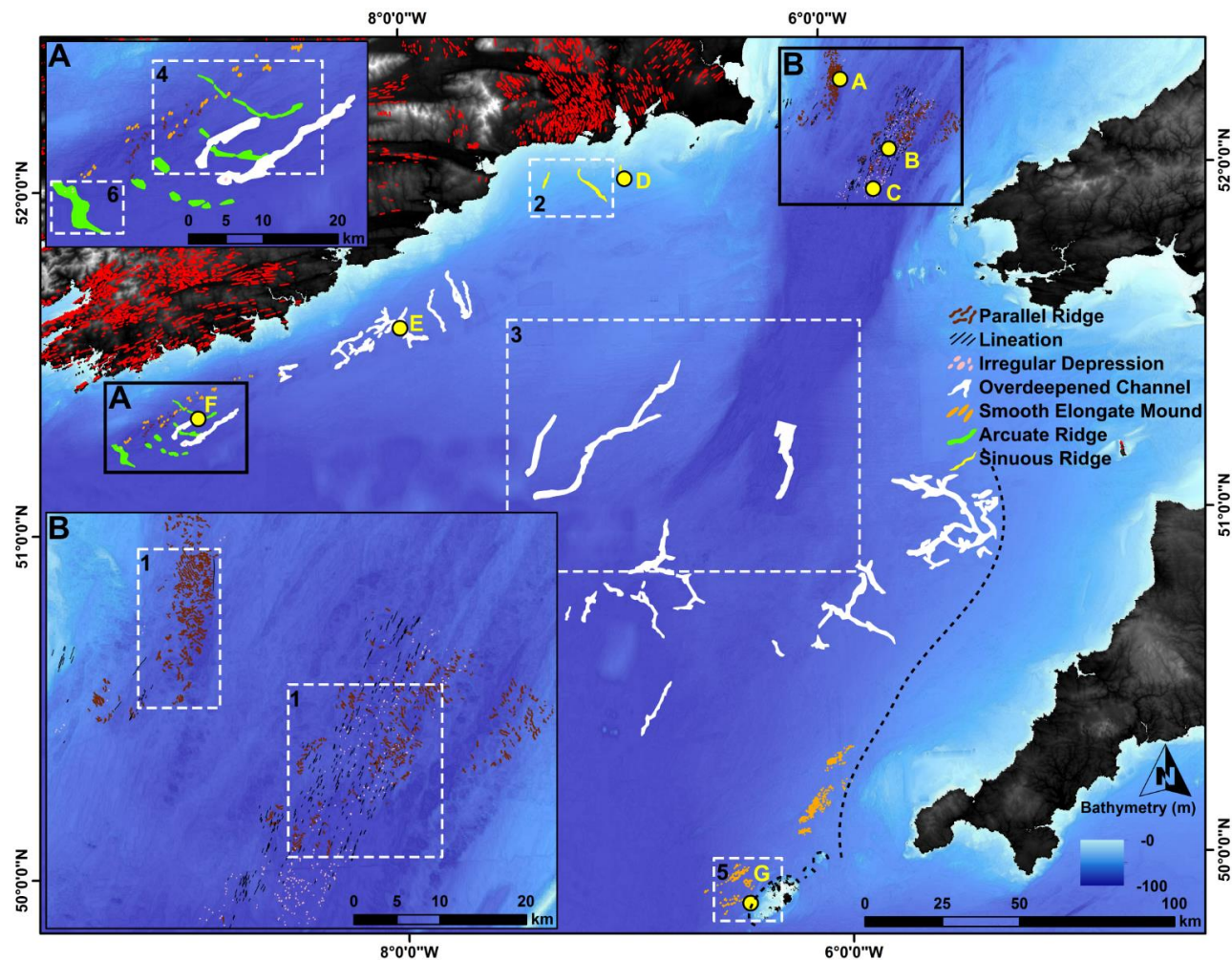
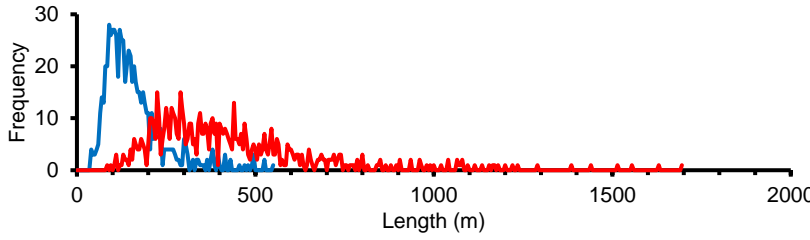
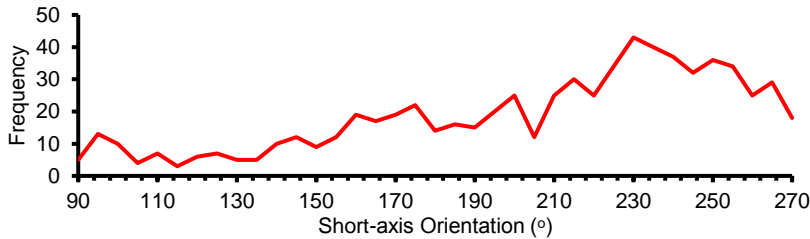
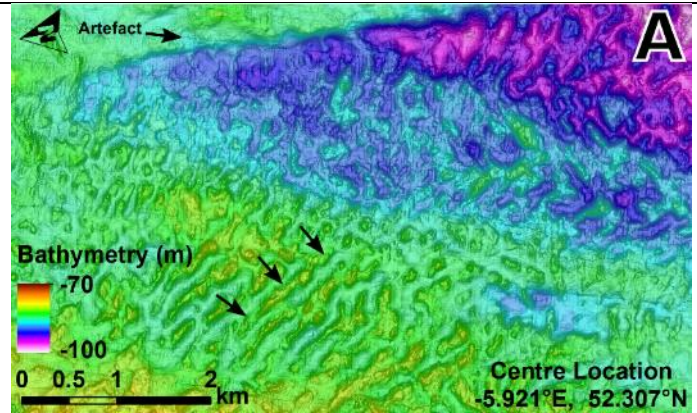
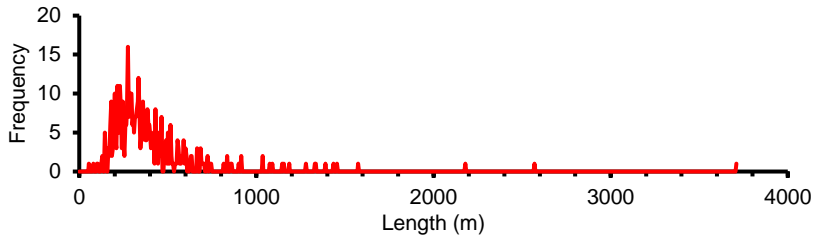
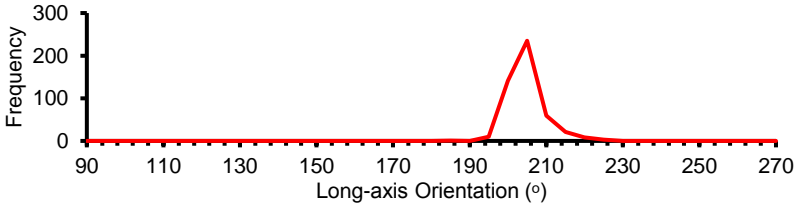
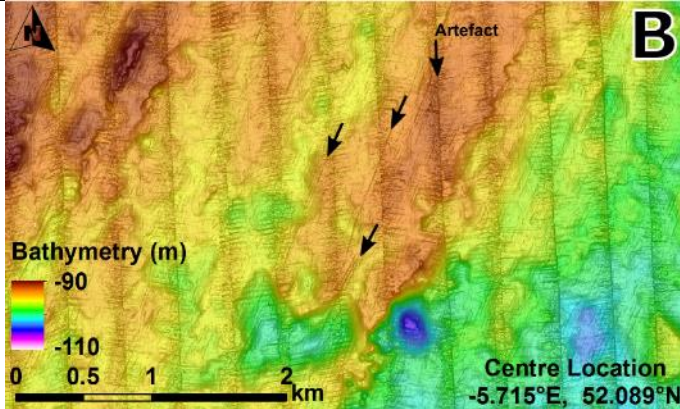


Figure 3.7 - Thematic map of inner-shelf seafloor features and image and figure locations. A wide variety of seafloor features are observed on the inner-shelf, including arcuate ridges, streamlined features and over-deepened channels. The long-axis orientation of similar lineations and streamlined bedrock from Clark et al. (2018) is shown in red for southern Ireland. The limit of this feature assemblage to the east is marked by a dashed line.

Table 3.1 - Feature classes and morphological descriptions with example images existing as either hillshades or slope maps. Some measurements were obtained numerous times per individual feature and these are marked with an asterisk. For image locations see Figure 3.7.

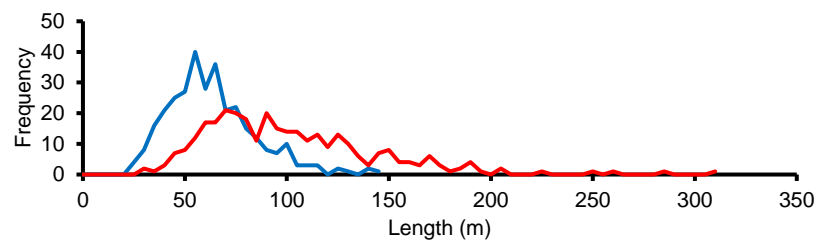
| Feature Type                             | Morphology and Spatial Information   | Example Image   |
|--|--|---|
| <b>Parallel Ridges</b><br><b>(n 695)</b> | <p><b>Plot A - Short- (blue) and Long-axis (red) Length</b></p>  <p><b>Plot B - Short-axis Orientation</b></p>  <p><b>Height (m):</b> Max 11, Min 0.5, Avg 2.8, SD 1.6, n 79</p> <p><b>Diagnostic Characteristics:</b></p> <ul style="list-style-type: none"> <li>• Tabular ridges</li> <li>• Perpendicular ridges which fit together</li> <li>• Uniform, tabular ridges form a continuous belt in the Irish sector but become discontinuous and chaotic to the south</li> <li>• Ridges are discontinuous and buried in the UK sector</li> </ul> <p><b>Dominant Areas:</b> St. George's Channel (Irish sector and UK sector)</p> |  |

|                                     |  |   |
|-------------------------------------|--|---|
| <b>Parallel Ridges</b>              | <b>Depth Range (m):</b> -75 to -100<br><b>Overprinted By:</b> Lineations   |   |
| <b>Lineations</b><br><b>(n 478)</b> | <p><b>Plot C - Length</b></p>  <p><b>Plot D - Long-axis Orientation</b></p>  <p><b>Diagnostic Characteristics:</b></p> <ul style="list-style-type: none"> <li>• Exist as linear breaks in slope</li> <li>• Overprint transverse ridges</li> <li>• Dominant southwest orientation</li> <li>• Do not deviate with topography variations</li> </ul> <p><b>Dominant Areas:</b> St. George's Channel (UK sector)</p> <p><b>Depth Range (m):</b> -90 to -110</p> <p><b>Overprints:</b> Parallel ridges</p> |  |

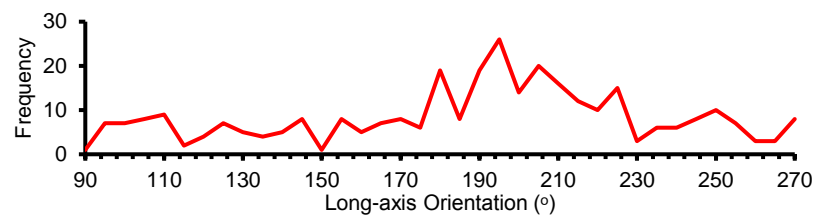


# Irregular Depressions (n 315)

**Plot E - Short- (blue) and Long-axis (red) Length**



**Plot F - Long-axis Orientation**



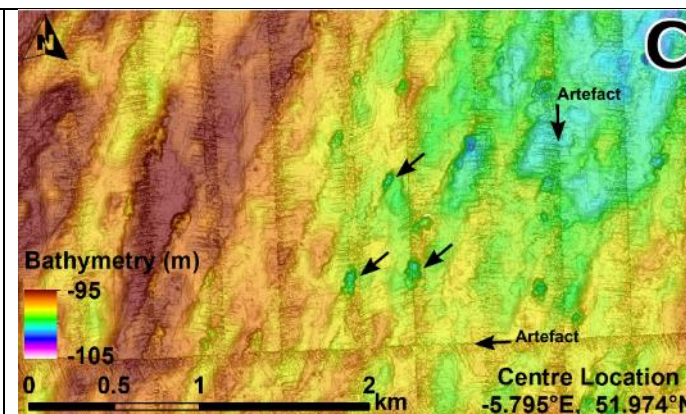
**Depression Depth (m):** Max 1.5, Min 0.5, Avg 0.8, SD 0.3, n 32

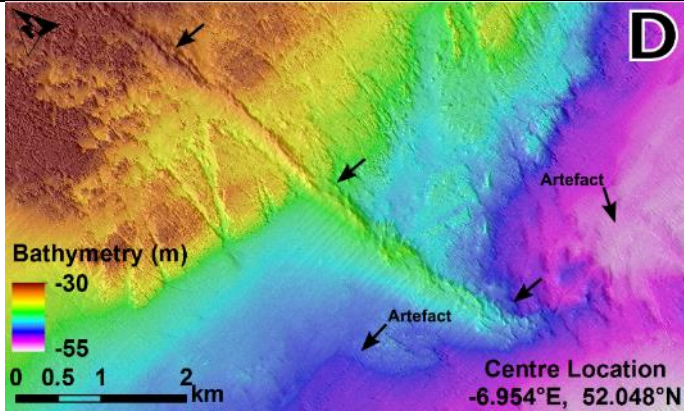
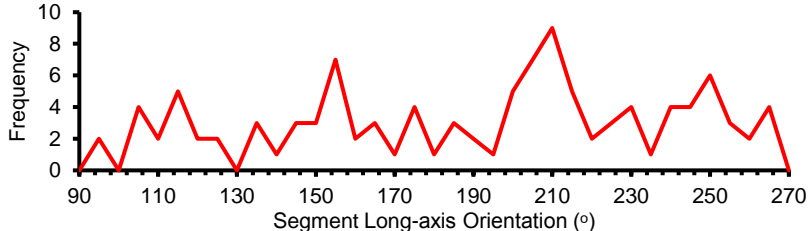
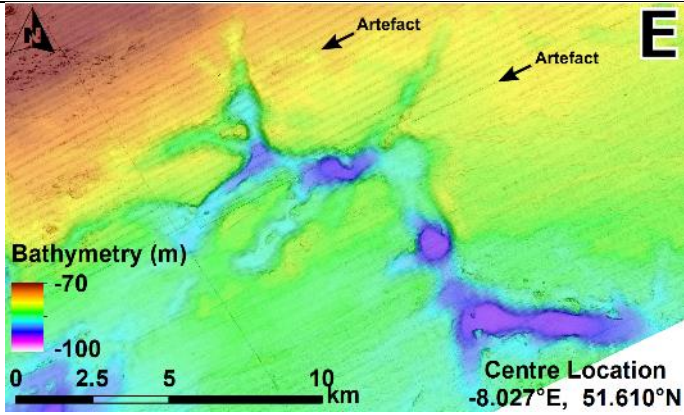
## Diagnostic Characteristics:

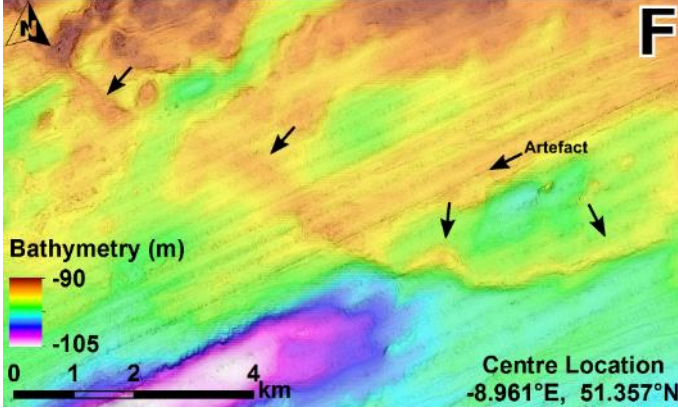
- Found on northern side of prominent areas of seafloor
- Sometimes associated with scours
- Elongated to the southwest
- Irregular boundaries with internal mounds and depressions

**Dominant Areas:** St. George's Channel (UK sector)

**Depth Range (m):** -85 to -105

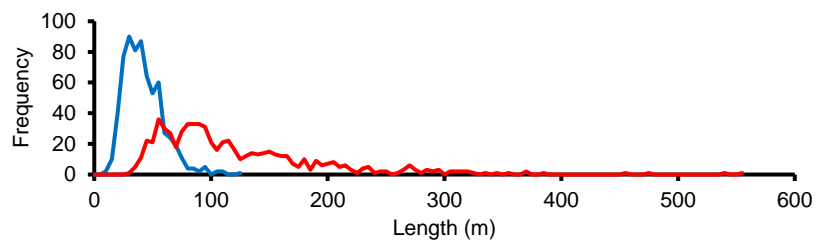


|   |   |  |
|---|---|--|
| <p><b>Sinuuous Ridges</b><br/>(n 3)</p> | <p><b>Long Axis (km):</b> Max 14.3, Min 5.3, Avg 8.9, SD 4.8, n 3</p> <p><b>Short Axis (m)*:</b> Max 804, Min 131, Avg 477, SD 257, n 9</p> <p><b>Height (m):</b> Max 2, Min 0.5, Avg 1.3, SD 0.8, n 3</p> <p><b>Diagnostic Characteristics:</b></p> <ul style="list-style-type: none"> <li>• Oriented perpendicular to the coastline</li> <li>• Can be continuous or discontinuous</li> <li>• Exist as single ridges, individual beads or fan-like</li> </ul> <p><b>Dominant Areas:</b> Southern Irish coastline (south of Brownstown Head)</p> <p><b>Depth Range (m):</b> -30 to -60</p>  |   |
| <p><b>Overdeepened Channels</b></p>     | <p><b>Plot G - 5 km Thalweg Segment Orientation (n 110)*</b></p>  <p><b>Long Axis (km):</b> Max 71.2, Min 4.5, Avg 20.4, SD 13.5, n 23</p> <p><b>Short Axis (km)*:</b> Max 2.9, Min 0.4, Avg 1.2, SD 0.6, n 54</p> <p><b>Channel Depth (m)*:</b> Max 33, Min 1.5, Avg 6.2, SD 6.3, n 30</p> <p><b>Diagnostic Characteristics:</b></p> <ul style="list-style-type: none"> <li>• Approximately 25 channel systems</li> <li>• Exist as individual channels or bifurcated systems</li> <li>• Display overdeepening</li> <li>• Abrupt termini</li> </ul> |  |

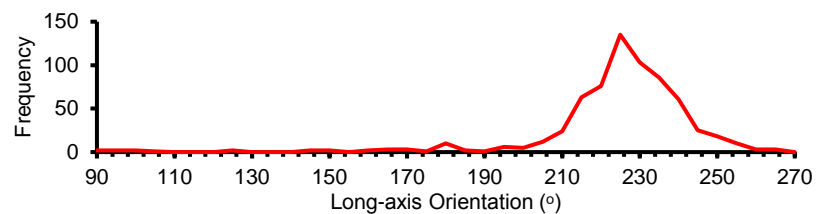
|                              |   |  |
|------------------------------|---|--|
| <b>Overdeepened Channels</b> | <ul style="list-style-type: none"> <li>• Generally oriented perpendicular to the coastline</li> <li>• The largest channel is located on the Nymphé Bank Platform</li> <li>• Found perpendicular to arcuate ridges where present</li> <li>• Located near geological boundaries and faults south of Ireland</li> </ul> <p><b>Dominant Areas:</b> Southern Irish coastline (20 km south of Ram Head to 25 km south of Galley Head); Inner shelf (Nymphé Bank Platform, Haig Fras Platform and Lundy Platform)</p> <p><b>Depth Range (m):</b> -70 to -100</p>   |  |
| <b>Arcuate Ridges</b>        | <p><b>Long Axis (km):</b> Max 10.1, Min 1.3, Avg 3.5, SD 2.8, n 12</p> <p><b>Short Axis (km):</b> Max 4, Min 0.2, Avg 1.4, SD 1.2, n 9</p> <p><b>Height (m):</b> Max 13, Min 0.5, Avg 2.1, SD 3.5, n 12</p> <p><b>Diagnostic Characteristics:</b></p> <ul style="list-style-type: none"> <li>• At least four main arcuate features comprised of 12 ridges</li> <li>• Outermost ridge is the largest and is overprinted by depressions and scours</li> <li>• Innermost ridge is the narrowest</li> <li>• Ridges have similar orientations</li> <li>• Can be continuous or discontinuous</li> </ul> <p><b>Dominant Areas:</b> Southern Irish coastline (20 km south of Galley Head to 30 km south of Toe Head)</p> <p><b>Depth Range (m):</b> -90 to -105</p> |  <p><b>Bathymetry (m)</b></p> <p>-90</p> <p>-105</p> <p>0 1 2 4 km</p> <p>Centre Location<br/>-8.961°E, 51.357°N</p> |

**Smooth Elongate  
Mounds  
(n 665)**

**Plot H - Short- (blue) and Long-axis (red) Length**



**Plot I - Long-axis Orientation**



**Height (m):** Max 7, Min 0.5, Avg 1.5, SD 1.1, n 67

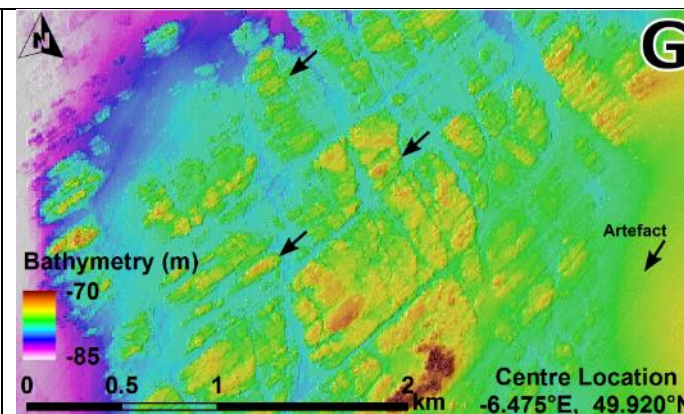
**Elongation Ratio:** Max 15, Min 1, Avg 3, SD 1, n 665

**Diagnostic Characteristics:**

- Dominant southwest orientation
- Smooth and elongated appearance
- Evident in areas of prominent seafloor

**Dominant Areas:** Isles of Scilly (37 km northwest of Land's End to 25 km west of the Isles of Scilly), Southern Irish coastline (20 km south of Galley Head to 30 km south of Toe Head)

**Depth Range (m):** -70 to -90





## Parallel Ridges

St. George's Channel (St. GC) contains the largest assemblage of parallel ridges in the study areas (Figure 3.7 and Table 3.1). In the Irish sector, these ridges exist between water depths of 70-100 m, forming a continuous belt of features in a bathymetric depression 5 km wide (Figure 3.8). In the UK sector, these features exist between 75-100 m water depth where they are more sporadic and discontinuous, forming isolated belts of ridges, in places filling depressions but also appearing on areas of prominent seafloor (Figure 3.8). These parallel ridges in places appear parallel to neighbouring ridges, all having similar orientations (Image A in Table 3.1). However, in places these features appear to mesh together, having convergent/divergent orientations overall (Plot B in Table 3.1). Heights can be up to 11 m, but generally heights of 3 m are observed. The upper surface of the ridges can be tabular in shape, but in places the topography is highly irregular, whereby smaller parallel ridges of a different orientation or mounds overprint the much larger underlying parallel ridges. In the UK sector of St. GC, isolated patches of parallel ridges appear in depressions.

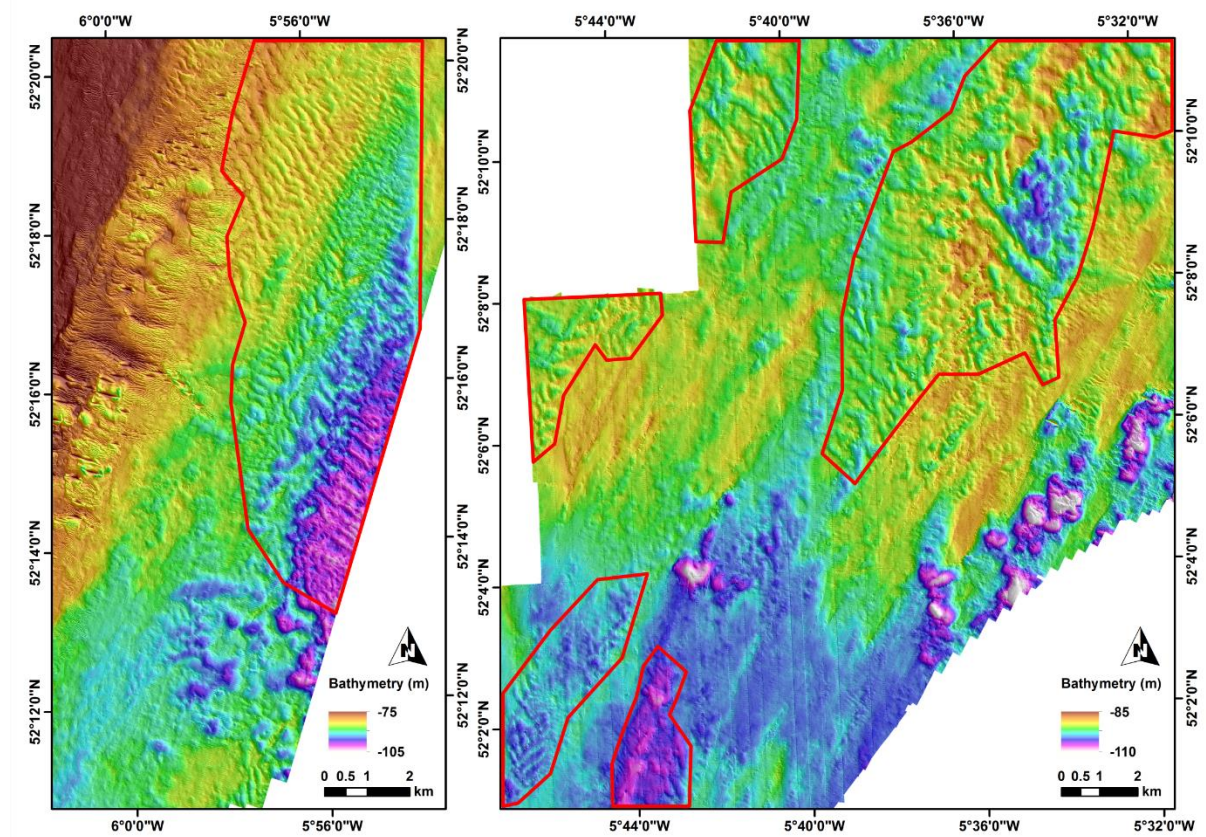


Figure 3.8 - INFOMAR (left) and UKHO (right) bathymetry and hillshaded relief (240° illumination for clarity) image of parallel ridges (red areas) in the Irish (left) and UK (right) sectors of St. George's Channel. For image location, see Area 1 in Figure 3.7.

### **Lineations**

Linear features at the seafloor in St. GC, are more abundant in the UK sector than in the Irish sector (Figure 3.7 and Table 3.1). In a few instances, these lineations overprint the previously described parallel ridges. The lineations do not generally exist as positive or negative features, but rather as distinct linear breaks of slope along the seafloor which do not appear to deviate due to topography (Image B in Table 3.1).

### **Irregular Depressions**

Distinct irregular depressions exist throughout the UK sector of St. GC (Figure 3.7 and Table 3.1). These features are up to 1.5 m deep and are more commonly found on a prominent area of seafloor rising to a water depth of 97 m to the south of St. GC. These depressions appear to be more common on the northern side of the seafloor rise and are elongated to the south and southwest (Plot F in Table 3.1). The features display an irregular boundary, and within the depression the topography can contain internal mounds and smaller depressions (Image C in Table 3.1).

### **Sinuuous Ridges**

In the surrounding area immediately south of Brownstown Head, several sinuous ridges exist in water depths of 30-60 m and are generally oriented perpendicular to the coastline (Figure 3.7 and Table 3.1). In places, the sinuous ridges appear discontinuous, appearing as separate segments, while others appear continuous (Image D in Table 3.1). However, significant variation occurs in their long-profile and in places a sinuous ridge transitions to a much wider fan-like morphology (Figure 3.9).

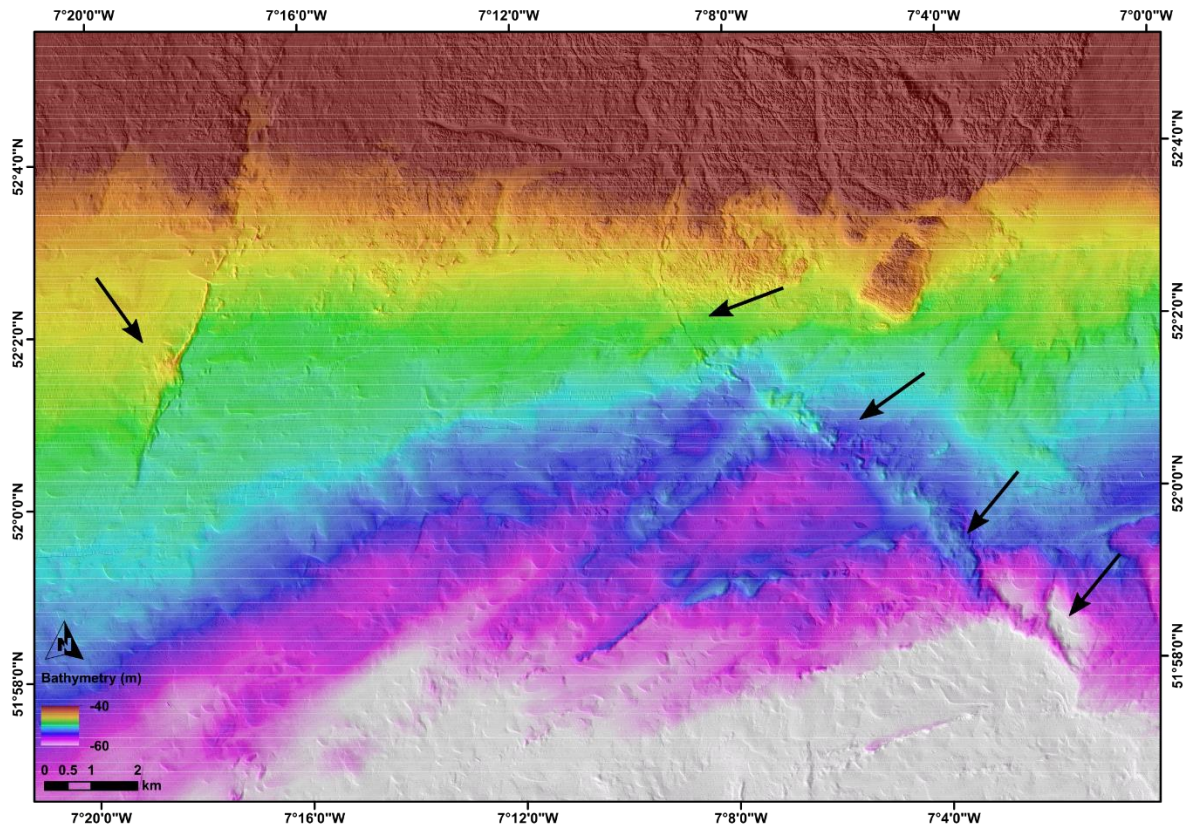


Figure 3.9 - INFOMAR bathymetry and hillshaded relief (240° illumination for clarity) image of sinuous ridges (black arrows) south of the southern Irish coastline. For image location, see Area 2 in Figure 3.7.

### Overdeepened Channels

Along the southern Irish coast between 20 km south of Ram Head and 25 km south of Galley Head are a series of large channels with evidence of overdeepening along their thalweg (Figure 3.7 and Image E in Table 3.1). In cross-section, the channels extend up to 14 m below the neighbouring banks and the channel mouths generally begin abruptly at 70 m water depth. The features extend beyond the dataset boundaries but are generally oriented coast-perpendicular in the north, but transition to almost coast-parallel in the southwest. Some channels exist as individual features, while others display complex bifurcation, in places with abrupt termini. To the southwest of the dataset, some channels are oriented perpendicular to large arcuate ridges (Area A in Figure 3.7).

Across the inner-shelf, regional bathymetric data show the presence of numerous channels of varying sizes. The largest of these channels is an individual feature on the Nymphe Bank Platform to the west of the southern boundary of the Celtic Deep (Figure 3.10). This feature is 71 km long, up to 3 km wide and overdeepened with a maximum cross-section relief of 33 m below its channel banks. Less prominent channels exist to the south and southeast of the Celtic Deep as both individual channels or bifurcated systems. The largest of these smaller channels is located on the eastern sector of the inner-



shelf and appears similar in size and morphology to those found on the southern Irish coast. Overdeepening of these features is not as observable, possibly due to the lower-resolution bathymetric data of the inner-shelf.

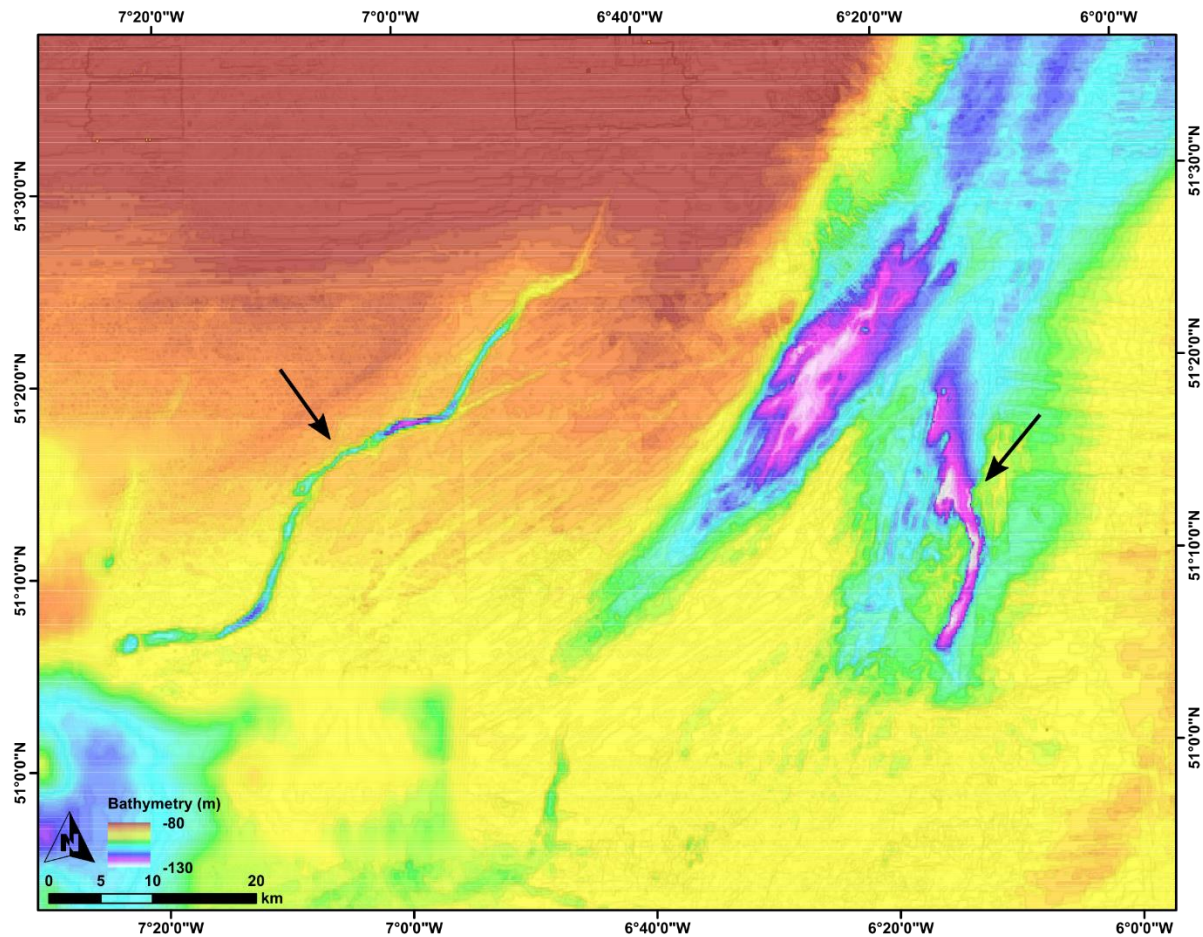


*Figure 3.10 - EMODnet bathymetry and slope map of prominent overdeepened channels (black arrows) on the Nymphe Bank Platform (left) and on the southern boundary of the Celtic Deep (right) adjacent to deep troughs. Dark and light areas denote steep and flat areas respectively. For image location, see Area 3 in Figure 3.7.*

These features are incised into areas of Upper Cretaceous chalk and Palaeogene deposits consisting of siliciclastic and argillaceous material and sandstone and have orientations and locations corresponding to changes in the underlying geology and its structure (Figure 1.6). Overdeepened channels found south of Ireland are oriented coast-parallel and coast-perpendicular to the southwest and northeast respectively. These orientations match those of local geological boundaries and faults, with channels commencing beyond the extent of Devonian and Carboniferous sandstone, mudstone and limestone. Similarly on the Lundy Platform, channels are bounded by Devonian and Carboniferous deposits to the southeast and Jurassic deposits to the north, with no apparent influence on channel orientation due to the underlying geological structures. The largest overdeepened channel, found on



the Nympe Bank Platform, overlies the southeast boundary of Upper Cretaceous chalk and aligns with the local geological boundary. Other channels in the central inner-shelf appear to have no correlation with the underlying geology or its structure.

### Arcuate Ridges

Large arcuate ridges exist between 30 km south of Toe head and 20 km south of Galley Head in water depths between 90-105 m (Figure 3.7 and Table 3.1). The ridges transition from narrow, continuous and more-defined ridges in the northeast (Image F in Table 3.1 and Figure 3.11) to wider and more discontinuous ridges in the southwest which are in places overprinted by irregular depressions.

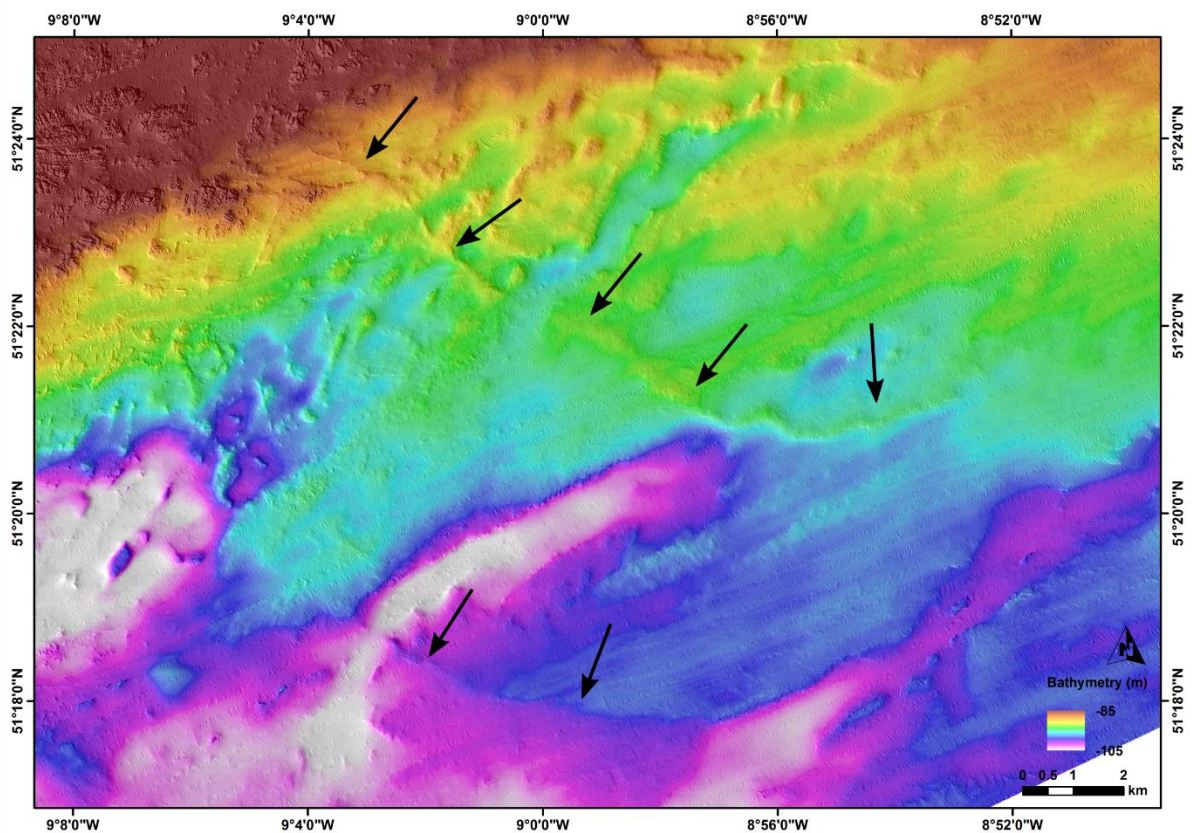


*Figure 3.11 - INFOMAR bathymetry and hillshaded relief (240° illumination for clarity) image of arcuate ridges (black arrows) and neighbouring features southwest of the southern Irish coastline. For image location, see Area 4 in Figure 3.7.*

### Smooth Elongate Mounds

To the northwest of Land's End there is a field of smooth and elongate mounds (Figure 3.12). The field extends southwest towards the northwest coast of the Isles of Scilly between water depths between 70-90 m (Figure 3.7 and Table 3.1). The elongate mounds have a consistent southwest orientation throughout the field (Plot I and Image G in Table 3.1). These features exist in an area of Devonian and Carboniferous sandstone, mudstone and limestone bedrock adjacent to the Isles of Scilly and offshore of the coast of Cornwall (Figure 1.6).

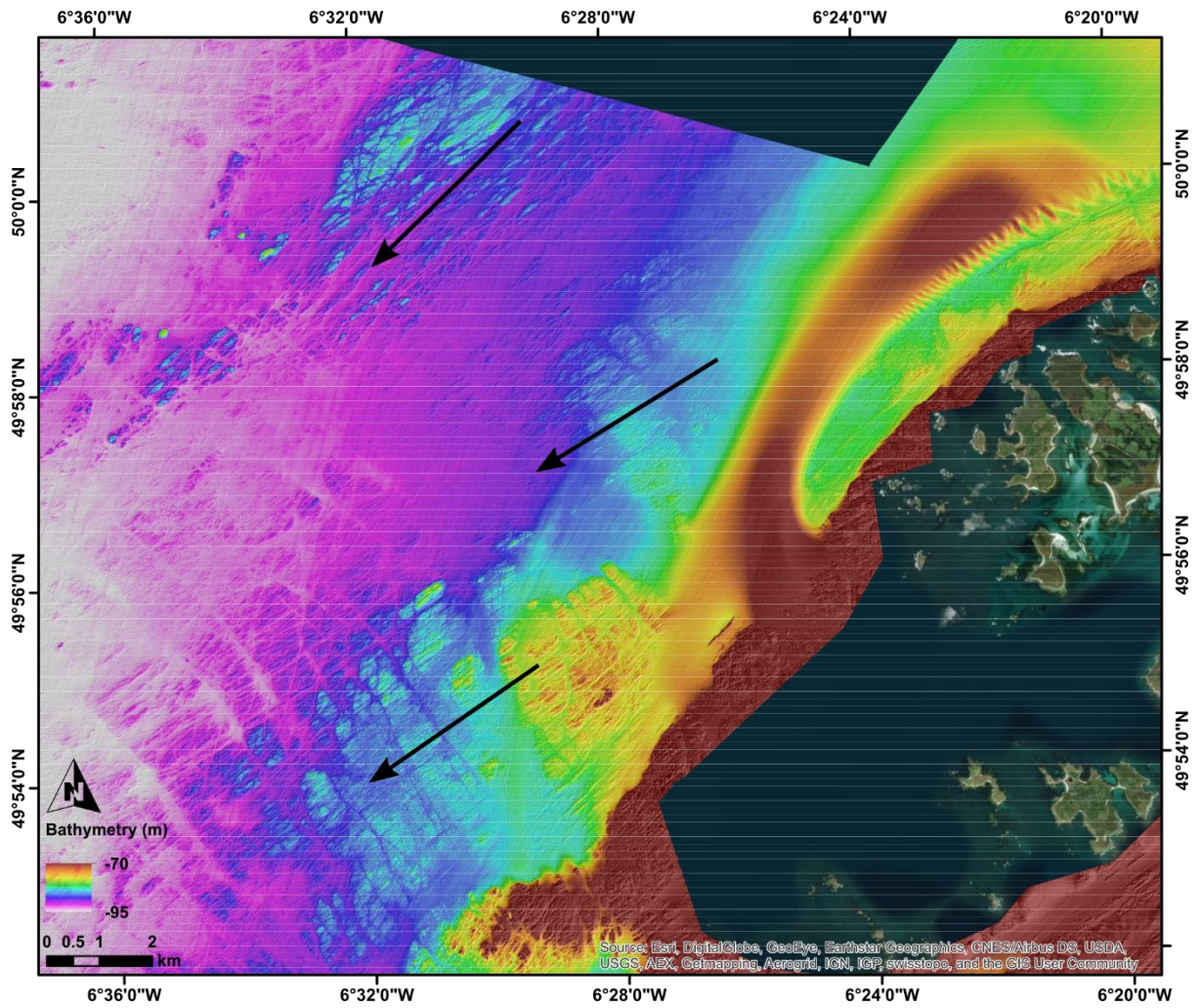


Figure 3.12 - UKHO bathymetry and hillshaded relief (140° illumination for clarity) image of southwest oriented (black arrows) smooth elongate mounds with satellite imagery. For image location, see Area 5 in Figure 3.7.



### 3.2 Sub-seafloor Stratigraphy

The following images represent acoustic cross-sections of the seafloor showing the underlying structure as represented by distinct reflections. Thus, the vertical scale is in two-way-time in ms and the sections are vertically exaggerated. The depth represented by the time in ms can be calculated using an assumed sound velocity in the underlying sediments, here assumed to be  $1600 \text{ m}\cdot\text{s}^{-1}$ . These individual sections provide detail on the various acoustic packets which comprise the shelf. These observations are then summarised to provide an overview as to the acoustic character and stratigraphic position of these units to aid with their correlation to previous observations.

#### 3.2.1 Seismic Sections and Seismic Facies

Seismic reflection data collected across the shelf reveal the shallow stratigraphy of the Celtic Sea. Twenty-seven seismic lines (Figure 3.13) highlight the acoustic character and stratigraphic position of 11 major Seismic Facies (SF) in various settings to show their spatial variability across the area as not all facies are present in each region.

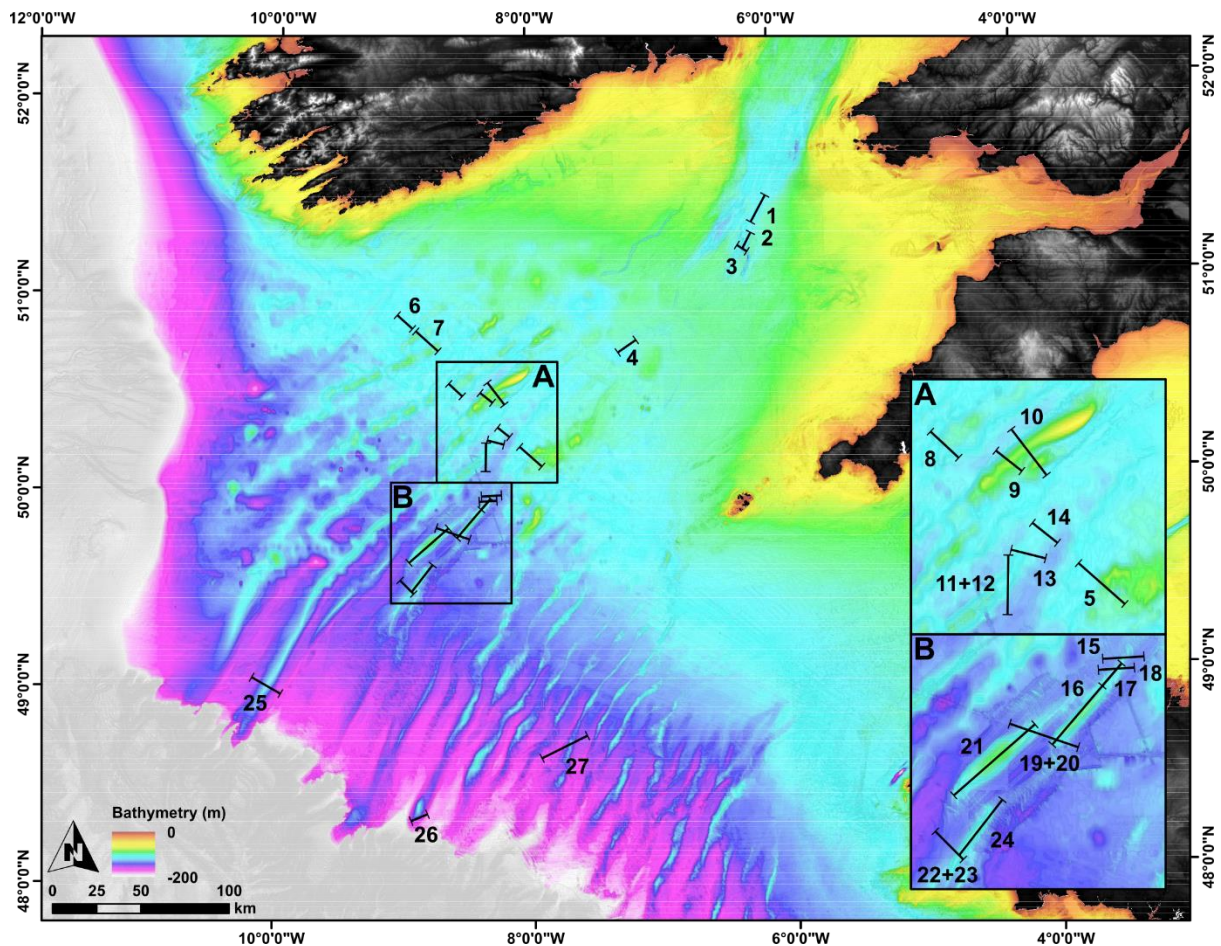


Figure 3.13 - EMODnet bathymetry and slope map showing the location of seismic lines referred to in this chapter.

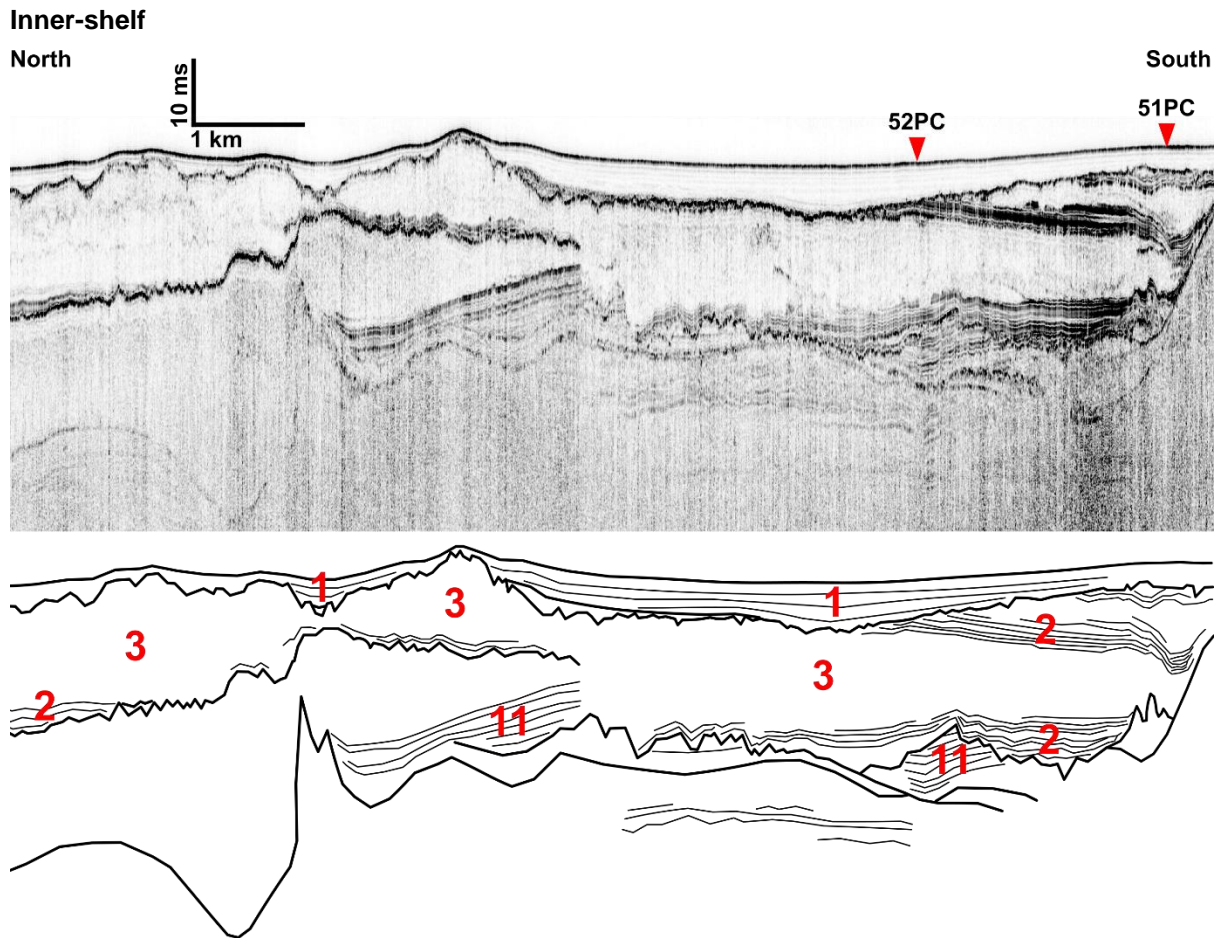


Figure 3.14 - JC-106 chirp seismic reflection data with selected physical sample locations and interpretation with seismic facies. See Line 1 in Figure 3.13 for location.

In the Celtic Deep, the uppermost seismic facies comprising the smooth seafloor is a low amplitude drape, transitioning downward to medium amplitude fill in places at its base (Figure 3.14). SF1 varies in thickness from less than 1 ms where an underlying unit rises to form a topographic high, to 7 ms in a basin between highs. The lower reflection of SF1 is of medium to high amplitude, continuous throughout this section but highly irregular, truncating reflections below.

Below this continuous reflection, SF2 and SF3 vary laterally, as if SF3 is low amplitude with bands of SF2, comprising medium to high amplitude parallel bands (Figure 3.14). The parallel bands of SF2 vary in thickness from 1 ms to 5 ms and are separated by SF3 comprising low amplitude fill up to 15 ms thick. The lower surface of SF2 and 3 is of low to medium amplitude and truncates reflections below, existing as an irregular surface. In places, this reflection is draped by a band of material up to 2 ms thick, consisting of parallel medium amplitude reflections similar to SF2. Therefore, it is possible that this reflection represents a continuation of the base of SF2. Additionally, this reflection continues for at least 19 km until the end of the dataset in the northeast. SF2 which drapes this reflection decreases in frequency and amplitude upward until it blends into SF3 where it often contains very discontinuous low amplitude reflections.

Below the base reflection of SF2, a variety of parallel facies are truncated by overlying reflections, comprising SF11 (Figure 3.14). This facies rests upon a smooth and highly undulating reflection which even appears to rise and form a sub-surface pinnacle.

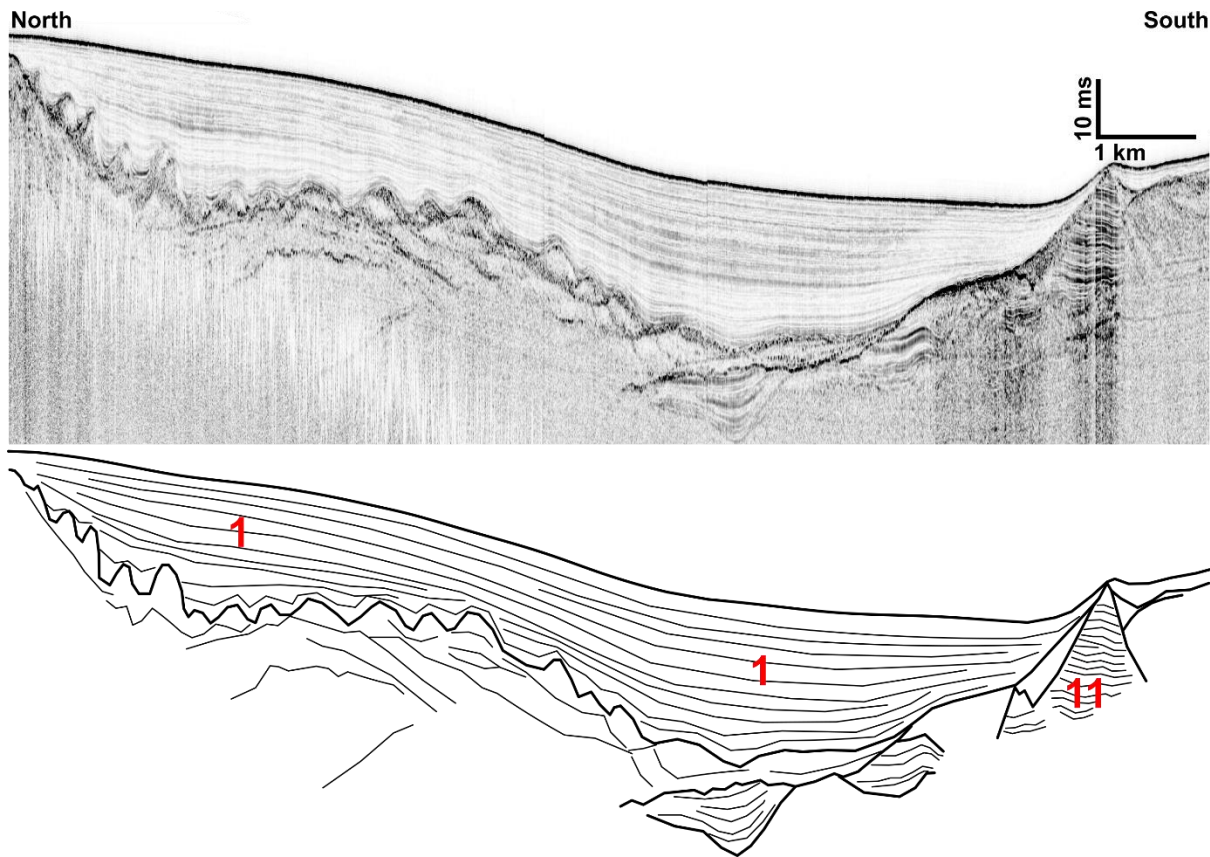


Figure 3.15 - JC-106 chirp seismic reflection data and interpretation with seismic facies. See Line 2 in Figure 3.13 for location.

At the southern boundary of the Celtic Deep, the seafloor appears smooth where a basin allows the thickest accumulation of SF1 which thins over topographic highs but extends up to 30 ms thick (Figure 3.15). SF1 comprises a low amplitude drape which overlies an undulating low to medium amplitude base reflection. There appears to be an upward transition in SF1 where reflections exist as sub-horizontal and the amplitude of reflections increases slightly. Underlying SF1 is a train of smooth mounds which produce an undulating surface. These mounds are up to 7 ms thick and comprise low to medium amplitude fill only on the north slope of the basin where some mound asymmetry is observed.

To the south of the section, a rising pinnacle comprises SF11 (Figure 3.15). This facies contains truncated sub-horizontal reflections of medium to high amplitude.



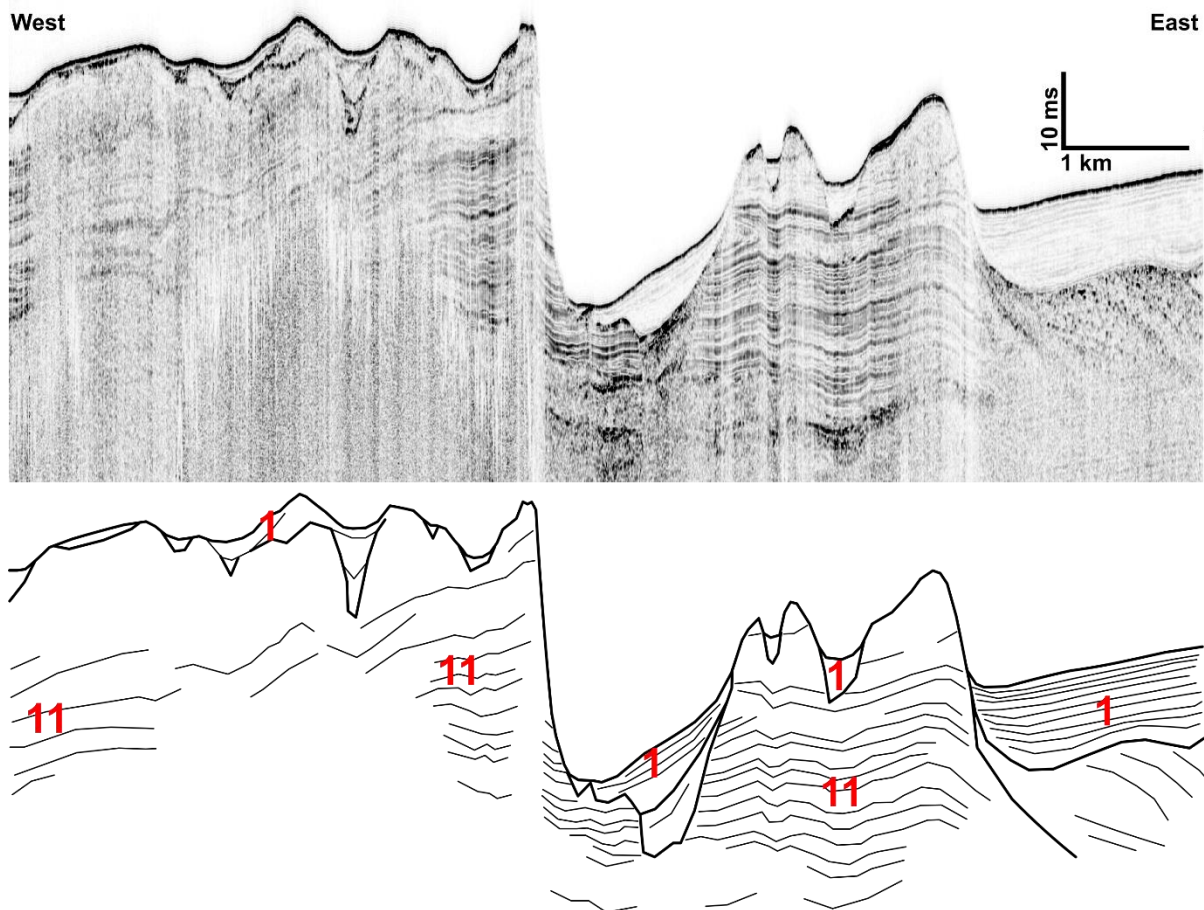


Figure 3.16 - JC-106 chirp seismic reflection data and interpretation with seismic facies. See Line 3 in Figure 3.13 for location.

Further south at the deepest section of the Celtic Deep the seafloor becomes more irregular (Figure 3.16). Here SF1 attains its thickest accumulation, up to 10 ms thick between rising pinnacles which outcrop at the seafloor where SF1 appears to not exist. The character of SF1 is consistent throughout the Celtic Deep where it drapes the bottom bathymetry of the basin in which it has accumulated and in places transitions downward into medium amplitude fill.

SF11 consists of truncated reflections which are sub-horizontal and appear to have a constant dip (Figure 3.16). These reflections are truncated against a smooth and undulating surface which incises SF11 to form channels which vary in size. This facies outcrops at the seafloor, resulting in SF1 being discontinuous.

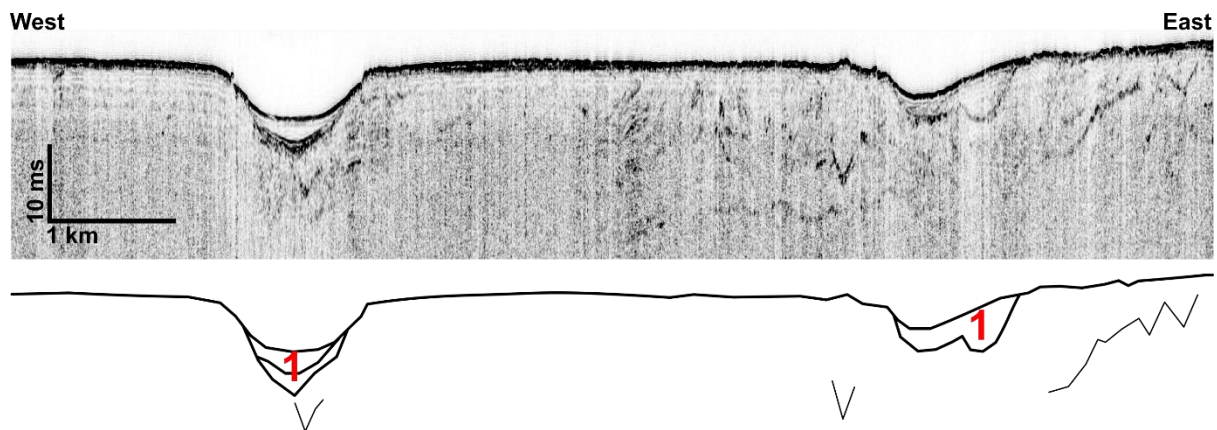


Figure 3.17 - JC-106 chirp seismic reflection data and interpretation with seismic facies. See Line 4 in Figure 3.13 for location.

Across the inner-shelf on the Haig Fras Platform, SF1 thins significantly and is up to 5 ms thick where it infills incised channels at the seafloor (Figure 3.17). These surface channels appear smooth and U-shaped, contrasting with channels which exist deeper in the section which are V-shaped.

#### Mid-shelf

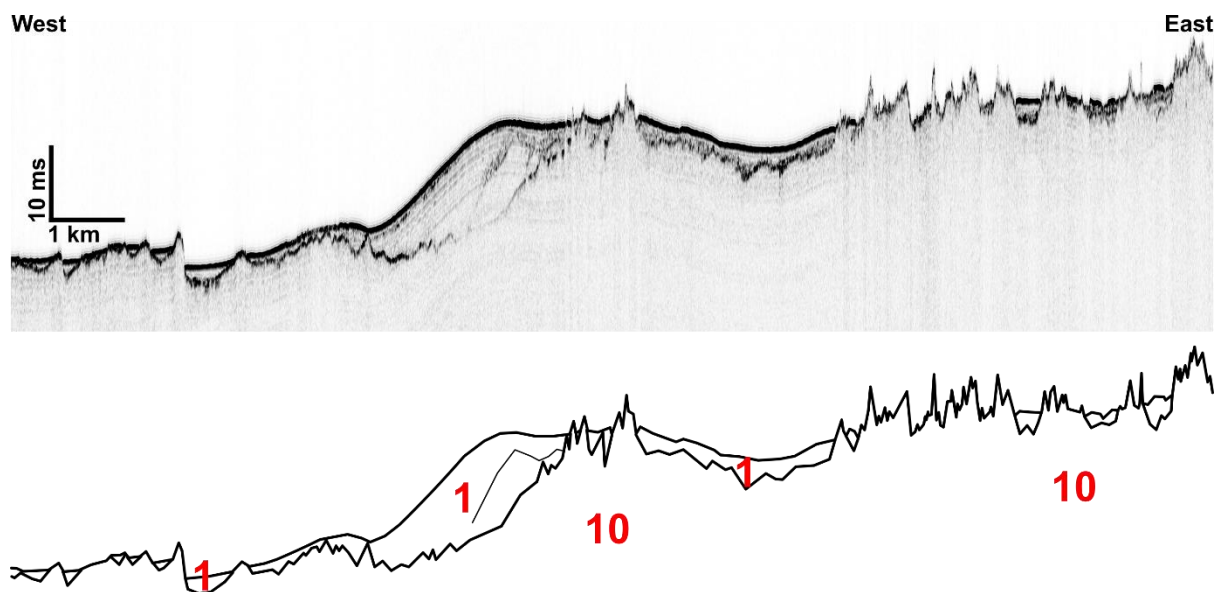
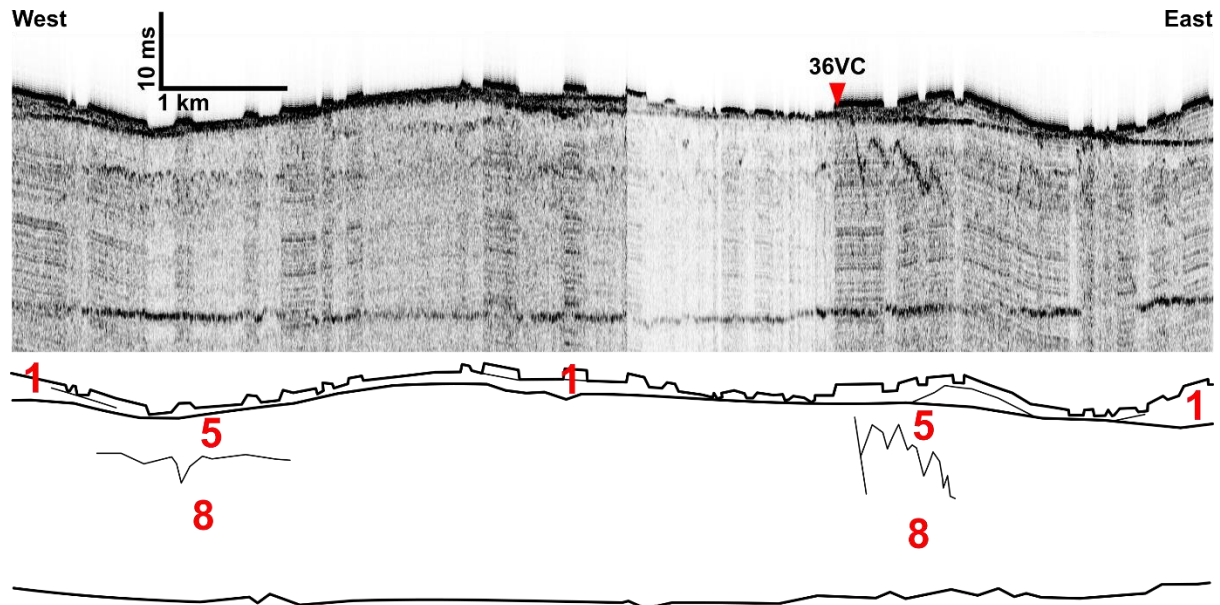


Figure 3.18 - JC-106 chirp seismic reflection data and interpretation with seismic facies. See Line 5 in Figure 3.13 for location.

To the west of Haig Fras, SF10 dips to the west where overlying facies become more continuous and thicker (Figure 3.18). SF1 is very discontinuous in this area as it infills depressions, existing as a low amplitude fill generally up to 3 ms thick. However, in places SF1 extends up to 12 ms thick.

SF10 outcrops at the seafloor and has no internal reflections (Figure 3.18). The upper surface of this facies is highly irregular throughout this section.



*Figure 3.19 - JC-106 chirp seismic reflection data with selected physical sample locations and interpretation with seismic facies. See Line 6 in Figure 3.13 for location.*

Beyond the ridge field to the northwest, a simple layered stratigraphy exists (Figure 3.19). SF1 comprises undulating mounds mantled by distinct raised platforms which are discontinuous and exist up to 3 ms thick. In places, these raised platforms overlie a reflection which then merges with the seafloor return. SF1 in its entirety extends up to 5 ms thick and this facies overlies a continuous medium to high amplitude reflection. This facies is of higher amplitude than equivalent facies in the Celtic Deep and other depressions on the inner-shelf.

Below this reflection is SF5, a discontinuous layer which is low amplitude in character, infilling an irregular low to medium amplitude surface (Figure 3.19). This facies can be up to 7 ms thick.

Below this irregular surface is SF8 which is up to 20 ms thick (Figure 3.19). The acoustic character of this facies is hard to define due to systematic noise in the seismic section, however its upper surface is irregular and it overlies a continuous high amplitude horizontal reflection.



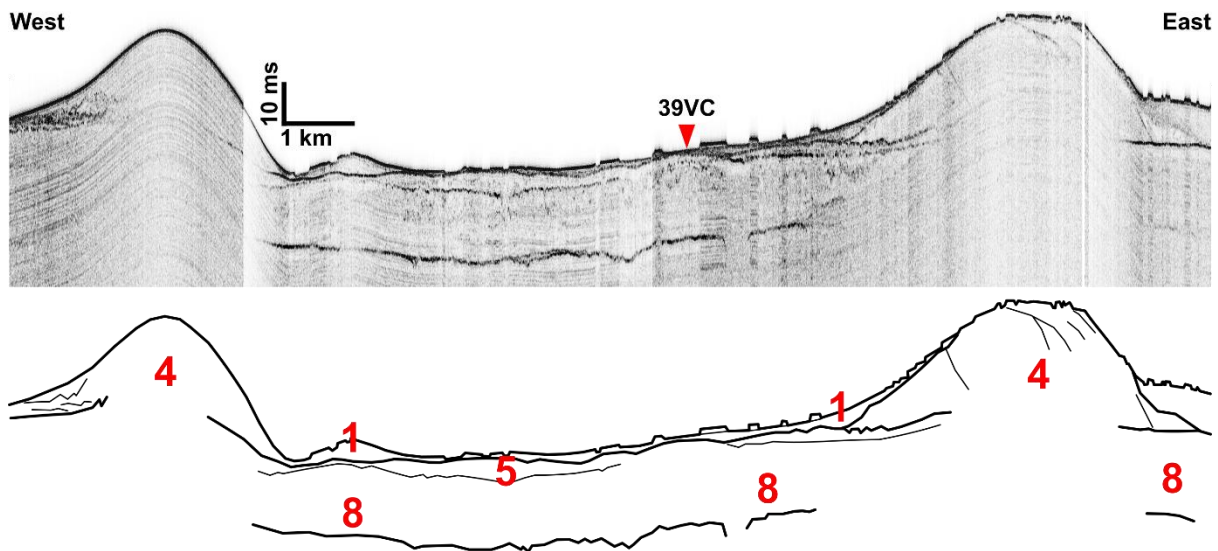


Figure 3.20 - JC-106 chirp seismic reflection data with selected physical sample locations and interpretation with seismic facies. See Line 7 in Figure 3.13 for location.

The previously described stratigraphy (Figure 3.19) is similar to that shown here within the ridge field apart from the addition of SF4 comprising the ridges (Figure 3.20).

SF1 comprises discontinuous raised platforms which exist across the section at the seafloor, overlying a medium amplitude reflection (Figure 3.20). The acoustic character of SF1 varies laterally throughout this section between low and medium amplitude and the layer is up to 5 ms thick.

SF4 contains dipping internal reflections which are truncated against the upper surface of the eastern ridge (Figure 3.20). Similar reflections are not observed on the ridge to the west. Both instances of SF4 overlie a medium to high amplitude horizontal reflection which is not observed directly under the crest of SF4 due to signal attenuation. However, it is likely that this reflection continues under SF4 and SF1 across the section, resulting in SF4 being up to 30 ms thick.

Below this reflection is SF5, a low amplitude thin layer which pinches out at its upper surface in places, and extends up to 5 ms thick (Figure 3.20). The base reflection of SF5 is of medium amplitude and partially discontinuous in places.

SF8 is up to 20 ms thick and contains very discontinuous low amplitude reflections (Figure 3.20). This facies overlies a distinct high amplitude reflection which appears to have been channelled and may traverse the entire section.

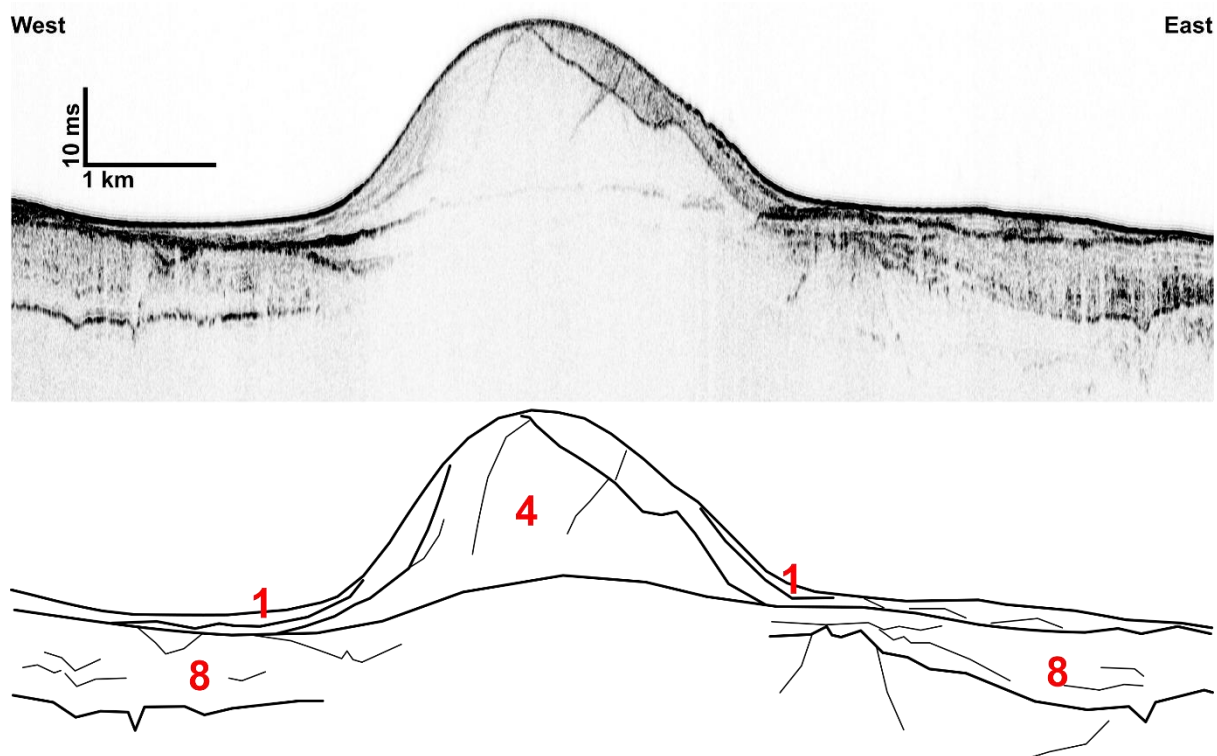


Figure 3.21 - JC-106 chirp seismic reflection data and interpretation with seismic facies. See Line 8 in Figure 3.13 for location.

SF1 is a discontinuous thin layer which is generally low amplitude in character and extends up to 3 ms thick on the flanks of SF4 (Figure 3.21).

SF4 forms the upper bulk of the ridge and displays internal reflections which have a consistent dip throughout the ridge bulk and are truncated against the upper surface (Figure 3.21). Here SF4 displays a transition from low amplitude to a medium amplitude drape which also contains a single dipping reflection. Together, SF4 is up to 20 ms thick and rests on a continuous base reflection which is imaged to be of high amplitude on the lower flanks of the ridge where SF1 overlies it. This base reflection rises, and this is attributed to acoustic pull-up because of increasing thickness of SF4 above which has a faster sound velocity compared to the water column either side of SF4.

Below this continuous reflection is SF8 which appears to comprise discontinuous low to medium amplitude parallel reflections which is in places truncated against internal medium amplitude reflections or by the upper surface (Figure 3.21).

SF8 is up to 12 ms thick and only thins due to a sub-surface pinnacle below the eastern flank of the ridge (Figure 3.21). The base reflection of this unit is of high amplitude and is somewhat continuous, possibly displaying some channelling in places.

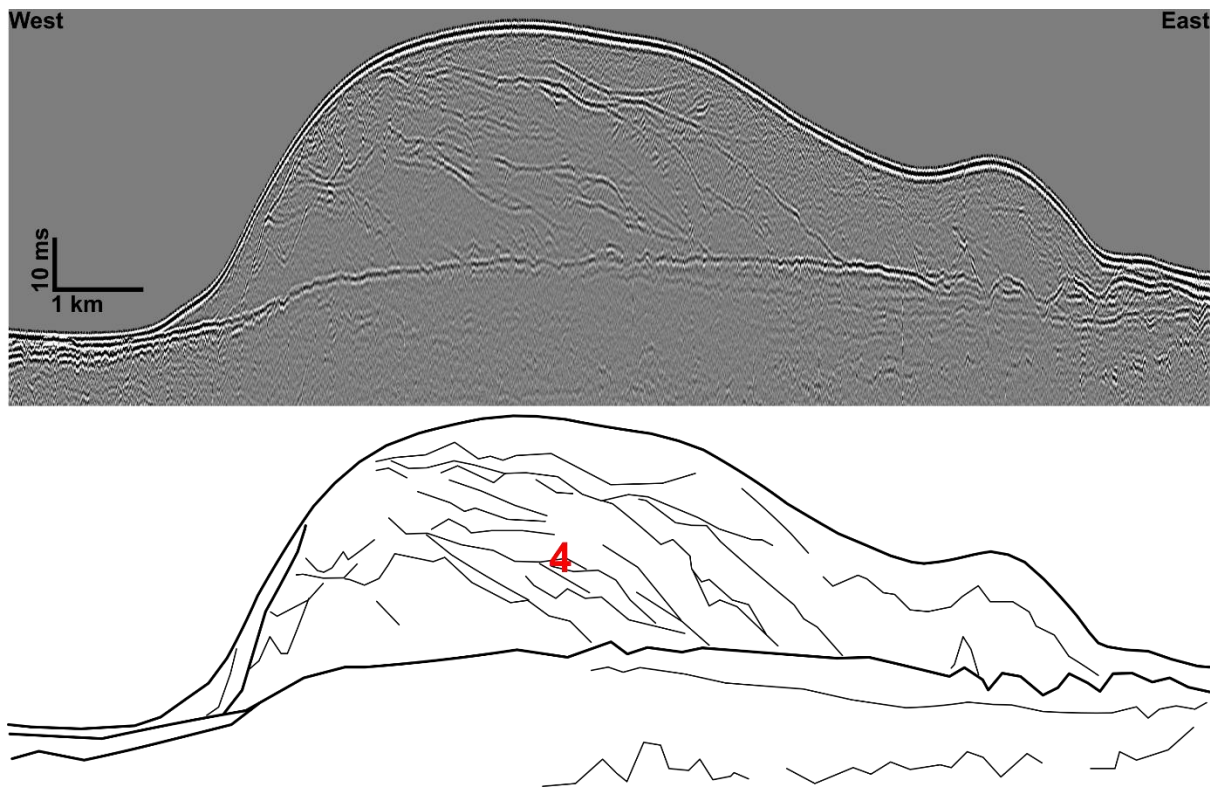


Figure 3.22 - CV14007 sparker seismic reflection data and interpretation with seismic facies. See Line 9 in Figure 3.13 for location.

At the largest ridge in this area, SF4 comprises the upper bulk of the feature where it is up to 40 ms thick (Figure 3.22). SF4 contains complex reflections which generally dip in a consistent direction throughout the bulk of the ridge which displays some asymmetry. These reflections appear truncated against the upper surface of the ridge and dip in the direction of the asymmetry. Underlying SF4 is a distinct base reflection against which the dipping reflections terminate. This base reflection appears to rise slightly, however this is most likely due to acoustic pull-up because of SF4 above.

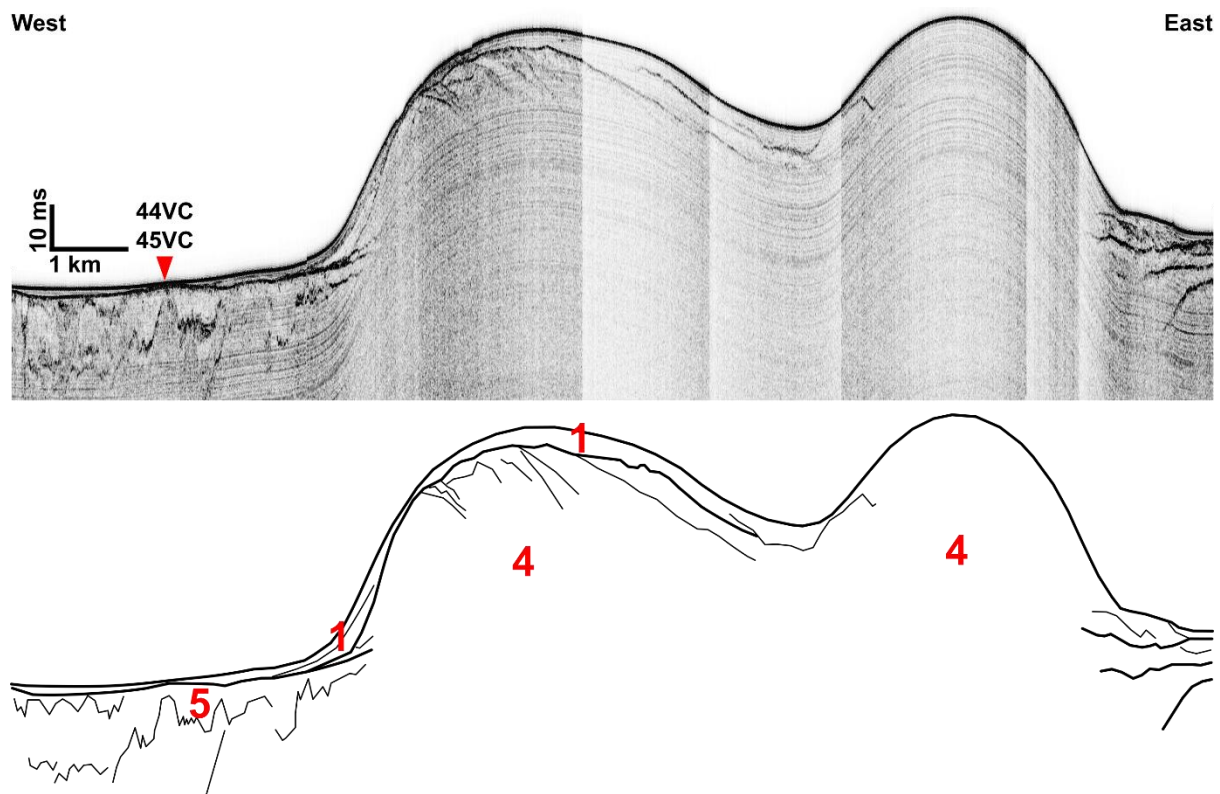


Figure 3.23 - JC-106 chirp seismic reflection data with selected physical sample locations and interpretation with seismic facies. See Line 10 in Figure 3.13 for location.

SF1 varies in thickness from less than 1 ms up to 8ms on a slope in proximity to SF4 but is commonly less than 2 ms in the low areas (Figure 3.23). This facies has a medium to low amplitude character which appears to vary laterally upslope. The lower surface of SF1 varies between a very high amplitude, smooth and continuous reflection in low-lying areas, and a low to medium amplitude continuous reflection which truncates the internal reflections of SF4.

The internal reflections of SF4 are truncated against the upper surface of the ridge (Figure 3.23) as similarly seen on sparker data to the south (Figure 3.22). In this section, two ridges have merged, both comprising SF4. However, no internal reflections have been identified within the adjoining ridge despite the fact that it also forms a positive feature overlying a high amplitude reflection imaged at its flank which may continue across the section to underlie the entirety of SF4 as seen on sparker data.

SF5 underlies the base reflection of SF4 up to 10 ms thick, thickening to the west while thinning to the east under SF4 (Figure 3.23). This facies is low amplitude in character, in places containing discontinuous and irregular low to medium amplitude reflections which are in places truncated against the upper surface. SF5 infills a highly irregular low to medium amplitude surface at its base which appears channelised. An acoustically comparable facies is not observed on the eastern flank of SF4.



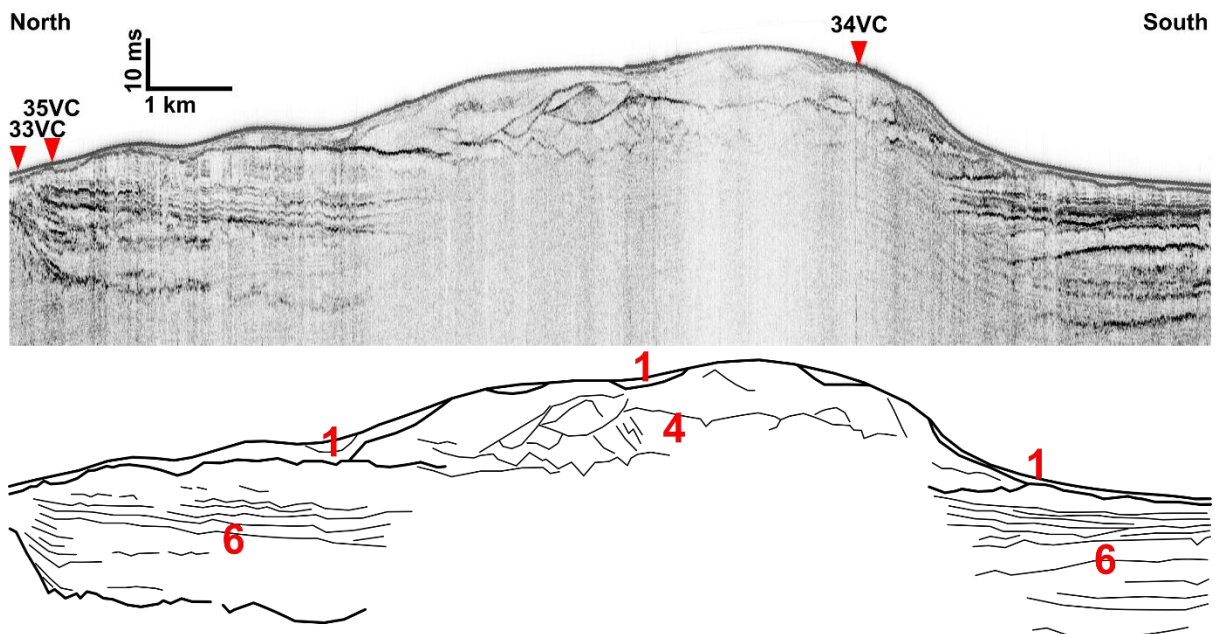
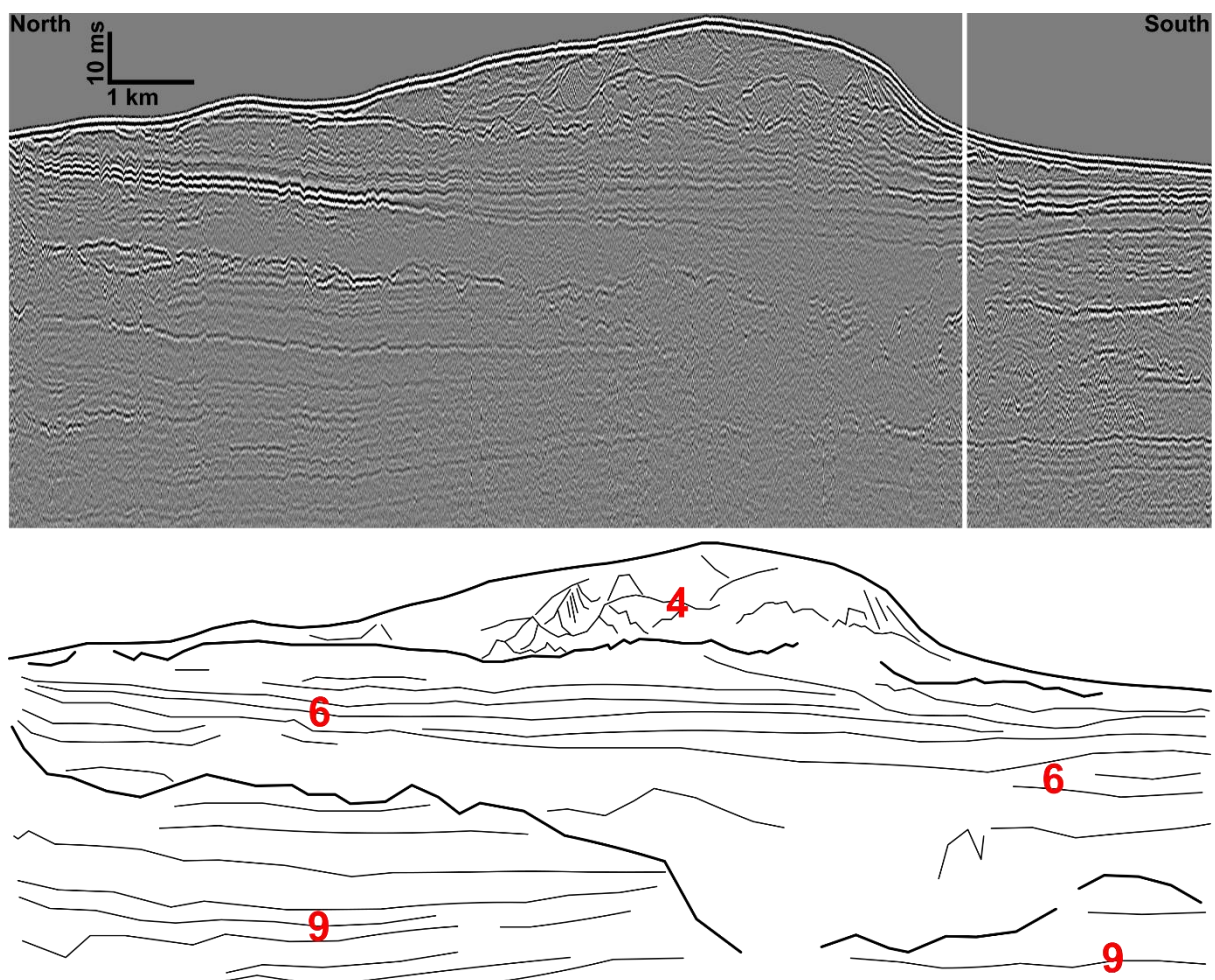


Figure 3.24 - JC-106 chirp seismic reflection data with selected physical sample locations along the same line as Figure 3.25 and interpretation with seismic facies. See Line 11 in Figure 3.13 for location.



*Figure 3.25 - CV14007 sparker seismic reflection data along the same line as Figure 3.24 and interpretation with seismic facies. See Line 12 in Figure 3.13 for location.*

SF1 consists of a low to medium amplitude layer which is discontinuous above SF4, varying in thickness up to 4 ms in depressions where it is mainly of low amplitude (Figure 3.24). In depressions flanking the ridge, SF1 overlies a high amplitude reflection, while above SF4 it is discontinuous, resting upon a low to medium amplitude reflection which pinches out at the seafloor in places. Where SF1 is discontinuous, it appears to have a higher amplitude compared to facies 1 in the flanking depressions.

SF4 comprises the ridge bulk, which is approximately 20 ms thick. SF4 displays complex internal reflections, where an upper acoustic packet is mostly low amplitude and contains a few low amplitude internal reflections, contrasting with a lower packet containing complex low to medium amplitude reflections (Figure 3.24). SF4 is bounded on its lower surface by a high amplitude reflection also overlain by SF1. Sparker data collected along the same line reveal the internal complexity of SF4 and suggest the continuation of the reflection underlying SF1 and 4 under the ridge. This reflection becomes somewhat irregular and difficult to trace under SF4 until it appears under the lower flank of the ridge to the south.

SF6 exists under this reflection which truncates internal reflections (Figure 3.24). This reflection rises on the ridge flank, forming the initial topographic control of the ridge slope. SF6 is up to 30 ms thick, with an upper layer comprising low to medium amplitude sub-parallel reflections which are discontinuous. This layer is imaged either side of the ridge below SF4 where it formed a raised plateau for SF4. With increasing depth through the upper layer of SF6, these reflections increase in amplitude and continuity before existing as medium to high amplitude parallel reflections that sparker data show are laterally continuous under SF4 (Figure 3.25). Toward the bottom of SF6, various discontinuous and low to medium amplitude reflections do not appear to be as continuous as the upper layer. These internal reflections drape SF9.

The upper surface of SF9 is an undulating reflection forming a surface that varies in height (Figure 3.25). It forms a plateau which appears to deepen to the south as seen on sparker data. These data show this upper surface to be laterally continuous despite areas where the reflection becomes very irregular and has a reduced amplitude due to signal attenuation from the ridge above. Below this surface are low to medium amplitude and parallel reflections which appear truncated against the upper surface of SF9 where it deepens and the horizontal reflections terminate.

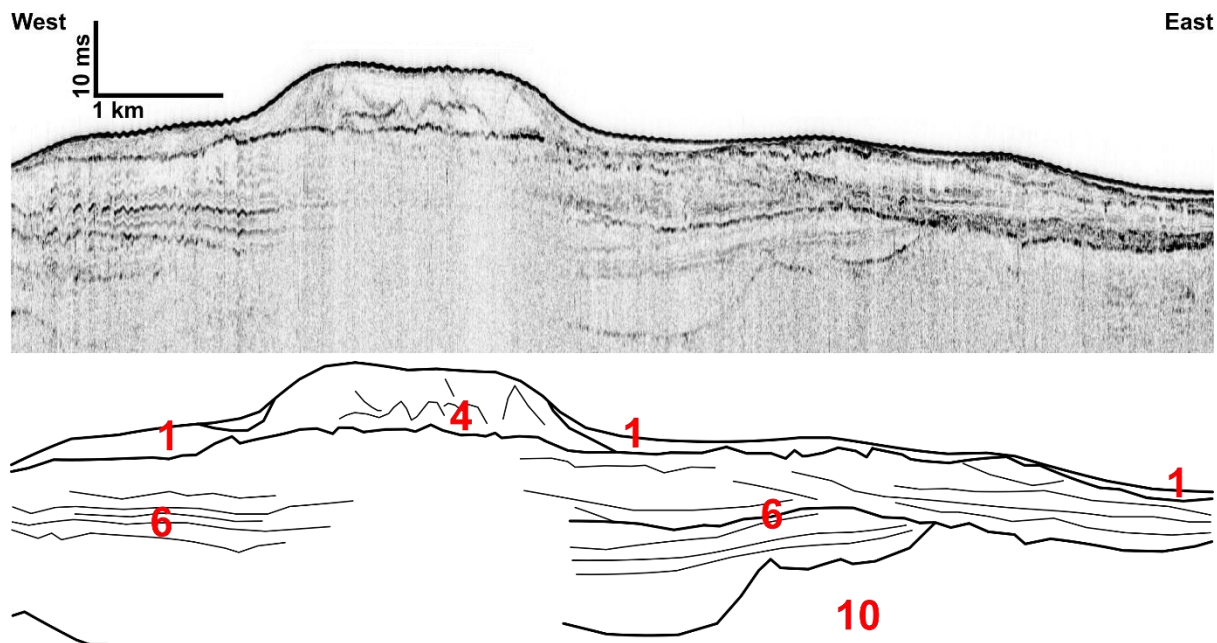


Figure 3.26 - JC-106 chirp seismic reflection data and interpretation with seismic facies. See Line 13 in Figure 3.13 for location.

To the north of the previous section, a similar stratigraphy is observed, however the height and width of the ridge has diminished. SF1 is a low amplitude layer up to 2 ms thick in depressions (Figure 3.26). This facies appears discontinuous across the section, especially to the west.

SF4 is thinner compared to previous sections, comprising a raised mound up to 9 ms thick (Figure 3.26). This facies contains low to medium amplitude reflections which appear regular, forming internal mounds or dipping surfaces. SF4 overlies a high to medium amplitude reflection which SF1 also overlies. This reflection is laterally continuous across the section and is generally sub-horizontal, forming a slight plateau for SF4.

The continuous reflection under SF1 and 4 appears to truncate reflections in SF6 which contains parallel reflections (Figure 3.26). SF6 is at least 25 ms thick, as it is not imaged in its entirety due to signal attenuation. The upper layer of SF6 contains low to medium amplitude discontinuous reflections which are in places truncated against the upper surface. To the west, the reflections within the upper layer of SF6 are of higher amplitude and become more continuous with increasing depth. Similar reflections exist to the east of the ridge. SF6 drapes a smoothly undulating surface of low to medium amplitude which forms a basin.

SF10 is of low amplitude and forms a basin topography which deepens toward the middle of the section (Figure 3.26).

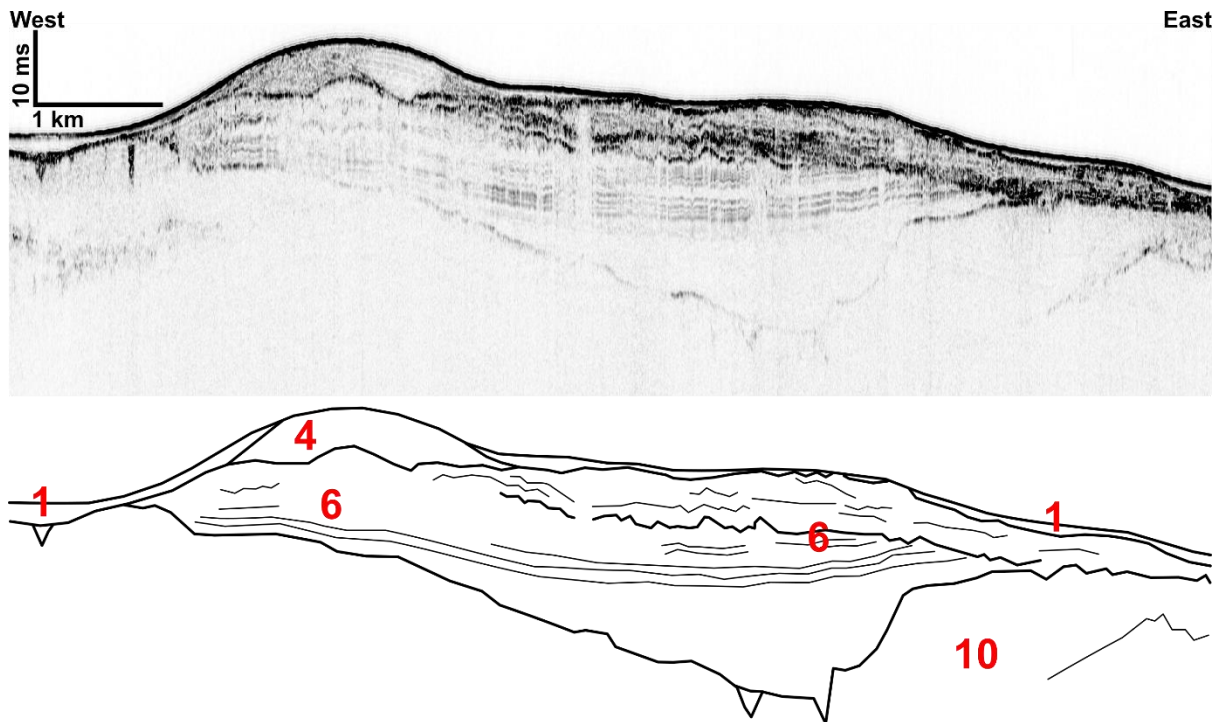


Figure 3.27 - JC-106 chirp seismic reflection data and interpretation with seismic facies. See Line 14 in Figure 3.13 for location.

At the northern end of the ridge, SF1 is of low amplitude in depressions and becomes discontinuous in places (Figure 3.27). This facies is up to 5 ms thick. SF1 overlies a distinct high amplitude continuous reflection either side of SF4.

SF4 is not easily distinguishable from SF1, as no distinct reflection separates them (Figure 3.27). SF4 is of higher amplitude than SF1 however, and forms a positive bank feature up to 7 ms thick. The medium amplitude fill of SF4 is disturbed in one instance where an area of low amplitude exists. This facies overlies a medium to high amplitude reflection which connects to the reflection underlying SF1. This reflection rises to form a plateau which in places is undulating.

SF6 comprises parallel low to medium amplitude reflections in upper and lower layers, both truncated against medium to high amplitude reflections forming the upper surfaces of each layer (Figure 3.27). The upper layer is up to 8 ms thick and is of higher amplitude and of a somewhat chaotic nature compared to the lower layer of up to 20 ms thick. This lower unit contains continuous reflections before transitioning downward to low amplitude fill with a lack of reflections.

The upper surface of SF10 is smooth and undulating, forming an asymmetric basin which deepens under SF6 (Figure 3.27). This surface appears to have been channelised.



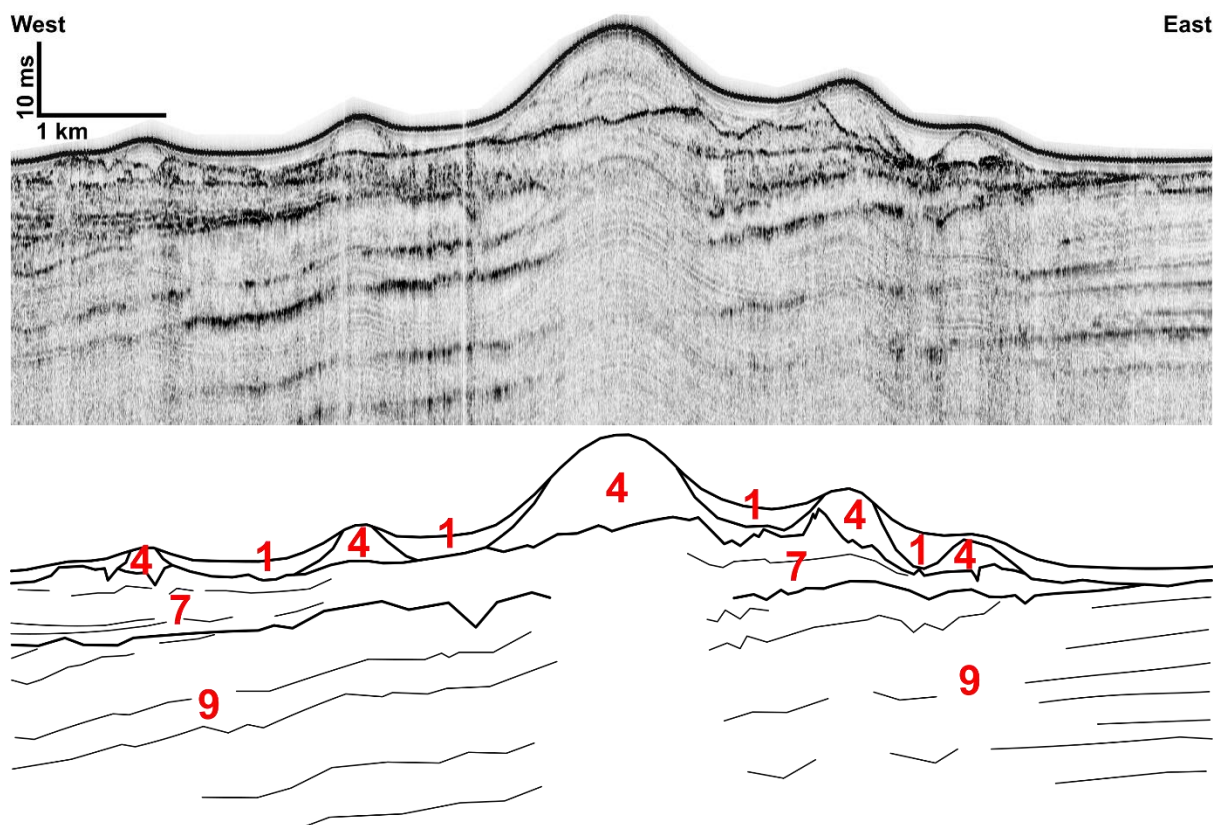


Figure 3.28 - JC-106 chirp seismic reflection data and interpretation with seismic facies. See Line 15 in Figure 3.13 for location.

On the northern flank of a mid-shelf ridge, SF1 varies in thickness from being discontinuous where underlying mounds outcrop near the seafloor to being up to 6 ms in depressions (Figure 3.28). Where SF1 infills depressions, it is of low amplitude.

SF4 comprises positive mounds, overlain by SF1 and resting upon a high amplitude reflection which undulates significantly in places (Figure 3.28). This facies is of low to medium amplitude with no internal reflections. The largest of these mounds is 13 ms thick and exists in the centre of the group of mounds which decrease in size away from the centre of the section. Outside of these mounds, SF4 is discontinuous.

SF7 is up to 10 ms thick and comprises various medium amplitude internal reflections which appear to be horizontally layered in places (Figure 3.28). The facies is of low to medium amplitude and is a layer which tapers out just beyond the horizontal extent of SF4. SF7 rests on a medium to high amplitude reflection which is also overlain by SF1 where SF4 is discontinuous. This base reflection can be irregular in places and in places is channelised.

SF9 comprises dipping low to high amplitude reflections which are parallel and are truncated against the upper surface (Figure 3.28). The dip of these reflections appears to steepen to the west, while reflections in the east have a gentler dip.

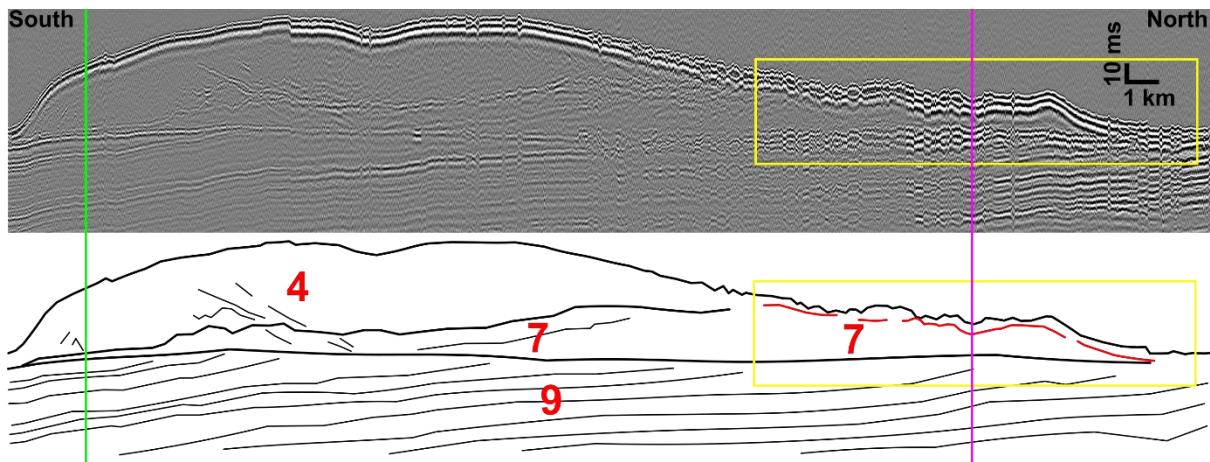


Figure 3.29 - IPY GLAMAR sparker seismic reflection data and interpretation with seismic facies. The yellow box indicates chirp data of Figure 3.30 with red showing the corresponding reflection depth. The green line indicates a tie point with Figure 3.33 and Figure 3.34. The magenta line indicates a tie point with the seismic section in Figure 3.30 and Figure 3.31. See Line 16 in Figure 3.13 for location.

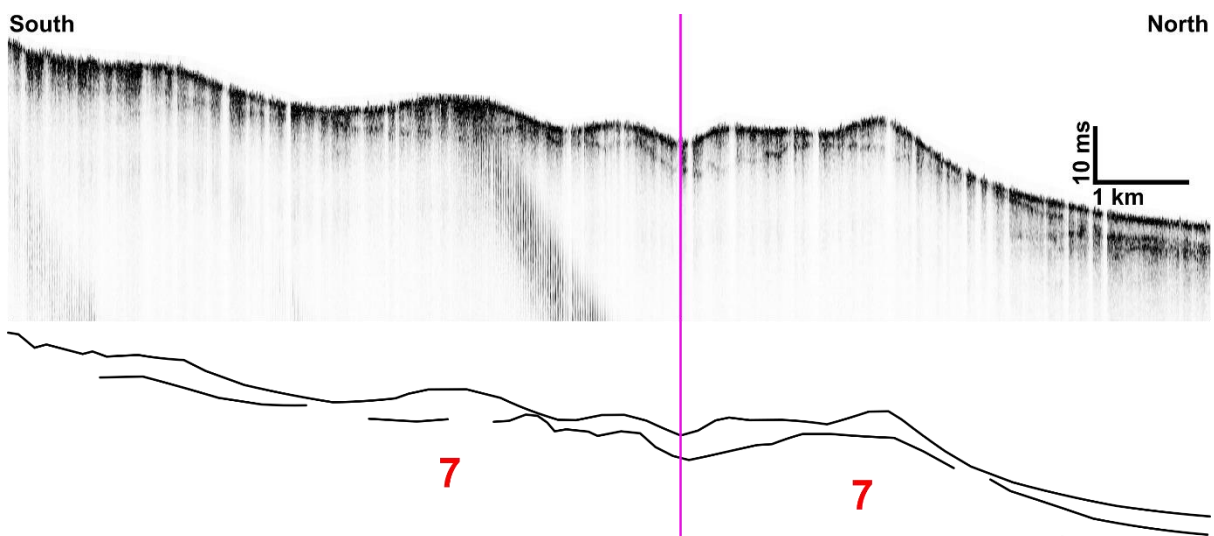


Figure 3.30 - IPY GLAMAR chirp seismic reflection data and interpretation with seismic facies. The magenta line indicates a tie point with the seismic section in Figure 3.29 and Figure 3.31. See Line 17 in Figure 3.13 for location.

On the mid-shelf, sparker data reveal the main facies along the crestline of a ridge (Figure 3.29). SF4 comprises the upper bulk of the ridge and appears to correspond to a smooth seafloor character towards the southern end of the ridge. This facies is up to 30 ms thick to the south, while to the north

SF4 thins as it overlies an additional facies which thickens to the north. SF4 contains low to medium amplitude reflections in places, some of which appear to dip. This facies rests above a surface which rises to the north within the ridge where this reflection cannot be distinguished from the seafloor return on sparker data. However, chirp data along the same line to the north (Figure 3.30) reveal a reflection at a similar height which may be the continuation of this reflection (Figure 3.29). Where this surface appears near the seafloor, the seabed is more irregular compared to that over SF4. Additionally, a break in slope is observed where SF4 initially thickens toward the south.

SF7 lies below this ridge-traversing reflection (Figure 3.29). This facies is up to 23 ms thick within the north of the ridge and it overlies a horizontal surface along its entirety, thinning to the south. This facies appears chaotic, containing some dipping reflections which appear truncated against its upper surface.

SF9 contains medium amplitude parallel reflections with a constant dip which are truncated against the upper horizontal surface of the facies (Figure 3.29).

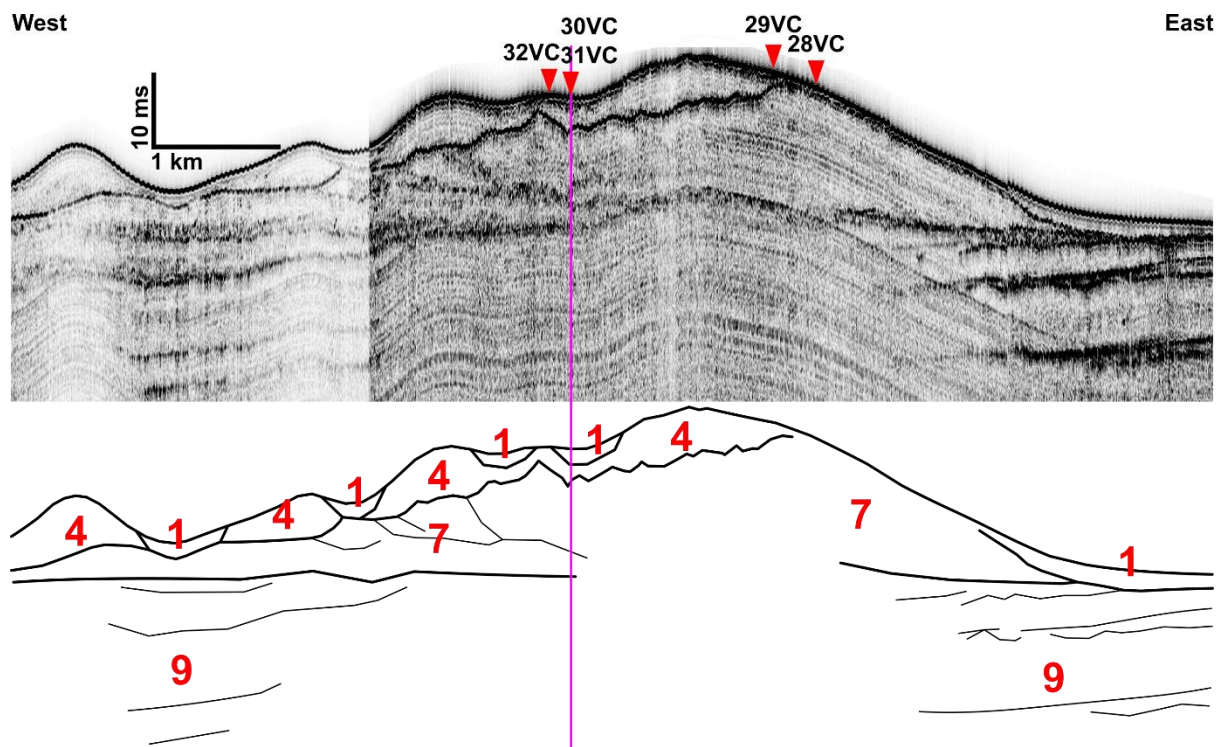


Figure 3.31 - JC-106 chirp seismic reflection data with selected physical sample locations and interpretation with seismic facies. The magenta line indicates a tie point with the seismic section in Figure 3.29 and Figure 3.30. See Line 18 in Figure 3.13 for location.

SF1 is a thin layer across the section, becoming discontinuous and forming isolated pockets of increased amplitude where it overlies SF4 and SF7 between raised mounds (Figure 3.31). In the neighbouring inter-ridge trough, SF1 is of low amplitude and is thicker at 4 ms.

SF4 comprises undulating mounds that appear reflection free and occur directly at the seafloor (Figure 3.31). These mounds overlie one side of SF7 and terminate laterally where SF7 is at its thickest.

The upper boundary of SF7 is high amplitude, continuous and irregular (Figure 3.31). This boundary rises to form an asymmetric mound comprising SF7 where it truncates reflections below. The acoustic character of this facies is of medium amplitude and containing dipping reflections. SF7 appears to overlie a flat base reflection.

SF9 exists below SF7 where it forms a flat base (Figure 3.31). The upper boundary of this facies truncates consistently dipping reflections comprising the internal acoustic character of the facies.

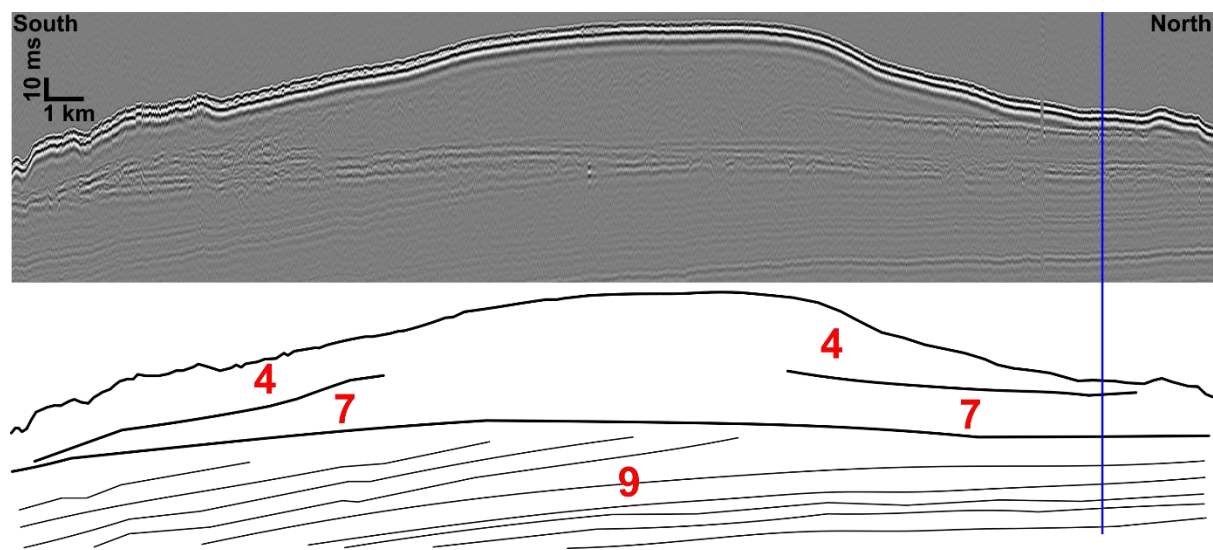


*Figure 3.32 - IPY GLAMAR sparker seismic reflection data and interpretation with seismic facies. The blue line indicates a tie point with the seismic section in Figure 3.33 and Figure 3.34. See Line 21 in Figure 3.13 for location.*

Along ridge data show that the upper bulk of the ridge comprises SF4 of up to 30 ms thick (Figure 3.32). This facies thins to the north and south. In these areas, the seafloor has an irregular surface, while the bulk of SF4 produces a smooth seafloor profile. Few internal reflections exist on sparker data. To the north, SF4 overlies a horizontal reflection which occurs near the seafloor. Throughout the ridge this reflection is discontinuous, and may be imaged on the southern end of the ridge.

SF7 contains chaotic reflections to the south where it gradually increases in thickness up to 15 ms (Figure 3.32). To the north, the upper surface appears irregular yet horizontal and no distinct internal reflections are observed. SF7 overlies a horizontal base which may possibly display channelling, however data quality does not allow for an accurate determination.



SF9 contains dipping parallel reflections which are truncated against the upper reflection (Figure 3.32). To the south, these reflections appear to dip more steeply compared to those observed to the north.

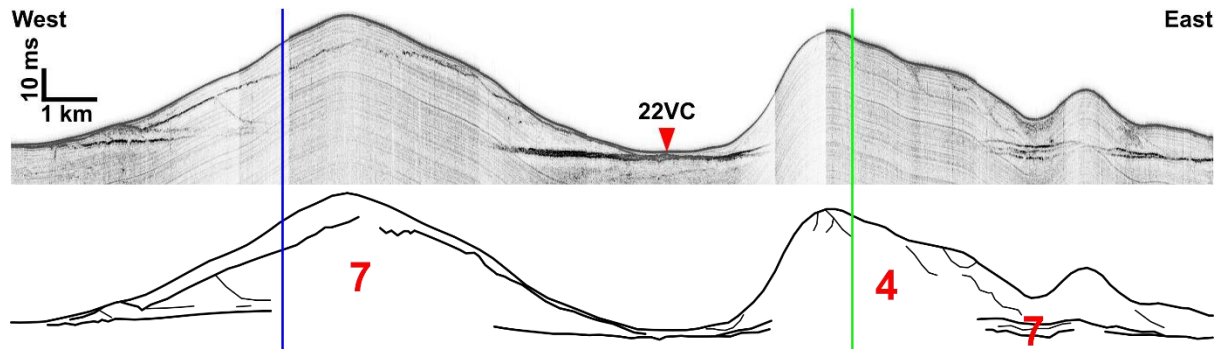


Figure 3.33 - JC-106 chirp seismic reflection data along the same line as Figure 3.34 with selected physical sample locations and interpretation with seismic facies. The green line indicates a tie point with the seismic section in Figure 3.29 and Figure 3.34. The blue line indicates a tie point with the seismic section in Figure 3.34 and Figure 3.32. See Line 19 in Figure 3.13 for location.

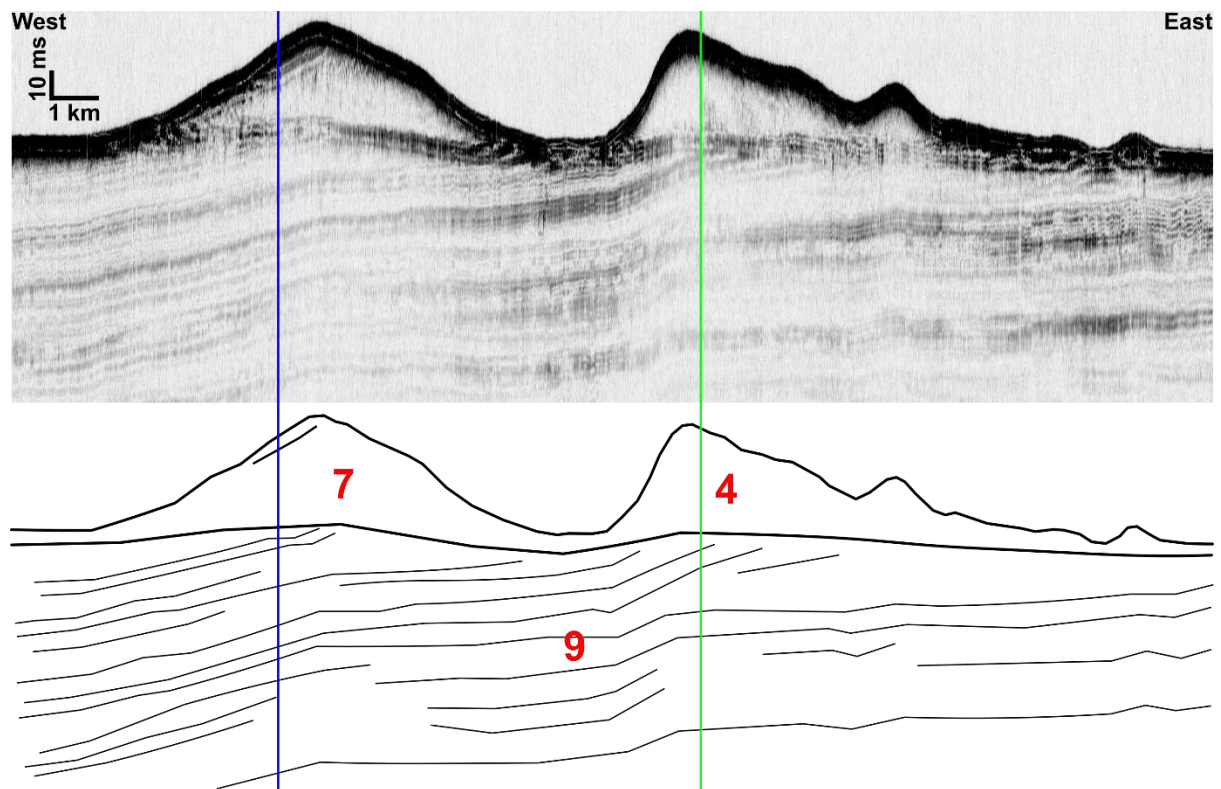


Figure 3.34 - IPY GLAMAR sparker seismic reflection data along the same line as Figure 3.33 and interpretation with seismic facies. The green line indicates a tie point with the seismic section in Figure 3.29 and Figure 3.33. The blue line indicates a tie point with the seismic section in Figure 3.33 and Figure 3.32. See Line 20 in Figure 3.13 for location.

Chirp (Figure 3.33) and sparker (Figure 3.34) data collected across two ridges show how the morphology of the ridge changes in response to internal facies present. The western ridge comprises SF7 where it produces a symmetrical ridge profile and is up to 30 ms thick (Figure 3.33). These chirp data show that SF7 has a medium to high amplitude upper reflection which appears irregular at the peak of the mound. This facies contains few internal reflections, but where they are observed they appear truncated against the upper surface.

This contrasts with the eastern ridge which has a distinct asymmetrical shape, comprising SF4 forming the bulk up to 35 ms thick which overlies a thinned SF7 as seen on chirp data (Figure 3.33). Some dipping reflections exist which are truncated against the upper surface of SF4. The seafloor undulates on the eastern side of the ridge due to the character of SF4.

Both ridges overlie SF9 where dipping parallel reflections are truncated against the upper horizontal surface (Figure 3.34).

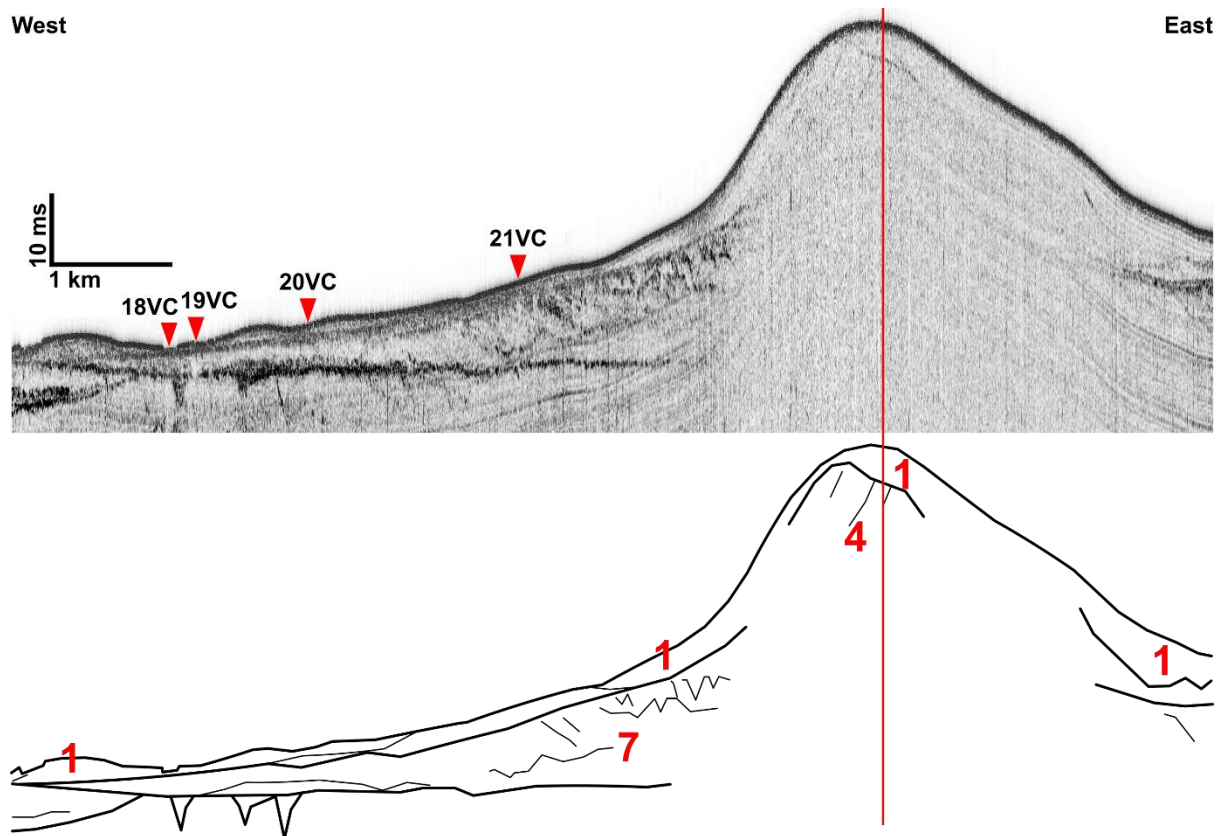
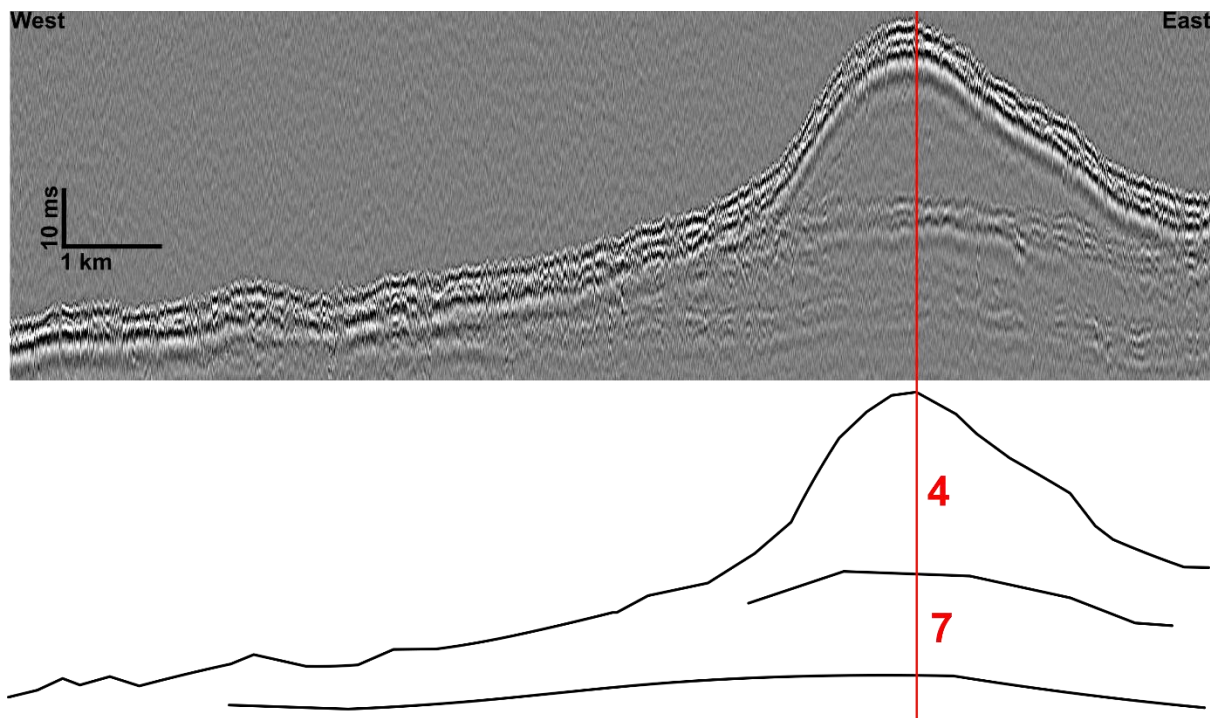


Figure 3.35 - JC-106 chirp seismic reflection data along the same line as Figure 3.36 with selected physical sample locations and interpretation with seismic facies. The red line indicates a tie point with the seismic section in Figure 3.36 and Figure 3.37. See Line 22 in Figure 3.13 for location.



*Figure 3.36 - IPY GLAMAR sparker seismic reflection data along the same line as Figure 3.35 and interpretation with seismic facies. The red line indicates a tie point with the seismic section in Figure 3.35 and Figure 3.37. See Line 23 in Figure 3.13 for location.*

SF1 consists of a thin layer of up to 5 ms thick and appears as a low to medium amplitude layer (Figure 3.35). This facies is at its thickest where it overlies SF4. In several places on the lower ridge flank, this unit becomes discontinuous, pinching out at the seafloor. Where this occurs, there is a noticeable notch in the seafloor profile.

SF4 makes up the ridge bulk and has a low amplitude upper surface which truncates equally low amplitude dipping internal reflections at the peak of the ridge (Figure 3.35). The base of this unit cannot be imaged on chirp data. However, sparker data for the same line show a medium amplitude reflection traversing across the ridge at depth, suggesting that SF4 is up to 25 ms thick (Figure 3.36). Where SF4 exists, its lateral extent corresponds to a distinct change in seafloor slope.

SF7 is up to 15 ms thick and bounded on its upper surface by a reflection which forms a base for SF1 and 4 (Figure 3.35 and Figure 3.36). This reflection rises on the ridge flank, forming the initial topographic control of the ridge slope and appears to truncate complex internal reflections of low to medium amplitude below. These complex and sometimes dipping reflections are only found in proximity to SF4 near the centre of the ridge. Toward the ridge flank, SF7 becomes low amplitude in character with a thin medium to high amplitude chaotic layer at its base. This facies overlies a horizontal reflection which is channelised.



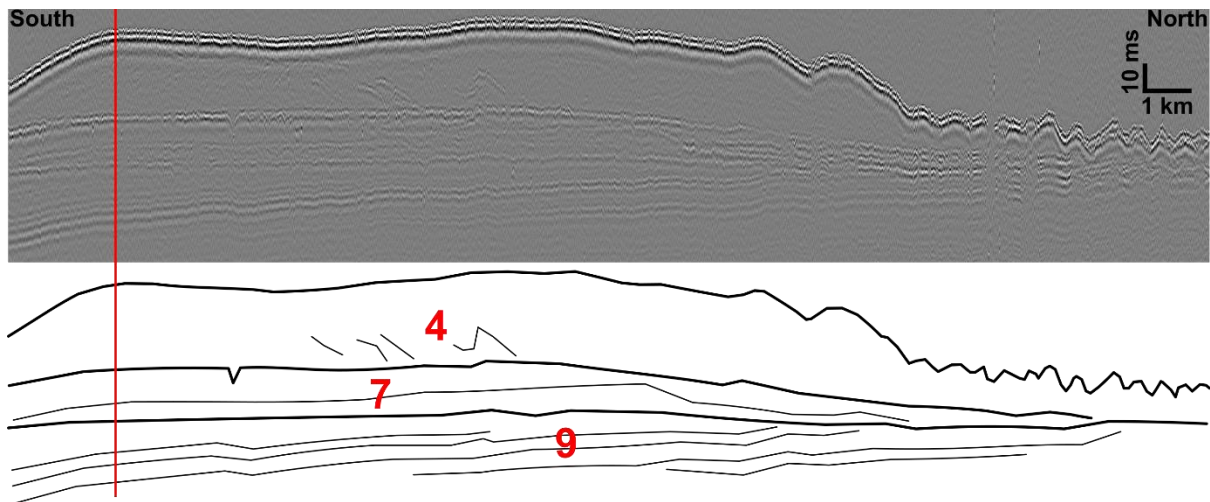


*Figure 3.37 - IPY GLAMAR sparker seismic reflection data and interpretation with seismic facies. The red line indicates a tie point with the seismic section in Figure 3.35 and Figure 3.36. See Line 24 in Figure 3.13 for location.*

The along-ridge profile shows the continuation of the ridge facies along its length (Figure 3.37). SF4 comprises the bulk of the ridge, resulting in a smooth seafloor profile until it thins out to the north where the seafloor then becomes highly undulating. Few internal reflections are observed within this facies, however those which do exist appear to dip in a consistent direction. This facies overlies a distinct reflection which gently curves, resulting in SF4 being up to 30 ms thick near its centre.

SF7 exists under this reflection, forming a layer up to 20 ms thick which thins to the north and south (Figure 3.37). Within this facies is an upper layer devoid of internal reflections. This then overlies a lower medium amplitude layer which contains chaotic reflections. This lower layer of SF7 overlies a horizontal base reflection.

The base reflection of SF7 truncates dipping parallel reflections comprising SF9 (Figure 3.37).

## Outer-shelf

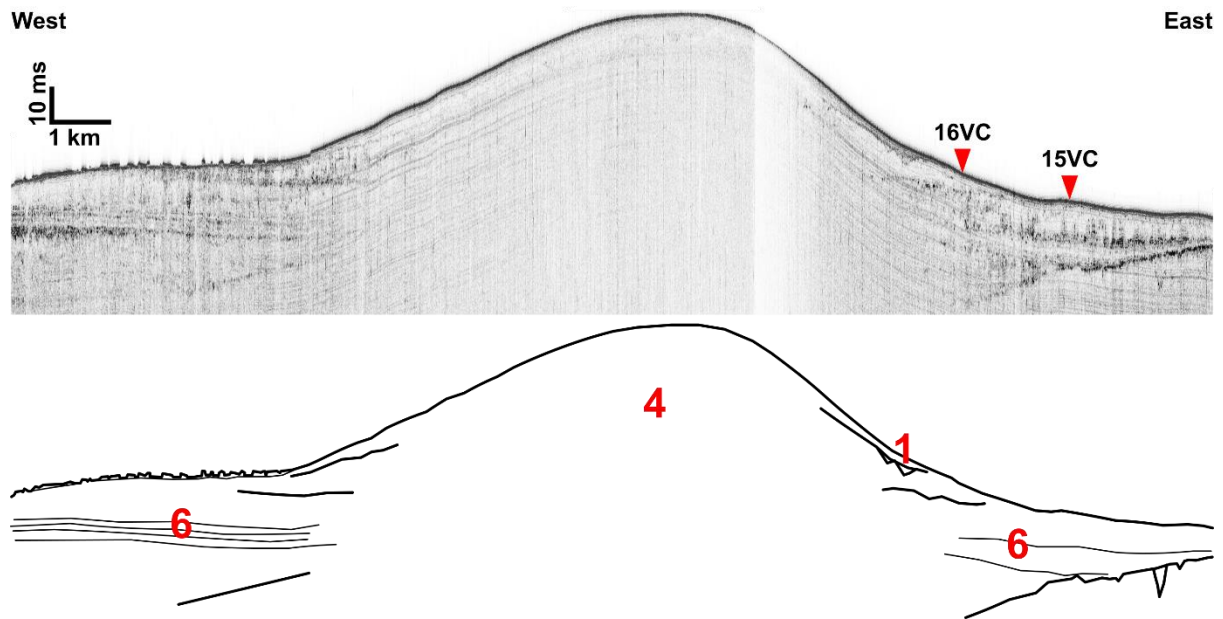


Figure 3.38 - JC-106 chirp seismic reflection data with selected physical sample locations and interpretation with seismic facies. See Line 25 in Figure 3.13 for location.

At the southwest shelf edge, SF1 is only observed where it increases in thickness, allowing it to be resolved acoustically (Figure 3.38). It forms a drape over SF4 on the eastern side of the ridge. It is a medium amplitude layer up to 3 ms thick that is discontinuous over the ridge and inter-ridge areas. SF1 also exists on the western side of the ridge where it comprises distinct crenulations on the lower flank of the ridge.

SF4 is not imaged in its entirety, but a possible base reflection is noted on each ridge flank (Figure 3.38). Over this base reflection, another reflection rises towards the ridge crest, suggesting that the layer increases in thickness towards the ridge crest similar to SF4 comprising the bulk of the ridge features. No distinct internal reflections are identified within SF4.

SF6 underlies SF4 and consists of low to medium amplitude parallel reflections that are horizontally layered (Figure 3.38). On the western side of the ridge, these reflections appear to decrease in amplitude and become more discontinuous upwards through the layer. On the eastern side of the ridge, discontinuous and chaotic reflections form parallel bands which may be a continuation of parallel reflections to the west. SF6 onlaps a dipping surface in the east which appears channelised.

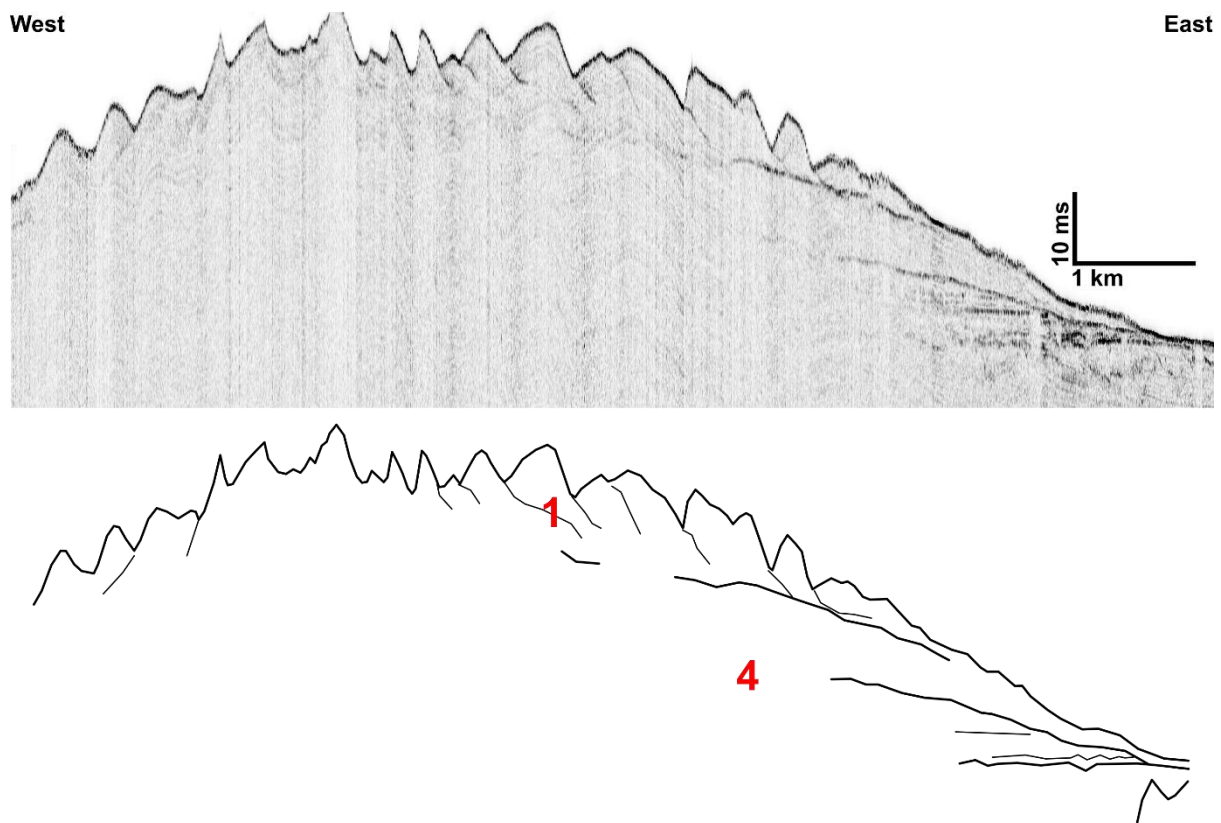
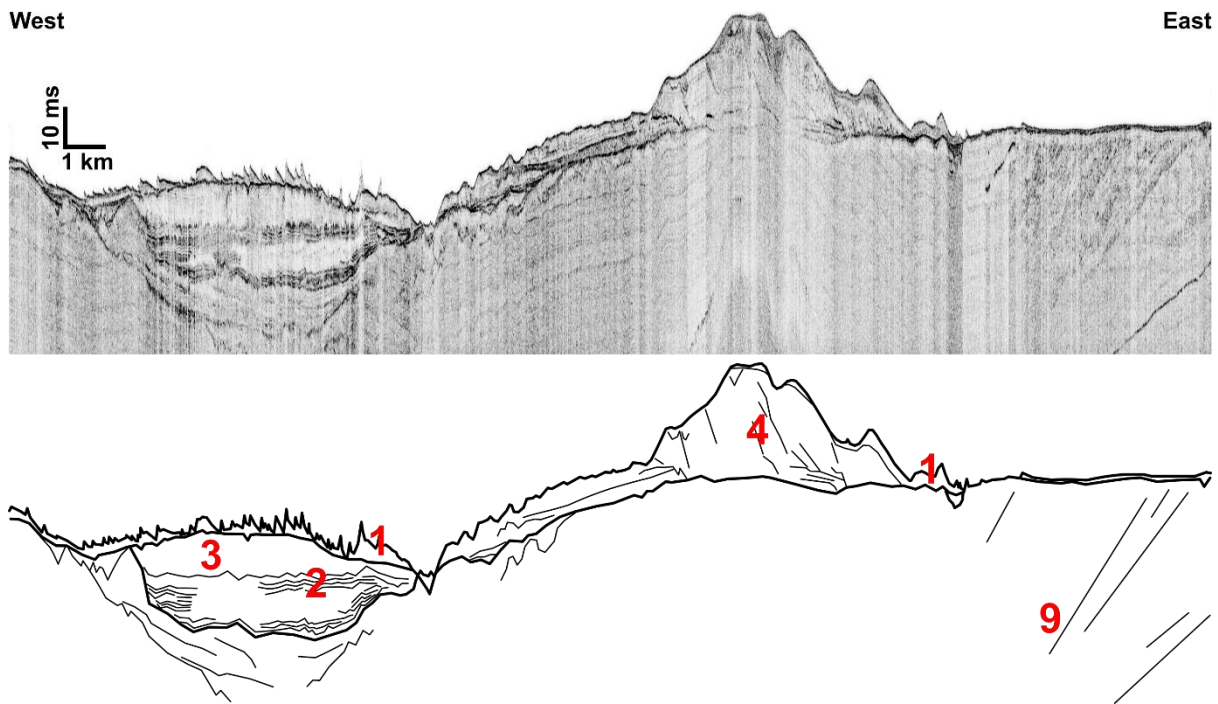


Figure 3.39 - JC-106 chirp seismic reflection data and interpretation with seismic facies. See Line 26 in Figure 3.13 for location.

On the southeast shelf edge, SF1 is at least 12 ms thick where it forms a highly irregular seafloor across the upper surface of the ridge (Figure 3.39). This facies contains dipping reflections which are directed away from the ridge crest, correlating to the direction of asymmetry of the seafloor features. Beyond this area, SF1 becomes discontinuous.

SF4 is designated based on the observation of a base reflection on the lower flank, and the occurrence of an overlying reflection which dips away from the ridge crest (Figure 3.39). This results in the facies increasing in thickness towards the ridge centre. The internal reflection geometry of the unit and the continuity of its upper surface and base reflection are not observed. However, on the lower flank of SF4, low to medium amplitude reflections may in places be truncated against the upper surface. However, this is speculative due to the clarity of the data.



*Figure 3.40 - JC-106 chirp seismic reflection data and interpretation with seismic facies. See Line 27 in Figure 3.13 for location.*

In the French sector of the outer-shelf, SF1 is generally found throughout the section (Figure 3.40). In places it forms a highly irregular seafloor where it is of low amplitude, producing undulating surface features up to 5 ms thick. This facies changes in acoustic character and is discontinuous. Where it overlies SF4, SF1 is of medium amplitude, resulting in an apparent decrease in amplitude with increasing water depth. This facies overlies a distinct medium to high amplitude reflection, the continuity of which across the section is undetermined.

SF3 is several low amplitude layers up to 10 ms thick and interbedded with SF2 comprising parallel reflections up to 5 ms thick (Figure 3.40). These facies infill a large channel feature which has a total depth of 20 ms.

SF4 comprises the bulk of the ridge and is up to 23 ms thick, containing dipping low to medium amplitude reflections (Figure 3.40). This facies displays a slight asymmetry and there is evidence of channelling on its upper surface in places. SF4 overlies a distinct medium to high amplitude reflection that truncates reflections below.

SF9 comprises steeply dipping low to medium amplitude reflections which are truncated against its upper surface (Figure 3.40). This surface is horizontal to the east, but becomes irregular to the west, where it dips and forms a basin before rising again.

### **3.2.2 Seismic Facies Summary**

Based upon the previous descriptions of seismic facies observed by different datasets and situated in various stratigraphic settings and spatial locations, the following summary descriptions are produced for each regional acoustic packet.

#### **Seismic Facies 1**

This facies is commonly discontinuous where it thins below the resolution of the seismic data. This unit is only imaged satisfactorily where it forms seafloor bedforms (Figure 3.39 and Figure 3.40) or it infills large basins or depressions where considerable thicknesses exist (Figure 3.15). At the seafloor, SF1 generally results in a smooth surface where it is of low amplitude (Figure 3.15). However, crenulations in places overlie a reflection (Figure 3.19 and Figure 3.20). The depth of the crenulations corresponds to the depth of this reflection, resulting in features that are up to 2 ms high/deep. Where SF1 forms bedforms, these features are asymmetrical; in places this asymmetry is directed in one consistent direction (Figure 3.39) or in the direction of a ridge crest (Figure 3.40).

#### **Seismic Facies 2 and 3**

These facies are commonly interbedded or overlie one another (Figure 3.14 and Figure 3.40). SF2 generally either forms the base of this interbedding, or forms intermediate bands separated by SF3 comprising a low amplitude layer with some sporadic internal reflections. Additionally, in instances SF2 can transition upward into SF3. These facies exist in the Celtic Deep where they are located in a large basin (Figure 3.14). In the French sector, a distinct channel feature is infilled by SF2 and SF3 (Figure 3.40).

#### **Seismic Facies 4**

This facies consistently comprises the upper bulk of the ridges found across the mid- and outer-shelf of the Celtic Sea. These features can be symmetrical (Figure 3.21) or asymmetrical (Figure 3.22). Additionally, the ridges can exist as single features with one crest (Figure 3.20), or as joined neighbouring ridges where SF4 has two crests (Figure 3.23). The lateral extent of this facies commonly corresponds to a distinct change in seafloor character or slope (Figure 3.36), as SF4 results in a bank with steep sides and smooth upper surface. SF4 contains various reflection geometries, however the most commonly occurring characteristics are dipping reflections which are truncated by the upper surface and extend throughout the bank (Figure 3.22). In places, SF4 lacks acoustic character (Figure 3.38) or displays complex internal reflections (Figure 3.24). In one case, several seismic profiles crossed the northern axial end of a ridge. These sections show that SF4 comprises single neighbouring mounds which decrease in thickness to the north from where the main bank is formed (Figure 3.24, Figure 3.26 and Figure 3.27). These isolated mounds of SF4 represent transverse bedforms (Figure 3.28) which the much larger ridges transition into, or are overlain by, axially (Figure 3.4 and Figure 3.37). In every occurrence of SF4, a base reflection truncates reflections below, however the character

and continuity of this reflection varies. The large ridges or transverse mounds comprising SF4 are overlain by SF1 which is discontinuous across the crest of the features.

### **Seismic Facies 5**

This facies is a discontinuous low amplitude layer which infills an irregular surface below, generally comprising SF8 (Figure 3.19 and Figure 3.23). SF5 underlies the base reflection of SF4 (Figure 3.20 and Figure 3.23), but is in places overlain directly by SF1 where SF4 is absent (Figure 3.19). This facies is primarily found in the Irish sector on the northwest mid-shelf.

### **Seismic Facies 6**

This facies forms a raised plateau which extends beyond the lateral extent of SF4 to produce the initial bathymetric expression of the ridge flanks (Figure 3.24, Figure 3.27 and Figure 3.38). Where SF6 extends laterally beyond SF4, a distinct change in seafloor slope occurs; here SF6 results in a gentler sloping seafloor compared to that produced by SF4 (Figure 3.38). Internal reflection geometry appears consistent between cases. SF6 comprises parallel reflections (Figure 3.24), similar to those of SF2 (Figure 3.14), which decrease in amplitude and continuity upward where any reflections are truncated against the upper surface which generally forms the base of SF1 or 4. The parallel reflections generally infill basins and depressions, the lower surface of which are channelised in places (Figure 3.27 and Figure 3.38).

### **Seismic Facies 7**

This facies forms mounds which overlie a distinctly flat base which is channelised in places (Figure 3.35). The mounds extend laterally and axially beyond the spatial extent of the overlying SF4 to produce the initial bathymetric expression of the ridge features (Figure 3.35). In such cases, SF7 is directly overlain by SF1 which can be discontinuous, resulting in SF7 being exposed close to the seafloor. Where SF7 extends beyond SF4, a distinct change in seafloor slope and character is observed where SF7 results in an irregular but more gently sloping seafloor compared to that produced by SF4 above (Figure 3.35). This is similar to the change in seafloor character produced when SF6 extends laterally and axially beyond the extent of SF4 (Figure 3.38). SF7 also is exposed on the northern axial ends of the investigated ridges, thinning to the south under SF4 (Figure 3.29 and Figure 3.32). Internal reflection geometries vary, ranging from horizontal sub-parallel reflections of medium amplitude (Figure 3.28) to some dipping reflections and a lack of acoustic character (Figure 3.33). Where internal reflections do exist, they appear to be truncated against the upper surface of SF7 (Figure 3.33 and Figure 3.35). In all cases, SF7 is underlain by SF9.

### **Seismic Facies 8**

This facies has an upper irregular surface which is discontinuous, while the facies itself lacks acoustic character. The lower reflection of SF8 is distinct and horizontal, extending beyond the available dataset.

This facies appears to contain some parallel reflections (Figure 3.21) and is overlain by SF5. SF8 is found on the northwest mid-shelf where it extends to the west towards the southern coastline of Ireland.

### **Seismic Facies 9**

SF9 has a horizontal upper surface directly overlain by SF1, SF7 or SF4 (Figure 3.34). Where overlain by SF1, SF9 is exposed close to the seafloor resulting in the flat appearance of the shelf and inter-ridge areas. The facies itself comprises dipping reflections which are truncated against the flat upper surface representing an angular unconformity. These reflections are parallel and inclined, however the slope of the dip increases or decreases in one consistent direction along individual reflections.

### **Seismic Facies 10**

On the northeast mid-shelf, SF10 outcrops at the seafloor where it forms a jagged upper surface (Figure 3.18). Depressions between these pinnacles are infilled by SF1. SF10 lacks internal acoustic character and has a smooth and undulating upper surface at depth where overlain by other layers such as SF6. In such cases, this upper surface is channelised.

### **Seismic Facies 11**

The internal acoustic character of SF11 comprises parallel reflections, comparable to SF2, which are truncated against the upper surface. This facies forms outcropping pinnacles in the Celtic Deep (Figure 3.16). The upper surface of SF11 is smooth and undulating, and in places channelling occurs at various heights along the surface ranging from U- to V-shaped channels.

### **3.2.3 Lithofacies Summary**

The following descriptions of the various core Lithofacies (LF) provide a general overview of their defining characteristics and stratigraphic position in each core. A litho-stratigraphic overview is shown for each sediment core in Table 3.2. Sediment core visual logs with lithofacies annotations and descriptions can be found in Lockhart et al. (2018) and Scourse et al. (2019) in the Appendix.



Table 3.2 - Lithofacies (LF) present per selected Vibrocore (VC) and Piston Core (PC) recovered during JC-106 with approximate thicknesses in metres, and converted into ms using a sound velocity of  $1600 \text{ m}\cdot\text{s}^{-1}$  to aid correlation between seismic profiles and cored lithofacies.

| Core          | 15VC | 16VC | 18VC | 19VC | 20VC | 21VC | 22VC | 28VC |
|---------------|------|------|------|------|------|------|------|------|
| Recovery (m)  | 2.17 | 1.68 | 1.86 | 1.62 | 1.52 | 1.40 | 1.28 | 1.42 |
| Recovery (ms) | 2.71 | 2.10 | 2.33 | 2.03 | 1.90 | 1.75 | 1.60 | 1.78 |
| Thickness (m) | 0.20 | 0.80 | 0.20 | 0.20 | 0.80 | 0.40 | 0.40 | 1.00 |
| TWT (ms)      | 0.25 | 1.00 | 0.25 | 0.25 | 1.00 | 0.50 | 0.50 | 1.25 |
|               | 0.10 | 0.10 | 0.40 | 0.25 | 0.10 | 0.90 | 0.20 | 0.10 |
|               | 0.13 | 0.13 | 0.50 | 0.31 | 0.13 | 1.13 | 0.25 | 0.13 |
|               | 1.80 | 0.90 | 1.20 | 1.10 | 0.60 | 0.10 | 0.60 | 0.25 |
|               | 2.25 | 1.13 | 1.50 | 1.38 | 0.75 | 0.13 | 0.75 | 0.31 |

| Core          | 29VC | 30VC | 31VC | 32VC | 33VC | 34VC | 35VC | 36VC |
|---------------|------|------|------|------|------|------|------|------|
| Recovery (m)  | 1.40 | 1.78 | 1.74 | 1.94 | 1.82 | 1.90 | 2.63 | 0.58 |
| Recovery (ms) | 1.75 | 2.23 | 2.18 | 2.43 | 2.28 | 2.38 | 3.29 | 0.73 |
| Thickness (m) | 0.30 | 1.20 | 1.05 | 0.25 | 0.90 | 0.45 | 0.35 | 0.15 |
| TWT (ms)      | 0.38 | 1.50 | 1.31 | 0.31 | 1.13 | 0.56 | 0.44 | 0.19 |
|               | 0.20 | 0.20 | 0.45 | 0.10 | 0.15 | 0.10 | 0.55 | 0.25 |
|               | 0.25 | 0.25 | 0.56 | 0.13 | 0.19 | 0.13 | 0.69 | 0.31 |
|               | 0.85 | 0.10 | 0.10 | 1.40 | 0.70 | 1.30 | 1.70 | 0.10 |
|               | 1.06 | 0.13 | 0.13 | 1.75 | 0.88 | 1.63 | 2.13 | 0.13 |

| Core          | 39VC | 44VC | 45VC | 51PC | 52PC | 53VC |      |
|---------------|------|------|------|------|------|------|------|
| Recovery (m)  | 0.79 | 2.02 | 2.17 | 6.29 | 7.58 | 4.47 | LF1  |
| Recovery (ms) | 0.99 | 2.53 | 2.71 | 7.86 | 9.48 | 5.59 | LF1a |
| Thickness (m) | 0.45 | 0.40 | 0.40 | 2.30 | 3.60 | 0.90 | LF2  |
| TWT (ms)      | 0.56 | 0.50 | 0.50 | 2.88 | 4.50 | 1.13 | LF3  |
|               | 0.15 | 0.10 | 0.20 | 0.08 | 0.08 | 0.30 | LF4  |
|               | 0.19 | 0.13 | 0.25 | 0.10 | 0.10 | 0.38 | LF5  |
|               | 0.15 | 0.80 | 0.80 | 1.60 | 1.70 | 0.60 | LF6  |
|               | 0.19 | 1.00 | 1.00 | 2.00 | 2.13 | 0.75 | LF7  |
|               |      | 0.60 | 0.65 | 2.20 | 2.10 | 2.60 | LF8  |
|               |      | 0.75 | 0.81 | 2.75 | 2.63 | 3.25 | LF9  |

### **Lithofacies 1**

LF1 represents sediments comprising the present-day seafloor as recovered in every sediment core. These sediments generally display a fining-upwards grainsize trend where medium or coarse sand at the base of LF1 transitions upwards into clay or fine sand. In places, LF1 displays no observable grainsize trend. In such instances, LF1 consists of a single grainsize which can range from mud to coarse sand. LF1 has thicknesses exceeding 3 m in isolated depressions such as the Celtic Deep but is generally <1 m thick across the mid- and outer- shelf.

### **Lithofacies 1a**

LF1a is less than 10 cm thick and only recovered in the Celtic Deep where it is a distinct shell fragment or clast layer in a clay to silt matrix. This facies is always overlain by finer variants of LF1.

### **Lithofacies 2**

LF2 consists of a coarse layer comprising medium sand to gravel with shell fragments and some clasts in places. LF1 either coarsens downwards into LF2, or LF2 itself forms a distinctly coarser layer than LF1 where there is no grainsize transition in LF1. This layer is generally <25 cm thick across the shelf and is always coarser than the overlying lithofacies. The base of LF2 is sharp and there is generally an abrupt transition in grainsize where the underlying lithofacies is finer. This facies is always overlain by LF1.

### **Lithofacies 3**

LF3 comprises soft mud with fine sand laminations and was only recovered in the Celtic Deep underlying LF1 and LF1a.

### **Lithofacies 4**

LF4 is a soft (undrained shear strengths up to 35 kPa) clay recovered in the Celtic Deep found underlying LF3.

### **Lithofacies 5**

LF5 comprises sands which exist as medium to coarse sand at the base of the facies. This facies in places fines upwards, containing abundant shell fragments which appear to form layers. In other places, LF5 display no observable grainsize trend. LF5 is overlain by coarser variants of LF1 and LF2.

### **Lithofacies 6**

LF6 is recovered as coarse sand which contains shell fragments and some clasts under coarser variants of LF1 and LF2.

**Lithofacies 7**

LF7 comprises medium to coarse sand, occasionally with abundant shell fragments which can result in abrupt grainsize trends in places. LF7 is overlain by coarser variants of LF1 and LF2.

**Lithofacies 8**

LF8 consists of stiff (shear strengths of up to 165 kPa) clay and silt which generally contain fine to medium sand laminations that, in places, exhibit deformation. The laminations allow the identification of subtle secondary deformation, which results in them being sub-horizontal and contorted. In places, LF8 can have a sandier grainsize composition which then contains finer-grained laminations. LF8 is overlain by finer variants of LF1 and LF2.

**Lithofacies 9**

LF9 consists of medium to coarse sand with shell fragments at its base which displays a fining-upwards trend to fine sand. LF9 is overlain by LF8.

### 3.3 Sediment Geotechnics

Geotechnical testing of LF8, recovered in Vibrocores (VC) 18VC to 45VC across the shelf, shows differences in physical characteristics to LF3 and LF4, recovered in Piston Cores (PC) 51PC, 52PC and 53VC from the Celtic Deep. Such differences provide detailed information and clues as to the depositional history of these deposits which cannot be provided by geophysical datasets alone. Core logs can be found in Lockhart et al. (2018) and Scourse et al. (2019) in the Appendix.

#### 3.3.1 Undrained Shear Strength

LF3 and LF4 has undrained shear strengths up to 35 kPa, contrasting with LF8 which has undrained shear strengths up to 165 kPa (Figure 3.41). Core 51PC appears to show increasing undrained shear strength with increasing depth while shelf cores do not appear to show any specific trend with depth.

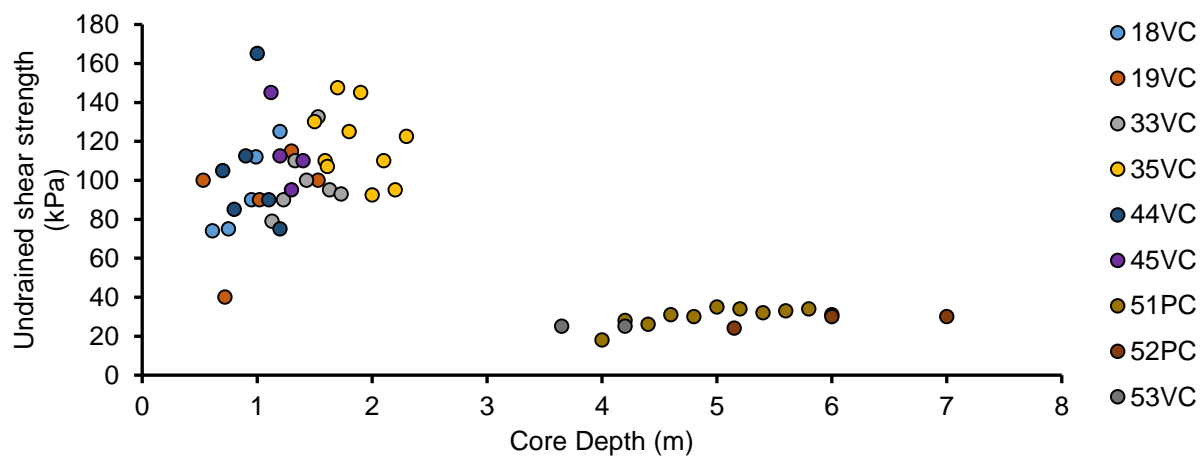


Figure 3.41 - Scatter plot showing undrained shear strength measurements for Vibrocore (VC) and Piston Core (PC) samples.

#### 3.3.2 Effective Stress

Effective stress increases with depth in all cores, with subtle deviations due to changes in the density of the litho-stratigraphy in each core which alters the imparted vertical stress (Figure 3.42). Shelf cores generally have higher effective stresses than Celtic Deep cores for similar depths due to their increased density.

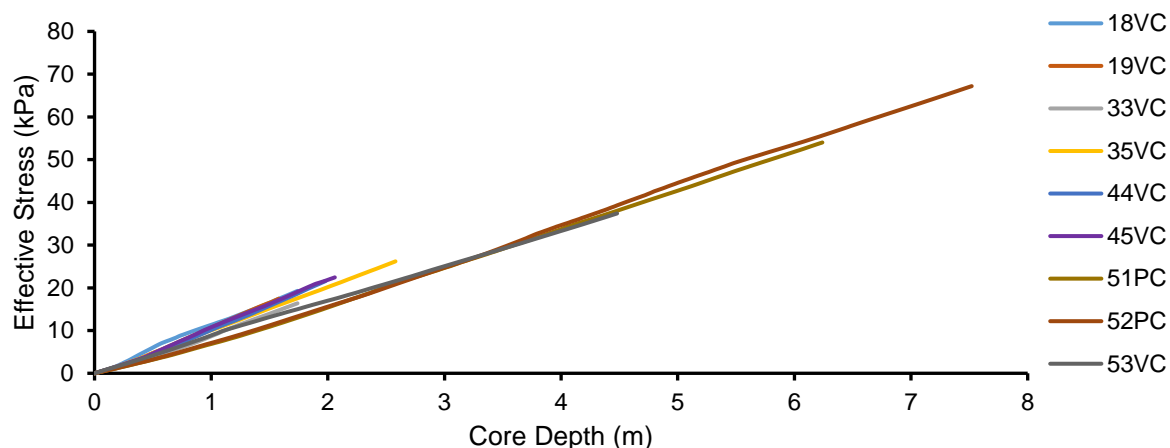


Figure 3.42 - Line graph showing effective stress with increasing depth for Vibrocores (VC) and Piston Cores (PC).

### 3.3.3 Atterberg Limits

Atterberg test results show that LF3, LF4 and LF8 display similar Atterberg limits, apart from LF8 in 44VC and 45VC which show lower plasticity indexes due to lower liquid limit values (Table 3.3). This could be due to subtle changes in grainsize composition in 44VC and 45VC in comparison to other cores. Despite this, these results show that LF8 on the mid-shelf and LF3 and LF4 in the Celtic Deep do not vary significantly in terms of their Atterberg limits and thus have similar plastic behaviour.

Table 3.3 - Plasticity Index ( $I_p$ ) and  $\alpha$  values for selected Vibrocore (VC) and Piston Core (PC) samples as derived from data in Table 3.4 and Table 3.5.

| Core | $w_L$ (%) | $w_P$ (%) | $I_p$ | $\alpha$ |
|------|-----------|-----------|-------|----------|
| 18VC | 62.29     | 29.99     | 32.30 | 4.15     |
| 33VC | 48.89     | 24.69     | 24.20 | 4.77     |
| 35VC | 48.03     | 23.78     | 24.25 | 4.76     |
| 44VC | 35.52     | 19.03     | 16.49 | 5.73     |
| 45VC | 37.00     | 25.76     | 11.24 | 6.89     |
| 51PC | 53.11     | 22.62     | 30.49 | 4.27     |
| 52PC | 59.92     | 26.92     | 33.00 | 4.11     |
| 53VC | 55.38     | 26.42     | 28.96 | 4.37     |
|      |           |           |       |          |
| Avg  | 50.02     | 24.90     | 25.12 | 4.88     |
| SD   | 9.80      | 3.25      | 7.80  | 0.97     |

Table 3.4 - Liquid limit ( $w_L$ ) mass and Moisture Content (MC) results for various Penetration (P) measurements for Vibrocore (VC) and Piston Core (PC) samples.

| Core | Tin (g) | Tin +<br>Wet (g) | Tin +<br>Dry (g) | P1 (mm) | P2 (mm) | P3 (mm) | Avg. P<br>(mm) | Wet (g) | Dry +<br>Salt (g) | Water<br>(g) | Pure<br>Dry (g) | MC (%) | $w_L$ MC<br>@ 20<br>mm (%) |
|------|---------|------------------|------------------|---------|---------|---------|----------------|---------|-------------------|--------------|-----------------|--------|----------------------------|
| 18VC | 5.34    | 20.97            | 15.21            | 14.1    | 14.2    |         | 14.2           | 15.63   | 9.87              | 5.76         | 9.67            | 59.6   | 62.29                      |
|      | 5.27    | 17.20            | 12.72            | 18.6    | 18.8    |         | 18.7           | 11.93   | 7.45              | 4.48         | 7.29            | 61.4   |                            |
|      | 5.29    | 17.69            | 13.00            | 21.2    | 20.9    |         | 21.1           | 12.40   | 7.71              | 4.69         | 7.55            | 62.2   |                            |
|      | 5.40    | 22.44            | 16.09            | 23.0    | 22.2    | 23.0    | 22.7           | 17.04   | 10.69             | 6.35         | 10.47           | 60.7   |                            |
|      | 5.42    | 24.49            | 16.82            | 25.5    | 25.1    |         | 25.3           | 19.07   | 11.40             | 7.67         | 11.13           | 68.9   |                            |
| 33VC | 5.43    | 21.04            | 16.27            | 14.9    | 14.9    |         | 14.9           | 15.61   | 10.84             | 4.77         | 10.67           | 44.7   | 48.89                      |
|      | 5.30    | 21.54            | 16.48            | 17.2    | 17.4    |         | 17.3           | 16.24   | 11.18             | 5.06         | 11.00           | 46.0   |                            |
|      | 5.65    | 23.61            | 17.81            | 19.4    | 19.4    |         | 19.4           | 17.96   | 12.16             | 5.80         | 11.96           | 48.5   |                            |
|      | 5.63    | 21.89            | 16.48            | 22.4    | 22.4    |         | 22.4           | 16.26   | 10.85             | 5.41         | 10.66           | 50.7   |                            |
|      | 5.38    | 28.22            | 20.39            | 24.5    | 24.4    |         | 24.5           | 22.84   | 15.01             | 7.83         | 14.74           | 53.1   |                            |
| 35VC | 5.42    | 18.38            | 14.38            | 17.2    | 17.3    |         | 17.3           | 12.96   | 8.96              | 4.00         | 8.82            | 45.4   | 48.03                      |
|      | 5.55    | 18.56            | 14.40            | 19.4    | 19.2    |         | 19.3           | 13.01   | 8.85              | 4.16         | 8.70            | 47.8   |                            |
|      | 5.43    | 18.53            | 14.21            | 22.2    | 22.6    |         | 22.4           | 13.10   | 8.78              | 4.32         | 8.63            | 50.1   |                            |
|      | 5.63    | 24.16            | 17.90            | 24.3    | 24.7    |         | 24.5           | 18.53   | 12.27             | 6.26         | 12.05           | 51.9   |                            |
| 44VC | 5.36    | 26.50            | 21.36            | 16.0    | 16.4    |         | 16.2           | 21.14   | 16.00             | 5.14         | 15.82           | 32.5   | 35.52                      |
|      | 5.44    | 27.77            | 21.65            | 23.5    | 23.8    |         | 23.7           | 22.33   | 16.21             | 6.12         | 16.00           | 38.3   |                            |
|      | 5.48    | 32.46            | 24.61            | 27.0    | 27.4    |         | 27.2           | 26.98   | 19.13             | 7.85         | 18.86           | 41.6   |                            |
| 45VC | 5.49    | 23.95            | 19.10            | 16.0    | 16.4    |         | 16.2           | 18.46   | 13.61             | 4.85         | 13.44           | 36.1   | 37.00                      |
|      | 5.26    | 32.19            | 24.92            | 23.2    | 23.4    |         | 23.3           | 26.93   | 19.66             | 7.27         | 19.41           | 37.5   |                            |



|      |      |       |       |      |      |      |      |       |       |       |       |      |       |
|------|------|-------|-------|------|------|------|------|-------|-------|-------|-------|------|-------|
|      | 5.33 | 31.88 | 24.51 | 26.0 | 25.6 |      | 25.8 | 26.55 | 19.18 | 7.37  | 18.92 | 38.9 |       |
| 51PC | 5.30 | 21.16 | 16.04 | 15.4 | 15.8 |      | 15.6 | 15.86 | 10.74 | 5.12  | 10.56 | 48.5 | 53.11 |
|      | 5.29 | 30.21 | 21.90 | 17.9 | 18.1 |      | 18.0 | 24.92 | 16.61 | 8.31  | 16.32 | 50.9 |       |
|      | 5.32 | 29.89 | 21.38 | 20.3 | 20.2 |      | 20.3 | 24.57 | 16.06 | 8.51  | 15.76 | 54.0 |       |
|      | 5.25 | 26.57 | 19.09 | 22.1 | 21.8 |      | 22.0 | 21.32 | 13.84 | 7.48  | 13.58 | 55.1 |       |
|      | 5.26 | 30.79 | 21.46 | 26.1 | 25.8 |      | 26.0 | 25.53 | 16.20 | 9.33  | 15.87 | 58.8 |       |
| 52PC | 5.43 | 27.93 | 20.12 | 15.4 | 15.2 |      | 15.3 | 22.50 | 14.69 | 7.81  | 14.42 | 54.2 | 59.92 |
|      | 5.29 | 26.29 | 18.66 | 17.9 | 18.5 | 17.9 | 18.1 | 21.00 | 13.37 | 7.63  | 13.10 | 58.2 |       |
|      | 5.44 | 24.78 | 17.51 | 21.0 | 21.4 |      | 21.2 | 19.34 | 12.07 | 7.27  | 11.82 | 61.5 |       |
|      | 5.37 | 32.97 | 22.33 | 24.2 | 23.8 |      | 24.0 | 27.60 | 16.96 | 10.64 | 16.59 | 64.1 |       |
| 53VC | 5.31 | 23.66 | 17.59 | 14.4 | 14.7 |      | 14.6 | 18.35 | 12.28 | 6.07  | 12.07 | 50.3 | 55.38 |
|      | 5.35 | 23.05 | 16.86 | 19.4 | 19.5 |      | 19.5 | 17.70 | 11.51 | 6.19  | 11.29 | 54.8 |       |
|      | 5.42 | 31.31 | 21.83 | 24.0 | 23.6 |      | 23.8 | 25.89 | 16.41 | 9.48  | 16.08 | 59.0 |       |

Table 3.5 - Plastic limit ( $w_p$ ) mass and Moisture Content (MC) results for Vibrocore (VC) and Piston Core (PC) samples.

| Core | Tin (g) | Tin +<br>Wet (g) | Tin +<br>Dry (g) | Wet (g) | Dry +<br>Salt (g) | Water<br>(g) | Pure<br>Dry (g) | $w_p$ MC<br>(%) |
|------|---------|------------------|------------------|---------|-------------------|--------------|-----------------|-----------------|
| 18VC | 5.44    | 21.30            | 17.67            | 15.86   | 12.23             | 3.63         | 12.10           | 29.99           |
| 33VC | 5.63    | 27.55            | 23.24            | 21.92   | 17.61             | 4.31         | 17.46           | 24.69           |
| 35VC | 5.21    | 24.18            | 20.56            | 18.97   | 15.35             | 3.62         | 15.22           | 23.78           |
| 44VC | 5.36    | 28.44            | 24.77            | 23.08   | 19.41             | 3.67         | 19.28           | 19.03           |
| 45VC | 5.27    | 14.17            | 12.36            | 8.90    | 7.09              | 1.81         | 7.03            | 25.76           |
| 51PC | 5.39    | 19.63            | 17.02            | 14.24   | 11.63             | 2.61         | 11.54           | 22.62           |
| 52PC | 5.40    | 26.11            | 21.75            | 20.71   | 16.35             | 4.36         | 16.20           | 26.92           |
| 53VC | 5.41    | 19.10            | 16.26            | 13.69   | 10.85             | 2.84         | 10.75           | 26.42           |

### 3.3.4 Over-consolidation Ratio

Over-consolidation ratio (OCR) results from all cores show two distinct populations, sorted by locality (Figure 3.43). LF8 recovered across the shelf has OCR values >20 and exist at core depths <2.5 m, showing a large variability of OCR values up to a maximum of 96. This contrasts with LF3 and LF4, recovered from the Celtic Deep, which have OCR values <3, despite existing at core depths between 3.6-7 m. LF8 generally shows trends of increasing OCR with decreasing core depth despite noticeable variability (Figure 3.44). These results show that LF8 is more over-consolidated in comparison to LF3 and LF4.

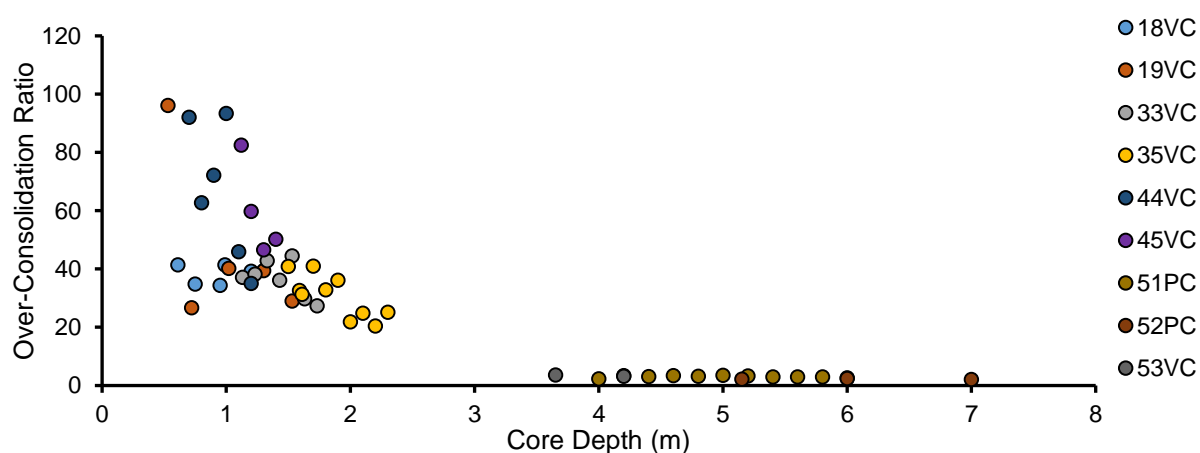


Figure 3.43 - Scatter plot showing OCR values at measurement depths for Vibrocore (VC) and Piston Core (PC) samples.

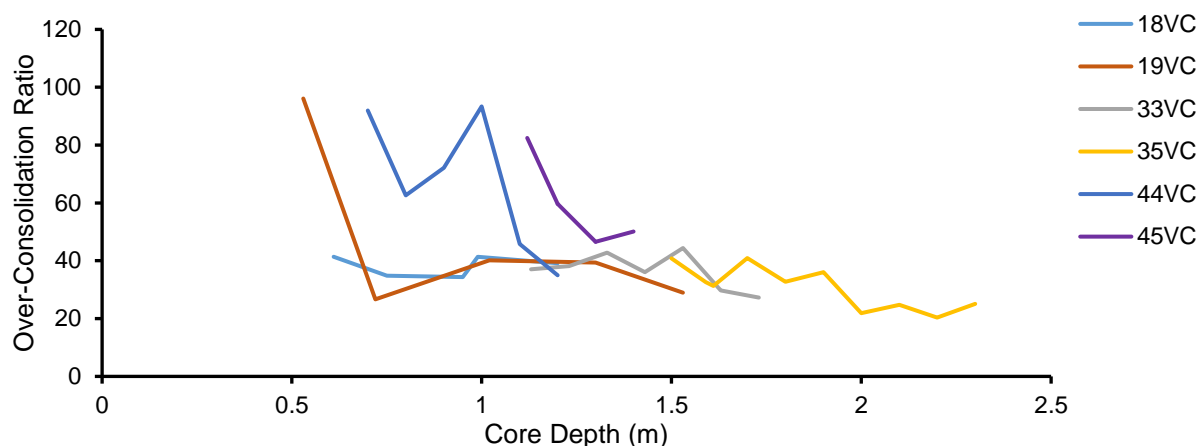


Figure 3.44 - Line graph showing OCR variability for Celtic Sea shelf Vibrocore (VC) samples.

### 3.3.5 Predicted Yield Stress

Figure 3.45 shows similar trends to that displayed in Figure 3.41. LF3 and LF4 have experienced predicted yield stresses <150 kPa at significantly greater depths than LF8 which exists at shallower depths but has predicted yield stresses from 195-999 kPa.

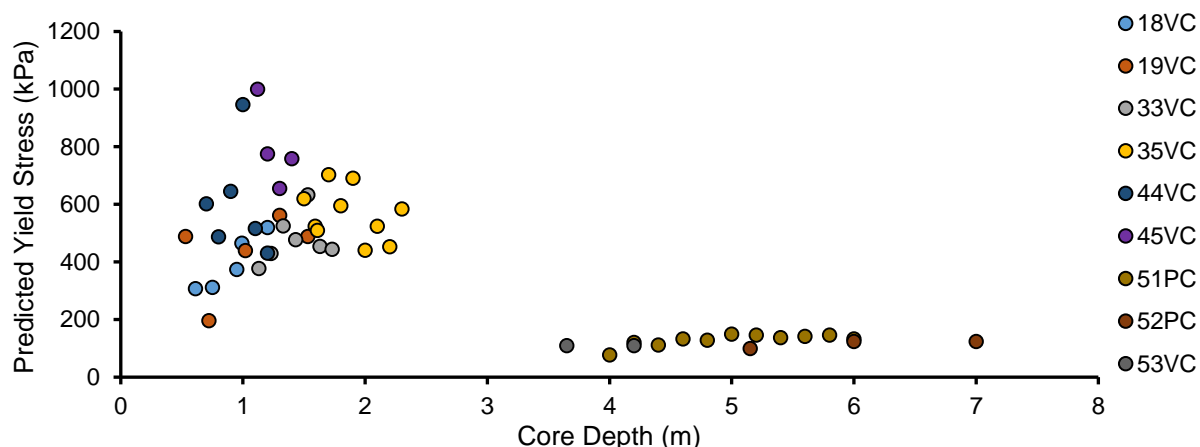


Figure 3.45 - Scatter plot showing the predicted yield stress with depth for Vibrocore (VC) and Piston Core (PC) samples.

### 3.3.6 Deformation

LF8 displays contorted sand laminations and minor fracturing in places, the intensity of which varies between cores (Figure 3.46). LF8 in core 33VC contains the most prominent deformed laminations. These appear partially deformed, still displaying some resemblance to horizontal laminations, and do not appear to display any vertical trend. In some instances, individual laminae appear to consistently dip and thin towards one direction, such as in 33VC. Other cores contain deformed laminations which consistently dip downwards away from the core centre, suggesting that this is a product of coring. Therefore, it is possible that some of the deformation structures in LF8 can be attributed to the effects

of the coring operation before being x-rayed. No such deformation structures exist in LF3 and LF4 in the Celtic Deep.

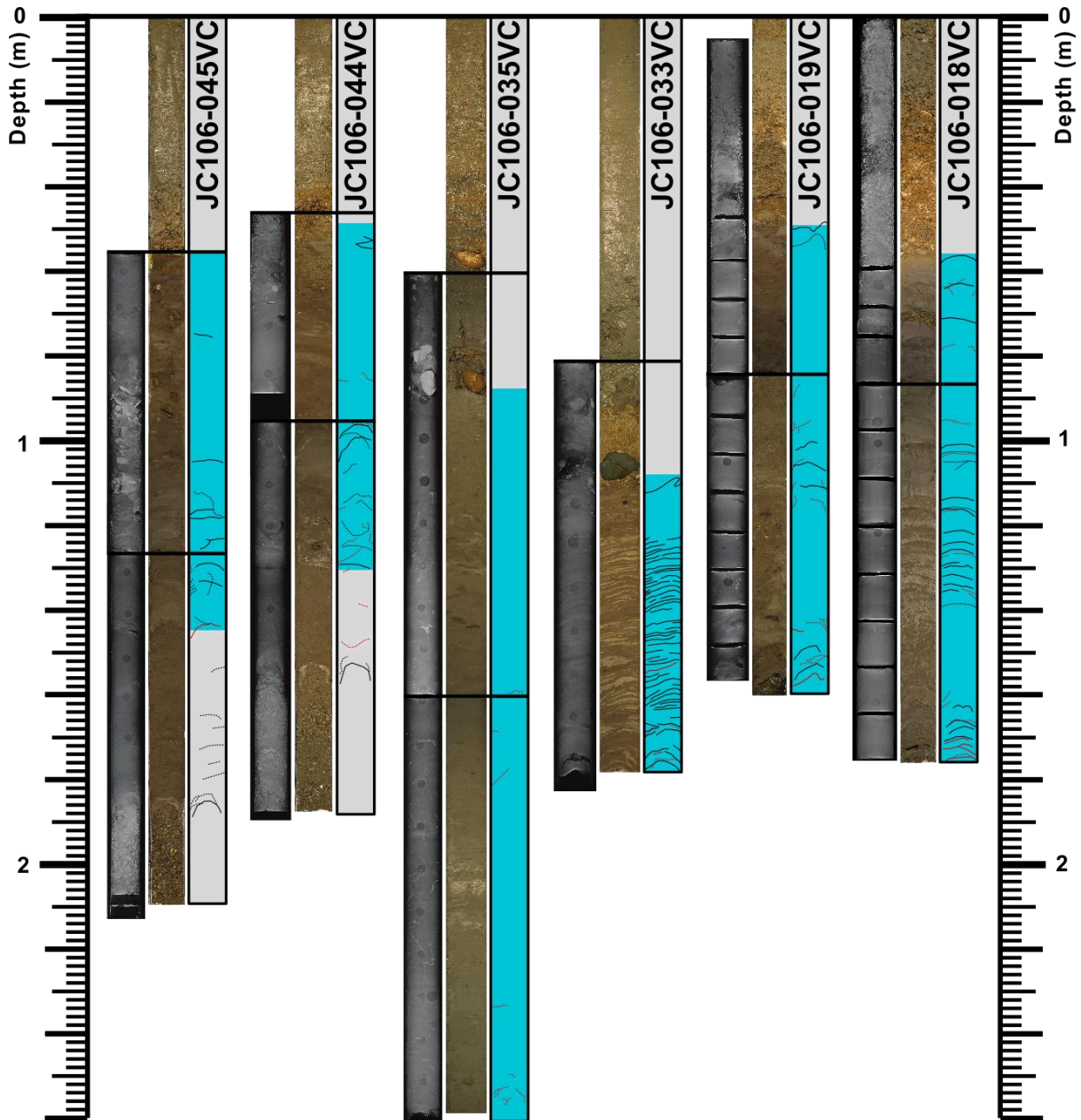


Figure 3.46 - Visible deformation structures (solid black) and fractures (solid red) with x-ray equivalent features (dashed) observed in Vibrocores (VC) containing Lithofacies (LF) LF8 (blue).

### 3.3.7 Summary of Findings

LF8, LF3 and LF4 exist as mud and silt deposits, which can be massive containing fine sand laminations. Atterberg limit tests show that mud component of these deposits has similar plastic and liquid behavioural properties, suggesting a similar clay type. LF8, recovered across the shelf is deformed and has undrained shear strengths of up to 165 kPa. Geotechnical tests show that LF8 is consistently over-consolidated, with OCRs between 20 and 96 within the top 2.5 m of core samples

which appear to increase with decreasing depth and show significant variability. These OCR results suggest that LF8 has experienced maximum yield stresses up to 999 kPa. This contrasts with LF3 and LF4 recovered from the Celtic Deep which have undrained shear strengths of up to 35 kPa and lacks any visible deformation up to depths of 7 m. OCRs for these sediments show that they are slightly over-consolidated with OCR values  $<3$  with no variability, suggesting maximum yield stresses of 150 kPa.

## **Chapter 4 - Interpretation**

### **4.1 Seafloor Geomorphology**

Bathymetric data reveal a large assemblage of seafloor features comprising many types which dominate in various regions of the shelf. The inner-shelf is dominated by glacially-related features, while the mid- and outer-shelf is characterised by large ridges. The morphology and distribution of these seafloor features provide information essential to their interpretation through comparison with other reported features with similar characteristics. The accurate interpretation of any feature is essential to ascertain its origin and the conditions during which it formed. Such information is essential for the reconstruction of the evolution of the shelf. This is particularly important for glacially-related features, information on which the current Celtic Sea glacial reconstruction certainly lacks. Therefore, such features provide key new information on past glacial dynamics which can be used to reconstruct such processes at ice stream scales.

#### **4.1.1 Large-scale Ridges**

Bathymetric data and morphological data produced through manual measurement of the ridge features suggest that, despite great variability in ridge morphology, three ridge populations can be delineated based upon morphological differences (Figure 3.1, Figure 3.2 and Figure 3.3). Two large populations of ridges exist to the northwest and the southeast which are separated by a band of vertically suppressed ridges in which small transverse ridges are more common. The ridges in the northwest consist of the longest and widest ridges, all having single crestlines. This northwest ridge population will be referred to as the megaridges. In places, the megaridges can be seen to overlie a mound which contributes to the bathymetric expression of the features (Figure 3.29, Figure 3.32 and Figure 3.36). This observation is most noticeable on seismic profiles which show a distinct change in seafloor slope either side of the ridge crest, representing the lateral extent of the uppermost of two vertically-stacked seismic facies (SF4) which commonly comprise the megaridges. A similar observation can be made from bathymetric data, where it is seen that some megaridges are asymmetric both laterally and axially where there is a change in seafloor character and slope similar to that observed on seismic profiles (Figure 3.4). Therefore, in places the lateral extent of the uppermost seismic facies comprising the megaridges can be observed on bathymetric data to overlie a gentler mound or plateau correlative to the lower seismic facies. The ridges to the southeast are thinner, more sinuous and have more complex crestlines, with some ridges appearing segmented with numerous crests which are joined by transverse ridges (Figure 3.4, Figure 3.5 and Figure 3.6). In places across the ridge field, counter-clockwise curvature of the ridge termini around their crest is observed (Figure 3.4) which is more common in the southeast where more sinuous ridges exist. Beyond the ridge ends, the ridges axially merge into much smaller transverse ridges (Figure 3.4) which in places link ridge crests to form large segmented ridges that are commonly observed in the southeast. These observations show that the ridges change in morphology laterally across the ridge field, which agrees with previous observations (Bouysse et al., 1976; Stride et al., 1982) while generally remaining axially uniform according to the characteristics of each ridge population.



The Celtic Sea ridges are significantly larger than sandbanks found elsewhere surrounding the British Isles (Stride, 1963; Stride et al., 1982). Stride et al. (1982) provide a comparison and overview of morphological differences between the Celtic Sea banks and other northwest European sandbanks. The Celtic Sea banks are significantly larger and have irregular crests compared to other sandbanks (Stride et al., 1982). These morphological characteristics are confirmed here; the features are up to 176 km long, 64 m high and 16 km wide (Figure 3.3), significantly longer and higher than the previously reported dimensions by Stride et al. (1982). It is also shown that the most-irregular crests dominate in the southeast while the longest, widest and most-uniform ridges exist in the northwest, which agrees with Stride et al. (1982). The ridges comprising the ridge field have been interpreted as tidal sandbanks which formed during lowered sea level based on their spatial extent and composition (Pantin and Evans, 1984), and the occurrence of a highly-energetic post-glacial marine transgression as suggested by palaeotidal model outputs (Scourse et al., 2009). The ridges are suggested to have formed by the entrainment of shelf sediment during the last post-glacial marine transgression due to exceptionally strong tidal currents which swept northeast across the shelf (Scourse et al., 2009). This post-glacial tidal mechanism can provide an explanation for the large size and coarse grainsize composition of the features, as energetic conditions persisted across the shelf for several ka (Scourse et al., 2009; Ward et al., 2016) with the energy capable of entraining coarse sand (Ward et al., 2015). Additionally, the spatial variability of shelf sediment, most notably that supplied by glaciation on the western shelf, is also suggested to have influenced the formation of the ridges (Scourse et al., 2009). The observed rotation, sinuosity of the ridges and axial transition into transverse ridges may be a product of flood and ebb tidal currents interacting with the features during their formation. These features are currently interpreted as being the largest examples of moribund sand banks in the world (Stride et al., 1982).

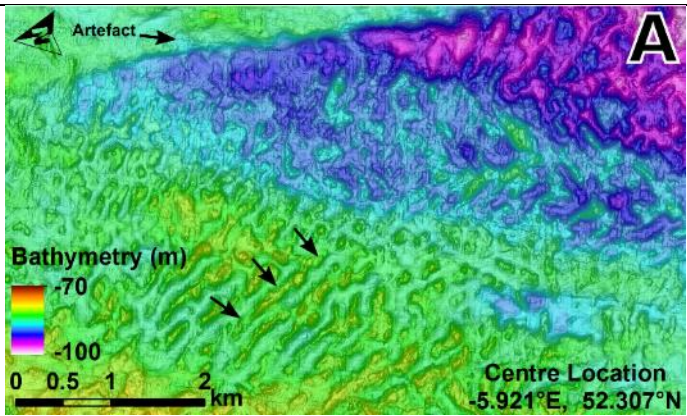
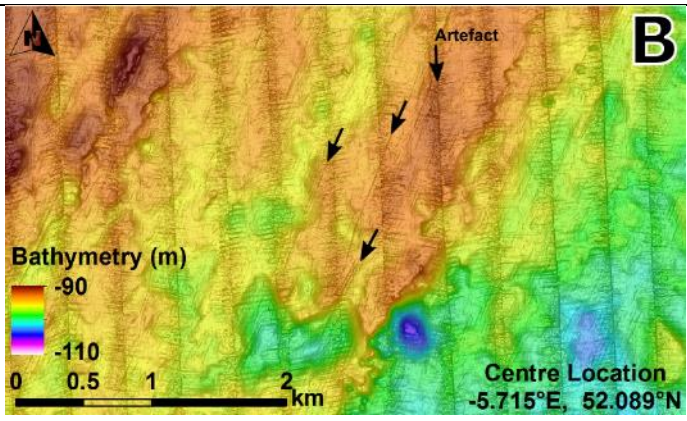
In an alternative interpretation, it has been suggested that the ridges may have formed as glacifluvial esker ridges, based on an interpretation that the ridges comprise glacial material (Praeg et al., 2015a). Such glacifluvial features can be hundreds of kilometres long and up to 80 m high, but commonly have widths <150 m while widths of several kilometres exist (Banerjee and McDonald, 1975; Mäkinen, 2003; Noormets and Flodén, 2002; Rust and Romanelli, 1975; Storrar et al., 2015; Veillette, 1986). Therefore, from a purely morphological perspective, the Celtic Sea ridges consistently reach or exceed the upper extreme size range for esker ridges. As the western shelf was glaciated (Praeg et al., 2015b; Scourse et al., 2019), it is also possible that the ridge field is not entirely glacifluvial in origin as this would invoke ice extension across the shelf with profound implications for glaciation. Therefore, a glacifluvial origin may explain the contrast in morphology between the ridges in the northwest and the southeast, with the former and latter representing eskers and tidal sand banks respectively. Eskers can display a wide variety of spatial configurations dictated by the glacial conditions during their formation, such configurations include dendritic networks, segmented ridges and long and continuous features which can be parallel or have no set arrangement (Storrar et al., 2014). Additionally, esker ridges are not commonly found in areas of fast ice flow or soft substrate (Livingstone et al., 2015), and are more commonly found in areas which experienced stable ice margin retreat as evidenced by the presence of continuous ridges (Storrar et al., 2014). As the Celtic Sea ridges are continuous for up to 176 km in the

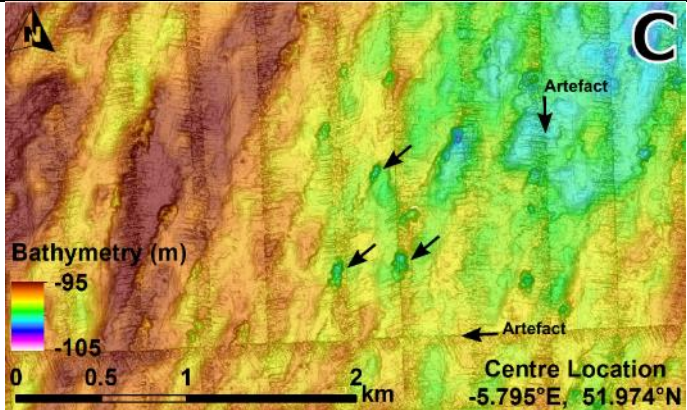
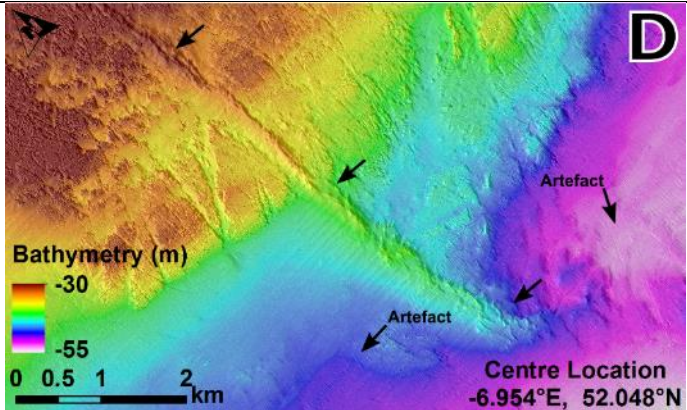
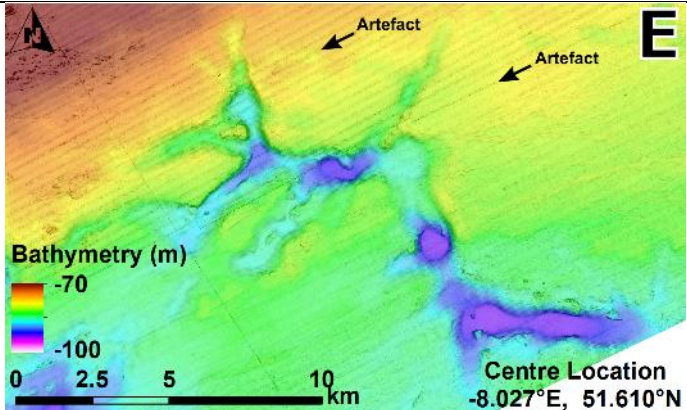
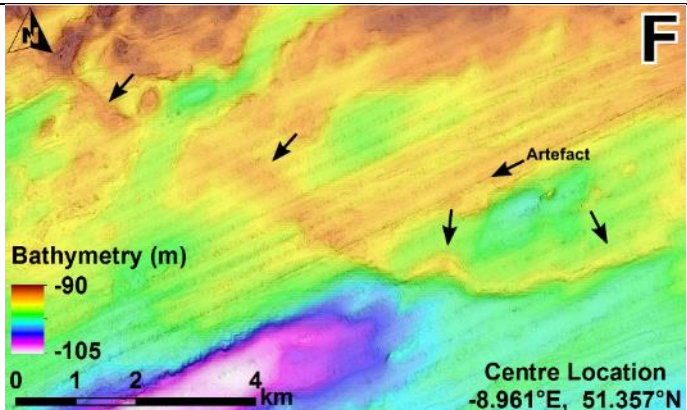
northwest, this would therefore suggest the gradual retreat of a non-streaming ice mass across the shelf. These observations need to be reconciled against the fact that these features are located on the bed of a probably surging ice stream which then retreated rapidly from the shelf (Scourse et al., 2019). However, some of the ridges also appear segmented, similar to the configuration observed in some eskers (Banerjee and McDonald, 1975). A glaciﬂuvial origin cannot explain the observed counter-clockwise rotation of the ridge ends, unless this characteristic is due to rotated post-glacial tidal deposits which have mantled the glaciﬂuvial ridges.

#### 4.1.2 Glacially-related Features

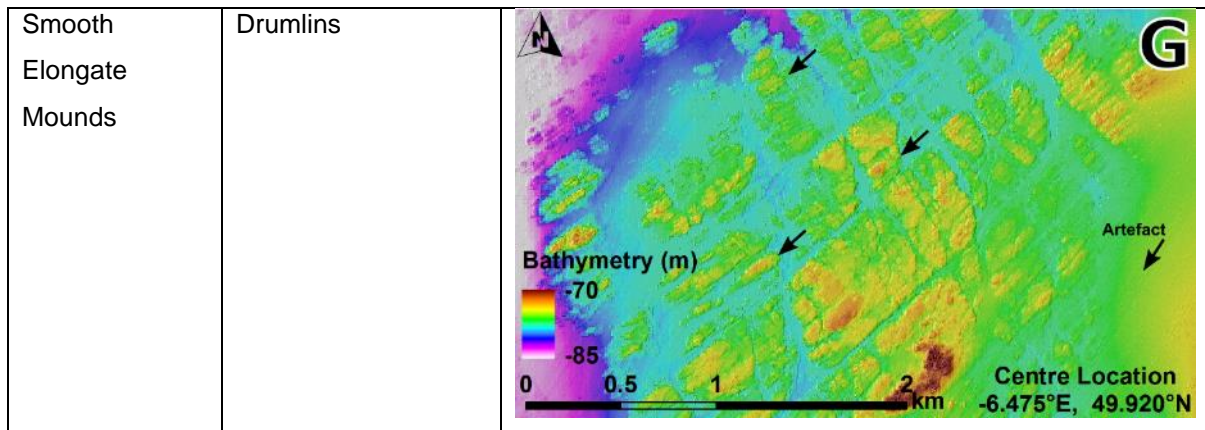
Multi-beam bathymetric data of the inner-shelf reveal a large assemblage of seafloor features associated with glaciation (Table 3.1, Figure 3.7 and Table 4.1), the majority of which have not been previously reported. Their presence records specific palaeo-glacial conditions which resulted in their formation and provides key new information on the glaciation of the Celtic Sea shelf lacking in previous reconstructions. Therefore, the accurate interpretation of these features is essential to understanding their palaeo-environmental contribution to a new reconstruction of palaeo-glacial dynamics in this region.

*Table 4.1 - Feature classes with example images existing as either hillshade or slope maps. For example image locations see Figure 3.7.*

| Feature Type    | Interpretation        | Example Image  |
|-----------------|-----------------------|--|
| Parallel Ridges | Ribbed Moraines       |  |
| Lineations      | Subglacial Lineations |  |

|                       |                                       |  |
|-----------------------|---------------------------------------|--|
| Irregular Depressions | Iceberg Grounding Pits                |  <p><b>C</b></p> <p>Bathymetry (m)</p> <p>-95</p> <p>-105</p> <p>0 0.5 1 2 km</p> <p>Artefact</p> <p>Centre Location<br/>-5.795°E, 51.974°N</p>    |
| Sinuuous Ridges       | Eskers                                |  <p><b>D</b></p> <p>Bathymetry (m)</p> <p>-30</p> <p>-55</p> <p>0 0.5 1 2 km</p> <p>Artefact</p> <p>Centre Location<br/>-6.954°E, 52.048°N</p>    |
| Overdeepened Channels | Tunnel Valleys and Meltwater Channels |  <p><b>E</b></p> <p>Bathymetry (m)</p> <p>-70</p> <p>-100</p> <p>0 2.5 5 10 km</p> <p>Artefact</p> <p>Centre Location<br/>-8.027°E, 51.610°N</p> |
| Arcuate Ridges        | Terminal Moraines                     |  <p><b>F</b></p> <p>Bathymetry (m)</p> <p>-90</p> <p>-105</p> <p>0 1 2 4 km</p> <p>Artefact</p> <p>Centre Location<br/>-8.961°E, 51.357°N</p>    |





### Parallel Ridges (Ribbed Moraines)

The observed parallel ridges cannot be explained as a result of the interaction between hydrodynamics and sediment transport, increasing confidence in a glacial origin. Ribbed moraine ridges can vary significantly in length and width (Dunlop and Clark, 2006), but horizontal dimensions are generally in the hundreds of metres (Ely et al., 2016) with heights of up to tens of metres. These features generally exist in fields or narrow bands of parallel and tabular ridges, with individual features displaying undulating crests (Clark and Meehan, 2001; Dunlop and Clark, 2006). These characteristics match the parallel ridge features in St. George's Channel (St. GC; Figure 3.8 and Image A in Table 4.1), which are interpreted as ribbed moraines. While parallel ridges are common in the current marine environment, such features form by currents and generally have similar orientations and have steep and sharp crestlines (Van Landeghem et al., 2009b). Ribbed moraines form transverse to ice flow at the transition from cold- to warm-based ice (Hättestrand, 1997; Hättestrand and Kleman, 1999) and are formed at the onset of ice streaming (Dunlop and Clark, 2006). Additionally, such features may be associated with cold-based ice forming sticky spots, where the features have been protected from reworking and have been preserved (Trommelen et al., 2014).

### Lineations (Subglacial Lineations)

Much more vertically pronounced linear features have been identified on the beds of ice streams, where they have been interpreted as glacial lineations parallel with ice flow direction of up to kilometre scale which can overprint glacial topography (Ottesen et al., 2017; Rydningen et al., 2013). In places, such features overprint underlying glacial depositional ridges (Dunlop and Clark, 2006), similarly observed here (Image B in Table 4.1). Curvilinear features can occur on the seafloor, where they represent patches of sand being transported by currents (Belderson et al., 1982). However, these features appear as distinct raised platforms, different to the linear features observed here which do not exist as positive or negative features. This characteristic can be explained by the dragging of an object along the seafloor which occurred over a significant area due to the consistent orientation of these features along with the observation that they do not deviate due to topography (Image B in Table 4.1). These characteristics cannot be produced by the interaction between hydrodynamics and sediment transport, as such a process would be influenced by the seafloor topography. Therefore, the observed

lineations in St. GC are interpreted to represent the product of subglacial abrasion under a grounded warm-based ice sheet, partially overprinting ribbed moraines.

### **Irregular Depressions (Iceberg Grounding Pits)**

The features observed here are similar to channels and pits produced by grounded icebergs which have scoured their keels across the seabed (Brown et al., 2017; Ottesen et al., 2017; Rydningen et al., 2013), similar to features observed here which can exist as slightly elongated pits. Such depressions are prominent on the northern side of a seafloor rise to the south of St. GC, consistent with icebergs grounding in shallower areas, originating from the north and travelling south. Such features cannot be explained by the interaction between hydrodynamics and sediment transport, as such features would not form sporadically across an area or form without an object acting as a nucleus for the depression. However, these features are elongated to the southwest (Plot F in Table 3.1 and Image C in Table 4.1), suggesting that hydrodynamics may have played a part in their development but not their initial formation. Gas-escape features produce near-circular depressions in the seafloor (Dunlop et al., 2010). The observed depressions are interpreted to be iceberg scour marks and pits, as in places these features display elongation, almost becoming scour-like, and are highly irregular which is not consistent with gas-escape.

### **Sinuuous Ridges (Eskers)**

The ridges observed here (Figure 3.9 and Image D in Table 4.1) are similar to sinuous eskers observed on the seafloor in other glaciated areas (Ottesen et al., 2008; Van Landeghem et al., 2009a) which generally have lengths of several kilometres and widths of tens to hundreds of metres (Mäkinen, 2003; Storrar et al., 2015, 2014). Such features can also be represented by beaded ridges and fan-like deposits, highlighting a high degree of variability in their morphology (Brennand, 2000; Gorrell and Shaw, 1991; Hebrand and Åmark, 1989). The sinuous ridges identified here have been previously interpreted as eskers by Tóth et al., (2016). Esker ridges are not commonly found in areas of fast ice flow or soft substrate (Livingstone et al., 2015), and are more commonly found in areas of stable ice retreat (Storrar et al., 2014). The features identified here appear similar in dimensions and morphology (Table 3.1) to esker ridges and are found on hard beds. Esker ridges can form time-transgressively behind the retreating ice margin, with continuous ridges represent deposition during gradual ice retreat (Storrar et al., 2014).

### **Overdeepened Channels (Tunnel Valleys and Meltwater Channels)**

Overdeepened channel systems of complex plan-form morphology include abrupt termini in places which are typical of subglacial meltwater drainage (Greenwood et al., 2007; Lonergan et al., 2006), formed by the incision of meltwater (Huuse and Lykke-Andersen, 2000). The large size of the features observed here (Table 3.1) are comparable to tunnel-valleys which have been identified on the inner-shelf in various stratigraphic positions (Eyles and McCabe, 1989; Tappin et al., 1994). Overdeepening is not necessarily observed in every subglacial channel (Grau et al., 2018). Therefore, such features

may be fluvial, requiring terrestrial conditions and an exposed shelf. However, such a scenario is hard to reconcile with the observation of iceberg grounding pits off the southern coastline of Ireland presented here and the recovery of deglacial muds indicative of deglaciation in contact with a pro-glacial waterbody across the shelf (Furze et al., 2014). Therefore, a subglacial meltwater origin of these channels is more likely as some of the features are significant in size, despite being located in areas of gentle slope (Figure 3.7). Meltwater drainage features are typically time-transgressive in origin, forming behind a warm-based ice margin during its retreat, and so may be used to determine the orientation of ice retreat, especially when combined with additional information such as topography or the presence of moraine ridges (Greenwood et al., 2007). The channels observed across the Celtic Sea display overdeepening, where the resolution of the data permit, and exist as either single channels or highly variable and bifurcated systems (Table 3.1, Figure 3.7, Figure 3.10 and Image E in Table 4.1). The orientation of these features indicates broad ice retreat patterns, with some influence on location and orientation driven by the underlying geology and its structure. These overdeepened channels are therefore interpreted as tunnel valleys and meltwater channels formed under grounded warm-based ice.

#### **Arcuate Ridges (Terminal Moraines)**

The arcuate ridges (Image F in Table 4.1) lie nearly perpendicular to the coastline and the overdeepened channels interpreted here as being formed by subglacial meltwater (Area A in Figure 3.7 and Figure 3.11). The upper surface of the largest ridge to the southwest is marked by depressions interpreted as iceberg scours, indicating deglaciation occurred in contact with an aqueous body in this area after the underlying arcuate ridges formed. Similar arcuate ridges have been identified in other glaciated areas where they have been interpreted as moraine ridges, representing deposition along a retreating ice margin (Dove et al., 2015; Howe et al., 2012; Ottesen et al., 2017, 2008; Shaw, 2003). Such features cannot be explained by the interaction between hydrodynamics and sediment transport as the orientation changes along each ridge and their crestlines are rounded and discontinuous, not consistent with the operation of marine currents. The observed arcuate ridges are interpreted to represent sequential moraine ridges marking individual ice margin positions during retreat.

#### **Smooth Elongate Mounds (Drumlins)**

Elongated mounds with a smooth upper surface found on the beds of former ice sheets have been interpreted as drumlins which formed subglacially and parallel to ice flow direction (Clark et al., 2009; Ottesen et al., 2017). Similar features are observed here, which are found in areas of prominent and irregular seafloor where the features appear to outcrop from the seabed on the eastern inner-shelf (Figure 3.12 and Image G in Table 4.1). This suggests that the features comprise exposed bedrock which has been glacially sculpted and abraded into the observed mounds. While bedrock may have inherent internal structure and alignment, predisposing any subglacial features to have a similar alignment, rounded bedrock features are generally indicative of subglacial erosion and can be used to infer ice flow direction (Krabbendam et al., 2016). Similar smooth elongate mounds are found on the



western shelf which do not appear to be formed on areas of prominent seafloor consistent with underlying bedrock composition. Therefore, these features may comprise glacigenic sediment instead. Such features have been used to interpret ice flow direction (Bradwell et al., 2008; Dove et al., 2015; Ottesen et al., 2017). Elongated mounds of smoothed bedrock or sediment are interpreted to represent drumlins formed by warm-based grounded ice and with an orientation indicative of ice flow direction.

## **4.2 Sub-seafloor Stratigraphy**

Eleven regional Seismic Facies (SF) were identified from seismic sections across the shelf, comprising most of the shallow stratigraphy of the region. A summary is shown in Figure 4.1. Sediment cores identified nine Lithofacies (LF) which provide essential composition information when correlated to the penetrated seismic facies. This integrated stratigraphy can then be combined with observations of previous stratigraphic investigations to provide the most accurate representation of the shallow stratigraphy of the shelf. This new stratigraphy provides the basis for interpreting the depositional environment on the shelf during deglaciation and the post-glacial and its evolution through time. Such information is critical for reconstructing palaeo-glacial conditions, improving on existing reconstructions which are based heavily on poorly correlated and spatially-positioned physical and geophysical data.

### **4.2.1 Seismic Facies Interpretation**

The interpretation of seismic facies based upon their acoustic character alone provides an objective foundation from which to correlate these facies to other regional seismic units. The character and reflection geometries of these seismic facies can also be used to infer their composition, formation mechanism and origin, providing information which may be useful when correlated to lithofacies and other regional units to critique the confidence of the correlation based upon what is most likely or expected.

#### **Seismic Facies 1**

The surface crenulations comprising SF1 may represent mobile sediment overlying an immobile layer at their base which is represented acoustically by an underlying reflection (Figure 3.19 and Figure 3.20). These features are found in places in both inter-ridge areas and overlying ridge crests, suggesting that present-day currents are active in such areas to maintain the features. The crenulations are associated with a medium amplitude fill, which may represent a coarse-grainsize composition compared to the low amplitude fill of SF1 seen in large basins (Figure 3.15) which suggests a more tranquil depositional environment associated with a fine-grainsize composition. In places, a downward transition is observed where SF1 increases in amplitude towards its base (Figure 3.14), which may suggest the presence of a fining-upwards transition in grainsize. Where the seafloor is highly irregular, SF1 comprises bedforms (Figure 3.39 and Figure 3.40) which suggest that current speeds are, or were, sufficient enough to entrain sediment to result in their formation and maintenance. The largest of such features exist at the southern shelf edge overlying a ridge crest. Where such bedforms are observed on ridge crests, they are asymmetrical with the steepest slope of the features appearing to face towards the crest of the ridge. This suggests that the bedforms are, or were, migratory, and that the direction of the features, and thus the currents resulting in their formation, are influenced by the presence of the ridge features. These crenulations and migratory bedforms do not occur everywhere across the shelf, as in places the seafloor is smooth (Figure 3.35 and Figure 3.38), suggesting that currents are not active in these areas, or that the sediment comprising the seafloor is immobile. Therefore, these observations suggest that

SF1 is most likely the product of the Holocene marine environment reworking the seafloor. The base of this facies truncates underlying reflections (Figure 3.14), suggesting that an erosion event took place.

### **Seismic Facies 2 and 3**

The parallel reflections of SF2 (Figure 3.14 and Figure 3.40) can be explained by deposition in a quiet subaqueous environment through suspension settling. The parallel reflections most likely represent individual depositional events in the sequence over a wide area due to their lateral traceability. The upward transition from SF2 to SF3 suggests that SF2 represents proximal deposition of material, while SF3 represents distal deposition of fine-grained material similar to the low amplitude fill of SF1 (Figure 3.14).

### **Seismic Facies 4**

SF4 makes up the upper bulk of the large ridges and much smaller transverse ridges. These ridges appear to mantle earlier features, as they can be seen to asymmetrically mantle underlying mounds or rest upon raised plateaux when observed in cross-section (Figure 3.29, Figure 3.32 and Figure 3.36). The extent of SF4 over such features is bounded by distinct lateral breaks in slope of the seafloor either side of the crest. Therefore, where seismic data are lacking, but high-resolution bathymetric data exist across the ridges, this change in seafloor character could indicate the lateral extent of SF4. The bedding within the ridges suggests a coarse-grainsize composition. The observation that these bedding planes are dipping throughout SF4 and are truncated against the upper surface (Figure 3.22) is consistent with a ridge built by the continuous action of currents. Such a process can provide an explanation for the occasionally observed asymmetry of the ridges, indicating migration of the features. However, where SF4 lacks acoustic character or contains complex reflections (Figure 3.24 and Figure 3.38), it is less consistent with a marine origin. The base reflection which appears prominent and truncates reflections below (Figure 3.24) might represent a regionally-extensive erosion surface. Additionally, the upper surface of SF4 is erosional in nature as dipping reflections are in places truncated against it. Therefore, SF4 is bounded by upper and lower erosion surfaces.

### **Seismic Facies 5**

Interpretation of SF5 is limited due to its lack of acoustic character. Where imaged, it has a low amplitude appearance which might suggest that it is fine-grained and homogenous in composition, similar to the low amplitude fill of SF1 and SF3.

### **Seismic Facies 6**

As similarly interpreted for SF2, the occurrence of parallel reflections may indicate that SF6 was deposited in a quiet subaqueous environment, with individual reflections representing unique depositional events over a wide area. However, the increasing discontinuity of these reflections upwards (Figure 3.24) may indicate some form of post-depositional reworking which only affected the upper

layers of SF6 while lower layers remained undisturbed. As the parallel reflections are horizontal and are truncated laterally either side of the mound (Figure 3.24), this suggests that SF6 was originally deposited as a sheet but was eroded into the shape of a mound.

#### **Seismic Facies 7**

As SF7 forms an underlying mound for SF4 (Figure 3.36), similar to SF6, then it might also have been sculpted during an erosion event as reflections appear laterally truncated against its upper surface. Some instances of bedding are observed in SF7 (Figure 3.29 and Figure 3.31) which may suggest a coarse grainsize composition, however this observation is rare due to the reduced penetration of the chirp data. Therefore, a thorough interpretation of this facies is not possible.

#### **Seismic Facies 8**

SF8 appears to contain in places subtle parallel reflection geometries (Figure 3.21) which may indicate deposition in a quiet subaqueous environment, similar to the interpretation of SF2 and SF6. The majority of this facies does not display any acoustic character, resulting in a limited interpretation partly due to inadequate penetration by chirp data.

#### **Seismic Facies 9**

The dipping laminations comprising SF9 (Figure 3.34) suggest deposition in a subaqueous environment. However, due to the steep dip of these reflections such a scenario must have occurred a significant time ago prior to tectonic disturbance as this facies has since been exposed to significant erosion events and channelling. Therefore, this facies may be lithified, comprising bedrock.

#### **Seismic Facies 10**

The outcropping nature and irregular surface of SF10 at the seafloor suggests that it is lithified, comprising bedrock (Figure 3.18).

#### **Seismic Facies 11**

Parallel laminations comprising SF11 (Figure 3.16) suggest deposition in a quiet subaqueous environment. However, due to the steep slopes bounding this facies, it is most likely lithified, comprising bedrock.

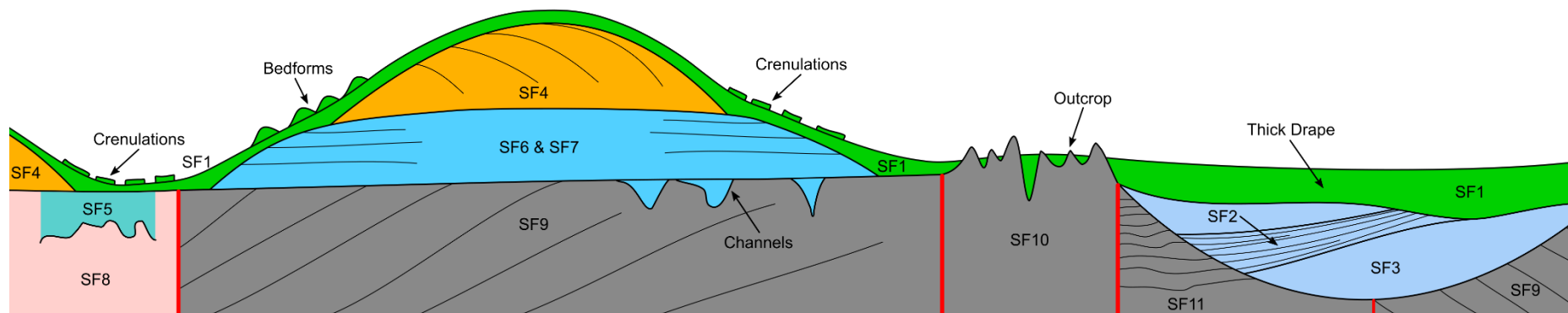


Figure 4.1 - Cartoon showing a summary of the stratigraphic relationships between the observed Seismic Facies (SF). Vertical red lines indicate different sections. Not to scale.

#### **4.2.2 Lithofacies Integration**

Correlation between the imaged seismic facies (Figure 4.1) and lithofacies (Table 3.2) recovered from Vibrocores (VC) and Piston Cores (PC) provide essential information on the composition of the imaged seismic facies where correlation is possible (Figure 4.2). This then permits the interpretation of the depositional environment resulting in the formation of the observed stratigraphy and correlation with other physical samples and regional seismic units based upon similar characteristics. This integrated stratigraphy provides the basis for the reconstruction of the depositional history and evolution of the shelf. Not all seismic facies were cored. Core logs can be found in Lockhart et al. (2018) and Scourse et al. (2019) in the Appendix.

#### **Seismic Facies 1**

This facies drapes the megaridges and older deposits across the shelf, comprising the seafloor which corresponds directly to LF1 recovered at the seafloor in all cores (Figure 4.2). These physical samples show that the grainsize composition of SF1 varies laterally due to a change in water depth, but generally consists of fine mud and sand in the inter-ridge depressions and the Celtic Deep (CD), and medium to coarse sand upslope from the megaridge flanks. This grainsize change can explain the low amplitude character of SF1 in the inter-ridge depressions, while on the ridge surfaces SF1 increases in amplitude due to coarsening. SF1 varies in thickness, in places thinning below the resolution of the seismic data in situations where it can still be observed in cores. LF1 generally transitions downwards into LF2 which forms the base of SF1. A similar stratigraphy is observed in the CD where LF1 overlies a much coarser LF1a comprising shelf fragments and clasts (cores 51PC, 52PC and 53VC in Figure 4.2), suggesting a similar origin to LF1 and LF2 on the mid- and outer-shelf.

#### **Seismic Facies 2 and 3**

Below the superficial drape of SF1 which comprises LF1 and LF1a in the CD, SF2 was cored as LF3, corresponding to soft mud containing fine sand laminations (cores 51PC, 52PC and 53VC in Figure 4.2). Such laminations must be represented by the parallel reflections observed in SF2. Below these laminations, SF3 was recovered as LF4 which comprises a massive soft clay which lacks structure (cores 51PC, 52PC and 53VC in Figure 4.2). This explains the lack of acoustic character of SF3.

#### **Seismic Facies 4**

Beneath the superficial drape of SF1, seismic data show that the megaridges on the mid- and outer-shelf mainly comprise two stacked seismic facies. The upper ridge bulk correlates to SF4 and was cored as LF5 beneath the superficial drape observed as LF1 and LF2 (cores 16VC, 29VC, 30VC, 31VC, 32VC and 34VC in Figure 4.2). LF5 comprises medium to coarse sand with shell fragments occasionally with subtle layering. Such layering may be represented in SF4 by dipping reflections.



### **Seismic Facies 5**

SF1 was imaged at the core sites and these physical samples penetrated LF1 and LF2 corresponding to SF1. Below this covering superficial drape, LF8 was recovered from SF5 which corresponds to stiff clay and silt, in places containing fine sand laminations which are deformed (cores 44VC, 45VC, 36VC and 39VC in Figure 4.2). The homogenous nature of LF8 provides an explanation for the lack of acoustic character of SF5 in places.

### **Seismic Facies 6**

Where SF1 thins below seismic resolution, this superficial drape remains as cores recover LF1 and LF2. Therefore, where SF6 is exposed close to the seafloor on the lower flank of the megaridges under SF1, it was cored as LF8 which comprises stiff clay and silt in places containing fine sand laminations which are deformed below LF1 and LF2 (cores 15VC, 33VC and 35VC in Figure 4.2).

### **Seismic Facies 7**

SF7 occurs under SF1 where it is exposed on the lower flank of the megaridges. Cores recovered from this area contained LF1 and LF2 corresponding to SF1, and LF8 which corresponds to SF7 (cores 18VC and 19VC in Figure 4.2). LF8 comprises stiff clay and silt in places containing fine sand laminations; some of these laminations are deformed. In another instance, SF6 may have been cored under the superficial drape of LF1 and LF2, corresponding to LF6 comprising coarse sand and shell fragments (cores 22VC and 28VC in Figure 4.2). However, this is not a confident correlation as LF6 may correlate to SF4 where it thins overlying SF7.

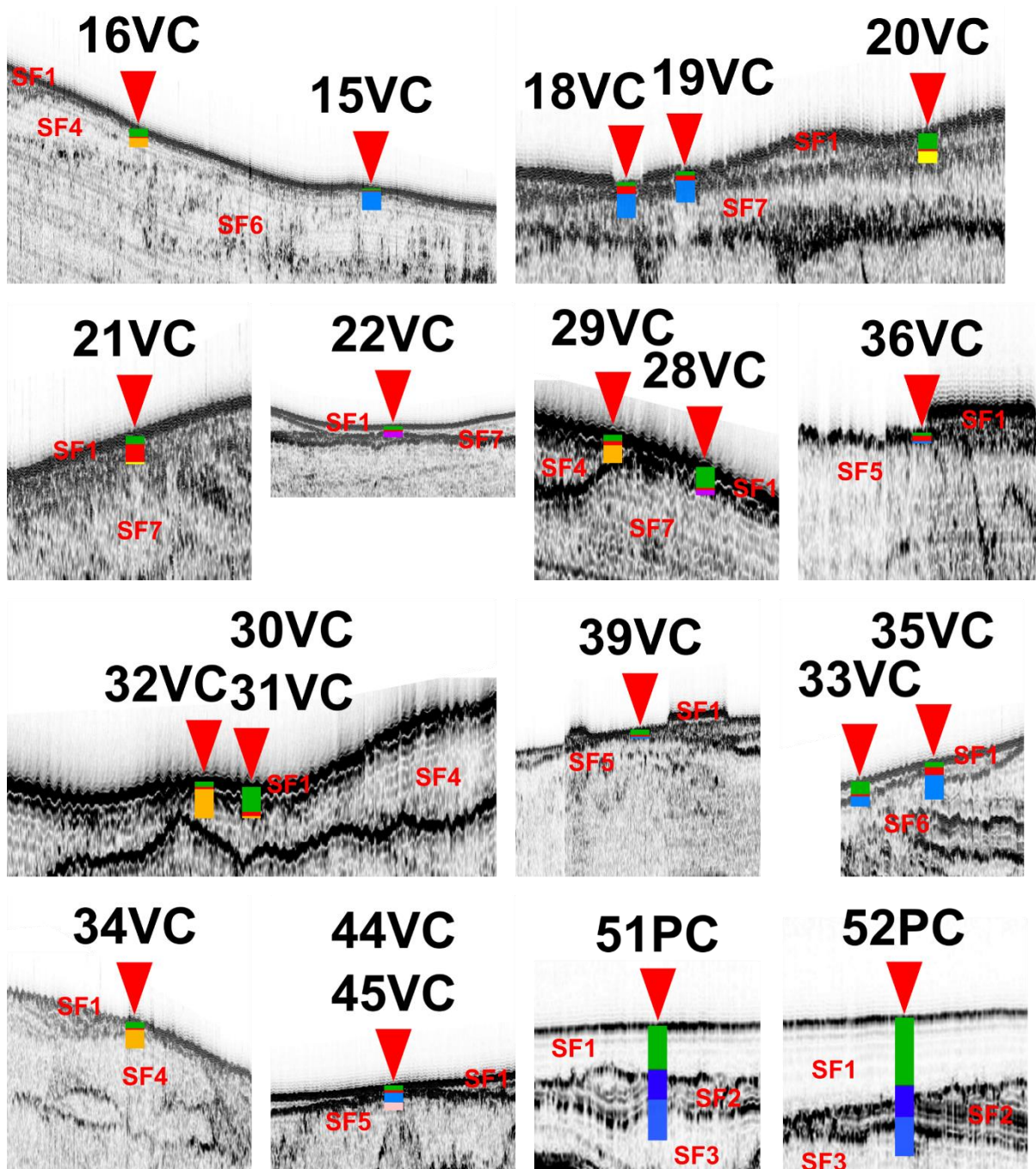


Figure 4.2 - Correlation between cored lithofacies and imaged Seismic Facies (SF). Lithofacies colours for each core correspond to those in Table 3.2.

#### 4.2.3 Stratigraphic Correlation to Other Investigations

Systematic surveying of the Celtic Sea shelf by the British Geological Survey (BGS) in the 1970s identified various seismic-stratigraphic units across the shelf, some of which were correlated to litho-stratigraphic units identified from sediment cores and other physical samples. However, direct correlation between these data was not always possible (Pantin and Evans, 1984) due to the reduced resolution of the available seismic data and the accuracy of the positioning system used; see Fannin (1989). Additionally, the detailed imaging of the internal structure and contact surfaces of shallow

seismic units was not always possible (Pantin and Evans, 1984) due to the seismic data having insufficient resolution and penetration. More recent seismic data presented and described here provide enhanced detail in comparison to previous datasets and adequately image the shallow stratigraphy of the Celtic Sea shelf and the seismic facies that comprise it. Such data allow the correlation of seismic facies presented here with shallow BGS litho-stratigraphic units and seismic-stratigraphic units which was not previously possible. However, not all of the seismic facies described here correlate with BGS units. The integration of these results with the BGS stratigraphy and other coring investigations provides the most-accurate representation of the shallow stratigraphy of the Celtic Sea shelf (Table 4.2). This fully integrated and updated shallow stratigraphy represents the best foundation from which to reconstruct the evolution of the depositional environment of the Celtic Sea shelf.

### **Seismic Facies 1 (Superficial Drape)**

A discontinuous seafloor seismic facies was noted in places by Pantin and Evans (1984) which formed superficial bedforms and crenulations in places. This superficial drape has been imaged as SF1 and is correlative to LF1 and LF2 identified from cores. LF1 and LF2 correspond to Layers A and B of Pantin and Evans (1984), and to Units I and II of Furze et al. (2014) respectively, the descriptions of which are similar to this study. In the CD, LF1a, existing as a basal lag under LF1, is additionally correlative to Unit II from Furze et al. (2014) and may have a similar origin to LF2 and Layer B recovered across the mid- and outer-shelf.

While BGS seismic data of Layers A and B was limited, seismic data presented here (Figure 3.13) show the spatial distribution of these superficial deposits in various locations and stratigraphic settings across the shelf and overlying the ridges. While the bulk of SF1 corresponds to Layer A from the BGS stratigraphy, Layer B comprises a coarse lag which may be contained within SF1. This scenario suggests that Layer A directly overlies Layer B in every instance of SF1, which fits the majority of core observations where LF1 consistently overlies LF2, the latter showing some variability in grainsize and thickness (Table 3.2 and Figure 4.2). However, some shallow physical samples showed that Layer B is missing in places (Pantin and Evans, 1984). Indeed, boulders which in places comprise Layer B have only been observed in the inter-ridge areas and on the lower flanks of the megaridges (Pantin and Evans, 1984). Such observations suggest that Layer B is not uniform at the base of SF1 across the shelf which may be due to the composition of the underlying units which were eroded during its formation.

Published dates on Layer B, the basal layer of SF1, from 12 cores recovered across the inner-shelf, extending from within the northern megaridges towards St. GC, have yielded a wide spread of radiocarbon ages. Ages of 13.9-4 ka BP were obtained from intertidal molluscs, the oldest of which were obtained from the CD and were suggested to represent the onset of Layer B formation during shallow marine conditions 14 ka BP (Furze et al., 2014). Other published dates show that Layer A in the CD has conformable ages from 13-3 ka BP (Scourse et al., 2002). This evidence suggests that SF1 is of post-glacial age on the inner-shelf, and records marine deposition during the late stages of

transgression prior to, and during, the Holocene (Furze et al., 2014). On the mid- and outer-shelf, the in places fining-upwards character of Layer B to Layer A in SF1 is consistent with deposition during decreasing energy associated with rising post-glacial sea level (Pantin and Evans, 1984). No published dates on this unit are available on the mid- to outer-shelf, therefore the age estimate of SF1 beyond the inner-shelf is inferred. However, due to the time-transgressive nature of post-glacial marine transgression, the age of SF1 is expected to become older towards the shelf edge, suggesting that SF1 formed before 14 ka BP on the mid- and outer-shelf. Here, SF1 must have formed after the seismic facies over which it rests. Therefore, SF1 must have commenced formation between 24-14ka BP on the mid- outer-shelf as the underlying LF8 glacial sediments have youngest ages of 24 ka BP (Praeg et al., 2015b; Scourse et al., 2019).

SF1 comprises the superficial drape across the shelf which has been shown to comprise transverse sand patches and other bedforms influenced by Holocene hydrodynamics (Belderson et al., 1982). The observed crenulations which overlie a reflection within SF1 are consistent with the observations of traverse sand patches which overlie a gravel bed across the Celtic Sea shelf (Belderson et al., 1982). Additionally, where SF1 forms bedforms with steep peaks, these features are actively migrating in response to currents (Belderson et al., 1982). Where these features are abundant, they may represent areas of the shelf where sediment accumulation has been active the longest (Belderson et al., 1982). Therefore, SF1 represents Holocene deposits formed by wave and tidal processes.

### **Seismic Facies 2 and 3**

The massive fine-grained and laminated sediments comprising SF2 and SF3 in the CD have been interpreted as being glacial in origin, equivalent to LF8 recovered across the mid- and outer-shelf (Scourse et al., 2019). While in the UK sector these facies have not been identified as a regional unit, SF2 and SF3 have been identified in the French sector of the shelf where they infill a channel under the Melville Formation (MFm). These channels have been correlated to the Upper Little Sole Formation (ULSFm), representing the eastward extension of the unit from the western outer-shelf (Bouysse et al., 1976). While no physical samples of the ULSFm channels exist in the French sector, the acoustic character and stratigraphic position of SF2 and SF3 under SF1 are remarkably similar between the CD and the French sector. Without physical samples to confirm the composition of SF2 and SF3 in the French sector, any interpretation is tentative. However, if SF2 and SF3 are glacial in origin in this region, then this has profound implications for ice limits and deglacial conditions on the outer-shelf beyond presently considered ice limits.

### **Seismic Facies 4 (Melville Formation)**

SF4 entirely comprises single prominent mounds or the upper bulk of the megaridges. SF4 contains clinoforms and other complex reflections which are generally truncated against the upper surface and is composed of LF5, comprising medium to coarse sand with shell fragments. The ridges are rounded in profile but can show some asymmetry both laterally and axially. The base of SF4 is in most places a

strong sub-horizontal or slightly dipping reflection, and it is here observed to mantle earlier deposits on the western shelf. These observations are consistent with the description of the MFm by Marsset et al. (1999), Pantin and Evans (1984) and Reynaud et al. (1999b). Therefore, SF4 correlates to the MFm which mantles the ULSFm.

Seismic data indicate that two major Erosion Events (EE) have occurred in the shallow stratigraphy, one truncating reflections in the underlying ULSFm (EE1), and the second truncating reflections in the MFm (EE2; Figure 4.3). EE1 occurred after the development of the ULSFm and prior to the development of the MFm, and EE2 occurred after the development of the MFm but before the development of SF1 as it only affected the MFm. The initial major erosion surface of EE1 which occurred after the development of the ULSFm but before the development of the MFm must have been regionally extensive, as the associated reflection truncates the ULSFm across the shelf (Figure 3.24, Figure 3.31 and Figure 3.38). This is consistent with the observation that a coarse lag deposit, similar in description to Layer B, exists at the base of the MFm which represents the product of an erosion event (Pantin and Evans, 1984). Any evidence of erosion which has impacted the ULSFm must therefore be attributed to the regionally-extensive EE1 which occurred prior to subsequent erosional events. EE2 appears to have been localised to the upper surface of the MFm (Figure 3.21 and Figure 3.23), possibly due to the MFm being prominent and thus being more exposed. It is also possible that EE2 may have been more spatially-extensive, overprinting EE1 in places on the lower flanks of the megaridges. If overprinting did occur, then the reflection associated with EE1 would be truncated by EE2 where the MFm tapers out which is not observed in every case (Figure 3.20, Figure 3.21, Figure 3.23 and Figure 3.24). This could be due either to the effective armouring of the EE1 coarse lag or the intensity of EE2 decreasing with increasing depth. Therefore in the latter scenario, EE2 may have been focused on the shallower upper surface of the MFm. Therefore, out of the two major erosion events, EE1 was regionally extensive, while EE2 was localised to the upper surface of the MFm, most likely due to its prominence. All cores penetrating SF1 consistently recovered a basal coarse lag which fines upwards into the main bulk of the unit, suggesting that a regionally-extensive erosion event (EE3) occurred during the formation of the unit, but its duration and intensity are unknown. If EE3 was a major regionally-extensive erosion event associated with the formation of SF1, then the EE1 reflection would be truncated against SF1 on the lower megaridge flanks where SF1 has significantly eroded into both units at the boundary. This is not observed in every case (Figure 3.20, Figure 3.21, Figure 3.23 and Figure 3.24), suggesting that EE3 was a minor regionally-extensive erosion event and not responsible for the truncation of reflections in the MFm. This agrees with the interpretation that SF1 represents Holocene marine deposits, with the basal coarse lag representing winnowing by shallow marine conditions which would be more pronounced on the MFm than in the inter-ridge areas. Therefore, three erosion events have occurred in the shallow stratigraphy, two major events identified on seismic data, EE1 being regionally-extensive and EE2 being localised to the MFm, and one minor regionally-extensive event cored at the base of SF1 (EE3) which has overprinted the earlier erosion surfaces (Figure 4.3).

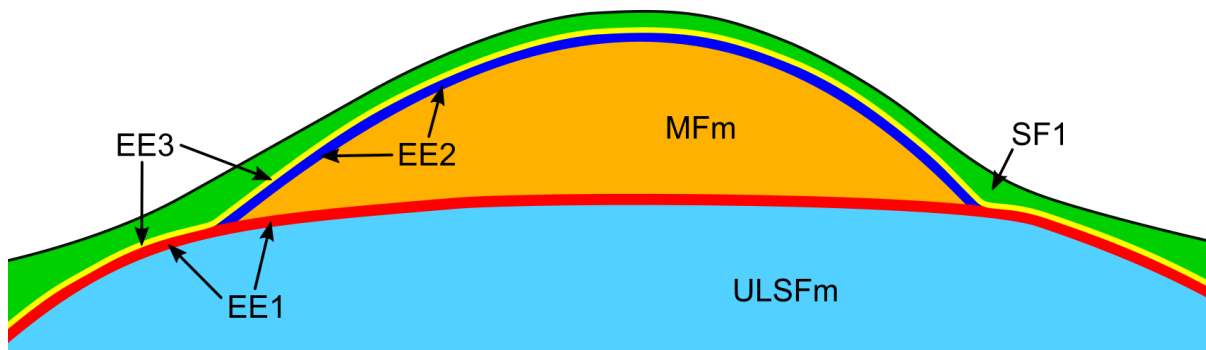


*Figure 4.3 - Schematic cross-section of a megaridge showing stratigraphic units and Erosion Events (EE) as indicated by cored physical samples and the truncation of reflections on seismic profiles across the mid- and outer-shelf. EE1 (red) is regionally extensive over the Upper Little Sole Formation (ULSFm) while EE2 (blue) is localised to the Melville Formation (MFm). The formation of the superficial drape (SF1) is associated with a regionally-extensive but minor EE3 (yellow).*

The stratigraphic position, varying intensity and overprinting of these erosion events results in a different character of the cored coarse lag at the base of SF1 in the inter-ridge and lower ridge flank areas compared to above the MFm because of the composition of the underlying units which were eroded (Figure 4.3). The composition alone of these lag deposits may not indicate which erosion event was stronger or lasted for a longer duration, as the composition of the lag deposits are a product of the underlying unit being eroded at the time of lag formation. Regardless, the laterally-varying composition of the coarse lag at the base of SF1 might explain the observation that Layer B was missing in places by Pantin and Evans (1984) as it would have a different physical character laterally across the varying stratigraphy, depending upon the composition of the underlying eroded deposits. The coarse lag deposits associated with EE1 and EE2 diverge above and below the MFm before being overprinted by EE3, resulting in numerous coarse layers which vary in composition and age, all of which were called Layer B by Pantin and Evans (1984) who lacked seismic data of sufficient resolution to identify the presence of numerous erosion events and their contacts. This confusion is due to the fact that Layers A and B could not be imaged on the original 1970s seismic data (Pantin and Evans, 1984). Therefore, Layer B was observed only through core samples without seismic data of sufficient resolution to observe the visible truncation representative of two major lag deposits which diverge above and below the MFm.

No dateable material has been recovered from the MFm to ascertain its age. However, the age of the unit can be constrained by dates obtained from over- and underlying units. The MFm overlies glacial sediments which have been radiocarbon dated to 27-24ka BP (Praeg et al., 2015b; Scourse et al., 2019) and the unit is unconformably overlain by SF1, deposition of which dates from at least 14 ka BP on the inner-shelf (Furze et al., 2014). Therefore, the MFm formed between sometime between 24-14 ka BP, with the outer-shelf ridges most likely forming before the mid-shelf ridges (Stride et al., 1982).



## **Seismic Facies 5**

SF5 exists below the MFm in the Irish sector of the mid-shelf where it correlates to glacial sediments which have been radiocarbon dated to 27-24ka BP (Scourse et al., 2019). Similar glacial sediments have been recovered from SF6 and SF7 which have similar ages (Praeg et al., 2015b; Scourse et al., 2019), suggesting a stratigraphic correlation between these seismic facies. However, the correlation of SF5 to any regional unit is difficult due to its lack of acoustic character.

## **Seismic Facies 6 (Upper Little Sole Formation)**

Praeg et al. (2015b) provide an alternative interpretation of the stratigraphy of an outer-shelf megaridge (Figure 4.4). Their interpretation is based on poor-quality pinger seismic data which suggest that the entire ridge flank comprises the MFm. This is because Praeg et al. (2015b) interpret the MFm-ULSFm boundary reflection to be further down the ridge flank based on the occurrence of a very weak horizontal reflection. This weak horizontal reflection is stratigraphically above a lower reflection which is channelised, both reflections thus delineating the ULSFm with the MFm resting above comprising the ridge bulk (Praeg et al., 2015b). This stratigraphy implies that the laminated and stiff fine sand and mud recovered from vibrocores VC-64, VC-63 and VC-60 on the lower flank of the ridge form a drape of glacial sediments, correlates to LF8 in this study, at the top of the MFm (Praeg et al., 2015b). Now that higher-quality seismic data and new sediment cores are available, these more-accurately reveal the facies comprising the flank of the megaridge (Figure 4.4) and permit the correlation of these facies to those observed in other megaridges, providing a new interpretation. This contested ridge (Figure 3.38) displays a similar stratigraphy to another ridge (Figure 3.24), where the base of the MFm forms a sub-horizontal surface overlying SF6 which coincides with a seafloor break in slope where the reflection terminates laterally on the megaridge flanks. At the outer-shelf megaridge, a sub-horizontal reflection which varies in continuity and amplitude is coincident with a seafloor break of slope and can be interpreted to delineate the boundary between the MFm and SF6 as presented here (Figure 4.4). Additionally, the character of this reflection also matches the description of the MFm base reflection by Pantin and Evans (1984). These observations suggest that the MFm-ULSFm boundary is the main reflection interpreted here between the SF4 and SF6 (Figure 3.38 and Figure 4.4). Either side of this reflection, the MFm and SF6 both consist of medium sand at their interface as evidenced by 15VC and 16VC. This similar lithology might account for the observed reduced amplitude reflection and explain why this distinct but low amplitude reflection was not identified on pinger data by Praeg et al. (2015b). The reflection interpreted by Praeg et al. (2015b) to be the MFm-ULSFm boundary is here suggested to be part of the internal acoustic character of SF6, forming a bed running parallel with the upper boundary of the unit (Figure 4.4) as similarly seen within SF6 in other megaridges (Figure 3.24). It is argued that the reduced quality of the pinger data used by Praeg et al. (2015b) provided insufficient clarity and penetration in order to reveal the true stratigraphy of the megaridge, resulting in the incorrect correlation of cored sediments to the observed seismic facies. The new interpretation presented here contrasts with that of Praeg et al. (2015b), in placing the lower boundary of the MFm higher up the flank the megaridge which correlates physical samples from 15VC, VC-64, VC-63 and VC-60 to SF6 instead

of the MFm (Figure 4.4). Therefore, the glaciogenic sediments of LF8 are thus interpreted to come from SF6 which is exposed on the lower megaridge flanks (Figure 3.38).

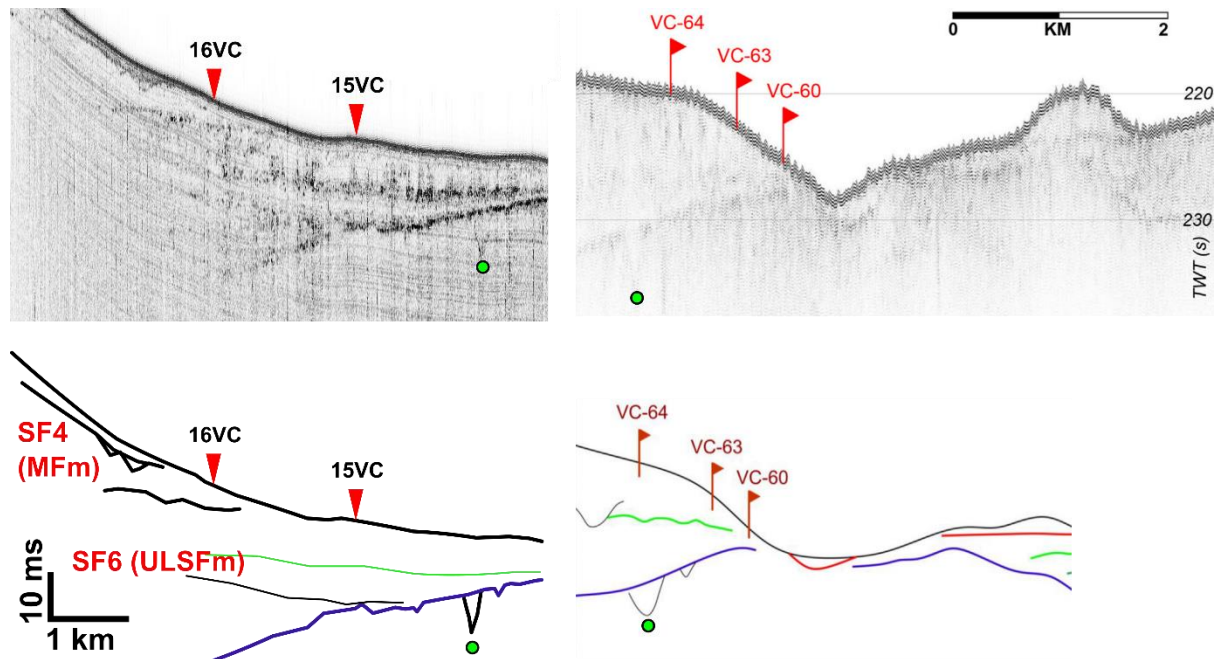


Figure 4.4 - Adjacent pinger data (right) collected by Praeg et al. (2015b) and JC-106 chirp data (left) with core locations, Seismic Facies (SF) and interpreted reflection configurations. A common channel feature is marked (green dot) to aid correlation along with the base of the Upper Little Sole Formation (ULSFm) in purple, and an overlying weak reflection in green interpreted as the Melville Formation (MFm)-ULSFm boundary reflection by Praeg et al. (2015b). The left interpretation is preferred due to improved data resolution, penetration and coverage.

Seismic data presented here consistently show that the MFm overlies a unit forming an underlying mound or plateau that is often exposed on the lower megaridge flanks comprising SF6 and SF7. These seismic facies are separated from the MFm by a sub-horizontal to slightly dipping reflection which in places truncates underlying reflections, most noticeably parallel reflections in SF6 (Figure 3.24 and Figure 3.38). The lower boundary of SF6 and SF7 either exists as an angular unconformity, truncating the Cockburn Formation (CbFm; Figure 3.28 and Figure 3.34), or in places displays channelling (Figure 3.27, Figure 3.35 and Figure 3.38). These observations are consistent with the description of the ULSFm by Pantin and Evans (1984) and Evans and Hughes (1984) who originally interpreted it to be confined to the outer-shelf. All cores recovered from SF6 contain stiff, laminated and fine-grained glaciogenic sediments (LF8) which have been radiocarbon dated to 27-24ka BP (Praeg et al., 2015b; Scourse et al., 2019). Therefore, SF6 is correlative to the ULSFm which is glacial in origin. Therefore, it follows that as SF5 and SF6 have both been imaged to exist under the MFm and have been cored as glaciogenic sediments, then SF5 may also be correlative to the ULSFm where it thins to the north and is not as vertically prominent as SF6 to the south. This suggests that the ULSFm extends further to the

north than originally suggested by Pantin and Evans (1984), as it is found throughout the megaridge field on the western shelf.

As the ULSFm has been demonstrated to be of glacial origin and composition, its extent within the megaridges can provide an explanation for the boulders recovered from a coarse lag referred to as Layer B by Pantin and Evans (1984) in inter-ridge areas. The ULSFm is exposed on the lower flanks of the megaridges and is covered by a coarse lag representing the product of numerous erosion events (Figure 4.3). EE1 resulted in the truncation of reflections in the ULSFm and the initial generation of a coarse lag deposit from this glacial material. Therefore, where Layer B was observed to contained boulders, these boulders must have originated from the eroded glacial ULSFm where the presence of such boulders can originally be explained by iceberg rafting or direct glacial transport.

### **Seismic Facies 7 (Upper Little Sole Formation)**

SF7 is correlative to the ULSFm as it exists below the MFm and above a channelised base or overlies the CbFm separated by an angular unconformity, similar in characteristics to SF6. These observations are consistent with those of the ULSFm by Pantin and Evans (1984) and Evans and Hughes (1984).

The reported Late Pliocene or Early Pleistocene age of the ULSFm by Evans and Hughes (1984) and Pantin and Evans (1984) is inconsistent with radiocarbon ages of 27-24ka BP obtained from LF8 across the shelf (Praeg et al., 2015b; Scourse et al., 2019) which has been correlated to the ULSFm. The Late Pliocene to Early Pleistocene age of the ULSFm was based on an analysis of foraminifera in muddy sands at the base of a single BGS core which was recovered between ridges on the outer-shelf (Evans and Hughes, 1984). The correlation of this core to the ULSFm was not illustrated by seismic data, which were of insufficient resolution for such a task (Pantin and Evans, 1984). Correlation of the underlying mud and sand to the ULSFm was most likely through the observation that the superficial drape had been penetrated entirely and that the core had terminated in an underlying unit thought to be the ULSFm. If the cored muddy sands are correlative to the ULSFm and the Late Pliocene or Early Pleistocene age of the muddy sands suggested by Evans and Hughes (1984) is considered accurate, then this needs to be explained in light of radiocarbon ages of 27-24 ka BP obtained from the ULSFm. Seismic data presented here show that the ULSFm is found under and extending slightly beyond the lateral extent of the MFm on the western shelf, beyond which it thins and becomes discontinuous. Therefore, the recovery of the BGS core between ridges on the outer-shelf suggests that the core studied by Evans and Hughes (1984) may have been recovered from an older deposit where the ULSFm is absent. This results in older deposits being exposed close to the seafloor under the superficial drape without seismic data of sufficient quality to determine an accurate correlation. Another possibility is that the muddy sand at the base of the core represents glacial sediments, being similar in grain size composition to LF8, which are correlative to the ULSFm and comprise glacially reworked foraminifera from older deposits. Regardless, here the ULSFm is reinterpreted as Late Pleistocene in age based upon numerous radiocarbon ages and being cored to contain glacial sediments across the shelf.

BGS core 49/-09/44 was located within 15 m of 30VC and 31VC and recovered 2 m of superficial sand and gravel above 3 m of Melville Laminated Clay (MLC) and 20 cm of Melville Till (MT; Scourse et al., 1990). Both MLC and MT were originally correlated to the MFm (Scourse et al., 1990). This stratigraphic correlation was complicated by seismic data of insufficient resolution and the use of the Decca Navigator positioning system which has a horizontal accuracy of 100s of metres for core and seismic data (Fannin, 1989), resulting in core 49/-09/44 having an ambiguous stratigraphic position. However, new seismic data show that core 49/-09/44 is located in an area where the MFm is thinning, and the underlying glacial ULSFm becomes more commonly exposed at the seafloor under superficial sediments surrounding the 49/-09/44 core site adjacent to 30VC and 31VC (Figure 3.31). Neither MLC nor MT were recovered in three neighbouring cores which were accurately positioned at the 49/-09/44 core site and correlated to seismic data. 30VC and 31VC were recovered up to 15 m away and core 32VC 160 m away, all recovering LF5 under a drape of Layers A and B instead of the MLC and MT observed in core 49/-09/44. This suggests that core 49/-09/44 is not accurately positioned as it does not penetrate a similar stratigraphy. It is more likely that core 49/-09/44 penetrated the ULSFm, comprising glacial sediments, where it exists close to the seafloor under SF1. In fact, no cores in this area confidently penetrated the ULSFm, therefore its lithology here can only be assumed based upon the consistent recovery of glacial sediments from the ULSFm elsewhere. Therefore, the MT and MLC in core 49/-09/44 may correlate to the ULSFm, based upon the approximate recovery of the core on the northern flank where the ULSFm is exposed near the seafloor (Figure 3.29 and Figure 3.31). If this assumption is correct, then the ULSFm correlates to every instance of Late Pleistocene glacial sediment recovery across the mid- and outer-shelf and that MLC and MT do not correlate to the MFm.

### **Seismic Facies 9 (Cockburn Formation)**

SF9 was not cored, but based upon its acoustic character alone, it has several similarities with the CbFm as described by Pantin and Evans (1984) and Evans and Hughes (1984). SF9 displays consistently dipping reflections which are truncated against the ULSFm above (Figure 3.28 and Figure 3.34), consistent with SF9 being correlative to the CbFm which is Oligocene-Miocene in age and lithified (Evans and Hughes, 1984).

Table 4.2 - Correlation of Seismic Facies (SF; Figure 4.1) and Lithofacies (LF; Table 3.2) to the Celtic Sea stratigraphic units of Layers A and B, the Melville Formation (MFm), Upper Little Sole Formation (ULSFm) and the Cockburn Formation (CbFm) by Pantin and Evans (1984), incorporating evidence from Scourse et al. (2002)<sup>1</sup>, Furze et al. (2014)<sup>2</sup>, Praeg et al. (2015b)<sup>3</sup>, Scourse et al. (2019)<sup>4</sup>, Pantin and Evans (1984)<sup>5</sup>, Bouysse et al. (1976)<sup>6</sup>, Marsset et al. (1999)<sup>7</sup>, Reynaud et al. (1999b)<sup>8</sup>, Scourse et al. (1990)<sup>9</sup> and Evans and Hughes (1984)<sup>10</sup>. Associated Erosion Events (EE) are noted from Figure 4.3.

| SF          | Seismic Description  | LF          | Lithology<br>(Interpretation)   | Updated Age<br>(Interpretation)                  | BGS Unit | Description  |
|-------------|--|-------------|---|--|----------|--|
| SF1         | Forms seafloor • Infills basins • Discontinuous over ridges • Forms a thin or thick drape, migratory bedforms or crenulations  | LF1         | LF1: Fining-upwards coarse sand to clay<br>(Deep water post-glacial)  | LF1: <13 ka BP in Celtic Deep <sup>1</sup>       | Layer A  | Seismic <sup>5</sup> : Forms migratory bedforms and crenulations at the seafloor • Is generally not imaged due to being thin<br>Litho <sup>5</sup> : Fining upward |
| SF1<br>base | Reflection at the base of SF1 • Overlies the shelf • Truncates reflections below (EE3)   | LF1a<br>LF2 | LF1a: Clay layer with shell fragments and clasts<br>LF2: Medium sand to gravel layer with shell fragments<br>(Shallow water post-glacial) | LF1a & LF2: 14 ka BP on inner-shelf <sup>2</sup> | Layer B  | Litho <sup>5</sup> : Basal coarse lag  |
| SF2         | Parallel reflections • Interbedded with, or transitions upward into, SF3 • Found in the Celtic Deep and in a channel in the French sector • Underlies SF4 in the French Sector | LF3         | Soft mud with fine sand laminations <sup>4</sup><br>(Glacimarine)   | Late Pleistocene<br>LF8 equivalent <sup>4</sup>  | (ULSFm?) | Seismic <sup>6</sup> : Forms channels under the MFm in the French sector   |

|     |   |                  |  |  |          |   |
|-----|---|------------------|--|--|----------|---|
| SF3 | Lacking acoustic character with some sporadic reflections • Interbedded with, or overlying, SF2 • Found in the Celtic Deep and in a channel in the French sector • Underlies SF4 in the French Sector   | LF4              | Soft structureless clay <sup>4</sup><br>( <i>Distal Glacimarine</i> )  | As above   | (ULSFm?) | As above  |
| SF4 | Forms upper bulk of the ridges and smaller transverse ridges across the shelf • Symmetrical or asymmetrical cross-section • Complex internal reflections truncated by the upper surface (EE2) • Parallel dipping reflections throughout the bulk have been imaged • Overlies horizontal base reflection which truncates various facies • Can overlie mounds of SF6 or SF7 | LF5              | Medium to coarse sand with abundant shell fragments<br>( <i>Marine tidal or glacifluvial</i> )                 | 24-14 ka BP<br>( <i>Constrained by SF1 above &amp; ULSFm below</i> )     | MFm      | Seismic <sup>5,7,8</sup> : Complex reflections that are truncated by the upper surface • Mantles earlier deposits • Overlies a horizontal base reflection |
| SF5 | Discontinuous layer • Infilling irregular surface of SF8 • Underlies SF4 • Found in the Irish sector of the mid-shelf   | LF8              | Stiff clay and silt in places with deformed sand laminations <sup>4</sup><br>( <i>Overridden glacimarine</i> ) | 27-24 ka BP <sup>4</sup>   | (ULSFm?) | Seismic <sup>5</sup> : Underlies the MFm • Overlies the CbFm <sup>10</sup> • Channelised base   |
| SF6 | Parallel reflections truncated by the upper surface (EE1) • Upward increase in reflection discontinuity • Forms raised plateau underlying SF4 • Infills depressions • Channelised base • Forms the initial bathymetric expression of the ridge • Found in the mid-shelf   | LF8              | As above • Stratified diamict and bedded muddy sands <sup>3</sup><br>( <i>Overridden glacimarine</i> )         | 27-24 ka BP <sup>3,4</sup>   | ULSFm    | As above  |
| SF7 | Various internal reflection geometries truncated by the upper surface (EE1) • Forms mound underlying SF4 • Overlies SF9 that can be channelised •   | LF8<br>MLC<br>MT | LF8: As above<br>MLC: Stiff laminated clay <sup>9</sup>  | LF8: 27-24 ka BP <sup>4</sup><br>MLC & MT: Late Pleistocene <sup>9</sup> | ULSFm    | As above  |



|      |  |  |  |                                 |      |   |
|------|--|--|--|---------------------------------|------|---|
| SF7  | Forms the initial bathymetric expression of the ridge • Found in the mid-shelf   |  | MT: Stiff clay with gravel and pebbles <sup>9</sup><br>( <i>Overridden glacimarine</i> ) |                                 |      |   |
| SF8  | Lacking acoustic character • Continuous layer with a discontinuous upper surface • Underlies SF5 • Continuous horizontal base • Found in the Irish sector of the mid-shelf       |  | ( <i>Subglacial?</i> )   |                                 |      |   |
| SF9  | Dipping parallel reflections truncated by the upper surface • Slope of dip can vary • Found in the mid-shelf   |  | ( <i>Lithified</i> )   | Oligocene-Miocene <sup>10</sup> | CbFm | Seismic <sup>10</sup> : Dipping parallel reflections truncated by the upper surface • Underlies the ULSFm • Varying dip slope |
| SF10 | Lacking acoustic character • Outcrops at the seafloor • Jagged upper surface at the seafloor • Undulating channelised surface at depth • Found in the UK sector of the mid-shelf |  | ( <i>Lithified</i> )   |                                 |      |   |
| SF11 | Parallel reflections truncated by the upper surface • Outcrops at the seafloor forming pinnacles • Has a smooth surface that can be channelised • Found in the Celtic Deep       |  | ( <i>Lithified</i> )   |                                 |      |   |

### **4.3 Sediment Geotechnics**

The observation that LF3 and LF4, recovered from the CD, are less consolidated and lack visible deformation in comparison to LF8, recovered across the shelf, suggests that LF8 has been overridden by ice (Scourse et al., 2019). These lithofacies are equivalent in origin (Scourse et al., 2019), representing glacialmarine deposits in a quiet marine environment which are typically soft, horizontally laminated and undeformed (Ó Cofaigh and Dowdeswell, 2001). Thus, it is assumed that LF8 was originally deposited in a physical state comparable to that observed in LF3 and LF4 and that its present state is due to post-depositional subglacial reworking and tectonism (Scourse et al., 2019). An alternative method to achieve over-consolidation is burial and erosion. Burial under significant thicknesses of sediment would result in normal-consolidation, after which a significant erosion event, such as that evidenced by EE1, would remove this upper stratigraphy to leave over-consolidated remnants. Therefore, the observation of high over-consolidation ratios and yield stresses has implications for the post-depositional history of LF8 and thus the evolution of the shelf, as readvancing ice represents a dramatic change in deglacial dynamics which has not been observed elsewhere.

#### **4.3.1 Burial and Erosion**

LF3 and LF4 do not reach ideal Over-Consolidation Ratio (OCR) values of 1 (Figure 3.43) which would indicate a state of perfect normal-consolidation solely due to gravity, whereby the present-day effective stress alone can explain the observed consolidation state of the sediment. Such a scenario is typical for undisturbed glacialaqueous sediments as they form through suspension settling in an subaqueous environment due to gravity and do not experience any additional loading (Ó Cofaigh and Dowdeswell, 2001). Therefore, even the undisturbed and soft LF3 and LF4 are over-consolidated. This may be due to the sequence of burial, normal-consolidation due to gravity and then subsequent erosion of overlying material, as evidenced by an overlying erosive lag (Furze et al., 2014) which truncates these deposits in the CD based on seismic data (Figure 3.14). This erosion surface was likely produced by energetic shallow water conditions during transgression (Furze et al., 2014). Based upon the maximum predicted yield stresses and bulk densities of LF3 and LF4, the thicknesses of equivalent sediment required to result in normal-consolidation can be calculated, thus simulating the thickness of sediment which was eroded. As LF3 and LF4 have low undrained shear strengths and lack visible deformation, it can be assumed that ice overriding did not occur here. In addition, the ice margin is suggested to have rapidly retreated into St. GC (Small et al., 2018), further suggesting that only continued glacialaqueous deposition occurred. Therefore, such sediments are likely to represent the removed stratigraphy. Using a sediment density of  $1900 \text{ kg}\cdot\text{m}^{-3}$ , thicknesses of between 6-8 m are required to achieve normal-consolidation (Figure 4.5). As the sample depths at which these values were calculated exist at depth under significant thickness of glacialaqueous deposits, subtracting the average observed overlying glacialgenic sediment thickness (2.5 m) yields values of 3.5-5.5 m. Therefore, assuming that LF3 and LF4 were allowed to maximally consolidate in situ due to gravity under equivalent sediments, then 3.5-5.5 m of glacialaqueous sediments were eroded to form the basal coarse lag of SF1 during transgression in the CD.

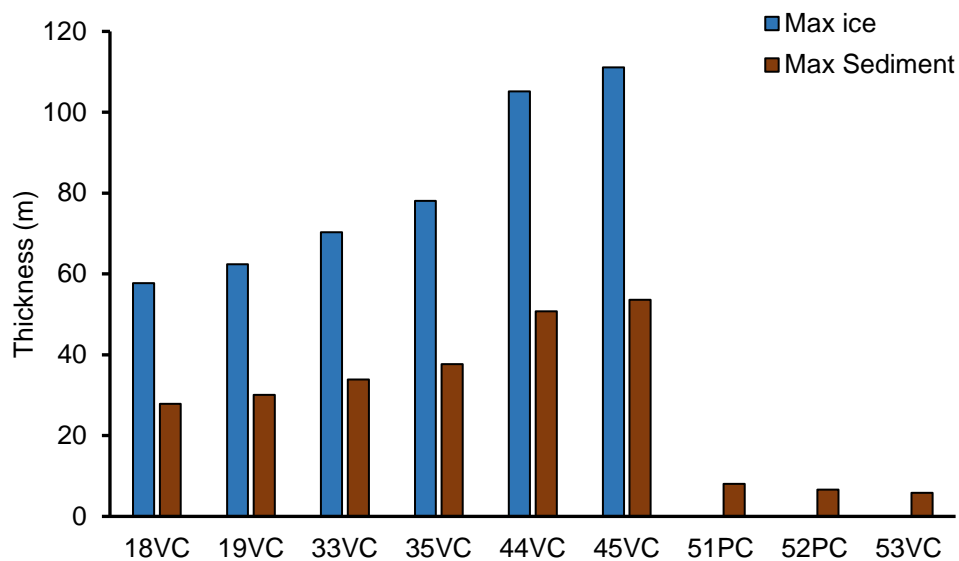


*Figure 4.5 - Column chart showing one-dimensional thicknesses of glacial ice ( $916.7 \text{ kg}\cdot\text{m}^{-3}$ ) and glaciaqueous sediment ( $1900 \text{ kg}\cdot\text{m}^{-3}$ ) required to result in the maximum predicted yield stresses for each Vibrocore (VC) and Piston Core (PC), not accounting for the observed overburden.*

The thicknesses of glacial sediment which were eroded by energetic conditions on the mid- and outer-shelf will be higher, as this area experienced significantly more-energetic and prolonged tidal currents compared to the CD (Scourse et al., 2009; Ward et al., 2016). Therefore, significant thicknesses of glacial sediment may have existed to produce the observed over-consolidation in LF8 prior to their erosion by EE1. Investigating burial as a possible mechanism, the thicknesses of typical glacial sediments ( $1900 \text{ kg}\cdot\text{m}^{-3}$ ) required to achieve normal-consolidation were calculated. To achieve such conditions, between 28-54 m of sediment are required (Figure 4.5). It is unlikely that such thicknesses of sediment existed in situ for such a duration to normally consolidate, as palaeotidal models suggest the presence of energetic marine conditions following deglaciation (Scourse et al., 2009; Ward et al., 2016) which would have easily eroded such deposits. The rate of consolidation of a sediment is dictated by its permeability, and the time required for consolidation to occur can be in the order of thousands of years for low-permeability sediments (Boulton and Hindmarsh, 1987). Therefore, it is unlikely that such sediments would have had sufficient time to normally consolidate between deposition at the retreating ice margin and erosion by tidal currents. Ice retreat had commenced at the shelf edge by 25ka BP (Praeg et al., 2015b; Scourse et al., 2019) and ice had evacuated the shelf by 24.2 ka BP (Small et al., 2018), suggesting that the short residence time of ice on the shelf may not have permitted the deposition of such thicknesses of glacial sediment in the first place. Therefore, the high undrained shear strengths and over-consolidation of LF8 are unlikely to have occurred through burial and subsequent erosion.

#### 4.3.2 Glacial Loading

Individual OCR values of LF8 (Figure 3.43) exceed those calculated for UK glacial tills which generally have OCR values of between 1-20 (Clarke, 2018). However, this may be due to the usage of different testing methodologies. The observed undrained shear strengths of LF8 (Figure 3.41) are comparable to, or exceed, those recovered from glacial tills at similar depths (Bell, 2002; Clarke et al., 2008). These comparisons suggest that LF8 is over-consolidated to a degree possible through direct loading by glacial ice. Additionally, increasing OCR with decreasing core depth observed in LF8 (Figure 3.43) cannot be attributed to simple gravitational-consolidation due to burial in a uniform sediment. During continued deposition, effective stress increases with depth which results in a more consolidated state with increasing core depth. This is generally represented by an increase in undrained shear strength with increasing depth over tens of metres in fine-grainsize sediments (Bartetzko and Kopf, 2007) which is not observed in this case. Due to the narrow depth range over which these measurements exist, it is possible that the OCR values do not represent an overall trend, but a sporadic section within a trend. Such sporadic measurements of consolidation state can be explained in a glacial setting, as complex vertical and horizontal deformation can occur beneath a glacial sole (Boulton et al., 2001; Knight, 2015; McCarroll and Rijdsdijk, 2003). Another explanation for increasing OCR with decreasing core depth can be provided through instantaneous vertical loading of the stratigraphy, with the upper surface acting as a drain. During such an event, a load is applied and the first surface to drain and consolidate due to the removal of porewater is the contact surface. As time and loading continue, deeper regions of the stratigraphy will consolidate, with a maximum at the contact surface for perfectly homogeneous sediments. As LF8 is not perfectly homogeneous, it is also possible that this OCR trend is a product of differential consolidation due to changes in grainsize, with coarser grainsize lenses acting as conduits for porewater escape. Regardless, either instantaneous vertical loading or complex deformation both suggest a glacial influence and not the product of simple one-dimensional burial and subsequent erosion. The most likely explanation is glacial overriding of LF8 after deposition. Assuming a glacial ice density of  $916.7 \text{ kg}\cdot\text{m}^{-3}$  (Shumskiy, 1960), ice thicknesses between 58-111 m are required to explain the maximum predicted yield stress values of LF8 (Figure 3.45). However, this assumes that glacial loading occurred directly in contact with the observed stratigraphy of LF8, which is unlikely as direct subglacial contact would have destroyed any sedimentary structures. It is more likely that glacial loading occurred, but in contact with a thicker stratigraphy, similar to LF3 and LF4, where the upper section was homogenised and the stress imparted by the glacial sole was partially transmitted at depth to form LF8. Even in the case of direct glacial loading, the bottom topography of a grounded ice mass can complicate one-dimensional results due to imparting extra stress on the sub-surface (O'Regan et al., 2010). Therefore, the calculated ice thicknesses are minimum estimates as they do not account for any removed stratigraphy or complex vertical and horizontal stresses imparted by a glacial sole.

Glacial overriding of LF8 can provide an explanation for the partial deformation observed in some cores (Figure 3.46). The partial deformation of laminations seen in LF8 is similar to that observed in sediment that has experienced low shear strain, resulting in partial preservation of the parent material being overridden (McCarroll and Rijdsdijk, 2003; Ó Cofaigh and Dowdeswell, 2001). This suggests that LF8,

as it is currently observed, existed in a transition between undisturbed parent material below and homogenous material above which was directly in contact with the glacial sole. This transition is indicative of a subglacial deforming bed which can occur over a depth of several metres (Evans et al., 2006). The deformed laminae of LF8 do not show any vertical trend representing such a deforming bed. However, this may be due to the narrow depth range over which these structures are observed, combined with the likelihood that the upper stratigraphy of LF8 has been removed by erosion to form the overlying coarse lag. Seismic data of the ULFSm show a trend of increasing discontinuity and decreasing amplitude upwards from distinct and continuous laminations over a depth of <10 m towards the upper termination (Figure 3.24). This transition may represent the seismic expression of a subglacial deforming bed, which exists as an upward transition from undisturbed parent material to homogenous and sheared sediment directly under the glacial sole (Hart and Boulton, 1991). The <10 m depth range over which this occurs on seismic data agrees with field evidence suggesting that such deformation can occur over a depth of several metres (Evans et al., 2006; Knight, 2015; Ó Cofaigh and Evans, 2001), and that a lack of acoustic structure has been suggested to acoustically represent direct subglacial reworking (O'Regan et al., 2010). In addition, the deformed laminae observed in cores can have a consistent dip direction (Core 33VC in Figure 3.46) which may suggest one principal direction of ductile simple shear deformation related to palaeo ice flow direction (McCarroll and Rijdsdijk, 2003). However, no core orientation data are available to allow such a determination. While the observed physical properties and deformation could result from iceberg ploughing (Dowdeswell et al., 1994), the lateral continuity of the reflections comprising the ULFSm and their vertical succession of distortion over a significant area is suggestive of a subglacial deforming layer. Due to the fine-grainsize and thus low-permeability of LF8, rising pore pressures in a subglacial environment would result in a dramatic reduction in effective stress and overall strength of LF8. This would make such sediment readily deformable (Benn and Evans, 1996), with the most complex deformation structures being produced when a wide assortment of grainsizes are present (Ó Cofaigh and Dowdeswell, 2001) such as the coarser laminations. This reduction in strength and the incorporation of sand laminations could facilitate noticeable deformation at even low shear strains and significant depths within a subglacial deforming layer. Therefore, the observations of deformation, high undrained shear strengths and the over-consolidated state of LF8 suggests that LF8 was originally deposited in a configuration similar to LF3 and LF4 in deglacial setting, before being overridden and deformed during ice margin readvance.

## **Chapter 5 - Discussion**

### **5.1 Inner-shelf**

Ice flow and retreat directions on the inner-shelf have primarily been reconstructed from onshore observations from Ireland and the Isles of Scilly in conjunction with offshore sediment core evidence from the mid- and outer-shelf. Therefore, this region of the shelf is distinctly lacking observations of seafloor features which can directly record palaeo-glacial dynamics in the main trunk of the Irish Sea Ice Stream (ISIS). Multi-beam and regional bathymetric data reveal a large and diverse assemblage of glacial features (Table 3.1, Figure 3.7 and Table 4.1) which record specific palaeo-glacial conditions during the time of their formation. Such features permit a spatial reconstruction at the ice stream scale with some temporal capacity depending upon whether the features formed during advance or retreat. By collating the distribution and indicative palaeo-glacial conditions recorded by the preserved glacial landform assemblage, the advance and retreat pattern and deglacial setting of the ISIS can be reconstructed on the inner-shelf. Such a reconstruction provides essential observations of the pattern of ice stream deglaciation and how the ice stream back stepped onto the coastline after evacuating the shelf. These observations of constrained ice flow and retreat are essential spatial components to combine with large scale chronological reconstructions. The integrated spatial and temporal reconstruction provides observations of ice stream deglaciation against which numerical whole ice sheet models can be validated to assess their ability to simulate palaeo-glacial dynamics.

#### **5.1.1 Ice flow Pathways and Extent**

##### **St. George's Channel & Inner-shelf**

New sediment core observations recording Celtic Sea glaciation by the ISIS suggest a southwest flowing ice stream which rapidly advanced through St. George's Channel (St. GC) towards the shelf edge (Praeg et al., 2015b; Scourse et al., 2019, 1990). The topographic constriction posed by Ireland and Wales may have reduced ice flow velocities, reducing the quantity of ice being supplied to the shelf from the ice catchment in the Irish Sea during the initial advance of the ISIS. South of this constriction, the trough of St. GC deepens towards the Celtic Deep (CD), suggesting that glacial erosion was more significant here than within the channel itself. This may indicate that ice streaming commenced south of St. GC. This trough and the CD would have facilitated warm-based ice streaming (Winsborrow et al., 2010), focusing the ISIS to flow along the trough thalweg as a fast-flowing ice lobe before expanding across the unconfined shelf.

Bounding the CD to the west, south and east are the Nymphe Bank Platform, Haig Fras Platform and Lundy Platform respectively (Tappin et al., 1994). The Haig Fras Platform rises 35 m to the south over 50 km from the southern boundary of the CD and is incised by large troughs and an isolated glacial channel (Figure 3.7). The bedrock here consists of Upper Cretaceous chalk and Palaeogene deposits, composed of siliciclastic and argillaceous material and sandstone (Figure 1.6) which would be susceptible to erosion by ice and subglacial meltwater due to the reduced strength of these rock types (Hoek, 2001). Either side of the ice lobe advancing through the CD, ice spread out on the flanks of the



lobe as evidenced by the presence of adjacent glacial channels (Figure 3.7). The Lundy Platform contains glacial channels which suggest that ice extended towards Cornwall, possibly resulting in a proglacial waterbody in the Bristol Channel. Mud drapes of interpreted glacialmarine origin have been identified at the coastline southeast of Lundy adjacent to the Bristol Channel (Eyles and McCabe, 1989). These deposits were subsequently reinterpreted as being glaciolacustrine, recording impoundment against the coastline by an offshore ice margin and subaqueous deposition (Scourse and Furze, 2001). It is known that the Lundy Platform was glaciated previously on two occasions prior to the last glaciation (Gibbard et al., 2017), so there is a possibility that these glacial channels were produced by a glacial event prior to the Last Glacial Maximum (LGM) and may have subsequently been reoccupied. South of the Haig Fras platform, the shelf bathymetry slopes towards a large field of sediment ridges (Figure 3.1), the largest of which mantle a preserved glacial topography on the western shelf. Ice flow continued southwest across the shelf and extended to the southern shelf edge (Praeg et al., 2015b; Scourse et al., 2019).

### **Isles of Scilly & Cornwall**

Ice advance northeast-southwest across the shelf was interpreted to have achieved a lateral limit along the northwest coastline of the Isles of Scilly (Scourse, 1991; Scourse et al., 1990), but the extent of ice towards the coastline of Cornwall is currently unknown. Subglacially smoothed bedrock with a consistent southwest orientation exists to the northwest of the Isles of Scilly and Land's End (Figure 3.7 and Image G in Table 4.2), suggesting that ice flowed southwest past the western Isles of Scilly with ice originating in the northeast. While the orientation of the smoothed bedrock features may be inherited from the structure of the parent geology, their smooth appearance is indicative of erosion by ice (Krabbendam et al., 2016). When the pre-existing bedrock structure is coincidentally orientated with ice flow direction, the elongation ratio of streamlined features may not represent a proxy for ice flow speed (Phillips et al., 2010), however the ice flow direction can still be inferred (Krabbendam et al., 2016). As these features appear to comprise sculpted bedrock, they may have been formed by an earlier glaciation and preserved. However, the recovery of Late Pleistocene sediments from the Isles of Scilly suggests that these features formed during the last glaciation as ice was grounded in this area. On the southeast side of the Isles of Scilly, bedrock outcrops also have a southwest orientation while appearing more prominent and irregular compared to subglacially smoothed bedrock to the northwest (Figure 5.1). Additionally, outcropping bedrock 10-20 km offshore of Cornwall has a similar character to bedrock exposed at the seafloor southeast of the Isles of Scilly, appearing sharp and irregular with no glacial signatures (Figure 5.2). This suggests that glacial sculpting of outcropping bedrock only occurred on the northwest side of the Isles of Scilly, coincident with the islands being interpreted as the lateral limit of the ISIS (Scourse, 1991; Scourse et al., 1990), as opposed to a terminal limit as suggested by John (2018). Therefore, these observations suggest that warm-based and grounded ice dominated the northwest side of the Isles of Scilly, flowing to the southwest, and did not reach the coastline of Cornwall.

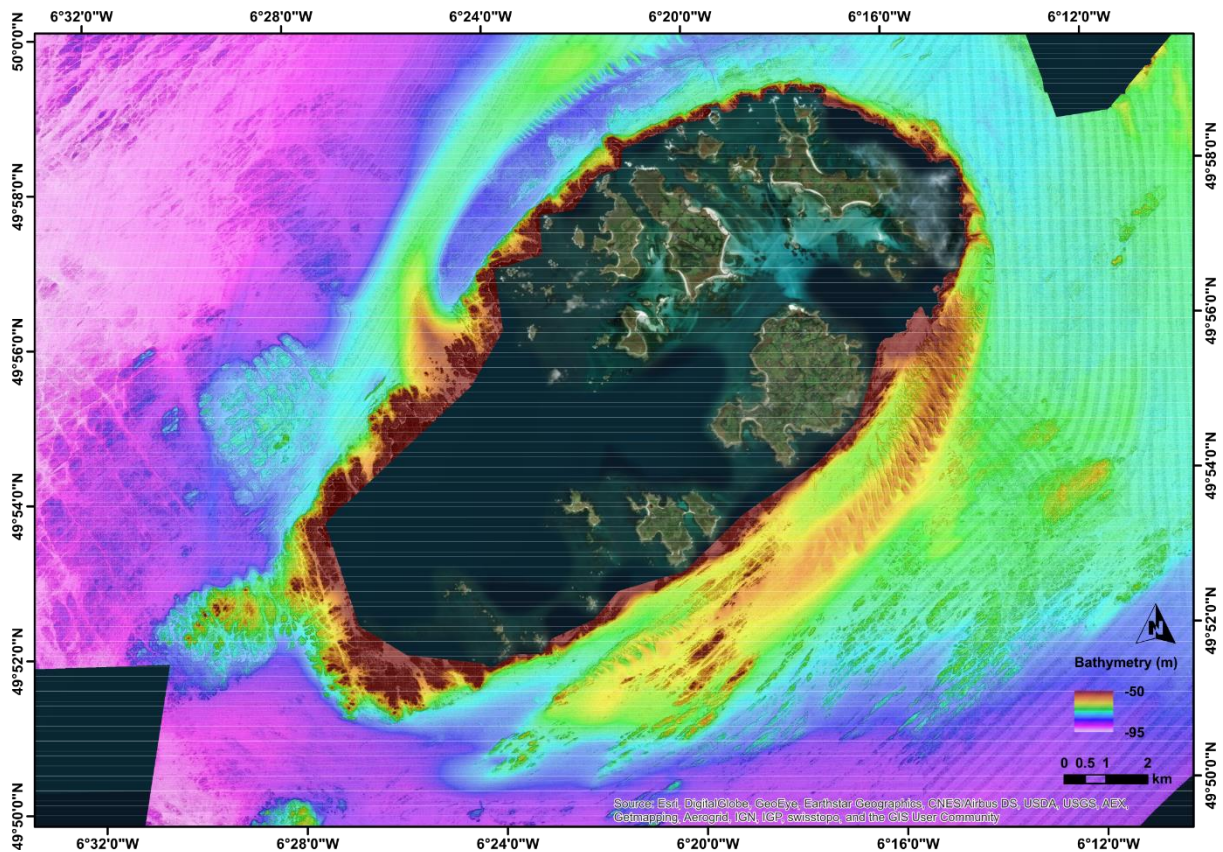


*Figure 5.1 - UKHO bathymetry and slope map of the seafloor surrounding the Isles of Scilly showing a deeper and flatter northwest seafloor and a shallower and irregular southeast seafloor with satellite imagery. Dark and light areas denote steep and flat areas respectively.*

Glacial sculpting of outcropping Devonian and Carboniferous rock adjacent to the Isles of Scilly and offshore of the coastline of Cornwall requires sediment-laden warm-based ice to abrade bedrock 4 km away from the islands yet did not result in them being overridden based on terrestrial observations. Such a configuration can be most simply accommodated by ice flow from the northeast to the southwest past the northwest coastline of the islands, abrading the bedrock further offshore (Figure 5.1) consistent with the southwest orientation of the rock drumlins (Plot I in Table 3.1). Therefore, ice on the eastern lateral periphery of the main ice stream trunk was in contact with the northwest coastline of the Isles of Scilly but did not advance beyond this. This configuration suggests that ice flowed parallel to the coastline of Cornwall from the Lundy Platform channels which must have been occupied during the LGM.

The water depth range of 70-90 m over which smoothed bedrock drumlins are found in this area (Table 3.1) suggests that sediment-laden warm-based ice dominated below the present-day -70 m isobath on the eastern inner-shelf. Therefore, an ice margin bordering the contemporary coastline of Cornwall seems unlikely, as there is no bathymetric expression of a glacial influence within 10-20 km offshore (Figure 5.2), nor any onshore evidence of glacial erosion and/or sedimentation. The Lundy Platform channels also occur below 70 m water depth (Table 3.1), similar to the shallowest occurrence of

smoothed bedrock. Therefore, the eastern ice margin for this region previously suggested by Sejrup et al. (2005) appears to best fit these observations which delineate a lateral ice margin position at the present-day -70 m isobath (Figure 5.3).

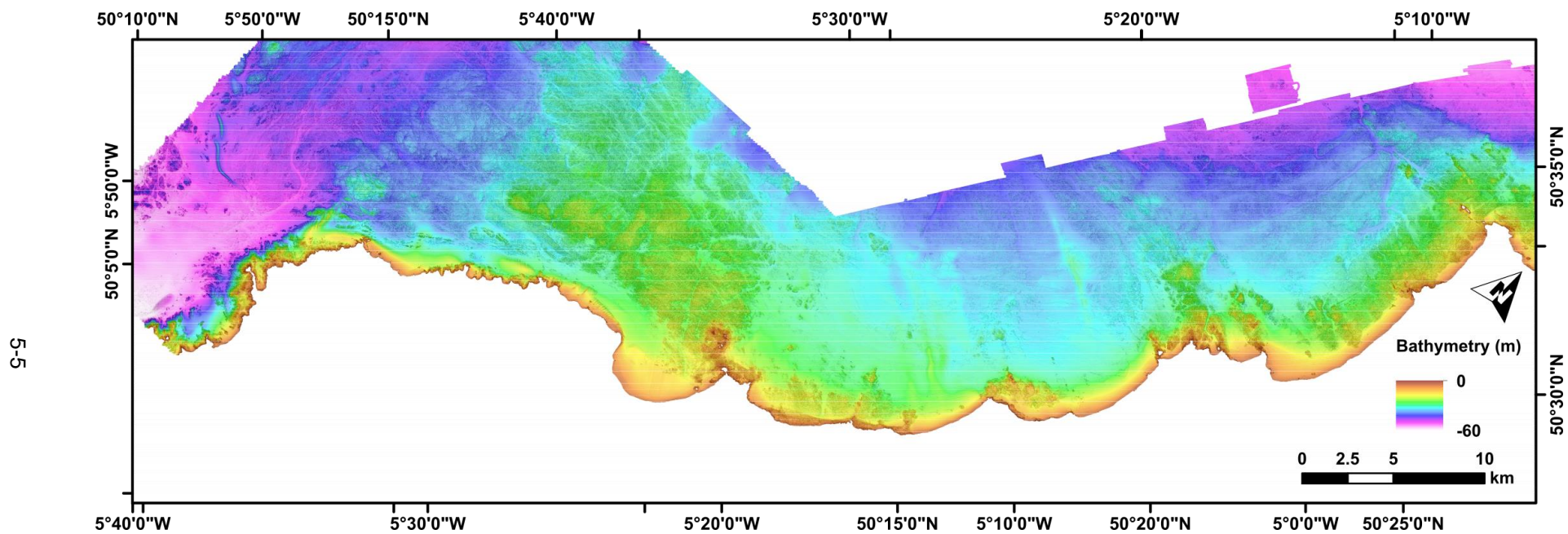


Figure 5.2 - UKHO bathymetry and slope map of the area immediately offshore of the coastline of Cornwall. Dark and light areas denote steep and flat areas respectively. See Area 1 in Figure 5.3.



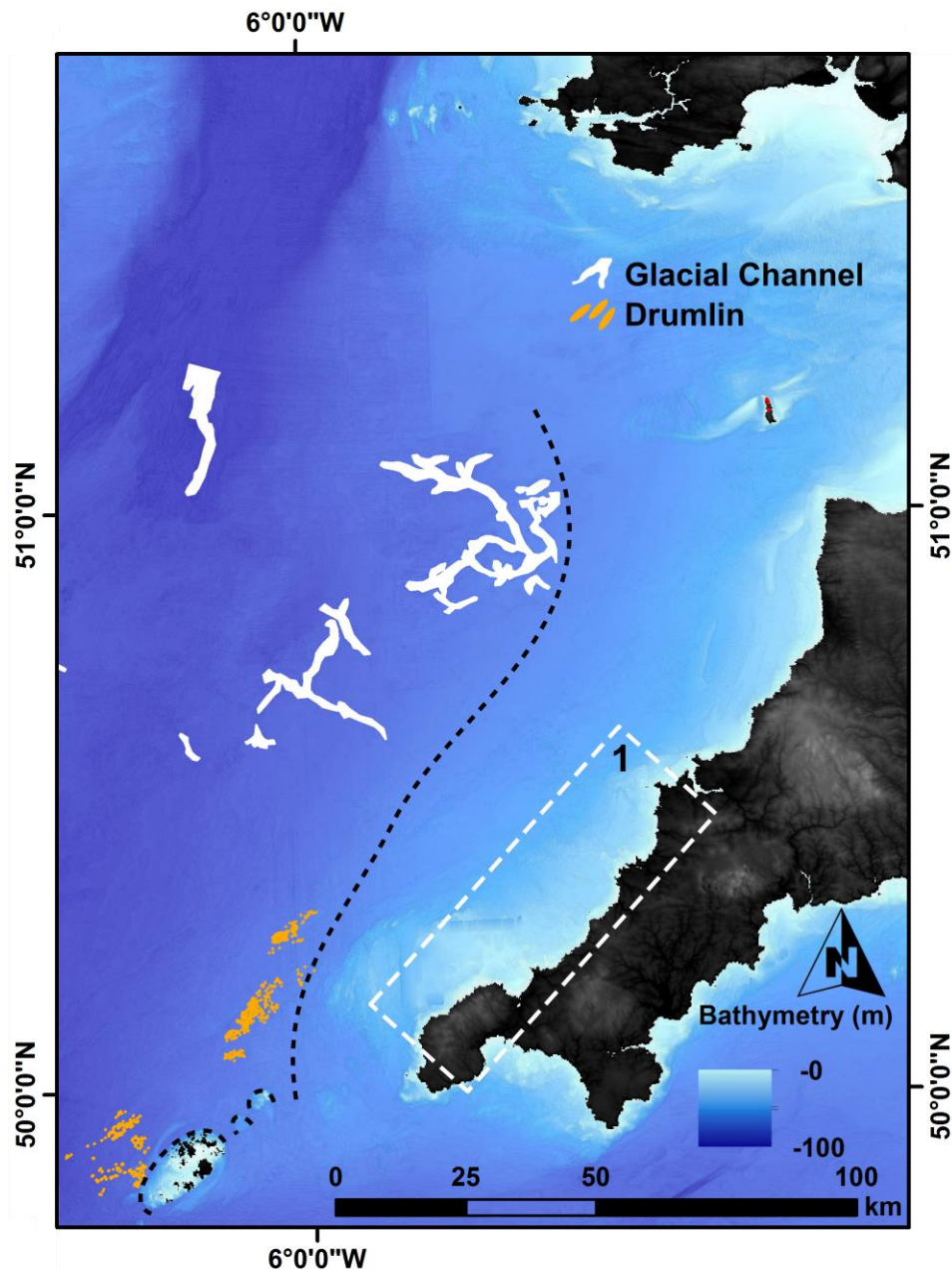


Figure 5.3 - Map showing the limit of glacial features on the eastern inner-shelf at the present-day 70 m isobath (dashed).

### 5.1.2 Retreat Configuration and Style

#### Southern Irish Coastline

The retreat of the ice margin along the southern coastline of Ireland is recorded by sequential moraine ridges (Area A in Figure 3.7), consistent with episodic ice margin retreat (Dowdeswell et al., 2008). These features are interpreted as being younger in age to the northeast, recording the landward withdrawal of a retreating ice margin during deglaciation from an older seaward position to the southwest. The most southwestern ridge, and therefore the oldest, is of significant size, up to 13 km wide, 10 km long and 13 m high and overprinted by iceberg grounding pits (Figure 5.4). Towards the

northeast, younger ridges appear discontinuous and then transition into narrower and more-continuous ridges (Figure 3.11). This transition in size may indicate that the positional pauses experienced at the ice margin became briefer to the northeast, resulting in less time for deposition compared to that which formed the larger ridge to the southwest. This suggests that the rate of ice margin retreat increased in this area after the formation of the most southwestern ridge. The upper surface of this ridge is pitted with iceberg grounding pits (Figure 5.4), consistent with ice margin retreat in contact with a proglacial waterbody after ridge deposition. As the ridges are located on an open shelf with no evidence of a confining morphology to allow the formation of a proglacial lake, it is more likely that ice margin retreat occurred in a marine setting (cf. Furze et al., 2014). Younger moraine ridges are not overprinted by iceberg grounding pits (Figure 3.11) which may be due to their reduced height which prevented the grounding of icebergs or that aqueous deglaciation did not occur here. The moraine ridges are oriented parallel to ribbed moraines and perpendicular to glacial channels and drumlins (Area A in Figure 3.7), typical of the landform assemblage associated with a retreating ice margin (Stokes and Clark, 1999). This assemblage of features and their orientations suggest that the ice margin did not retreat directly towards the Irish coastline, but along the coastline towards the northeast, similarly represented onshore by coast-parallel streamlined features (Figure 3.7). The orientation of the offshore features is consistent with ice margin retreat forced by relative sea-level rise, as palaeotidal model outputs suggest that marine transgression initially advanced northwest across this area before subsequently rising towards the present-day coastline (Scourse et al., 2009b; Ward et al., 2016). This configuration indicates that the ice margin did not retreat directly towards the coastline and the nearest ice dome, comprising the Kerry-Cork ice cap which covered southwest Ireland (Ballantyne et al., 2011), as would be expected. This suggests that ice margin retreat was forced by relative sea-level rise which agrees with the offshore feature assemblage which records marine deglaciation in this area.

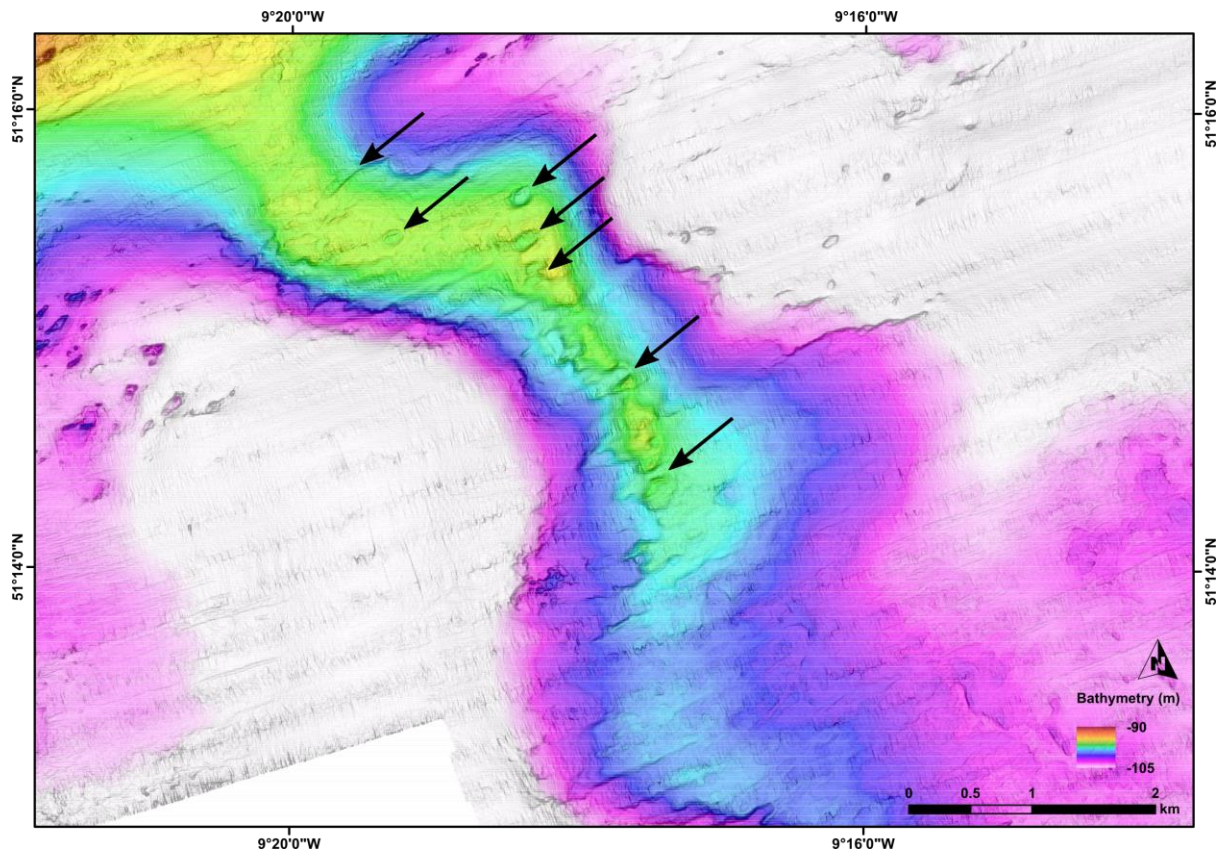


*Figure 5.4 - INFOMAR bathymetry and slope map showing the southwestern moraine overprinted by pits (black arrows) produced by the grounding of icebergs. Dark and light areas denote steep and flat areas respectively. See Area 6 in Figure 3.7.*

Glacial channels and meltwater channels are found neighbouring the moraine ridge assemblage are oriented parallel to the coastline, consistent with a coast-parallel ice margin retreat direction suggested by the ridges (Area A in Figure 3.7). Other channels located further northeast validate this ice margin retreat vector, but they also change in orientation from being coast-parallel to coast-perpendicular towards the northeast (Figure 3.7). This orientation change may have been facilitated by the presence of underlying geological structures, as in this area the main geological boundaries are coast-parallel and intersected by coast-perpendicular faults (Figure 5.5). The presence of such geological structures is significant, as they can influence the orientation and location of glacial channels through the erosion of pre-existing weaknesses (Lloyd, 2015; Preusser et al., 2010). The glacial channels terminate abruptly to the northwest at the boundary with Devonian and Carboniferous sandstone, mudstone and limestone (Figure 5.5). This geology is generally regarded as being more resistant than the geology incised by the observed channels (Hoek, 2001). Therefore, the incision of Devonian and Carboniferous rock by meltwater may have been more difficult, resulting in abrupt channel terminations where this rock type dominates. Meltwater channels can be used to infer ice margin retreat direction, as the channel axes should lie perpendicular to the ice margin (Greenwood et al., 2007), but a geological influence on their orientation introduces some ambiguity as to the exact pattern of ice margin retreat. Despite this, the change in channel orientation can be attributed to an overall change in ice margin retreat direction,



whereby changing retreat vectors resulted in the incision of either coast-parallel geological boundaries or coast-perpendicular faults. The various orientations of these weaknesses would result in certain weaknesses being more-closely oriented perpendicular to the ice margin to result in their incision. Therefore, a change in ice margin retreat direction occurred along the southern coastline of Ireland, changing from coast-parallel in the southwest to coast-perpendicular in the northeast. Landward of the northwestern glacial channel terminations, there are no glacial or meltwater-related features which record final ice withdrawal towards the coastline (Figure 3.7). This may be due to rapid ice margin retreat, resulting in the lack of a glacial landform assemblage, or because of shallow-water post-glacial processes which subsequently eroded any glacial features.

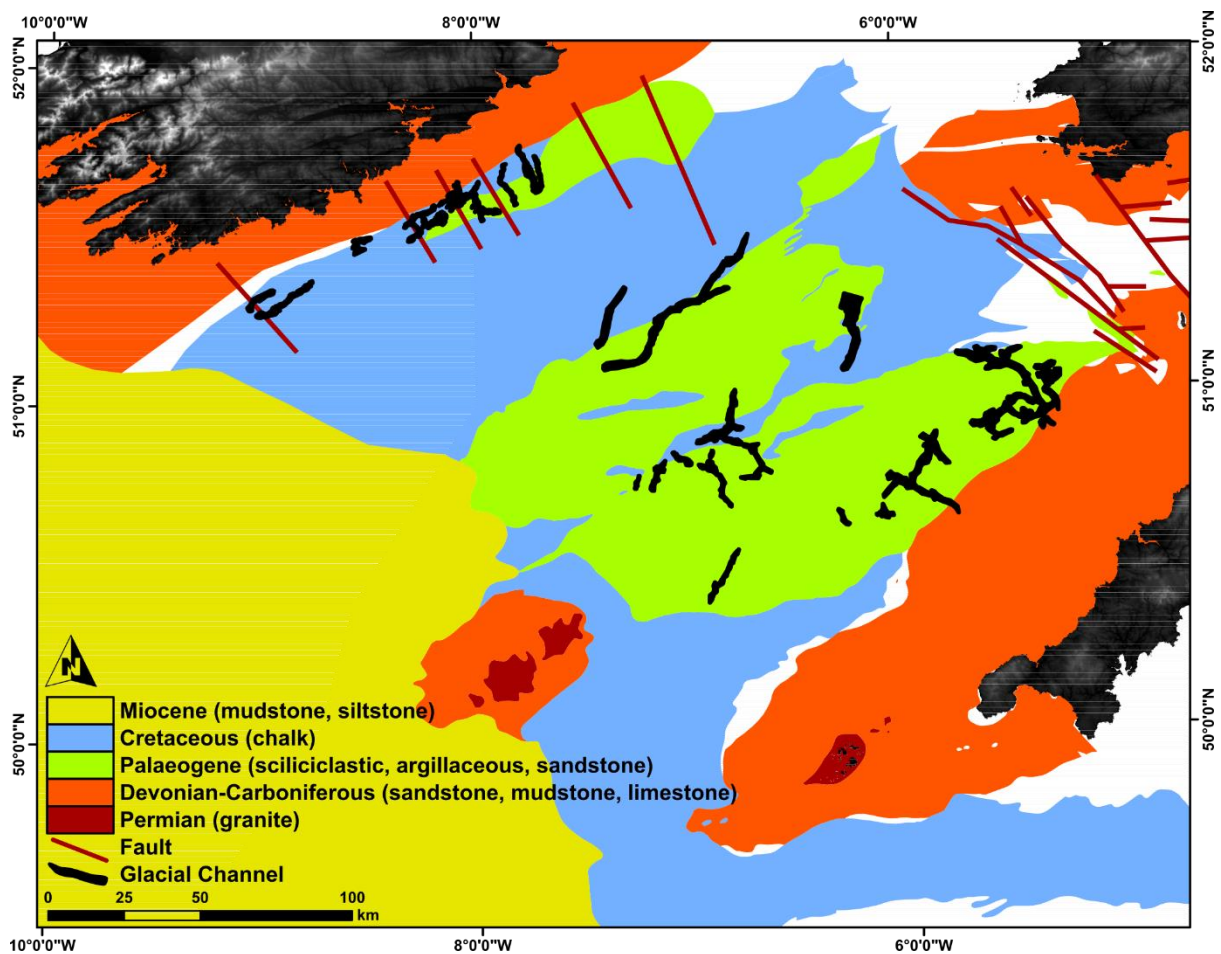


*Figure 5.5 - Map showing the primary sub-Quaternary geology of the Celtic Sea shelf (BGS, 2013, 1979) with glacial channel locations.*

South of Brownstown Head, sinuous esker ridges (Figure 3.7) record coast-perpendicular ice margin retreat, parallel to an incised palaeochannel located just inshore (Gallagher, 2002) which may represent an infilled glacial channel recording the continuation of ice margin retreat towards the contemporary coastline. These eskers are found overlying the resistant Devonian and Carboniferous bedrock found along the southern coastline of Ireland (Figure 1.6) and may have formed due to the increased difficulty

of glacial meltwater to incise this substrate, whereby subglacial meltwater conduits formed within the ice instead of incising the substrate. During ice margin retreat, sedimentation in these conduits then formed esker ridges which are oriented parallel to the ice margin retreat direction (Livingstone et al., 2015). Such features are found elsewhere on hard beds (Livingstone et al., 2015), supporting the interpretation here, and when ice margin retreat is stable and gradual (Storrar et al., 2014). This suggests that ice margin retreat in this area was gradual, possibly contrasting to other areas along the southern coastline of Ireland which may have experienced rapid ice margin retreat, preventing the formation of eskers despite abundant meltwater.

The ice margin retreat vectors across the southern coastline of Ireland suggested here appear similar to the inferred direction of ISIS advance interpreted by Greenwood and Clark (2009) at 24 ka BP based on the onshore glacial landform assemblage. In combination with the new offshore evidence, the observed glacial landform assemblage suggests that the ice margin retreated axially back along its initial offshore advance pathway from Ireland. Firstly, coast-parallel ice margin retreat occurred in the southwest where the ice margin retreated past the local onshore Kerry-Cork ice cap, forced by rising relative sea level which resulted in episodic marine deglaciation. A change in ice margin retreat direction occurred in the northeast, with ice withdrawing directly back onto the coastline when the rate of landward ice margin retreat became more gradual.

### **Inner-shelf & St. George's Channel**

Glacial channels across the central inner-shelf (Figure 3.7) record the retreat of the ice margin from the Haig Fras Platform and Lundy Platform towards the CD, assuming that the ice margin retreat direction occurred parallel to the channel axes due to the incision of meltwater (Greenwood et al., 2007). This orthogonal relationship between the ice margin and the glacial channels has already been observed on the southern coastline of Ireland, indicated by neighbouring terminal moraines and glacial channels (Area A in Figure 3.7). Ice margin retreat vectors on the inner-shelf can be more confidently reconstructed from the observed channels due to fewer significant geological boundaries and faults (Figure 5.5) which influence channel orientation as observed south of Ireland. On the Nympe Bank Platform, the orientation of the largest observed glacial channel records ice margin retreat parallel to the CD towards St. GC (Figure 3.10). Despite great variability, the orientation of linear thalweg segments of up to 5 km long within these channels show a dominant southwest orientation recording retreat towards St. GC, and a secondary southeast orientation recording retreat towards the coastline of Ireland and from the Lundy Platform towards the CD (Plot G in Table 3.1). The Nympe Bank Platform glacial channel is located along one of a few inner-shelf geological boundaries (Figure 5.5), constituting a line of weakness which might have influenced channel orientation and expression (Lloyd, 2015; Preusser et al., 2010). The large size of the Nympe Bank Platform channel can be most easily explained by the underlying geological boundary which is sub-linear over 150 km distance and is oriented southwest, coincident with the main advance and retreat vector of the ISIS. This geological boundary would have provided an exploitable weakness at an ideal orientation to ice flow and ice margin retreat for meltwater incision. Therefore, the formation of this channel may have commenced during the

initial ice advance of the ISIS across the shelf and continued growing through to final ice withdrawal. On the Lundy Platform, a lack of channels on Devonian and Carboniferous bedrock indicates that channel development was confined to areas of much weaker Upper Cretaceous chalk and Palaeogene deposits as similarly observed south of the Irish coastline (Figure 5.5). The ice margin retreat pattern inferred from the orientation of the glacial channels suggests that the majority of the ice mass in the Celtic Sea retreated towards the CD and subsequently towards St. GC. The large size and number of these channels indicate that meltwater was an important subglacial element which conditioned deglaciation across the inner-shelf. Other incised valleys which have been infilled exist at various stratigraphic positions on the inner-shelf which also appear to originate from St. GC (Eyles and McCabe, 1989; Tappin et al., 1994). These features may represent the sub-surface continuation of the observed seafloor glacial channels which have been infilled. The large quantity of meltwater may be due to the lower-latitude location of the Celtic Sea which may have enhanced melting, especially later during ice margin retreat when warming increased in intensity during Greenland Interstadial 2 (Rasmussen et al., 2014). However, the timing of the initial retreat of the ice margin across the mid- and outer shelf appears to pre-date any warming events (Scourse et al., 2019; Small et al., 2018).

As the ice margin retreated into the CD, the adverse slope would have encouraged ice margin instability and rapid retreat (Schoof, 2007), especially if marine inundation and filling of the deep occurred. Therefore, it can be assumed that if such a situation occurred, the ice margin on the adjacent Nympe Bank Platform would have retreated more slowly due to the platform being higher and having a positive slope, promoting ice margin stability and reducing its susceptibility to relative sea-level rise. It is likely that the ice margin lingered on the Nympe Bank Platform and gradually retreated towards the southern coastline of Ireland, as evidenced by eskers (Figure 3.7) which indicate gradual ice margin retreat (Storror et al., 2014), while deglaciation into St. GC was occurring or had already occurred along the CD. Seismic data collected in the CD show the presence of a buried undulating topography (Figure 3.15) which may represent the cross-section of subglacial features such as moraines or drumlins. Therefore, the 3D investigation of this topography may provide insight into the pattern and style of deglaciation in the CD.

The geomorphological imprint left by warm-based ice typically represents the last ice flows that occurred during deglaciation whereby cold-based conditions transition into a warm-based regime. The observed overprinting of ribbed moraines by glacial lineations in the UK sector of St. GC suggests that the lineations formed as sliding warm-based ice overprinted earlier features. Therefore, these lineations most likely formed during retreat. These lineations have a dominant southwest orientation (Plot D in Table 3.1), coincident with the long-axis thalweg orientation of St. GC along which ice would have flowed (Winsborrow et al., 2010). In the UK sector of St. GC, some ribbed moraines appear buried under an unknown sediment thickness (Figure 3.8), which may be due to sedimentation or reworking during final deglaciation or during Holocene reworking of the seafloor by waves and currents. In contrast, the north of the Irish sector has ribbed moraines which appear near-perfectly preserved (Figure 3.8). To the south beyond the delineated ribbed moraine field in the Irish sector, ribbed moraines

appear discontinuous, similar to those observed in some areas of the UK sector, resulting in a spatial transition where features are more discontinuous to the south (Figure 3.8). These features are generally oriented southwest (Plot B in Table 3.1), also coincident with the long-axis orientation of St. GC and the orientation of inferred ice flow. The presence of significant ribbed moraine fields at the southern entrance of St. GC suggests that this area was up-ice from the point where streaming occurred, as such features are associated with the transition zone between frozen- and warm-based ice (Hättestrand and Kleman, 1999; Kleman and Hättestrand, 1999). During a fast ice margin retreat phase, glacial landform assemblages may have been overprinted by lineations formed beneath the flowing ice margin (Dowdeswell et al., 2008; Kleman and Hättestrand, 1999), consistent with the observed landform assemblage of overprinted ribbed moraines but inconsistent with retreat chronologies which suggest that the ice margin resided over the features for several ka (Small et al., 2018). Therefore, the preservation of these ribbed moraines requires either the sediment to have resisted the flow of the passing ice margin, or that the ice margin did not rework the features through decoupling from the bed or due to being stagnant. One mechanism to make the substrate resistant to erosion which can explain the preservation of the ribbed moraines is through sticky spots in the subglacial environment (Trommelen et al., 2014). Sticky spots reduce the basal sliding of grounded ice to the point where subglacial erosion does not take place, and thus the landform assemblage is preserved. Such sticky spots can occur due to de-watering of the substrate, which increases the effective stress and thus the strength of the sediment, or to basal freezing of ice to the bed; see Stokes et al. (2007) for a review. Addressing the former de-watering scenario, there is no seafloor evidence to suggest that a channelised subglacial drainage system existed in St. GC (Figure 3.8), inferring that meltwater was evenly distributed at the ice-bed interface and not confined to specific conduits which would have left some areas of the seafloor well-drained enough to create sticky spots. This indicates that localised de-watering was unlikely in this area. Basal freeze-on is also unlikely, as warming was increasing in intensity during Greenland Interstadial 2 (Rasmussen et al., 2014) which forced continued retreat of the ice margin (Chiverrell et al., 2013; Smedley et al., 2017). Additionally, the presence of smoothed bedrock, glacial lineations and glacial channels on the inner-shelf record warm subglacial conditions not conducive to basal freezing. Therefore, sticky spots are unlikely to have occurred in St. GC. Ice margin flotation due to rising relative sea level is suggested to have occurred in the Irish Sea where the ISIS finally decoupled from its bed to result in a lack of subglacial seafloor features (Van Landeghem et al., 2009). Within the southern entrance to St. GC, a similar scenario could explain the preservation of ribbed moraines in the Irish sector, while other areas were partially overridden by warm-based ice to form lineations. However, such a rise in relative sea level to result in ice margin flotation is unlikely as this would have triggered rapid retreat of the ice margin which is not compatible with chronological reconstructions that suggest ice margin stability in the southern entrance of St. GC for several ka (Small et al., 2018). Due to the long residence time of the ice margin in this area, subglacial reworking of the ribbed moraines would have been significant if continuous flow occurred at the ice margin. The southern entrance to St. GC represents a constriction where the ice margin would have been pinned laterally at the coastlines of Ireland and Wales, enhancing ice margin stability (Small et al., 2018). Therefore, it is possible that this constriction resulted in a reduction in ice flow velocity whereby the ribbed moraines

where only partially overprinted, with areas of severely-reduced ice flow permitting the best preservation of ribbed moraines.

As there is a lack of confining morphology to produce a lacustrine environment within St. GC, the presence of iceberg grounding pits in the UK sector (Figure 3.7) suggests that ice margin retreat most likely occurred in a marine setting. As iceberg scours are found on an area of prominent seafloor, this suggests that water depths were significant enough for iceberg flotation to occur and only ground in shallow areas. These features are oriented to the south and southwest (Plot F in Table 3.1), which may represent the drifting of icebergs away from an ice margin in St. GC to the northeast due to currents when they subsequently grounded in shallow areas to the south. Due to the topography of St. GC, the margin width of the ISIS would have reduced, decreasing the rate of calving and thus slowing ice margin retreat rate (Small et al., 2018). This provides an explanation for the lack of evidence of extensive iceberg scouring in comparison to that observed in other aqueous deglacial settings (e.g. Ottesen et al., 2017).

While the signature of marine deglaciation is clear on the outer-shelf based upon sediment core evidence (Praeg et al., 2015b; Scourse et al., 2019), the deglacial setting on the mid- to inner-shelf is more ambiguous (Furze et al., 2014). Two competing hypotheses were proposed by Furze et al. (2014) to explain the occurrence of glaciaqueous muds lacking fossils diagnostic of marine or lacustrine deposition across the inner- and mid-shelf. Marine deglaciation may have been characterised by higher sedimentation rates, lower salinity and higher relative sea level to result in an aqueous environment with low primary productivity. This contrasts with lacustrine deglaciation which may have had lower relative sea level, resulting in a subaerially exposed shelf with confining morphology to result in impounded proglacial waterbodies. The glacial landform assemblage observed in coastal areas does not directly allow the differentiation of marine or lacustrine ice margin retreat on the inner-shelf, only that aqueous deglaciation occurred. However, the location of iceberg grounding pits in areas located on an open shelf (Figure 5.4 and Image B in Table 3.1) which lacks confining morphology to produce lacustrine waterbodies suggests a marine deglacial environment where sea level kept pace with the retreating ice margin during deglaciation across the shelf, requiring a high relative sea-level environment. On the mid- and outer-shelf, the stratigraphic investigation of the sediment ridges shows that significant quantities of coarse sediment overlies over-consolidated deglacial muds to form the upper bulk of the ridges, indicating that significant sedimentation occurred during deglaciation which could have produced a turbid aqueous environment. Numerous glacial channels observed across the inner-shelf (Figure 3.7) may also indicate that higher sedimentation rates were possible due to the availability of significant quantities of meltwater during deglaciation, combined with the large size of the ice catchment to the north which would have supplied large quantities of sediment through these conduits. These observations suggest that marine deglaciation across the inner-shelf is more likely than lacustrine deglaciation due to geomorphological evidence suggesting a higher relative sea-level environment and higher sedimentation rates consistent with the model suggested by Furze et al. (2014).

### 5.1.3 Regional Reconstruction

The glacial landform assemblage presented here provides the first spatially-extensive submarine geomorphological evidence of the glaciation of the Celtic Sea shelf by the ISIS as far south as the Isles of Scilly and as far west as the southern coastline of Ireland. These glacial features provide new observations of palaeo-glacial advance and retreat vectors and deglacial setting in key areas which can be combined with Bayesian modelling of ice stream-scale deglaciation chronologies (e.g. Chiverrell et al., 2013; Small et al., 2018) to provide essential basis for ice stream reconstructions.

It is generally assumed that the spatial distribution of glacial features is due to glaciation. However, as observed for channel channels where the strength and structure of the underlying geology has influenced channel position and orientation (Figure 5.5), the distribution of glacial features can be due to processes or environments not related to glaciation. The Celtic Sea experienced very energetic hydrodynamics and a complex sea-level history which can alter the spatial distribution of glacial features due to burial or erosion. Such an explanation has been provided elsewhere to account for the lack of glacial features in deep areas due to post-glacial burial and in shallow areas due to wave erosion (Dove et al., 2015). Palaeo sea level reconstructions from palaeotidal model and GIA outputs (Bradley et al., 2011; Ward et al., 2016) suggest that areas of the northern inner-shelf experienced a prolonged relative sea-level position of -70 to -60 m from 20 to 15 ka BP (Figure 1.8). At this point in time, tidal amplitudes were reduced on the northern inner-shelf but were elevated along the southwestern coastline of Ireland and the mid- to outer-shelf (Figure 1.9). As sea level began to rise from this inner-shelf low position from 15 to 10 ka BP, tidal amplitudes increased, subsequently dominating along the coastline of the eastern inner-shelf from the Isles of Scilly to St. GC while amplitudes reduced along the southwestern coastline of Ireland. Therefore, lowered sea level and the subsequent increased tidal amplitudes may have influenced the preservation of glacial features and sediments in coastal areas of the inner-shelf. Such glacial features dominate in water depths greater than 70 m (Figure 3.7), corresponding to the lowered sea-level position of -70 to -60 m from 20 to 15 ka BP (Figure 1.8). The only glacial features to exist in shallower water depths up to 30 m occur to the west of St. GC (Figure 3.7), corresponding to the only coastal area of the inner-shelf which did not experience increased tidal amplitudes during transgression (Figure 1.9). The seafloor of the southern coastline of Ireland and of the eastern inner-shelf can appear highly irregular and consistent with outcropping bedrock distinctly lacking in sediment coverage as partly indicated by seabed composition (Figure 1.5) and seabed character (Figure 5.1 and Figure 5.2). This outcropping bedrock in coastal areas contrasts with significant post-glacial sediment thicknesses observed in the adjacent Celtic Deep (Figure 3.15) which record significant post-glacial deposition on the inner-shelf. The lack of such sediment accumulation in coastal areas to drape the outcropping bedrock indicates that post-glacial hydrodynamics are preventing the deposition of fine-grained material. These hydrodynamics, which would have been more energetic during lowered sea-level conditions, may have eroded glacial deposits in coastal regions shallower than 70 m water depth while only subglacially-sculpted rock or significantly large features remain. Therefore, it is likely that post-glacial hydrodynamics had the potential to remove glacial sediments in areas shallower than 70 m water depth.



At a regional scale, the seafloor glacial landforms presented here suggest that the ISIS advance and retreat cycle took place via two primary pathways (Figure 5.6). This advance and retreat configuration is very similar to that based on offshore sediment cores and terrestrial observations, together depicting a southwest flowing lobe of ice originating from St. GC with a lateral eastern limit bordering the Isles of Scilly (Scourse, 1991; Scourse et al., 1990). The reconstruction presented here records the pattern of deglaciation, showing that the ice margin did not retreat directly towards the coastline, and the nearest ice dome, as would be expected. This most likely represents a forced ice margin retreat direction due to rising relative sea level which subsequently forced the ice margin to retreat directly onto the coastline later during deglaciation. Rising relative sea level resulted in marine deglaciation within St. GC, suggesting that sea-level rise kept pace with the ice margin as it retreated across the shelf. In addition, the subglacial geology influenced the organisation of the subglacial drainage network which most likely altered glacial dynamics during deglaciation. These findings highlight that ice margin retreat can be complicated by physical and environmental factors which can result in unusual retreat patterns. Therefore, these observations provide a retreat model against which numerical whole ice sheet models can be tested in order to accurately simulate the deglacial dynamics of marine-terminating ice streams.

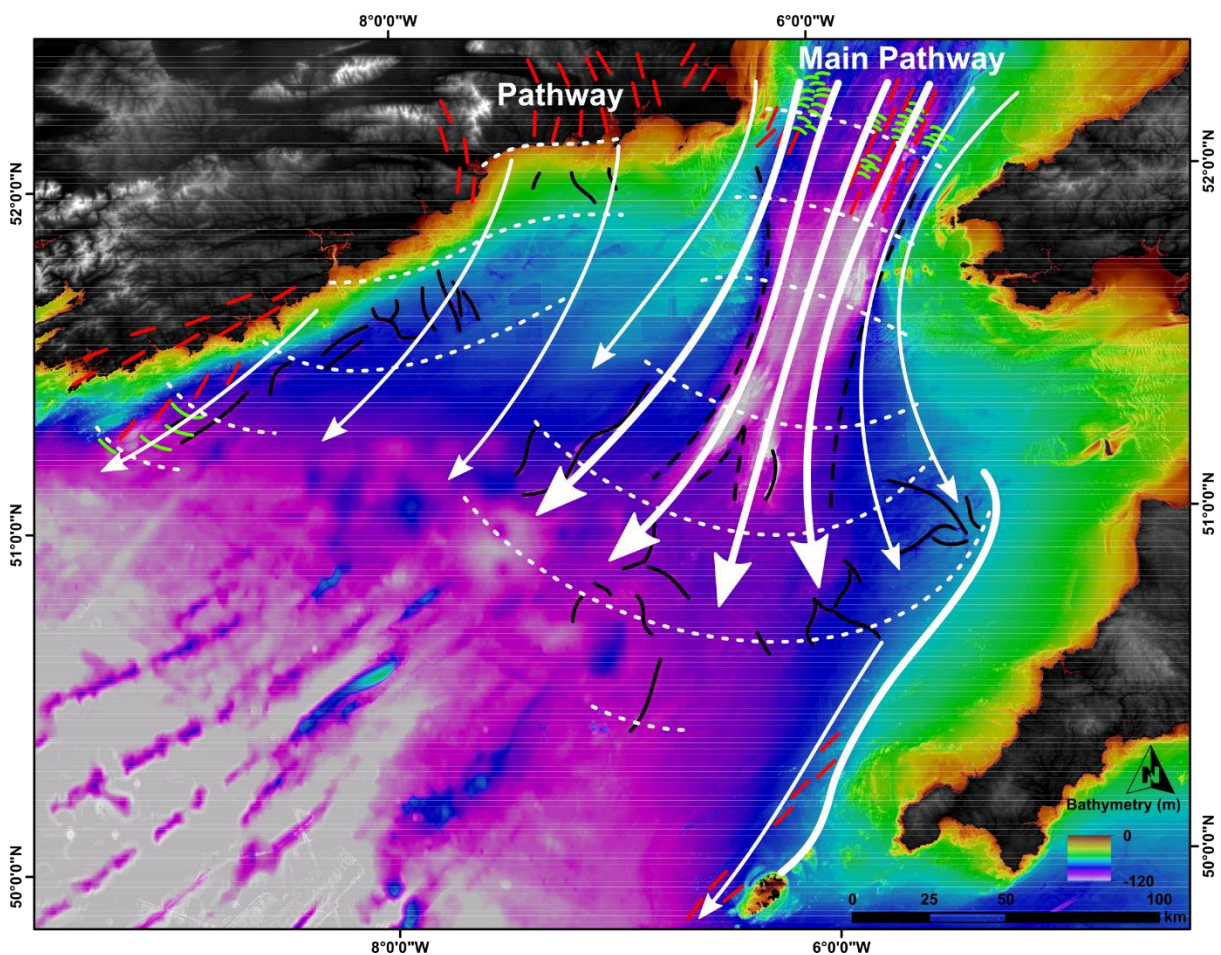


Figure 5.6 - The two primary advance and retreat pathways of the Irish Sea Ice Stream on the inner-shelf. White arrows denote the generalised ice flow pathways as evidenced by regional bathymetry and mapped features, with thicker arrows indicating the main ice stream. The eastern margin is

*marked as a solid white line and generalised ice margin retreat positions are indicated with white dashed lines. The general orientation of features aligned parallel to ice flow direction (red), parallel to ice retreat direction (black) and parallel to the ice margin (green) are marked along with the banks bounding major troughs through which ice would have flowed (dashed). Onshore features are from Clark et al. (2018).*

The inferred sequence of events produced from the interpretation of the observed glacial landform assemblage and regional bathymetry is as follows, integrating other work providing chronological constraints (Praeg et al., 2015b; Scourse et al., 2019, 2018; Small et al., 2018):

1. The main grounded ice lobe advanced southwest through St. GC, directed along the thalweg of the CD while ice spread out over the flanks of the deep, merging with ice advancing offshore from southern Ireland (>27 ka BP)
2. Grounded, fast-flowing and warm-based ice advanced southwest onto the mid-shelf, adjacent to the Isles of Scilly and parallel to the coastline of Cornwall but did not reach the coastline (>27 ka BP)
3. This southwest advancing ice lobe extended onto the mid- and outer-shelf before deglaciating back towards the inner-shelf
4. To the southwest of the southern coastline of Ireland, grounded and marine ice margin retreat occurred parallel to the coastline
5. Significant quantities of meltwater incised pre-existing geological weaknesses on the inner-shelf as the ice margin retreated towards the CD in response to rising relative sea level
6. The CD was breached and became inundated, triggering rapid retreat of the ice margin towards St. GC due to the adverse slope
7. Further northeast along the southern coastline of Ireland, a change in ice margin retreat orientation occurred where the grounded ice margin retreated directly towards the coastline
8. The grounded ice margin stabilised in the southern entrance of St. GC where ice flow velocities reduced due to narrowing of the ice margin width (24.2-22.1 ka BP)
9. Adjacent to St. GC on the southern coastline of Ireland, stable and grounded ice margin retreat occurred from the Nymph Bank Platform towards the coastline

## **5.2 Mid- and Outer-shelf**

The previous mid- and outer-shelf reconstruction of glaciation is primarily based upon terrestrial observations from the Isles of Scilly and from sporadic sediment cores recovered offshore which contained glacial sediments that were poorly spatially-positioned and correlated to regional stratigraphic units. Whilst regional bathymetric data provide some information as to the morphology of the mid- and outer-shelf, this region is dominated by a large assemblage of ridges and lacks any distinct glacial landforms such as those which are observed on the inner-shelf. Therefore, the reconstruction of the mid- and outer-shelf relies primarily on the interpretation of the stratigraphy of the ridges as either post-glacial tidal banks (Scourse et al., 2009b) or as glacifluvial ridges (Praeg et al., 2015a) to establish their relationship to the cored glacial sediments. Only when the stratigraphy of the mid- and outer-shelf has been elucidated can an accurate reconstruction of the evolution of the shelf emerge. Such a reconstruction of the terminal region of the ISIS will yield essential information as to the maximum extent of glaciation and under what conditions rapid deglaciation occurred to ascertain the primary deglacial forcing mechanisms. The answers to such questions are essential for understanding how deglaciation of marine-terminating ice streams occurs, providing clues as to what mechanisms can precondition irreversible ice stream collapse. The initial reconstruction can be combined with chronological data to produce a final reconstruction against which the validity of whole ice sheet numerical models can be tested to determine their ability to recreate the observed palaeo-glacial dynamics. Additionally, such a reconstruction can elucidate how glaciation of the shelf has influenced its post-glacial evolution.

### **5.2.1 The Megaridges**

The origin of the megaridges on the western shelf as either post-glacial tidal sand banks or glacifluvial eskers has profound implications for the reconstruction of the glacial and post-glacial evolution of the Celtic Sea shelf. The integration of Seismic Facies (SF) and Lithofacies (LF) provides new insight into the shallow stratigraphy of the shelf, updating the previous BGS stratigraphy produced in the 1970s (Table 4.2), and permitting the investigation of the megaridge origin hypotheses. The typical stratigraphy comprising the megaridges is summarised as follows:

The megaridges and older shelf deposits are draped by superficial sediments (SF1) which comprise fining-upwards coarse sand to clay which are finer in bathymetric depressions and coarser overlying the ridges and other prominent features where SF1 becomes discontinuous. These deposits overlie a distinct medium sand to gravel layer containing abundant shell fragments comprising the base of the unit, formed during Erosion Event (EE) EE3 (Figure 4.3). The superficial drape is younger than 24 ka BP across the shelf and commenced formation at 14 ka BP on the mid- to inner-shelf. This unit has been interpreted to form migratory bedforms and transverse sand patches which exist sporadically across the shelf.

The Melville Formation (MFm) makes up the upper bulk of the megaridges (SF4) comprising medium to coarse sand with abundant shell fragments. These sediments form a positive mound which seismic data show contain various reflection geometries which are truncated against the upper surface,

representing EE2 (Figure 4.3). Truncated dipping reflections are the most common; these exist throughout the unit. The MFm overlies a sub-horizontal base which truncates reflections in various facies below. No direct chronological data exist for the MFm, however it formed after the ULSFm which it overlies across the western shelf.

The Upper Little Sole Formation (ULSFm) is glacial in origin, comprising stiff clay and silt which in places have deformed sand laminations representing subglacially overridden deglacial muds. Seismic data show that the ULSFm (SF5, SF6 and SF7) forms raised mounds and plateaus which originally existed in places as horizontal sheets before being sculpted by EE1 (Figure 4.3) into mounds which the MFm mantles. Glacigenic sediments recovered from the ULSFm constrain its age to between 27-24 ka BP across the western shelf.

The interpretation of this shallow stratigraphy suggests that two major erosion events occurred (Figure 4.3). After the ULSFm was deposited in glacial conditions, it experienced regionally-extensive EE1 to sculpt it into the observed positive features. After this erosion event, the MFm formed. Subsequent to this, the MFm was then exposed to localised EE2 to truncate dipping reflections.

### **The Megaridges as Post-glacial Tidal Banks**

The oldest age of 14 ka BP from the superficial drape (Table 4.2) is consistent with numerical palaeotidal model outputs of the post-glacial marine transgression (Scourse et al., 2009b; Ward et al., 2016), showing a time-transgressive landward reduction in tidal bed stress between 16-12 ka BP across the Celtic Sea (Figure 1.9). This modelled reduction in energy suffers from the uncertainties linked to palaeotidal modelling, such as relative sea-level history, ice extent and chronological uncertainties. However, several palaeotidal model outputs using various inputs all show that the Celtic Sea experienced megatidal conditions during marine transgression (Ward et al., 2016), increasing confidence in this overall interpretation. The reduction in tidal current intensity towards the present-day could be represented by the in places fining-upwards succession from a basal coarse layer (LF2 and LF1a) observed in the superficial drape. Prior to 16-12 ka BP, energetic tidal conditions occurred during the peak of marine transgression, commencing by at least 21 ka BP (Figure 1.9; Scourse et al., 2009b; Ward et al., 2016), limited by the temporal limit of the models. These energetic tidal currents were suggested to provide the primary mechanism for the erosion of shelf sediment and the formation of the MFm as post-glacial tidal sand banks (Scourse et al., 2009b). As these tidal currents reduced in intensity, due to increasing water depth resulting the loss of resonance on the shelf as marine transgression progressed, wave action continued to rework the ridges (Reynaud et al., 1999b). Water depths shallower than 145 m, encompassing the ridge surfaces across the shelf at present, are exposed to wave action as evidenced by the presence of superficial bedforms (Reynaud et al., 1999a). This constant supply of energy prevents the deposition of superficial fine muds, consistent with the observation that fine-grained SF1 sediments are generally found in the inter-ridge troughs and other depressions while coarse-grained SF1 sediments exist on the upper ridge surfaces. Reduced water depths during the early stages of marine transgression would have resulted in the wave energy

envelope, which presently only focuses on the upper ridge surfaces, encompassing the megaridges and their neighbouring troughs entirely, resulting in their winnowing during marine transgression. This wave energy surface, representing the mechanism forming EE3 (Figure 4.3), may have partially overprinted earlier major erosion event surfaces comprising the upper surface of the MFm (EE2) and the upper boundary of the ULSFm (EE1). As SF1 may represent the sedimentary expression of wave action and rising sea level, these processes can explain the origin of LF1 and LF2 in Vibrocore (VC) 34VC (see the annotated core log in Lockhart et al., 2018 in the Appendix), recovered from the upper surface of the MFm. Here, continued wave action is preventing the deposition of fine-grained deposits, forming LF1, while LF2 represents the winnowing of the upper surface of the MFm during EE3 (Figure 4.3) when relative sea level was lower and thus wave conditions were more energetic. Wave action during lowered sea level can also account for the angular unconformity at the base of the superficial drape in the CD (Figure 3.14), where several metres of deglacial mud was eroded. Therefore, the superficial drape could be interpreted solely as the sedimentary product of wave action and deep-water deposition during rising relative sea level in the final stages of marine transgression after tidal currents diminished between 16-12 ka BP (Figure 1.9).

Wave action alone during the later stages of marine transgression most likely cannot account for the truncation of clinoforms observed in the MFm because this would require very energetic conditions to entrain such coarse sediment. Clinoforms are imaged throughout the full thickness of the MFm in places (Figure 3.22), suggesting that the MFm formed through a single mechanism which resulted in the progressive layering of sediment to produce these clinoforms. Such a process can be accommodated by a marine tidal origin, where sediment is transported by tidal currents over the surface of the bank, resulting in sequential bedding which dips in the dominant direction of sediment transport. This results in clinoforms which are truncated against the upper surface of the bank due to the transport of sediment across this surface in response to energetic hydrodynamics. Therefore, EE2 (Figure 4.3) is interpreted to represent the acoustic expression of the end of energetic tidal current conditions and does not represent the product of a single instantaneous erosion event. Palaeotidal model reconstructions show that tidal currents had maximum bed stresses generally aligned with the megaridge axes, providing a mechanism for MFm growth (Scourse et al., 2009b). The palaeotidal model outputs suggest that energetic tidal conditions commenced at least 21 ka BP and persisted until 16-12 ka BP (Figure 1.9; Scourse et al., 2009b; Ward et al., 2016), and had sufficient energy to erode coarse sand (Ward et al., 2015). It is interpreted that the time period during which these energetic tidal currents existed on the shelf encompass the time during which the MFm developed (Scourse et al., 2009b). This is consistent with the age of the MFm being constrained to be between 27-24 ka BP to 14 ka BP by the observed bounding stratigraphy (Table 4.2). Cores show that the MFm consists of uniform massive shelly medium to coarse sand, similar to sediments associated with tidal bedforms (Davis and Balson, 1992; Houbolt, 1968) and the grainsizes entrainable by the predicted tidal current energies. When tidal currents diminished between 16-12 ka BP (Figure 1.9) and the banks stopped growing, the MFm clinoforms remained truncated against the upper surface as sediment transport over their upper surfaces ceased, forming EE2 (Figure 4.3). These truncated clinoforms effectively represent a snapshot in time when

tidal currents reduced in intensity below the threshold required for continued sediment transport and bank growth. Therefore, after the MFm ceased development, the truncated clinoforms were overprinted by wave action during EE3 (Figure 4.3) and the formation of SF1. If tidal currents are responsible for the development of the MFm, then the Huthnance (1982a, 1982b) numerical model predicts that the megaridges in the west and ridges in the east formed in water depths of 88 m and 40-60 m respectively along their lengths, based upon their observed spacing. The observed sinuosity and rotated ends of the MFm (Figure 3.4) appear similar to characteristics of tidal sand banks in the North Sea at various stages of formation (Caston, 1972; de Swart and Yuan, 2018) and those reproduced by simple tidal sand bank formation models (Huthnance, 1982a), suggesting a similar tidal formation process.

The base reflection of the MFm has been interpreted to represent a coarse layer formed during one or more Pleistocene erosion phases (Pantin and Evans, 1984) that in places truncates glacial deposits of the ULSFm (Figure 3.24) which originally existed as a sheet. This surface represents the regionally-extensive EE1 (Figure 4.3), produced during the onset of energetic tidal conditions as suggested for another Celtic Sea ridge (Reynaud et al., 1999b). EE1 is indeed regionally-extensive, as palaeotidal model outputs suggest energetic conditions existed across the mid- and outer-shelf (Figure 1.9) (Scourse et al., 2009b; Ward et al., 2016). The MFm generally overlies isolated and discontinuous glacial mounds of the ULSFm which are separated from the MFm by the distinct reflection of EE1 (Figure 4.3), consistent with erosion during the onset of energetic tidal conditions following deglaciation. This supports the suggestion that the topography of the partially eroded ULSFm may have influenced the orientation and formation of the MFm (Pantin and Evans, 1984), as glacial deposits most likely would have induced seafloor instabilities due to having an uneven surface. Such seafloor instabilities can act as nuclei for tidal ridge development as suggested by numerical models (Huthnance, 1982a, 1982b). As EE1 formed (Figure 4.3), representing the onset of energetic tidal conditions, the MFm was deposited which armoured sections of the ULSFm while erosion of the inter-ridge areas continued. Therefore, the ULSFm was sculpted into discontinuous mounds from an initial glacial sheet deposit while these mounds were mantled by sand ridges that grew axially towards the inner-shelf.

The inferred sequence of events to produce a post-glacial tidal origin of the MFm is as follows, integrating other work providing chronological constraints (Furze et al., 2014; Praeg et al., 2015b; Scourse et al., 2019; Ward et al., 2016):

1. Glacial deposition occurs as a sheet deposit (ULSFm) extending across the western shelf during rising relative sea level (27-24 ka BP; Image A in Figure 5.7)
2. Tidal resonance drives a regionally-extensive erosion event (EE1) produced by tidal currents which begins to erode the ULSFm (25-21 ka BP; Image B in Figure 5.7)
3. The MFm grows axially due to sediment transport over the crest of the banks (EE2), armouring the underlying ULSFm from further erosion, which continues in the inter-ridge areas (21-16 ka BP; Image C and Image D in Figure 5.7)



4. Tidal resonance is lost and the MFm ceases to grow but is still exposed to localised wave action (EE3) while a superficial drape is deposited across the shelf as sea-level rises (16 ka BP to present-day; Image E in Figure 5.7)

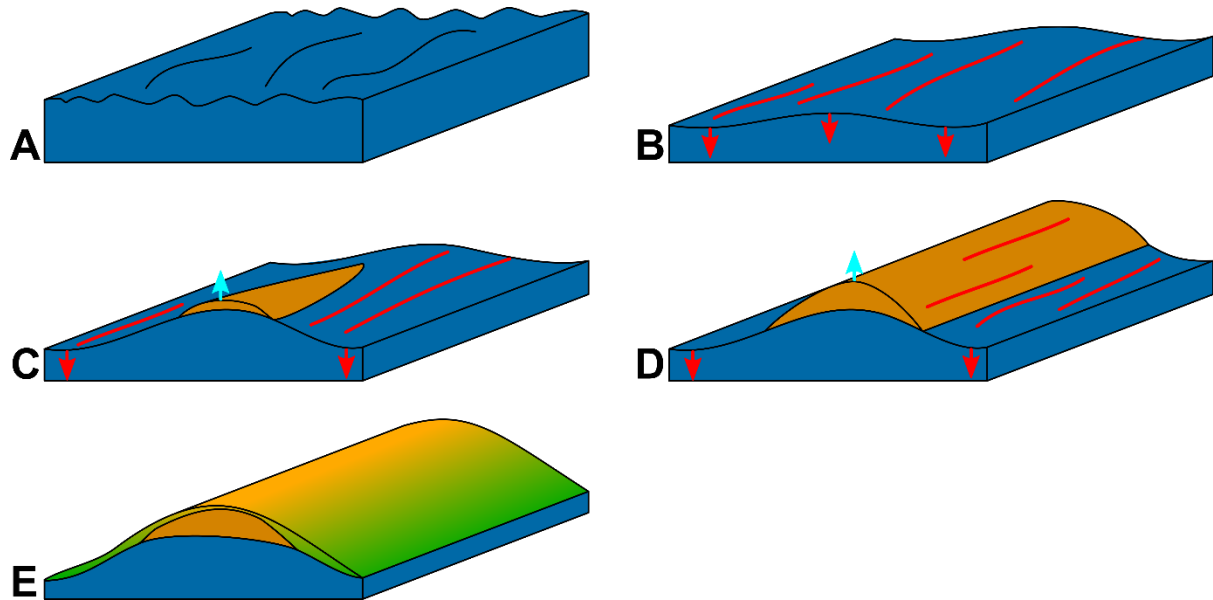


*Figure 5.7 - Cartoon showing stages of the tidal formation model showing areas of erosion (red) and deposition (blue) due to post-glacial tidal currents (red lines). A glacial topography (A) is then exposed to a regional erosion event (B) where a sand bank nucleates on a seafloor irregularity (C) which grows (D) until tidal currents diminish and the seafloor is draped (E).*

### **The Megaridges as Eroded Eskers**

The sedimentary composition of eskers varies both vertically and laterally, commonly containing a core of boulders and cobbles which fines upward and outward towards bedded sand, representing decreasing meltwater pressure in the later stages of development (Gorrell and Shaw, 1991). Such a fining-upward trend exists in LF5 in 34VC, recovered from the upper surface of the MFm (see the annotated core log in Lockhart et al., 2018 in the Appendix). Meltwater drainage can result in highly variable internal structures, varying from plane- to cross-bedding (Brennand and Shaw, 1996; Owen, 1997). This is consistent with seismic observations of complex internal geometry within the MFm (Figure 3.24) and internal bedding (Figure 3.22). In addition, eskers can overlie, underlie or contain layers or lenses of glacial deposits (Banerjee and McDonald, 1975). Therefore, the initial interpretation of the stratigraphy of an outer-shelf ridge presented by Praeg et al. (2015b) suggested that subglacial and glacial marine sediments represented an eroded carapace at the top of the MFm composed mainly of sand which comprises the bulk of an esker. This was similarly interpreted for a mid-shelf ridge by Praeg et al. (2015a) where subglacial till at the base of core 49/-09/44 was suggested to also record a glacial carapace over the MFm. However, new data enable updated interpretations of these ridges and for the stratigraphic position of glacial sediments in relation to the MFm (Table 4.2). All

glacigenic sediments are correlated to the ULSFm which is confidently found as a separate unit underlying the MFm but exposed near the seafloor on the lower megaridge flanks. These new observations still allow for a glacifluvial interpretation of the MFm however, as eskers can be found overlying glacigenic sediments (Banerjee and McDonald, 1975). A glacifluvial origin is consistent with the age of the MFm being constrained by the stratigraphy to be between 27-24 ka BP and 14 ka BP (Table 4.2) which initially encompasses the period of rapid retreat of the ice margin across the shelf (Scourse et al., 2019). Therefore, the flat base on which the MFm rests which truncates the ULSFm could be a product of localised meltwater scouring immediately prior to the deposition of bedded sands and gravels as an esker.

EE2 (Figure 4.3), which truncates the MFm under the superficial drape, has an unknown duration, although it occurred at or before 14 ka BP on the inner- and mid-shelf based upon the age of SF1 (Table 4.2). Therefore, this unconformity could represent the localised product of energetic tidal conditions which reworked the MFm and ULSFm. Palaeotidal model outputs (Figure 1.9) suggest that such conditions had commenced by at least 21 ka BP across the shelf and persisted until 16-12 ka BP (Scourse et al., 2009b; Ward et al., 2016). This scenario can most simply facilitate an esker formation model of the MFm, where glacifluvial features have largely survived several thousand years of energetic tidal currents during marine transgression which eroded the upper surface of the MFm (EE2) and some of the ULSFm (EE1; Figure 4.3). This implies that no deposition occurred during the period of 21 ka BP until 16-12 ka BP when energetic tidal currents existed across the shelf (Figure 1.9). This is because no significant deposits exist between the MFm, of assumed deglacial age, and the superficial drape which formed 14 ka BP after tidal currents diminished. This gap would result in a depositional hiatus of 10 ka during which strong tidal currents existed. A scenario where only erosion of the glacifluvial MFm and the partly-exposed ULSFm occurs at the peak of marine transgression is plausible considering the high energies involved. Therefore, the superficial drape would represent the first deposits to form after the peak of transgression which diminished at 16 ka BP (Figure 1.9) while wave action continued to form EE3 (Figure 4.3) during sea-level rise.

The inferred sequence of events to produce a glacifluvial origin of the MFm is as follows, integrating other work providing chronological constraints (Furze et al., 2014; Praeg et al., 2015b; Scourse et al., 2019; Ward et al., 2016):

1. Glacial deposition occurs as a sheet deposit (ULSFm) extending across the western shelf during rising relative sea level (27-24 ka BP; Image A in Figure 5.8)
2. Glacifluvial deposition during ice margin retreat partially scours the ULSFm (EE1) and results in the formation of eskers (MFm; Image B in Figure 5.8)
3. Tidal resonance drives an erosion event (EE2) produced by tidal currents which begins to erode the MFm and ULSFm (25-21 ka BP; Image C in Figure 5.8)
4. Energetic tidal currents persist across the shelf as marine transgression continues, during which no deposition occurs (21-16 ka BP; Image D in Figure 5.8)

5. Tidal resonance is lost and erosion ceases. The MFm is still exposed to localised wave action (EE3) while a superficial drape is deposited across the shelf as sea-level rises (16 ka BP to present-day; Image E in Figure 5.8)

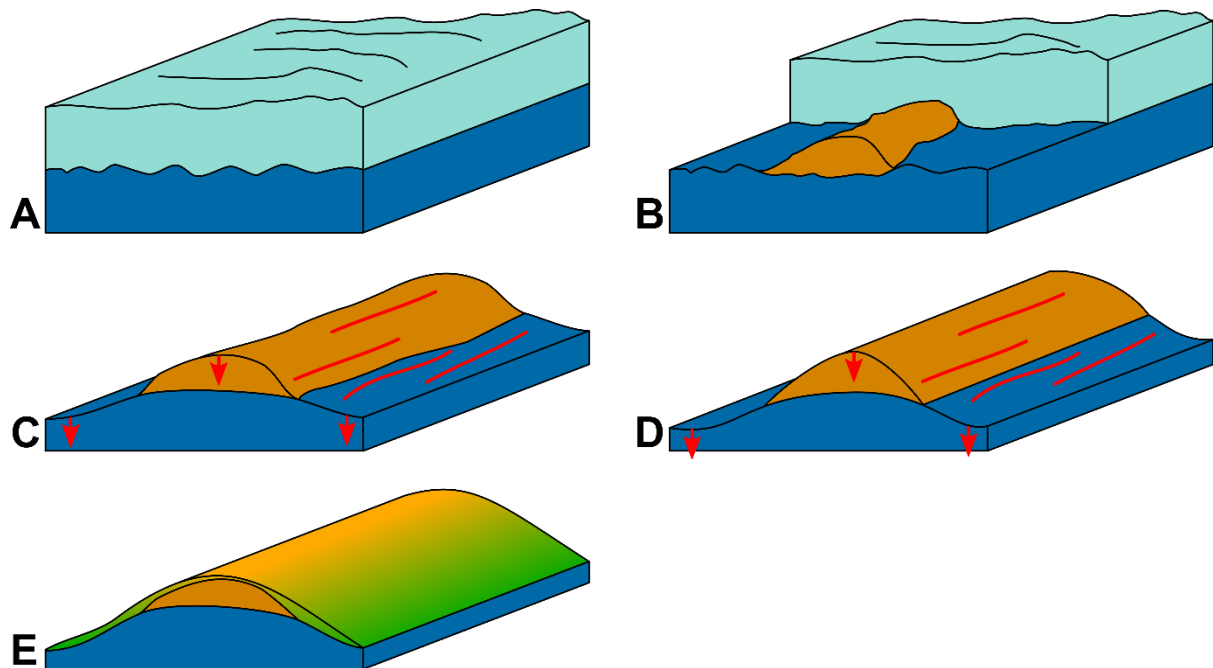


*Figure 5.8 - Cartoon showing stages of the esker formation model showing areas of erosion (red arrows) due to post-glacial tidal currents (red lines). Glaciation (A) results in the deposition of an esker (B) which is exposed to a regional erosion event (C) which sculpts the ridge (D) until tidal currents diminish and the seafloor is draped (E).*

### **Evaluation of Megaridge Origin Formation Models**

The MFm is chronologically constrained by over- and underlying units on the inner- to mid-shelf to have formed between 27-24 ka BP and 14 ka BP (Table 4.2). This coincides with deglaciation of the shelf (Praeg et al., 2015b; Scourse et al., 2019) and the ensuing main phase of marine transgression which palaeotidal model outputs suggest was characterised by large tidal amplitudes, producing energetic tidal currents for several thousand years (Scourse et al., 2009b; Ward et al., 2016). Therefore, the constraints on the age of the MFm do not unequivocally allow the differentiation between a tidal or glaci-fluvial origin for the MFm. In addition, the available geophysical and physical sample data on the internal character of the MFm can be accommodated by both tidal and glaci-fluvial formation models.

The initial advance of the ISIS into the Celtic Sea occurred after 25-24 ka BP (Ó Cofaigh and Evans, 2007) and ice margin retreat started from the shelf edge by at least 24.3 ka BP (Praeg et al., 2015b). The ice margin had reached St. GC and evacuated the shelf by 24.2 ka BP (Small et al., 2018), indicating that ice margin retreat rate was rapid (Chiverrell et al., 2013; Small et al., 2018) and most likely due to instability (Scourse et al., 2019) induced by a deformable substrate (Scourse et al., 1990).

If the MFm is glacifluvial in origin, this timing implies that the large quantity of sediment comprising the MFm was deposited during a short interval of a few hundred years of the ISIS on the shelf during its retreat. In contrast, eskers are typically observed to be absent in areas of high ice flow velocities (Livingstone et al., 2015) and large and continuous esker generation is favoured during a regime of gradual and stable ice margin retreat (Storror et al., 2014). This is not consistent with the rapid ice margin retreat rate of the ISIS from the Celtic Sea as reconstructed from offshore radiocarbon ages (Praeg et al., 2015b; Scourse et al., 2019) and the Bayesian analysis of luminescence and cosmogenic exposure ages in the Celtic and Irish Seas (Small et al., 2018; Smedley et al., 2017). Additionally, the volume of sediment comprising the MFm seems vast in comparison to that which may possibly have been deposited by the unstable and over-extended ISIS, especially during a rapid advance and retreat cycle. This suggests that the deposition of such quantities of sediment may not have been possible.

Eskers are always formed subglacially, yet the MFm is found in the French sector of the Celtic Sea, well outside currently defined lateral ice limits. Therefore, the esker formation model of the MFm cannot explain the occurrence of the MFm beyond the extent of glaciation on the eastern shelf without invoking a major extension of the glaciation of the Celtic Sea as far south as 47.5° latitude. Eskers have been identified on the inner-shelf (Figure 3.9) but they are significantly smaller than the MFm observed on the mid- to outer-shelf and display a variable along-ridge morphology, consistent with previously described glacifluvial features (Brennand, 2000; Gorrell and Shaw, 1991; Hebrand and Åmark, 1989). Such variable morphology is not observed to the same degree in the MFm (Figure 3.1) apart from where the megaridges comprise segments (Figure 3.4 and Figure 3.5) which could be explained by a glacifluvial origin. Regardless, the MFm is significantly larger (Figure 3.3) than esker and glacial channel systems observed on the inner-shelf (Table 3.1, Figure 3.7 and Figure 3.10), suggesting that either meltwater and sediment supply was more abundant on the mid- and outer-shelf than on the inner-shelf, or that the MFm is not glacifluvial in origin. The latter is more likely, as melting, and meltwater availability would have been even more enhanced during retreat on the inner-shelf, compared to the mid- and outer-shelf, due to warming which increased in intensity during Greenland Interstadial 2 (Rasmussen et al., 2014).

The preservation of the MFm as large glacifluvial ridges surviving a high-energy post-glacial marine transgression is difficult to explain in relation to palaeotidal models which suggest that energy was sufficient enough to continuously entrain coarse sediment (Ward et al., 2015) for several thousands of years (Scourse et al., 2009b; Ward et al., 2016). The erosion of such pronounced ridges comprising unconsolidated non-cohesive sediments is highly likely, and the survival of the megaridges is thus surprising unless they were sufficiently armoured by the development of a coarse lag. Only a single lag deposit exists above the MFm, and this lag deposit is in places not sufficiently coarse or thick to provide armouring as seen in LF2 in 34VC recovered from the upper surface of the MFm (see the annotated core log in Lockhart et al., 2018 in the Appendix). Therefore, the ability of this coarse lag deposit to protect the MFm from several thousand years of energetic tidal currents is questionable and probably unlikely. In the absence of sufficient armouring, this implies that the ridges originally existed as much

larger features than those which are presently observed before being eroded by tidal currents. The deposition of such uncharacteristically large eskers may not have been possible by the brief, unstable and over-extended ISIS. Alternatively, palaeotidal model outputs could be incorrect, and marine transgression may not have been as energetic as predicted.

The tidal ridge formation model provides a mechanism which can explain the occurrence of the MFm beyond present ice limits on the shelf, whereby shelf sediment was eroded by energetic southwest oriented tidal currents which transgressed the shelf to the northwest, entraining sediment to form sand ridges (Scourse et al., 2009b) according to the Huthnance (1982a, 1982b) model. Such a model can explain the varying morphology and internal bedding of the ridges across the shelf, similar to typical tidal bedforms which appear as slightly sinuous single ridges with numerous subtle crests in places; see de Swart and Yuan (2018) for a review. Caston (1981) suggested that offshore tidal ridges may owe their morphology and orientation to being anchored to an underlying feature as suggested here. In such a scenario, the anchoring of a sand body to an underlying feature or seafloor instability can allow ridge growth through the Huthnance (1982a, 1982b) mechanism as tidal currents and sediment transport interact with, and feed, the bed instability. The ridges grow as they experience deposition across their upper surface towards the down current side of the crest when flood and ebb tides are asymmetrical, as is suggested to have been the case at the peak of marine transgression by palaeotidal model outputs (Scourse et al., 2009b; Ward et al., 2016). Such a seafloor instability was most likely provided by the ULSFm where spatially varying glacial processes during deglaciation produced an undulating topography with varying physical characteristics, influencing the erodibility of the ULSFm which tidal currents exploited during marine transgression. The MFm may have also played a protective role, armouring the underlying ULSFm from further erosion by tidal currents after the onset of MFm deposition as sand banks. Additionally, the over-consolidated glacial sediments comprising the ULSFm would be less erodible and therefore would have produced remnant mounds to which the MFm anchored during its formation. The combination of these processes results in the megaridges on the western shelf appearing longer, wider and more uniform along their length, different in morphology to the ridges on the eastern shelf where the MFm does not mantle an eroded glacial unit (Figure 3.1). Therefore, the ridges on the eastern shelf are interpreted to have formed through a purely tidal mechanism with no glacial influence. One issue with a tidal origin of the MFm is that it cannot explain the observation that the ridges across the shelf sometimes have numerous prominent crests along their length and appear distinctly segmented whilst neighbouring ridges sometimes have a distinctly different morphology (Figure 3.5). This may be due to the interaction of tidal currents with an unknown precursor topography prior to erosion of the ULSFm which could have profoundly influenced sand ridge development.

Based upon the rapid advance and withdrawal of an unstable ice margin, the predicted intensity and duration of marine transgression following deglaciation, and the extent of the MFm in addition to its large volume, it is suggested that the MFm is less likely to represent eskers as the deposition and preservation of such features is questionable. It is therefore more likely that the MFm represents post-

glacial tidal deposits which mantle a partially eroded glacial topography comprising the ULSFm, having experienced a regionally-extensive tidal erosion event followed by deposition of the MFm to armour the ULSFm from further erosion. Therefore, the tidal formation model of events most likely describes the post-glacial evolution of the Celtic Sea shelf. As tidal sand banks overlie the ULSFm which was deposited during the final withdrawal of the ISIS at the LGM, the quantity of coarse sediment comprising the MFm indicates that significant sedimentation occurred between the commencement of deglaciation at 25 ka BP (Praeg et al., 2015b; Scourse et al., 2019) and the onset of megatidal conditions at or before 21 ka BP (Scourse et al., 2009b; Ward et al., 2016). It is likely that this sedimentation occurred due to deglaciation which occurred during this period. Therefore, the glacial sediments which dominate on the western shelf were harvested by energetic tidal currents during marine transgression and fuelled the growth of the MFm in this region of the shelf. Such sediments must have comprised subglacial, glacial and proglacial deposits, the coarsest grain size fraction of which was incorporated into the MFm by tidal currents while finer grain sizes were eroded and transported off the shelf. Such ample sediment supply in this region of the shelf allowed the MFm to grow for as long as megatidal conditions persisted, providing an explanation as to why the megaridges on the western shelf are some of the longest and widest ridges, despite being exposed to less-energetic tidal currents for a shorter period compared to the eastern shelf (Figure 1.9) which was sediment starved (Scourse et al., 2009b). As the eroded ULSFm is discontinuous under the MFm on the western mid-shelf, underlying lithified units are exposed near the seafloor (Figure 3.33). This indicates that megatidal conditions had nearly exhausted the available glacial deposits, having eroded down to the lithified base. In contrast, significantly thick glacial facies are continuous under the megaridges towards the western inner-shelf (Figure 3.20). This spatial contrast suggests that seaward glacial deposits were more heavily eroded by megatidal conditions, agreeing with palaeotidal model outputs which suggest that seaward areas experienced megatidal conditions for a longer duration than landward areas before megatidal conditions ceased (Scourse et al., 2009b).

### **5.2.2 Reconstruction of Palaeo-glacial Dynamics**

The revised shallow Quaternary stratigraphy presented here (Table 4.2) provides the first data-rich determination of the stratigraphic position of glacial sediments and their relationship to the megaridges on the western shelf. This stratigraphic framework provides the best foundation from which to reconstruct the palaeo-glacial environment as it records both the spatial distribution of glacial sediments across the shelf as well as their stratigraphic position. It is now possible to assess the observed stratigraphy to ascertain the maximum extent of glaciation on the shelf as well as in what setting deglaciation occurred. These observations from the terminal region of the ISIS are essential for studying how marine-terminating ice streams deglaciate and the primary mechanisms driving such events.

### **Extent of Maximum Ice Advance**

The revised composition and extent of the ULSFm can be used to infer the extent of glaciation across the mid- and outer-shelf due to it comprising stiff, over-consolidated and sometimes deformed

glacimarine sediments (LF8) and subglacial till (MT) which are consistent with the action of localised grounded ice. In addition, the extent of soft and undeformed glacigenic sediments can provide information on areas where grounded ice did not exist.

The ULFSm encompasses glacigenic sediments recovered from the megaridges across the western shelf which extend out towards the shelf edge (Figure 3.1). As the MFm is most likely to be post-glacial tidal in origin, the megaridges indirectly provide insight into the extent of glaciation based on their morphology from regional bathymetric data. The occurrence of glacigenic material contributing to the bathymetric expression of the megaridges may explain the contrasting morphology with the smaller ridges on the eastern shelf. The megaridges on the western shelf are distinctly longer, wider and more axially-uniform (Figure 3.1), most likely because these features comprise post-glacial tidal deposits which have mantled, and have been influenced by, the remnant glacigenic topography. It is possible that the megaridges only developed on the western shelf because of the existence of stiff or significant thicknesses of glacigenic sediment which enhanced their preservation and provided a sufficiently-entrainable sediment supply. A glacial influence on ridge development may not have occurred on the eastern shelf where ridges appear distinctly more sinuous, narrower and more irregular (Figure 3.1), and are suggested here to have formed through a purely tidal process. Therefore, if the updated stratigraphic model of the megaridges presented here is applicable to other megaridges of a similar morphology on the western shelf which were not investigated, then this similarity suggests that the ULFSm exists in this area. Thus, the extent of the megaridges could record the extension of the ISIS to the shelf edge adjacent to the Goban Spur and merge with the shelf edge limit suggested by Praeg et al. (2015b). An advancing ice lobe would not have been confined by topography on the mid- and outer-shelf, which would have encouraged lateral spreading as a piedmont lobe. The extent of glaciation towards the French sector of the outer-shelf is difficult to determine due to the lack of high-resolution ridge seismic data and new sediment cores. It is possible that glaciation extended into the French sector, but the thicknesses or physical properties of any glacigenic sediments might not have been conducive to their preservation during marine transgression, and therefore they were removed before ridge development. Additionally, the French sector of the shelf is suggested to have experienced tidal conditions which were more energetic than those on the western shelf (Figure 1.9; Scourse et al., 2009b; Ward et al., 2016) which may have completely eroded any glacigenic sediments. Therefore, the extent of glaciation into the French sector is difficult to determine based upon the available stratigraphic, sediment core and ridge morphological data, though the megaridges provide a minimum extent to the west.

Beyond the megaridges to the northwest, LF8 is recovered from SF5 which extends towards the southern coastline of Ireland beyond the dataset (Figure 3.19), representing the furthest northwest extent of a seismic facies which has been correlated to cored glacigenic sediments. The extent of this facies and the ULFSm in the megaridges agree with the extent of glaciation from previous observations which suggest that the entire western shelf was glaciated south of Ireland due to the offshore advance



of ice (Ó Cofaigh et al., 2012) which extended out to the shelf break (Praeg et al., 2015b; Scourse et al., 2019).

However, not all glacially-correlative seismic facies or glacial sediments are restricted to the western region of the shelf. Scourse et al. (2019) report a stiff matrix-supported diamict in core 3VC at the shelf break (Figure 1.4) to the southeast, in the region of purely tidal ridges where similar sediments interpreted as ice-rafted debris have also been recovered (Scourse et al., 1990). This glacial lithofacies (see the annotated core log for 3VC in Scourse et al., 2019 in the Appendix) was interpreted to be subglacial till deposited by the ISIS, based upon its geochemical similarity to LF8 and physical similarity to MT recovered on the mid-shelf, together suggesting grounded ice extent to the southeast beyond the megaridges (Scourse et al., 2019). These characteristics suggest that this till correlates with the glacial sediments which comprise the ULSFm located under and adjacent to the MFm, forming the megaridges on the western shelf. However, seismic data at the shelf edge core site do not allow for a stratigraphic correlation of this till to a seismic facies, as no distinct boundaries or reflections exist below the seafloor (Scourse et al., 2019). All that can be determined from the seismic data is that the till was recovered adjacent to and stratigraphically below the MFm, similar in location and stratigraphic position to the ULSFm and the recovery sites of other glacial sediments across the western shelf (Table 4.2). Seaward of core 3VC, Piston Core (PC) 2PC (see the annotated core log in Scourse et al., 2019 in the Appendix) recovered soft muds which were interpreted as undisturbed glacial marine sediments, therefore constraining a grounded ice margin along the shelf break in the southeast (Scourse et al., 2019). The glacial extent suggested by the morphology and stratigraphy of the megaridges must therefore represent the area where the most-significant glacial deposition and preservation occurred and should be regarded as a minimum indication of ice extent. This ice extent to the southeast agrees with streamlined features adjacent to the Isles of Scilly on the inner-shelf which record grounded ice flowing to the southwest onto the shelf (Plot I in Table 3.1 and Figure 5.6) which would produce a flow directed towards this region of the outer-shelf. As mentioned previously, it is likely that such an ice flow spread out laterally on the flat and unconfined shelf to form a piedmont lobe. Therefore, if the grounded extent of the ISIS at the shelf edge (Line 26 in Figure 3.13) as suggested by Scourse et al. (2019) is accepted, then it is not impossible that glacial conditions existed in parts of the French sector of the shelf during this lateral spread.

The French sector of the shelf contains channels which exist under the MFm and comprise sediments of the ULSFm (Figure 1.16) which incise pre-Quaternary deposits (Bouysse et al., 1976). The landward termini of these channels are observed in bathymetric data which terminate along the northeast boundary of the ridge field (Figure 3.6) and extend towards the shelf break (Figure 1.16). One of the ULSFm channels mapped in the French sector by Bouysse et al. (1976) was imaged on chirp seismic data (Figure 3.40), representing the first high-resolution image of the ULSFm in this sector of the shelf since the initial discovery and mapping of the channels. Seismic data from the channel show that it is incised into a lithified unit of similar acoustic character to the Cockburn Formation (CbFm) and is infilled by SF2 and SF3 which appear to have been deposited in an subaqueous setting, consistent with

equivalent seismic facies in the CD (Figure 3.14) which were cored as undisturbed glacialaqueous deposits (Table 4.2). These observations suggest that SF2 and SF3 are in a similar stratigraphic position to the ULSFm on the western shelf where the ULSFm in places infills a channelised surface (Figure 3.27) or overlies the CbFm (Figure 3.34). Additionally, SF2 and SF3 have been interpreted to be glacialgenic in origin in the CD (Table 4.2), similar to the ULSFm. These similar characteristics suggest that the ULSFm in the French sector comprises glacialaqueous deposits which infill channels. However, even though the acoustic similarity of the facies and the stratigraphic correlation to other glacialgenic facies is striking, further investigation of these and other channels comprising the ULSFm in the French sector is required to determine their exact composition. If the seismic facies comprising ULSFm here do indeed consist of glacialaqueous deposits, then they would further extend the ice limits of the Celtic Sea into the French sector south of the Isles of Scilly. These seismic facies may represent glacialaqueous deposition beyond a laterally spreading ice margin which may have initially occupied the channels before subsequently infilling them with deglacial sediments during retreat. Such a scenario can explain the undulating seismic facies within the base of this channel, possibly representing subglacial sediments. If the infilling seismic facies are glacialgenic then they provide a minimum ice extent limit in the French sector. However, the preservation of undisturbed glacialaqueous deposits in the French sector channels is unlikely, as this area experienced more-energetic tidal currents than the western shelf (Ward et al., 2016) where only stiff and deformed deglacial sediments were partially preserved. However, it is also possible that the channel provided shelter from tidal currents, as exposed deposits of positive relief on a flat seafloor would have been more readily eroded. Lacking physical samples, the seismic facies infilling the channel may not be glacialgenic in origin. If this is the case, then their undisturbed appearance may suggest that the ice margin did not reach the French sector of the shelf as such sediments would have been contorted by the advancing ice margin.

The combined evidence of Celtic Sea glaciation implies that a significantly larger ice lobe occupied the Celtic Sea than that first suggested by Scourse et al. (1990) which was limited to a mid-shelf position in the UK sector. Observations suggest that the ISIS reached the western shelf edge and may have even encroached into the French sector of the shelf. This large extent would imply that the ISIS spread as a piedmont lobe and was very over-extended and thin which would have promoted rapid ice margin retreat.

### **Configuration of Ice Retreat and the Deglacial Environment**

Over-consolidated and sometimes deformed glacialmarine sediments (LF8) and other deglacial deposits provide key evidence of depositional and deglaciation conditions which occurred across the shelf. Such observations permit the reconstruction of the retreat of the ISIS where direct glacial geomorphological evidence of ice margin positions is absent.

The suggested mechanism of initial deglaciation of the Celtic Sea is that the associated rise in relative sea level caused initially by glacio-isostatic depression due to greater ice extent (Scourse et al., 2019), and subsequently by Heinrich Event 2 (H2; Haapaniemi et al., 2010). Relative sea-level rise resulted in

marine deglaciation at 25 ka BP, after which warming was the primary driver for northward retreat (Smedley et al., 2017) during Greenland Interstadial 2 (Rasmussen et al., 2014). As marine deglaciation commenced, the subaqueous deposition of mud and silt deposits occurred beyond the ice margin across the shelf (Praeg et al., 2015b; Scourse et al., 2019, 1990). The presence of such fine-grained and laminated deposits requires there to be a quiet subaqueous environment to result in their deposition through suspension-settling (Ó Cofaigh and Dowdeswell, 2001) before they were overridden by the ice margin. Such quiet aqueous conditions across the shelf could have been facilitated by either proglacial lacustrine waterbodies on a subaerially exposed shelf, or a calm and turbid marine environment (Furze et al., 2014). Core observations of glacialmarine deposition are clear across the outer-shelf (Praeg et al., 2015b; Scourse et al., 2019, 1990), while conditions on the inner- to mid-shelf are ambiguous (Furze et al., 2014). High relative sea level, high sedimentation rates and low salinities in a marine environment can explain the lack of diagnostic fossils in deglacial muds on the inner- and mid-shelf (Furze et al., 2014). High sedimentation rates can be evidenced by the presence of significant quantities of sediment comprising the MFm which was harvested from glacialine sediments during the post-glacial marine transgression (Figure 5.7). High relative sea-level conditions are evidenced on the inner-shelf by the presence of iceberg scouring (Figure 3.7 and Image C in Table 4.1). Finally, the presence of numerous glacial channels and eskers on the inner-shelf (Figure 3.7, Figure 3.9 and Figure 3.10) record the presence of abundant meltwater. Therefore, this evidence suggests that marine deglaciation is more likely to have occurred across the entire shelf, as a lacustrine depositional model requires low relative sea-level conditions and confining glacial morphology, neither of which are apparent. Marine deglaciation can provide an initial driving mechanism in the form of a pulse of relative sea-level rise during glacio-isostatic depression (Scourse et al., 2019), and by H2 (Haapaniemi et al., 2010) which destabilised the ice margin and can explain the observed peaks in ISIS-sourced Ice Rafted Debris (IRD) recovered offshore (Haapaniemi et al., 2010; Scourse et al., 2009a).

After the onset of marine deglaciation, energetic megatidal conditions existed across the Celtic Sea shelf, having commenced by 21 ka BP as suggested by palaeotidal model outputs (Figure 1.6; Scourse et al., 2009b; Ward et al., 2016). These energetic megatidal and shallow marine conditions contrast with the occurrence of fine-grained deglacial deposits requiring quiet marine conditions. If the observed glacialmarine deposits had been exposed to such an energetic marine environment, then they would have remained in suspension and would not have been deposited through settling. Therefore, the deposition of such sediments in an energetic marine environment needs to be explained. One mechanism to facilitate a calm marine environment along the ice margin could be provided by the abundance of icebergs and freshwater from melting. H2 was characterised by vast armadas of icebergs being calved into the North Atlantic by the Laurentide Ice Sheet (Hemming, 2004) which drifted towards the Celtic Sea shelf (Wagner et al., 2018). These icebergs could have congregated at the Celtic Sea shelf edge ice margin and buffered it from energetic marine conditions while still allowing the ice margin to be susceptible to retreat triggered by relative sea-level rise. During the retreat of the ice margin in response to the eustatic pulse associated with H2, abundant calving at the ice margin must have occurred due to buoyancy stresses being imparted on the thin and fractured ice margin (Ma et al.,

2017). Such conditions are likely, as indicated by ISIS-sourced IRD at this time (Haapaniemi et al., 2010) especially considering the rapid pace of ice margin retreat, as calving provides the fastest mechanism for ice mass loss, especially for an over-extended and fast-flowing ice stream (Benn et al., 2007). These numerous and freshly calved icebergs, in addition to those that have traversed the North Atlantic during H2, could have continued to buffer the ice margin from energetic marine conditions during deglaciation across the shelf. Additionally, abundant freshwater input from meltwater sourced from the ice margin and icebergs may have produced a strong local halocline in the water column which could provide some protection from energetic tidal conditions (Syvitski, 1991; Syvitski and Praeg, 1989). Such a scenario is possible, as the low-latitude location of the ISIS may have enhanced melting, and the presence of abundant meltwater during deglaciation is evidenced by the presence of eskers and glacial channels observed on the inner-shelf (Figure 3.7, Figure 3.9 and Figure 3.10). The formation of a freshwater layer and a sheltered subaqueous environment provided by the presence of numerous icebergs could then additionally facilitate the temporary formation of sea ice to further buffer energetic marine conditions (Wagner et al., 2018). These processes may have combined to facilitate a quiet glacimarine environment around the ice margin to allow for the deposition of glacimarine muds across the shelf even during energetic marine conditions.

After deposition in a quiet aqueous environment, the glacimarine muds were exposed to subglacial overriding resulting in the observed deformation and over-consolidation. This overriding event must have occurred between the start of retreat at the shelf edge at 25 ka BP (Praeg et al., 2015b; Scourse et al., 2019) and final ice evacuation of the shelf at 24.2 ka BP (Small et al., 2018), and could have occurred as either a large advance or minor oscillations of the ice margin (Scourse et al., 2019). If marine deglaciation continuously occurred across the mid- and outer-shelf, then any readvance event is more likely to have occurred as minor ice margin oscillations as opposed to a major readvance. A major readvance scenario is unlikely, as a thin ice margin would be unable to advance into the marine environment for a considerable distance without floating. This would result in stress being imparted on the ice margin (Ma et al., 2017) and an increase in ice flow velocity, both of which would promote rapid breakup through calving (Benn et al., 2007). Even if such a major readvance was possible, it is unlikely that the ISIS had sufficient ice accumulation to facilitate such an event, as it was most likely over-extended and thin. Therefore, the overriding event to deform and over-consolidate glacimarine muds across the shelf is more likely to have occurred through multiple minor oscillations of the ice margin during deglaciation. The fine grainsize, and thus low permeability, of the saturated glacimarine muds would result in their tendency to deform when loaded by ice due to a dramatic increase in pore pressure. Therefore, their presence in the proglacial environment could result in ice margin instability (Ó Cofaigh and Evans, 2001) and allow the rapid adjustment of the ice margin to internal and external dynamics. During deglaciation, the ice margin may have repeatedly “slipped” on the glacimarine sediments in response to reduced subglacial friction induced by flotation as relative sea level continued to rise during deglaciation (Figure 5.9). As sea-level rose, the thin and grounded ice margin began to float which imparted stress on the ice margin (Image B in Figure 5.9; Ma et al., 2017). This also reduced subglacial friction, causing the ice margin to axially-extend and deform proglacial sediments which further

decreased subglacial friction (Image C in Figure 5.9). The heavily fractured ice margin then broke up through calving (Image D in Figure 5.9), after which the cycle repeated to leave behind a trail of deformed glacimarine sediments. The spatial distribution of cores containing LF8 suggests that such minor ice margin oscillations occurred only on the mid- and outer-shelf, as similar physical properties are absent from equivalent deglacial sediments recovered from the CD. On the mid- and outer-shelf, the slope is not adverse which would have provided some stability for the ice margin, facilitating ice margin oscillations during deglaciation. These ice margin oscillations must have been brief and minor as they did not hinder the overall northward retreat of the ice margin, as the uniform bio- and litho-stratigraphy and radiocarbon ages of the deglacial sediments indicate rapid ice margin retreat rates (Furze et al., 2014; Scourse et al., 2019). During deglaciation, the raised area of seafloor comprising the Haig Fras Platform most likely provided stability for the ice margin and temporary alleviation from rising relative sea level. At this position, the ice margin would be pinned laterally in the west to the southern coastline of Ireland and in the east to the Isles of Scilly.

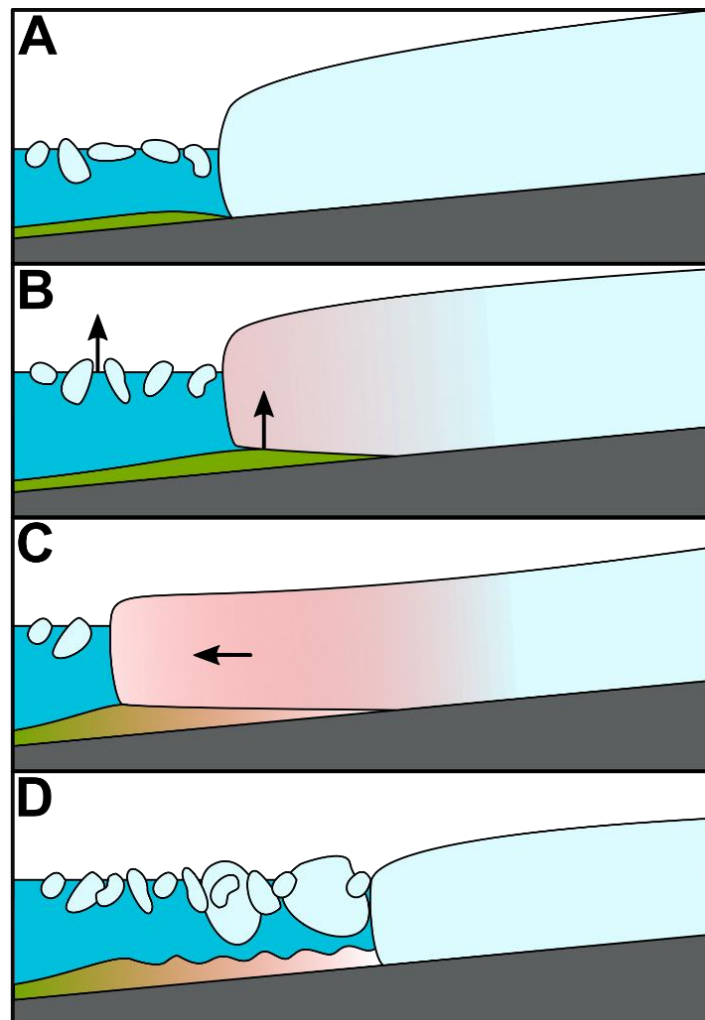


*Figure 5.9 - Cartoon showing the stages of an ice margin oscillation during deglaciation. A marine-terminating ice margin (A) experiences relative sea-level rise which imparts stress on the margin due to flotation (B). This flotation results in a reduction in basal friction and an unstable advance to*

*override deformable proglacial sediments along with the production of even more stress (C). Due to intense fracturing and over-extension, the ice margin subsequently breaks up through calving (D).*

### **5.2.3 Regional Reconstruction**

The stratigraphy and morphology of the megaridges provides key information for the interpretation of the minimum extent of glaciation across the western shelf, with the ice margin reaching the shelf break as interpreted by Praeg et al. (2015b) and Scourse et al. (2019). This interpretation is enhanced by the spatial extent of glacial sediments comprising the ULSFm on the western shelf, providing an integrated reconstruction of the ISIS on the mid- and outer-shelf (Figure 5.10). Undisturbed seismic facies infilling channels in the French sector may provide a minimum ice margin extent position if glacial (Figure 5.10), or may delineate an ice-free area if pre-glacial in age. These observations do not directly record ice margin advance and retreat direction as the mid- and outer-shelf lacks complex topography. Therefore, it can be assumed that spreading as a piedmont lobe occurred, but the exact extent of this spreading into the French sector of the shelf is unknown. In addition to the extent of glaciation, deglacial muds record glacial deposition across the mid- and outer-shelf, most likely representing glacial deposits which were then overridden by the ice margin during minor oscillations. This represents a profound change in deglacial dynamics in response to external factors such as a deformable substrate and flotation due to relative sea-level rise. This deglacial mechanism facilitates rapid ice margin retreat, preconditioned only by the presence of a thin ice margin and deformable proglacial sediments in a rising sea-level environment (Figure 5.9). Such conditions will exist in the future for contemporary marine-terminating ice streams in response to rising relative sea level and increased atmospheric and marine warming. Therefore, where similar physical characteristics exist for other ancient and contemporary ice streams, such a combination of mechanisms invokes rapid ice margin retreat which can lead to irreversible collapse of the ice sheet.

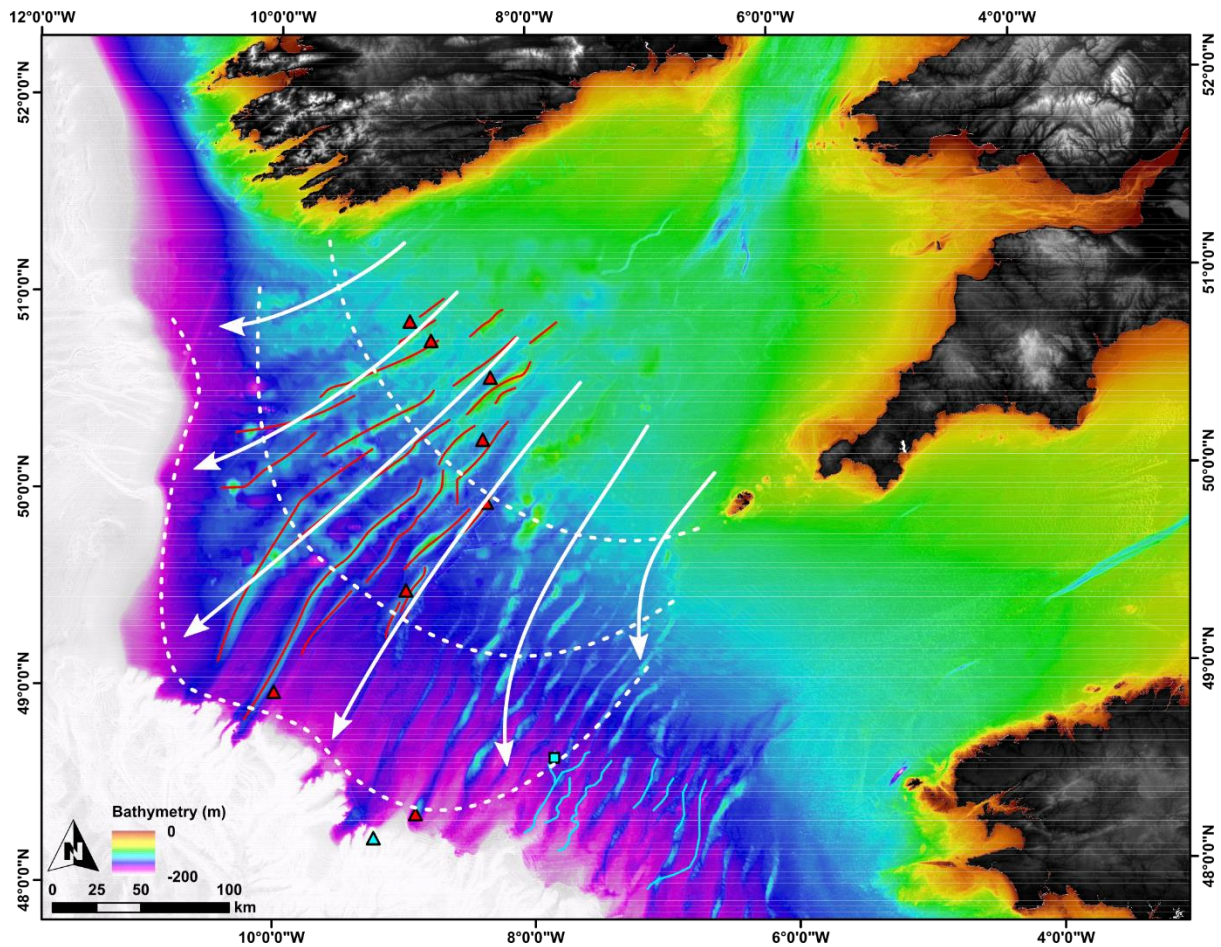


Figure 5.10 - The advance and retreat pathways of the Irish Sea Ice Stream on the mid- and outer-shelf based on ice flow direction reconstructed on the inner-shelf (Figure 5.6). White arrows denote generalised ice flow pathways while generalised ice margin retreat positions are indicated with white dashed lines. The extent of the Upper Little Sole Formation (ULSFm), comprising cored subglacial sediments (red triangles), within the megaridges (red lines) is marked on the western shelf. Cored undisturbed glaciaqueous sediments (blue triangle) are marked with ULSFm channels (blue lines) which are imaged to contain undisturbed seismic facies (blue square).

The inferred sequence of events to explain the spatial and stratigraphic distribution of glacial sediments and glacially-related seismic facies on the mid- and outer-shelf is as follows, integrating other work providing chronological constraints (Praeg et al., 2015b; Scourse et al., 2019, 2018):

1. The grounded ice lobe advanced onto the mid- and outer-shelf, spreading out laterally (>27 ka BP)
2. The grounded ice margin attained a position at the shelf edge, covering the western shelf and infringing on parts of the French sector (27-25 ka BP)



3. Ice margin retreat commenced in response to a rise in relative sea level, resulting in marine deglaciation where abundant calving provided quiet aqueous conditions to allow glacimarine deposition (25 ka BP)
4. During marine deglaciation across the mid- and outer-shelf, the grounded ice margin experienced minor oscillations, overriding and deforming the recently deposited glacimarine sediments
5. The ice margin stabilised between the inner- and mid-shelf, where the southern coastline of Ireland, Haig Fras and the Isles of Scilly provided pinning points while the raised area of the Haig Fras Platform south of the CD provided a positive slope

## Chapter 6 - Synthesis

### 6.1 Glaciation of the Celtic Sea Shelf

Based on the regional reconstructions of the inner-shelf and the mid- and outer-shelf, the advance and retreat pattern of the Irish Sea Ice Stream (ISIS) can be inferred (Figure 6.1). The advance and retreat configuration on the inner-shelf is more accurately determined due to being based on direct observations of glacial features recording ice margin advance and retreat direction. In contrast, the reconstruction on the mid- and outer-shelf is less reliable as such features are not observed. However, due to the flat topography of the mid- and outer-shelf and the location of the main ice mass to the north, the ice flow patterns in this area most likely occurred through simple spreading as a piedmont lobe. Therefore, the main ice lobe advanced southwest as a single trunk through the St. George's Channel (St. GC) and Celtic Deep (CD) trough and spread out across the Celtic Sea shelf to attain its maximum extent at the shelf edge. As relative sea level rose, this initiated the simple northwest retreat of the ice margin across the shelf. Upon reaching the inner-shelf, the complex topography in combination with rising relative sea level produced spatially-varying ice margin retreat rates, such as rapid retreat in the CD compared to slower retreat immediately adjacent to the west on the southern coastline of Ireland.

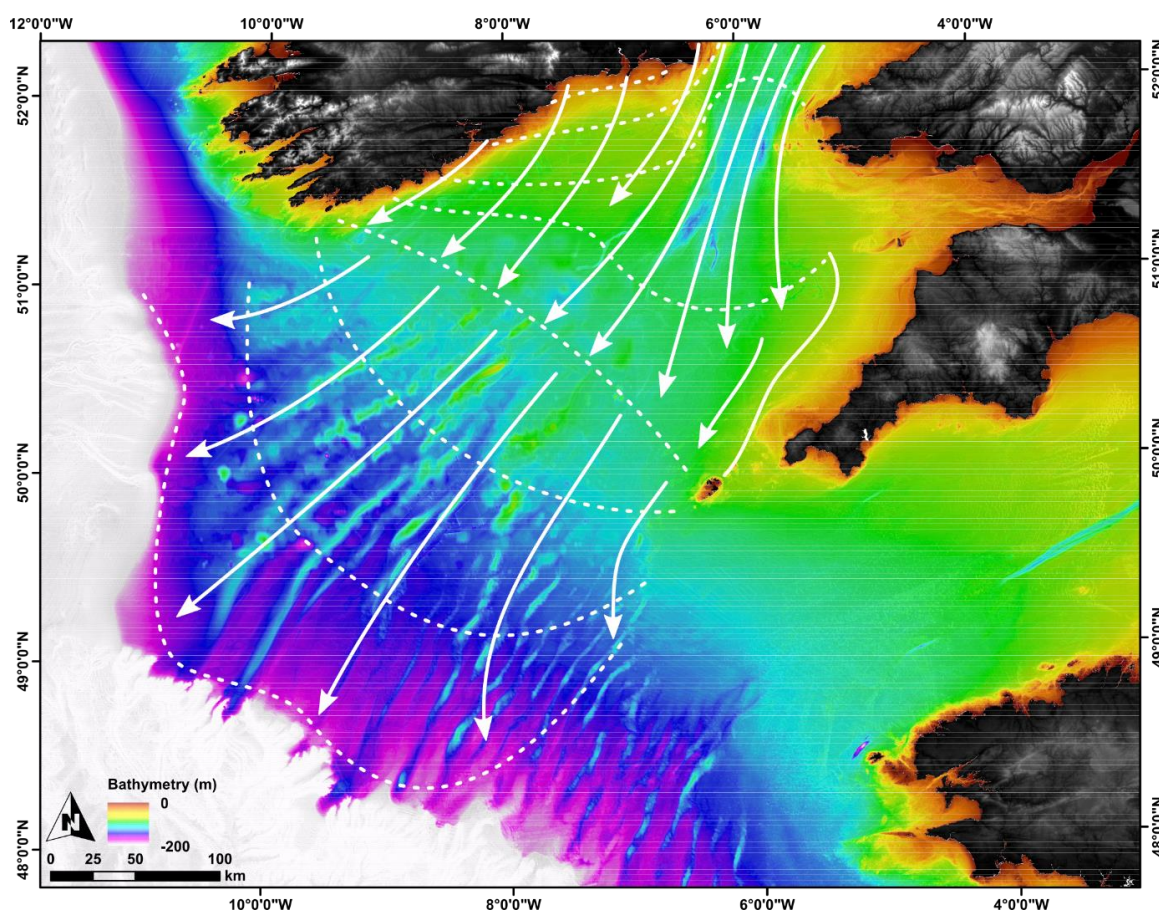


Figure 6.1 - The inferred advance and retreat pathways of the Irish Sea Ice Stream on the Celtic Sea shelf. White arrows denote generalised ice flow pathways while generalised ice margin retreat positions are indicated with white dashed lines, solid white represents the eastern margin limit north of the Isles of Scilly.

The inferred sequence of events of the advance and retreat of the ISIS on the Celtic Sea shelf is as follows, integrating other work providing chronological constraints (Praeg et al., 2015b; Scourse et al., 2019, 2018; Small et al., 2018):

1. The main grounded ice lobe advanced southwest through St. GC, directed along the thalweg of the CD while ice spread out over the flanks of the deep, merging with ice advancing offshore from southern Ireland (>27 ka BP)
2. Grounded, fast-flowing and warm-based ice advanced southwest onto the mid-shelf, adjacent to the Isles of Scilly and parallel to the coastline of Cornwall but did not reach the coastline (>27 ka BP)
3. The grounded ice lobe advanced onto the mid-and outer-shelf, spreading out laterally (>27 ka BP)
4. The grounded ice margin attained a position at the shelf edge, covering the western shelf and infringing on parts of the French sector (27-25 ka BP)
5. Ice margin retreat commenced in response to a rise in relative sea level, resulting in marine deglaciation where abundant calving provided quiet aqueous conditions to allow glacimarine deposition (25 ka BP)
6. During marine deglaciation across the mid- and outer-shelf, the grounded ice margin experienced minor oscillations, overriding and deforming the recently deposited glacimarine sediments
7. The ice margin stabilised between the inner- and mid-shelf, where the southern coastline of Ireland, Haig Fras and the Isles of Scilly provided pinning points while the raised area of the Haig Fras Platform south of the CD provided a positive slope
8. To the southwest of the southern coastline of Ireland, grounded and marine ice margin retreat occurred parallel to the coastline
9. Significant quantities of meltwater incised pre-existing geological weaknesses on the inner-shelf as the ice margin retreated towards the CD in response to rising relative sea level
10. The CD was breached and became inundated, triggering rapid retreat of the ice margin towards St. GC due to the adverse slope
11. Further northeast along the southern coastline of Ireland, a change in ice margin retreat orientation occurred where the grounded ice margin retreated directly towards the coastline
12. The grounded ice margin stabilised in the southern entrance of St. GC where ice flow velocities reduced due to narrowing of the ice margin width (24.2-22.1 ka BP)
13. Adjacent to St. GC on the southern coastline of Ireland, stable and grounded ice margin retreat occurred from the Nympe Bank Platform towards the coastline

The extent of the ISIS across the outer-shelf suggests that the advance occurred as a piedmont lobe which spread out to the shelf edge, fed by a single trunk which drained the interior of the British-Irish Ice Sheet (BIIS) through St. GC. This configuration is similar to that of the Hudson Strait Ice Stream of the Laurentide Ice Sheet (Margold et al., 2015; Scourse et al., 2019) which also drained the interior of

the ice sheet and experienced a dramatic marine deglaciation which culminated in Heinrich Event 2 (Hemming, 2004). The ISIS is also similar in configuration to the contemporary Thwaites Ice Stream of the Antarctic Ice Sheet (Scourse et al., 2019) which is dynamically thinning while in contact with the marine environment (Milillo et al., 2019). Therefore, the present-day Thwaites Ice Stream may suffer the same fate as the Hudson Strait and Irish Sea ice streams, both of which can provide valuable information as to how rapidly such a system may collapse and the what the driving mechanisms are. The extent of the ISIS and the lack of a significantly large feeder catchment, in comparison to those comprising the Hudson Strait and Thwaites ice streams, suggests that the ISIS advance was in response to external conditions, such as a deformable bed (Scourse et al., 1990), and that the ice stream was unstable and short-lived (Scourse et al., 2019; Small et al., 2018). It is unlikely that the ice stream trunk flowing through St. GC and the catchment in the Irish Sea were able to supply enough ice mass for the advance of the ISIS to be stable, considering the 800 km long ice stream and 200 km wide feeder catchment supplying ice to the margin through a 70 km wide channel. For comparison, the 1400 km long Hudson Strait Ice Stream had a 700 km wide catchment while the contemporary Thwaites Ice Stream is 400 km long and is fed by a 300 km wide catchment (Margold et al., 2015), providing adequate ice supply. The insufficient supply of ice through St. GC would have resulted in the main advancing lobe of the ISIS having a finite quantity of ice mass which rapidly spread across the shelf due to the presence of a deformable substrate and a lack of confining morphology on the mid- and outer-shelf. The presence of a deformable substrate would reduce subglacial friction and increase ice flow velocities, resulting in an over-extended and unstable piedmont ice lobe which was most likely fractured and thin due to lateral spreading and axial extension. This unstable ice advance resulted in the dramatic draw-down of the internal ice sheet surrounding the Irish Sea which was a major factor conditioning the deglaciation of the BIIS. The observed extent of the ISIS is ~60000 km<sup>2</sup> greater than previous reconstructions by Scourse and Furze (2001), incorporating the observations presented here and from Praeg et al. (2015b) and Scourse et al. (2019). This increased extent of the ISIS is not taken into account in northwest Europe glacial isostatic adjustment and palaeotidal models, which rely upon a constrained ice sheet chronology to produce accurate sea-level reconstructions (Bradley et al., 2011). Such an extent can result in glacio-isostatic depression, subsequent relative sea-level rise and ice margin retreat (Scourse et al., 2019). Therefore, these new observations feed back into the regional palaeo-environmental and sea-level history of the Celtic Sea.

The influence of the substrate was not only profound during the advance of the ISIS, but also during its deglaciation. Minor ice margin oscillations occurred during deglaciation in response to ice margin flotation due to relative sea-level rise. Flotation of the thin ice margin reduced subglacial friction and increased the ice flow velocity which resulted in the overriding of freshly deposited and readily deformable deglacial muds. These saturated sediments would have dramatically reduced in strength when loaded and would have further increased ice flow velocities and caused the ice margin to destabilise and continue advancing into the marine environment until it fractured. This process of ice margin flotation and axial advance would impart stresses on the already fractured, thin and near-buoyant ice lobe, resulting in further fracturing and crevasse formation (Benn et al., 2007; Ma et al.,

2017). Such a heavily fractured ice lobe would precondition the margin for rapid breakup in a marine environment through calving, the rate of which would be enhanced by the significant width of the ice margin. Such a mechanism can explain the rapid retreat rate of the ice margin and the presence of significant quantities of ISIS-sourced ice rafted debris delivered into the adjacent North Atlantic for the period 25-24 ka BP (Haapaniemi et al., 2010) when deglaciation was occurring. On the inner-shelf, the underlying geology influenced the distribution and organisation of subglacial drainage conduits due to subglacial meltwater exploiting structural weaknesses such as faults and geological boundaries. Those weaknesses which lay oriented along the ice margin retreat direction were the most heavily exploited. The organisation of the subglacial drainage network into defined conduits suggests that some areas of the substrate may have been well-drained, encouraging the formation of sticky spots which readily reduce basal sliding (Stokes et al., 2007). Additionally, the availability of meltwater supplied by the subglacial drainage network can profoundly affect ice flow velocities, with implications for ice sheet stability (Schoof, 2010). Therefore, the advance and retreat reconstruction of the ISIS in the Celtic Sea highlights how the substrate can affect the dynamics of ice streams in response to environmental changes such as sea-level rise and tidal conditions.

The trough of St. GC contained the main supply trunk of the ice stream which flowed through the CD before spreading and over-extending to the shelf edge due to the presence of a deformable and smooth substrate. These physical characteristics made the Celtic Sea shelf suitable for enhanced ice streaming (Winsborrow et al., 2010), explaining the over-extension of the ISIS. Numerical whole ice sheet models have not been able to recreate the maximum shelf edge extent of the ISIS in the Celtic Sea (Boulton and Hagdorn, 2006; Hubbard et al., 2009; Patton et al., 2017). This suggests that important mechanisms or conditions are unaccounted for in these numerical models, such as the influence of the substrate on glacial dynamics during the initial advance of the ISIS. The inability of these numerical models to recreate the observed extent and deglaciation of the ISIS has profound implications for the accuracy of such models to simulate glacial dynamics in forecasting of present-day ice sheet stability. In order to partially recreate earlier less-extensive reconstructions of the ISIS in the Celtic Sea, a large area of deformable substrate had to be invoked in previous numerical whole ice sheet models (Boulton and Hagdorn, 2006). Therefore, the new maximum extent of the ISIS implies that more extensive areas of a deformable substrate need to be invoked in such simulations. However, this should be informed by observations of the geology of the shelf. The substrate of the shelf also profoundly influenced the deglacial dynamics of the ISIS in combination with its over-extension and rising sea level, resulting in a perfect example of rapid ice margin retreat due to marine ice sheet instability. The accurate representation of substrate conditions in numerical models is therefore essential in order to predict major changes in ice stream dynamics such as over-extension and ice margin oscillations which can punctuate and pre-condition rapid retreat. Not only is the substrate important for glacial dynamics during the initial advance, but freshly-deposited proglacial sediments during deglaciation also play a role in ice margin instability as suggested here. Therefore, both may need to be incorporated into numerical ice sheet models where the proglacial substrate changes in physical properties from ice margin advance through to retreat. As the subglacial environment is difficult to observe for many contemporary ice

sheets, the representation of the substrate may represent the next challenge in numerical whole ice sheet modelling. It is essential that numerical whole ice sheet models are constrained and validated against palaeo-glacial observations which describe instability (Stokes et al., 2015), such as the reconstruction of the advance and retreat of the ISIS presented here. This reconstruction combines direct observations of palaeo-glacial and environmental conditions and their change through time, integrated with published geochronological information. Only when validated against such a framework can such numerical models be used to accurately predict the stability of present-day marine-terminating ice streams to forecast their contribution to future sea-level rise in response to environmental change.

## **6.2 Post-glacial Evolution of the Celtic Sea Shelf**

The seafloor of the Celtic Sea varies both locally, regionally and with depth in composition and thickness due to spatial and temporal variability of erosion and deposition throughout its post-glacial evolution. This evolution was most profoundly influenced by megatidal conditions which existed during marine transgression of the shelf (Scourse et al., 2009; Ward et al., 2016) which resulted in the erosion of shelf sediment and fuelled the formation of some of the world's largest tidal sand banks. Glaciation also played a pivotal role in the post-glacial evolution of the shelf, as glacigenic sediments were harvested by megatidal conditions to form these sand banks which nucleated on glacial seafloor irregularities on the western shelf. As relative sea level continued to increase towards and through the Holocene, these megatidal conditions declined and quiet deep-water deposition occurred across the shelf, dominating in deeps which were spared from continuing wave action.

The inferred sequence of events of the post-glacial evolution of the Celtic Sea shelf is as follows, integrating other work providing chronological constraints (Furze et al., 2014; Praeg et al., 2015; Scourse et al., 2019, 2018; Ward et al., 2016):

1. Glacial deposition occurs as a sheet deposit extending across the glaciated shelf during rising relative sea level (27-24 ka BP)
2. Tidal resonance drives a regionally-extensive erosion event (EE1) produced by tidal currents which begins to erode glacigenic deposits (25-21 ka BP)
3. The glacigenic deposits survive this erosion event on the western shelf, while glacigenic deposits in the French sector are eroded
4. The coarse fraction of the glacigenic deposits entrained by tidal currents is deposited as sand banks which grow axially due to sediment transport over the crest of the banks (EE2), armouring the underlying glacigenic sediments from further erosion, which continues in the inter-ridge areas and in the French sector (21-16 ka BP)
5. Tidal resonance is lost and the sand banks cease to grow but are still exposed to localised wave action (EE3) while a superficial drape is deposited across the shelf as sea level rises (16 ka BP to present-day)

Within the Bristol Channel and St. GC of the inner-shelf, large areas of seafloor bedforms exist, comprising superficial linear features and large sand waves of varying heights up to 40 m (Tappin et al., 1994). The occurrence of such bedforms corresponds to areas of strong currents enhanced by tidal flow through the channels and around exposed headlands (Ward et al., 2015). In deeper and sheltered regions such as the CD, the quiet deposition of mud occurs and forms vast drapes over the underlying topography which may in places be glacial in origin (Figure 3.15), warranting further geophysical investigation. The action of present-day tidal currents and the influence of the bathymetry explains the majority of the observed composition of the inner-shelf seafloor (Ward et al., 2015). However, areas of coarse grainsize sediment south of Ireland may have been inherited from shallower and more energetic conditions during transgression which winnowed glacigenic deposits, and are thus not in equilibrium



with present-day hydrodynamics (Ward et al., 2015). Such energetic tidal current conditions responsible for the mobilisation of coarse sediment occurred on the shelf during the later stages of marine transgression prior to the Holocene (Scourse et al., 2009; Ward et al., 2016). These conditions dominated on the mid-and outer-shelf, evidenced by the lack of significantly large relict hydrodynamic features on the inner-shelf comparable to the outer-shelf ridges. The northward termination of the ridges is attributed to an abrupt reduction in tidal amplitudes and bed stresses as relative sea level rose towards the present-day (Scourse et al., 2009). Such conditions are required in combination with entrainable sediment to form sand ridges (Scourse et al., 2009) and the inner-shelf lacked the former, as glacigenic sediments are abundant in places. The bathymetry of the inner-shelf is characterised by deep troughs such as the CD where significant thicknesses of Quaternary sediments exist (Tappin et al., 1994), contrasting with surrounding areas of near-surface bedrock which lack sediment coverage greater than 5 m (BGS, 2014). Therefore, the inner-shelf yields the best prospect for the identification of glacial features and the recovery of glacigenic sediments, as it is likely that such deposits remain preserved under a post-glacial drape, especially in the CD, or preserved in glacially-sculpted near-surface bedrock.

The mid- and outer-shelf is devoid of glacial features, primarily due to erosion by energetic tidal currents during marine transgression. Here, only mounds of stiff glacigenic sediments were preserved due to armouring by the formation of post-glacial tidal sand banks on the western shelf, highlighting that sand banks may have a capacity to preserve ancient deposits valuable for palaeo-environmental reconstructions. Therefore, such features may be worth investigating if they exist in areas of glaciation such as the North Sea. In this region, Dogger Bank contains a glacial core comprising moraine ridges (Roberts et al., 2018). Therefore, neighbouring sand ridges might also contain glacigenic cores. Palaeotidal model outputs suggest that the North Sea did not experience as energetic a transgression in comparison to the Celtic Sea (Ward et al., 2016), suggesting that it is more likely that glacigenic sediments and features have been preserved, forming seafloor instabilities on which sand banks may have nucleated. The existence and extent of the sand banks on the Celtic Sea shelf reflects the extent, intensity and duration of tidal current conditions during the post-glacial marine transgression as predicted by palaeotidal model outputs (Scourse et al., 2009; Ward et al., 2016). Despite updated palaeotidal models revealing that the western shelf experienced less energetic tidal currents in comparison to the eastern shelf (Ward et al., 2016), the influence of a glacial topography and abundant sediment supply can account for the existence of significantly large ridges in the west. The change in ridge morphology across the shelf provides an indication of the typical morphology of sand banks which have formed through a purely tidal process on a flat bed in the east, contrasting with those that developed on an undulating topography in the west. Therefore, where sandbanks are observed to have morphologies that deviate from the tidal norm, this may indicate the influence and presence of a preserved core and warrant further investigation. Due to megatidal conditions experienced during marine transgression, the features which characterise the seafloor of mid- and outer-shelf are dominantly moribund tidal features preserved from a prior hydrodynamic regime which are draped by a thin veneer of sediment being reworked by present-day hydrodynamics.

### **6.3 Future Work**

This integrated reconstruction of the glacial and post-glacial evolution of the shelf addresses fundamental issues of previous reconstructions identified from the literature:

- The unknown stratigraphic position of glacial sediments
- The tidal or glacial origin of the mid- to outer-shelf ridges
- A lack of direct observations of palaeo glacial dynamics recorded by preserved features

It is now shown that Last Glacial Maximum glacial sediments correlate not to the Melville Formation, but to the underlying Upper Little Sole Formation (ULSFm) consistently across the shelf, providing a framework for future work regarding the stratigraphy of the shelf and the investigation of shelf glaciation. Combined with radiocarbon dates, the correlation of glacial sediments to the ULSFm is a key observation with implications for the origin of the MFm which comprises the bulk of the ridges across the mid- to outer-shelf. The interpretation that the MFm is post-glacial and tidal in origin is based on the balance of probabilities, heavily determined by the prediction of prolonged and energetic tidal conditions during marine transgression and the rapid speed of ice margin retreat across the shelf. New glacial features identified on the inner-shelf directly record palaeo glacial conditions at the time of formation which complement the onshore and offshore evidence of glaciation to strengthen the overall reconstruction.

However, several specific issues remain unaddressed and warrant further investigation:

- Not all historical sediment cores containing glacial sediments were investigated, therefore geophysical surveying of their recovery locations may validate the stratigraphic model proposed here. In addition, the composition and origin of the ULSFm channel infill in the French sector has implications for the extent of glaciation across the shelf and warrants coring and further geophysical investigation of the remaining channels.
- Further investigation of the mid- to outer-shelf ridges would benefit greatly from 3D seismic data of high resolution to provide more observations from which to determine their origin. Such data would allow the detailed 3D investigation of the internal ridge structures to determine their individual evolution. Such an approach would benefit from significantly long cores through the features to study their internal stratigraphy in greater detail to complement the geophysical data.
- An additional avenue to investigate the influence of glaciation on shelf evolution and the origin of the ridges presents itself through numerical modelling of an evolving bed forced by hydrodynamic conditions informed by palaeotidal model outputs. By producing variations in initial seafloor topography and studying how palaeotidal conditions would interact with such a surface through time, this may strengthen the interpretation that the ridges are tidal in origin and provide key information as to what glacial and non-glacial topography may have existed previously to explain the contrasting morphology of the ridges.

- A marine deglacial setting on the inner-shelf is proposed based on the observation of iceberg grounding pits in areas of an open shelf which alone is not diagnostic of marine deglaciation, only aqueous deglaciation. Therefore, deglacial muds recovered across the inner-shelf and northern mid-shelf which lack a diagnostic fossil assemblage may provide further information through geochemical investigations. Such analyses may determine a diagnostic elemental signature representative of subaqueous deposition in lacustrine or marine conditions when compared to the elemental signatures of deglacial sediments from known depositional conditions.

These specific issues warrant further investigation in order to accurately reconstruct the glaciation of the Celtic Sea and its post-glacial evolution in increasing detail. Therefore, by determining the origin of the ridges and the deglacial setting, and adjusting the reconstruction accordingly, the behaviour of the ISIS can be studied in greater detail. Such a reconstruction is a vital component of the overall reconstruction of the BIIS, as the response of the over-extended ISIS to megatidal conditions, relative sea-level rise and warming provides a unique opportunity to study just how fast ice streams can deglacialate due to marine instability forced by environmental change. Such observations of deglaciation are essential, as instrumental records of ice sheet behaviour do not represent the long-term behaviour of ice sheets due to the fact that the complete deglaciation of a marine-terminating ice mass has never been directly observed. Therefore, the instrumental record only provides a limited representation of present-day ice sheet behaviour. Because of this fundamental limitation, it is unknown how present-day marine-terminating ice sheets will respond to current and future sea-level rise and atmospheric and oceanic warming, and thus their contribution to sea-level rise is also unknown (IPCC, 2014). This is of great concern for West Antarctica which has a reverse bed slope inland (Fretwell et al., 2013) in addition to being marine-terminating, physical characteristics which can precondition rapid and irreversible deglaciation (Benn et al., 2007; Schoof, 2007), resulting in 3 m of global sea-level rise (Bamber et al., 2009). One of the largest ice streams in West Antarctica, the Thwaites ice stream, is currently thinning (Milillo et al., 2019). This response represents the initial phase of instability which can precondition irreversible deglaciation once critical tipping points have been surpassed (Benn et al., 2007). If irreversible deglaciation of the Thwaites ice stream occurs, such an event can threaten the interior of West Antarctica and destabilise neighbouring ice masses in this region (Feldmann and Levermann, 2015), producing a domino effect where deglaciation could progress rapidly due to the reverse bed slope. Therefore, the prediction of such an event occurring in the future is only possible through the application of numerical models which are validated against ice sheet reconstructions with a robust chronological framework (Stokes et al., 2015). Until such a numerical model exists, the long-term behaviour of ice sheets and their contribution to future sea-level rise represent major uncertainties in a warming world with the capability to dramatically affect oceanic circulation and climate and displace coastal populations around the world.

## References

- Ballantyne, C.K., McCarroll, D., Stone, J.O., 2011. Periglacial trimlines and the extent of the Kerry-Cork Ice Cap, SW Ireland. *Quat. Sci. Rev.* 30, 3834–3845.  
<https://doi.org/10.1016/j.quascirev.2011.10.006>
- Bamber, J.L., Alley, R.B., Joughin, I., 2007. Rapid response of modern day ice sheets to external forcing. *Earth Planet. Sci. Lett.* 257, 1–13. <https://doi.org/10.1016/j.epsl.2007.03.005>
- Bamber, J.L., Riva, R.E.M., Vermeersen, B.L.A., LeBrocq, A.M., 2009. Reassessment of the potential sea-level rise from a collapse of the West Antarctic Ice Sheet. *Science* (80-. ). 324, 901–903.  
<https://doi.org/10.1126/science.1169335>
- Banerjee, I., McDonald, B.C., 1975. Nature of esker sedimentation, in: Jopling, A.V., McDonald, B.C. (Eds.), *Glacifluvial and Glaciolacustrine Sedimentation*. SPEM Special Publication 23, Tulsa, Okla, pp. 372–410.
- Bartetzko, A., Kopf, A.J., 2007. The relationship of undrained shear strength and porosity with depth in shallow (<50 m) marine sediments. *Sediment. Geol.* 196, 235–249.  
<https://doi.org/10.1016/j.sedgeo.2006.04.005>
- Belderson, R.H., Johnson, M.A., Kenyon, N.H., 1982. Bedforms, in: Stride, A. (Ed.), *Offshore Tidal Sands: Processes and Deposits*. Chapman & Hall, New York, pp. 27–55.
- Belderson, R.H., Pingree, R.D., Griffiths, D.K., 1986. Low sea-level tidal origin of Celtic Sea sand banks - evidence from numerical modelling of M2 tidal streams. *Mar. Geol.* 73, 99–108.  
[https://doi.org/10.1016/0025-3227\(86\)90113-1](https://doi.org/10.1016/0025-3227(86)90113-1)
- Bell, F.G., 2002. The geotechnical properties of some till deposits occurring along the coastal areas of eastern England. *Eng. Geol.* 63, 49–68. [https://doi.org/10.1016/S0013-7952\(01\)00068-0](https://doi.org/10.1016/S0013-7952(01)00068-0)
- Benn, D.I., Evans, D.J.A., 1996. The interpretation and classification of subglacially-deformed materials. *Quat. Sci. Rev.* 15, 23–52.
- Benn, D.I., Warren, C.R., Mottram, R.H., 2007. Calving processes and the dynamics of calving glaciers. *Earth-Science Rev.* 82, 143–179. <https://doi.org/10.1016/j.earscirev.2007.02.002>
- Berné, S., Lericolais, G., Marsset, T., Bourillet, J.F., De Batist, M., 1998. Erosional offshore sand ridges and lowstand shorefaces: examples from tide- and wave-dominated environments of France. *J. Sediment. Res.* 68, 540–555. <https://doi.org/10.2110/jsr.68.540>

- Berné, S., Trentesaux, A., Stolk, A., Missiaen, T., De Batist, M., 1994. Architecture and long term evolution of a tidal sandbank: The Middelkerke Bank (southern North Sea). *Mar. Geol.* 121, 57–72. [https://doi.org/10.1016/0025-3227\(94\)90156-2](https://doi.org/10.1016/0025-3227(94)90156-2)
- BGS, 2014. Quaternary deposits thickness (map).
- BGS, 2013. Offshore bedrock geology (1:250k scale map).
- BGS, 2011. Offshore seabed sediment types (1:250k scale map).
- BGS, 1979. Sub-Pleistocene geology of the British Isles and the adjacent continental shelf (1:2500k scale map).
- Boulton, G., Hagdorn, M., 2006. Glaciology of the British Isles Ice Sheet during the last glacial cycle: form, flow, streams and lobes. *Quat. Sci. Rev.* 25, 3359–3390. <https://doi.org/10.1016/j.quascirev.2006.10.013>
- Boulton, G.S., Dobbie, K.E., Zatsepin, S., 2001. Sediment deformation beneath glaciers and its coupling to the subglacial hydraulic system. *Quat. Int.* 86, 3–28.
- Boulton, G.S., Hindmarsh, R.C.A., 1987. Sediment deformation beneath glaciers: rheology and geological consequences. *J. Geophys. Res.* 92, 9059–9082. <https://doi.org/10.1029/JB092iB09p09059>
- Bouysse, P., Horn, R., Lapierre, F., Le Lann, F., 1976. Étude des grands bancs de sable du sud-est de la Mer Celtique. *Mar. Geol.* 20, 251–275.
- Bradley, S.L., Milne, G.A., Shennan, I., Edwards, R., 2011. An improved glacial isostatic adjustment model for the British Isles. *J. Quat. Sci.* 26, 541–552. <https://doi.org/10.1002/jqs.1481>
- Bradwell, T., Stoker, M., Krabbendam, M., 2008. Megagrooves and streamlined bedrock in NW Scotland: the role of ice streams in landscape evolution. *Geomorphology* 97, 135–156.
- Brennand, T.A., 2000. Deglacial meltwater drainage and glaciodynamics: inferences from Laurentide eskers, Canada. *Geomorphology* 32, 263–293. [https://doi.org/10.1016/S0169-555X\(99\)00100-2](https://doi.org/10.1016/S0169-555X(99)00100-2)
- Brennand, T.A., Shaw, J., 1996. The Harricana glaciofluvial complex, Abitibi region, Quebec: its genesis and implications for meltwater regime and ice-sheet dynamics. *Sediment. Geol.* 102, 221–262. [https://doi.org/10.1016/0037-0738\(95\)00069-0](https://doi.org/10.1016/0037-0738(95)00069-0)

- Brown, C.S., Newton, A.M.W., Huuse, M., Buckley, F., 2017. Iceberg scours, pits, and pockmarks in the North Falkland Basin. *Mar. Geol.* 386, 140–152.  
<https://doi.org/10.1016/j.margeo.2017.03.001>
- Caesar, L., Rahmstorf, S., Robinson, A., Feulner, G., Saba, V., 2018. Observed fingerprint of a weakening Atlantic Ocean overturning circulation. *Nature* 556, 191–196.  
<https://doi.org/10.1038/s41586-018-0006-5>
- Callard, S.L., Ó Cofaigh, C., Benetti, S., Chiverrell, R.C., Van Landeghem, K.J.J., Saher, M.H., Gales, J.A., Small, D., Clark, C.D., Livingstone, Stephen, J., Fabel, D., Moreton, S.G., 2018. Extent and retreat history of the Barra Fan Ice Stream offshore western Scotland and northern Ireland during the last glaciation. *Quat. Sci. Rev.* 201, 280–302.  
<https://doi.org/10.1016/j.quascirev.2018.10.002>
- Caston, G.F., 1981. Potential gain and loss of sand by some sand banks in the Southern Bight of the North Sea. *Mar. Geol.* 41, 239–250. [https://doi.org/10.1016/0025-3227\(81\)90083-9](https://doi.org/10.1016/0025-3227(81)90083-9)
- Caston, V.N.D., 1972. Linear sand banks in the southern North Sea. *Sedimentology* 18, 63–78.
- Chandler, B.M.P., Lovell, H., Boston, C.M., Lukas, S., Barr, I.D., Benediktsson, Í.Ö., Benn, D.I., Clark, C.D., Darvill, C.M., Evans, D.J.A., Ewertowski, M.W., Loibl, D., Margold, M., Otto, J.-C., Roberts, D.H., Stokes, C.R., Storrar, R.D., Stroeve, A.P., 2018. Glacial geomorphological mapping: a review of approaches and frameworks for best practice. *Earth-Science Rev.* 185, 806–846.  
<https://doi.org/10.1016/j.earscirev.2018.07.015>
- Chiverrell, R.C., Thrasher, I.M., Thomas, G.S.P., Lang, A., Scourse, J.D., Van Landeghem, K.J.J., Mccarroll, D., Clark, C.D., Ó Cofaigh, C., Evans, D.J.A., Ballantyne, C.K., 2013. Bayesian modelling the retreat of the Irish Sea Ice Stream. *J. Quat. Sci.* 28, 200–209.  
<https://doi.org/10.1002/jqs.2616>
- Clark, C.D., 1997. Reconstructing the evolutionary dynamics of former ice sheets using multi-temporal evidence, remote sensing and GIS. *Quat. Sci. Rev.* 16, 1067–1092.
- Clark, C.D., Ely, J.C., Greenwood, S.L., Hughes, A.L.C., Meehan, R., Barr, I.D., Bateman, M.D., Bradwell, T., Doole, J., Evans, D.J.A., Jordan, C.J., Monteys, X., Pellicer, X.M., Sheehy, M., 2018. BRITICE Glacial Map, version 2: a map and GIS database of glacial landforms of the last British-Irish Ice Sheet. *Boreas* 47, 11–27. <https://doi.org/10.1111/bor.12273>

- Clark, C.D., Hughes, A.L.C., Greenwood, S.L., Jordan, C., Sejrup, H.P., 2012. Pattern and timing of retreat of the last British-Irish Ice Sheet. *Quat. Sci. Rev.* 44, 112–146.  
<https://doi.org/10.1016/j.quascirev.2010.07.019>
- Clark, C.D., Hughes, A.L.C., Greenwood, S.L., Spagnolo, M., Ng, F.S.L., 2009. Size and shape characteristics of drumlins, derived from a large sample, and associated scaling laws. *Quat. Sci. Rev.* 28, 677–692. <https://doi.org/10.1016/j.quascirev.2008.08.035>
- Clark, C.D., Meehan, R.T., 2001. Subglacial bedform geomorphology of the Irish Ice Sheet reveals major configuration changes during growth and decay. *J. Quat. Sci.* 16, 483–496.  
<https://doi.org/10.1002/jqs.627>
- Clark, J., McCabe, A.M., Bowen, D.Q., Clark, P.U., 2012. Response of the Irish Ice Sheet to abrupt climate change during the last deglaciation. *Quat. Sci. Rev.* 35, 100–115.  
<https://doi.org/10.1016/j.quascirev.2012.01.001>
- Clark, P.U., Dyke, A.S., Shakun, J.D., Carlson, A.E., Clark, J., Wohlfarth, B., Mitrovica, J.X., Hostetler, S.W., McCabe, A.M., 2009. The Last Glacial Maximum. *Science* (80-. ). 325, 710–714.  
<https://doi.org/10.1126/science.1172873>
- Clarke, B.G., 2018. The engineering properties of glacial tills. *Geotech. Res.* 1–16.  
<https://doi.org/10.1680/jgere.18.00020>
- Clarke, B.G., Hughes, D.B., Hashemi, S., 2008. Physical characteristics of subglacial tills. *Géotechniques* 58, 67–76. <https://doi.org/10.1680/geot.2008.58.1.67>
- Davis, R.A., Balson, P.S., 1992. Stratigraphy of a North Sea tidal sand ridge. *J. Sediment. Petrol.* 62, 116–121. <https://doi.org/10.1306/D42678A2-2B26-11D7-8648000102C1865D>
- de Swart, H.E., Yuan, B., 2018. Dynamics of offshore tidal sand ridges, a review. *Environ. Fluid Mech.* 1–25. <https://doi.org/10.1007/s10652-018-9630-8>
- Dove, D., Arosio, R., Finlayson, A., Bradwell, T., Howe, J. a., 2015. Submarine glacial landforms record Late Pleistocene ice-sheet dynamics, Inner Hebrides, Scotland. *Quat. Sci. Rev.* 123, 76–90. <https://doi.org/10.1016/j.quascirev.2015.06.012>



- Dove, D., Bradwell, T., Carter, G., Cotterill, C., Gaferia, J., Green, S., Krabbendam, M., Mellet, C., Stevenson, A., Stewart, H., Westhead, K., Scott, G., Guinan, J., Judge, M., Monteys, X., Elvenes, S., Baeten, N., Dolan, M., Thorsnes, T., Bjarnadóttir, L., Ottesen, D., 2016. Seabed Geomorphology: a two-part classification system. <https://doi.org/10.1111/j.1365-2656.2009.01617.x>
- Dowdeswell, J.A., Canals, M., Jakobsson, M., Todd, B.J., Dowdeswell, E.K., Hogan, K.A., 2016. Atlas of submarine glacial landforms: modern, Quaternary and ancient, Geological Society, London, Memoirs. Geological Society, London. <https://doi.org/10.1674/0003-0031-162.1.43>
- Dowdeswell, J.A., Ottesen, D., Evans, J., Ó Cofaigh, C., Anderson, J.B., 2008. Submarine glacial landforms and rates of ice-stream collapse. *Geology* 36, 819–822. <https://doi.org/10.1130/G24808A.1>
- Dowdeswell, J.A., Whittington, R.J., Marienfeld, P., 1994. The origin of massive diamicton facies by iceberg rafting and scouring, Scoresby Sund, East Greenland. *Sedimentology* 41, 21–35. <https://doi.org/10.1111/j.1365-3091.1994.tb01390.x>
- Dunlop, P., Clark, C.D., 2006. The morphological characteristics of ribbed moraine. *Quat. Sci. Rev.* 25, 1668–1691. <https://doi.org/10.1016/j.quascirev.2006.01.002>
- Dunlop, P., Shannon, R., McCabe, M., Quinn, R., Doyle, E., 2010. Marine geophysical evidence for ice sheet extension and recession on the Malin Shelf: new evidence for the western limits of the British Irish Ice Sheet. *Mar. Geol.* 276, 86–99. <https://doi.org/10.1016/j.margeo.2010.07.010>
- Ely, J.C., Clark, C.D., Spagnolo, M., Stokes, C.R., Greenwood, S.L., Hughes, A.L.C., Dunlop, P., Hess, D., 2016. Do subglacial bedforms comprise a size and shape continuum? *Geomorphology* 257, 108–119. <https://doi.org/10.1016/j.geomorph.2016.01.001>
- EMODnet, n.d. EMODnet-bathymetry portal [WWW Document]. URL <http://www.emodnet-bathymetry.eu/>
- Evans, C.D.R., 1990. United Kingdom offshore regional report: the geology of the western English Channel and its western approaches. British Geological Survey.
- Evans, C.D.R., Hughes, M.J., 1984. The Neogene succession of the south western approaches, Great Britain. *J. Geol. Soc. London.* 141, 315–326.

- Evans, D.J.A., Phillips, E.R., Hiemstra, J.F., Auton, C.A., 2006. Subglacial till: formation, sedimentary characteristics and classification. *Earth-Science Rev.* 78, 115–176.  
<https://doi.org/10.1016/j.earscirev.2006.04.001>
- Eyles, N., McCabe, A.M., 1989. The Late Devensian (<22,000 BP) Irish Sea Basin: the sedimentary record of a collapsed ice sheet margin. *Quat. Sci. Rev.* 8, 307–351.  
[https://doi.org/10.1016/0277-3791\(89\)90034-6](https://doi.org/10.1016/0277-3791(89)90034-6)
- Fannin, N., 1989. Offshore investigations 1966-87. British Geological Survey.
- Feldmann, J., Levermann, A., 2015. Collapse of the West Antarctic Ice Sheet after local destabilization of the Amundsen Basin. *Proc. Natl. Acad. Sci.* 112, 14191–14196.  
<https://doi.org/10.1073/pnas.1512482112>
- Field, K., Beale, L., 2016. Terrain tools [WWW Document]. URL  
<http://www.arcgis.com/home/item.html?id=4b2ea7c5f87d476a8849c804b81667aa>
- Fretwell, P., Pritchard, H.D., Vaughan, D.G., Bamber, J.L., Barrand, N.E., Bell, R., Bianchi, C., Bingham, R.G., Blankenship, D.D., Casassa, G., Catania, G., Callens, D., Conway, H., Cook, A.J., Corr, H.F.J., Damaske, D., Damm, V., Ferraccioli, F., Forsberg, R., Fujita, S., Gim, Y., Gogineni, P., Griggs, J.A., Hindmarsh, R.C.A., Holmlund, P., Holt, J.W., Jacobel, R.W., Jenkins, A., Jokat, W., Jordan, T., King, E.C., Kohler, J., Krabill, W., Riger-Kusk, M., Langley, K.A., Leitchenkov, G., Leuschen, C., Luyendyk, B.P., Matsuoka, K., Mouginot, J., Nitsche, F.O., Nogi, Y., Nost, O.A., Popov, S. V., Rignot, E., Rippin, D.M., Rivera, A., Roberts, J., Ross, N., Siegert, M.J., Smith, A.M., Steinhage, D., Studinger, M., Sun, B., Tinto, B.K., Welch, B.C., Wilson, D., Young, D.A., Xiangbin, C., Zirizzotti, A., 2013. Bedmap2: improved ice bed, surface and thickness datasets for Antarctica. *Cryosph.* 7, 375–393. <https://doi.org/10.5194/tc-7-375-2013>
- Furze, M.F.A., Scourse, J.D., Pieńkowski, A.J., Marret, F., Hobbs, W.O., Carter, R.A., Long, B.T., 2014. Deglacial to postglacial palaeoenvironments of the Celtic Sea: lacustrine conditions versus a continuous marine sequence. *Boreas* 43, 149–174. <https://doi.org/10.1111/bor.12028>
- Gallagher, C., 2002. The morphology and palaeohydrology of a submerged glaciofluvial channel emerging from Waterford Harbour onto the nearshore continental shelf of the Celtic Sea. *Irish Geogr.* 35, 111–132.
- Gibbard, P.L., Hughes, P.D., Rolfe, C.J., 2017. New insights into the Quaternary evolution of the Bristol Channel, UK. *J. Quat. Sci.* 32, 564–578. <https://doi.org/10.1002/jqs.2951>

- Glasser, N.F., Bennett, M.R., 2004. Glacial erosional landforms: origins and significance for palaeoglaciology. *Prog. Phys. Geogr.* 28, 43–75. <https://doi.org/10.1191/0309133304pp401ra>
- Gorrell, G., Shaw, J., 1991. Deposition in an esker, bead and fan complex, Lanark, Ontario, Canada. *Sediment. Geol.* 72, 285–314. [https://doi.org/10.1016/0037-0738\(91\)90016-7](https://doi.org/10.1016/0037-0738(91)90016-7)
- Grau, A.G., Jellinek, A.M., Osinski, G.R., Zanetti, M., Kukko, A., 2018. Subglacial drainage patterns of Devon Island, Canada: detailed comparison of river and tunnel valleys. *Cryosph.* 12, 1461–1478. <https://doi.org/10.5194/tc-12-1461-2018>
- Greenwood, S.L., Clark, C.D., 2009. Reconstructing the last Irish Ice Sheet 2: a geomorphologically-driven model of ice sheet growth, retreat and dynamics. *Quat. Sci. Rev.* 28, 3101–3123. <https://doi.org/10.1016/j.quascirev.2009.09.014>
- Greenwood, S.L., Clark, C.D., Hughes, A.L.C., 2007. Formalising an inversion methodology for reconstructing ice-sheet retreat patterns from meltwater channels: application to the British Ice Sheet. *J. Quat. Sci.* 22, 637–645. <https://doi.org/10.1002/jqs.1083>
- GSI, n.d. Geological Survey Ireland interactive web data delivery system [WWW Document]. URL <https://jetstream.gsi.ie/iwdds/map.jsp>
- Haapaniemi, A.I., Scourse, J.D., Peck, V.L., Kennedy, H., Kennedy, P., Hemming, S.R., Furze, M.F.A., Pieńkowski, A.J., Austin, W.E.N., Walden, J., Wadsworth, E., Hall, I.R., 2010. Source, timing, frequency and flux of ice-rafted detritus to the Northeast Atlantic margin, 30–12 ka: testing the Heinrich precursor hypothesis. *Boreas* 39, 576–591. <https://doi.org/10.1111/j.1502-3885.2010.00141.x>
- Hallet, B., 1996. Glacial quarrying: a simple theoretical model. *Ann. Glaciol.* 22, 1–8.
- Hallet, B., 1981. Glacial abrasion and sliding: their dependence on the debris concentration in basal ice. *Ann. Glaciol.* 2, 23–28.
- Harig, C., Simons, F.J., 2015. Accelerated West Antarctic ice mass loss continues to outpace East Antarctic gains. *Earth Planet. Sci. Lett.* 415, 134–141. <https://doi.org/10.1016/j.epsl.2015.01.029>
- Hart, J.K., Boulton, G.S., 1991. The interrelation of glaciotectonic and glaciodepositional processes within the glacial environment. *Quat. Res.* 10, 335–350.
- Hättestrand, C., 1997. Ribbed moraines in Sweden - distribution pattern and palaeoglaciological implications. *Sediment. Geol.* 111, 41–56.

- Hättestrand, C., Kleman, J., 1999. Ribbed moraine formation. *Quat. Sci. Rev.* 18, 43–61.  
[https://doi.org/10.1016/S0277-3791\(97\)00094-2](https://doi.org/10.1016/S0277-3791(97)00094-2)
- Hebrand, M., Åmark, M., 1989. Esker formation and glacier dynamics in eastern Skåne and adjacent areas, southern Sweden. *Boreas* 18, 67–81. <https://doi.org/10.1111/j.1502-3885.1989.tb00372.x>
- Hemming, S.R., 2004. Heinrich events: massive Late Pleistocene detritus layers of the North Atlantic and their global climate imprint. *Rev. Geophys.* 42, 1–43.
- Hiemstra, J.F., Evans, D.J.A., Ó Cofaigh, C., 2007. The role of glaciectonic rafting and comminution in the production of subglacial tills: examples from southwest Ireland and Antarctica. *Boreas* 36, 386–399. <https://doi.org/10.1080/03009480701213521>
- Hoek, E., 2001. Rock mass properties for underground mines, in: Hustrulid, W.A., Bullock, R. (Eds.), *Underground Mining Methods: Engineering Fundamentals and International Case Studies*. Society for Mining, Metallurgy and Exploration, Littleton, Colorado, pp. 1–20.
- Houbolt, J.J.H.C., 1968. Recent sediments in the southern bight of the North Sea. *Geol. en Mijnb.* 47, 245–273.
- Howe, J.A., Dove, D., Bradwell, T., Gafeira, J., 2012. Submarine geomorphology and glacial history of the Sea of the Hebrides, UK. *Mar. Geol.* 315–318, 64–76.  
<https://doi.org/10.1016/j.margeo.2012.06.005>
- Hubbard, A., Bradwell, T., Golledge, N., Hall, A., Patton, H., Sugden, D., Cooper, R., Stoker, M., 2009. Dynamic cycles, ice streams and their impact on the extent, chronology and deglaciation of the British–Irish ice sheet. *Quat. Sci. Rev.* 28, 758–776.  
<https://doi.org/10.1016/j.quascirev.2008.12.026>
- Huthnance, J.M., 1982a. On the formation of sand banks of finite extent. *Estuar. Coast. Shelf Sci.* 15, 277–299. <https://doi.org/10.1017/S0022112006009256>
- Huthnance, J.M., 1982b. On one mechanism forming linear sand banks. *Estuar. Coast. Shelf Sci.* 14, 79–99.
- Huuse, M., Lykke-Andersen, H., 2000. Overdeepened Quaternary valleys in the eastern Danish North Sea: morphology and origin. *Quat. Sci. Rev.* 19, 1233–1253. [https://doi.org/10.1016/S0277-3791\(99\)00103-1](https://doi.org/10.1016/S0277-3791(99)00103-1)

- IMBIE, 2018. Mass balance of the Antarctic Ice Sheet from 1992 to 2017. *Nature* 558, 219–222.  
<https://doi.org/10.1098/rsta.2006.1792>
- IPCC, 2018. Impacts of 1.5°C of global warming on natural and human systems, in: *Global Warming of 1.5 °C*.
- IPCC, 2014. *Climate change 2014: synthesis report*.
- ISO, 2018. ISO 17892-12: determination of liquid and plastic limits, in: *Laboratory Testing of Soil*.
- John, B., 2018. Evidence for extensive ice cover on the Isles of Scilly. *Quat. Newsl.* 146, 3–27.  
<https://doi.org/10.1144/SP433.CITATIONS>
- Keary, P., Brooks, M., Hill, I., 2002. Seismic reflection surveying, in: *An Introduction to Geophysical Exploration*. Blackwell Science Ltd, pp. 43–98.
- Kelley, J.T., Cooper, J.A.G., Jackson, D.W.T., Belknap, D.F., Quinn, R.J., 2006. Sea-level change and inner shelf stratigraphy off Northern Ireland. *Mar. Geol.* 232, 1–15.  
<https://doi.org/10.1016/j.margeo.2006.04.002>
- Kleman, J., Borgström, I., 1996. Reconstruction of palaeo-ice sheets: the use of geomorphological data. *Earth Surf. Process. Landforms* 21, 893–909.
- Kleman, J., Hättestrand, C., 1999. Frozen-bed Fennoscandian and Laurentide ice sheets during the Last Glacial Maximum. *Nature* 402, 63–66. <https://doi.org/10.1038/47005>
- Knaapen, M.A.F., 2005. Sandwave migration predictor based on shape information. *J. Geophys. Res.* 110, 1–9. <https://doi.org/10.1029/2004JF000195>
- Knight, J., 2015. Ductile and brittle styles of subglacial sediment deformation: an example from western Ireland. *Sediment. Geol.* 318, 85–96. <https://doi.org/10.1016/j.sedgeo.2015.01.002>
- Krabbendam, M., Eyles, N., Putkinen, N., Bradwell, T., Arbelaez-Moreno, L., 2016. Streamlined hard beds formed by palaeo-ice streams: a review. *Sediment. Geol.* 338, 24–50.  
<https://doi.org/10.1016/j.sedgeo.2015.12.007>
- Lambeck, K., Yokoyama, Y., Purcell, T., 2002. Into and out of the Last Glacial Maximum: sea-level change during Oxygen Isotope Stages 3 and 2. *Quat. Sci. Rev.* 21, 343–360.  
[https://doi.org/10.1016/S0277-3791\(01\)00071-3](https://doi.org/10.1016/S0277-3791(01)00071-3)

- Liu, Z., Berné, S., Saito, Y., Yu, H., Trentesaux, A., Uehara, K., Yin, P., Liu, J.P., Li, C., Hu, G., Wang, X., 2007. Internal architecture and mobility of tidal sand ridges in the East China Sea. *Cont. Shelf Res.* 27, 1820–1834. <https://doi.org/10.1016/j.csr.2007.03.002>
- Livingstone, S., Storrar, R., Hillier, J.K., Stokes, C., Clark, C., Tarasov, L., 2015. An ice-sheet scale comparison of diagnosed subglacial drainage routes with esker networks. *Geomorphology* 246, 104–112. <https://doi.org/10.1016/j.geomorph.2015.06.016>
- Lloyd, C.T., 2015. Controls upon the location and size of glacial overdeepenings. Unpublished PhD Thesis. University of Sheffield.
- Lockhart, E.A., Scourse, J.D., Praeg, D., Van Landeghem, K.J.J., Mellett, C., Saher, M., Callard, L., Chiverrell, R.C., Benetti, S., Ó Cofaigh, C., 2018. A stratigraphic investigation of the Celtic Sea megaridges based on seismic and core data from the Irish-UK sectors. *Quat. Sci. Rev.* 198, 156–170. <https://doi.org/10.1016/j.quascirev.2018.08.029>
- Loneragan, L., Maidment, S.C.R., Collier, J.S., 2006. Pleistocene subglacial tunnel valleys in the central North Sea basin: 3-D morphology and evolution. *J. Quat. Sci.* 21, 891–903. <https://doi.org/10.1002/jqs.1015>
- Lønne, I., Syvitski, J.P., 1997. Effects of the readvance of an ice margin on the seismic character of the underlying sediment. *Mar. Geol.* 143, 81–102. [https://doi.org/10.1016/S0025-3227\(97\)00091-1](https://doi.org/10.1016/S0025-3227(97)00091-1)
- Ma, Y., Tripathy, C.S., Bassis, J.N., 2017. Bounds on the calving cliff height of marine terminating glaciers. *Geophys. Res. Lett.* 44, 1369–1375. <https://doi.org/10.1002/2016GL071560>
- Mäkinen, J., 2003. Time-transgressive deposits of repeated depositional sequences within interlobate glaciofluvial (esker) sediments in Köyliö, SW Finland. *Sedimentology* 50, 327–360. <https://doi.org/10.1046/j.1365-3091.2003.00557.x>
- Margold, M., Stokes, C.R., Clark, C.D., 2015. Ice streams in the Laurentide Ice Sheet: identification, characteristics and comparison to modern ice sheets. *Earth-Science Rev.* 143, 117–146. <https://doi.org/10.1016/j.earscirev.2015.01.011>
- Marsset, T., Tessier, B., Reynaud, J.-Y., De Batist, M., Plagnol, C., 1999. The Celtic Sea banks: an example of sand body analysis from very high-resolution seismic data. *Mar. Geol.* 158, 89–109. [https://doi.org/10.1016/S0025-3227\(98\)00188-1](https://doi.org/10.1016/S0025-3227(98)00188-1)

- Mayne, P.W., Mitchell, J.K., 1988. Profiling of overconsolidation ratio in clays by field vane. *Can. Geotech. J.* 25, 150–157. <https://doi.org/10.1139/t88-015>
- McCabe, A.M., Clark, P.U., Clark, J., 2005. AMS 14C dating of deglacial events in the Irish Sea Basin and other sectors of the British–Irish ice sheet. *Quat. Sci. Rev.* 24, 1673–1690. <https://doi.org/10.1016/j.quascirev.2004.06.019>
- McCarroll, D., Rijdsdijk, K.F., 2003. Deformation styles as a key for interpreting glacial depositional environments. *J. Quat. Sci.* 18, 473–489. <https://doi.org/10.1002/jqs.780>
- Milillo, P., Rignot, E., Rizzoli, P., Scheuchl, B., Mougnot, J., Bueso-Bello, J., Prats-Iraola, P., 2019. Heterogeneous retreat and ice melt of Thwaites Glacier, West Antarctica. *Sci. Adv.* 5, 1–8. <https://doi.org/10.1126/sciadv.aau3433>
- Mitchum, R.M., Vail, P.R., Sangree, J.B., 1977. Seismic stratigraphy and global changes of sea level, Part 6: stratigraphic interpretation of seismic reflection patterns on depositional sequences, in: Payton, C.E. (Ed.), *Seismic Stratigraphy - Applications to Hydrocarbon Exploration*. American Association of Petroleum Geologists.
- Mohajerani, Y., Velicogna, I., Rignot, E., 2018. Mass loss of Totten and Moscow University Glaciers, East Antarctica, using regionally optimized GRACE mascons. *Geophys. Res. Lett.* 45, 7010–7018. <https://doi.org/10.1029/2018GL078173>
- Noormets, R., Flodén, T., 2002. Glacial deposits and ice-sheet dynamic in the north-central Baltic Sea during the last deglaciation. *Boreas* 31, 362–377. <https://doi.org/10.1111/j.1502-3885.2002.tb01080.x>
- O'Regan, M., Jakobsson, M., Kirchner, N., 2010. Glacial geological implications of overconsolidated sediments on the Lomonosov Ridge and Yermak Plateau. *Quat. Sci. Rev.* 29, 3532–3544. <https://doi.org/10.1016/j.quascirev.2010.09.009>
- Ó Cofaigh, C., 2014. Cruise JC-106 - RRS James Cook.
- Ó Cofaigh, C., Dowdeswell, J.A., 2001. Laminated sediments in glacialmarine environments: diagnostic criteria for their interpretation. *Quat. Sci. Rev.* 20, 1411–1436. [https://doi.org/10.1016/S0277-3791\(00\)00177-3](https://doi.org/10.1016/S0277-3791(00)00177-3)
- Ó Cofaigh, C., Evans, D.J.A., 2007. Radiocarbon constraints on the age of the maximum advance of the British-Irish Ice Sheet in the Celtic Sea. *Quat. Sci. Rev.* 26, 1197–1203. <https://doi.org/10.1016/j.quascirev.2007.03.008>



- Ó Cofaigh, C., Evans, D.J.A., 2001. Sedimentary evidence for deforming bed conditions associated with a grounded Irish Sea glacier, southern Ireland. *J. Quat. Sci.* 16, 435–454.  
<https://doi.org/10.1002/jqs.631>
- Ó Cofaigh, C., Telfer, M.W., Bailey, R.M., Evans, D.J.A., 2012. Late Pleistocene chronostratigraphy and ice sheet limits, southern Ireland. *Quat. Sci. Rev.* 44, 160–179.  
<https://doi.org/10.1016/j.quascirev.2010.01.011>
- Ottesen, D., Dowdeswell, J.A., Bellec, V.K., Bjarnadóttir, L.R., 2017. The geomorphic imprint of glacier surges into open-marine waters: examples from eastern Svalbard. *Mar. Geol.* 392, 1–29.  
<https://doi.org/10.1016/j.margeo.2017.08.007>
- Ottesen, D., Dowdeswell, J.A., Benn, D.I., Kristensen, L., Christiansen, H.H., Christensen, O., Hansen, L., Lebesbye, E., Forwick, M., Vorren, T.O., 2008. Submarine landforms characteristic of glacier surges in two Spitsbergen fjords. *Quat. Sci. Rev.* 27, 1583–1599.  
<https://doi.org/10.1016/j.quascirev.2008.05.007>
- Owen, G., 1997. Origin of an esker-like ridge - erosion or channel-fill? Sedimentology of the Monington “esker” in southwest Wales. *Quat. Sci. Rev.* 16, 675–684.  
[https://doi.org/10.1016/S0277-3791\(97\)00015-2](https://doi.org/10.1016/S0277-3791(97)00015-2)
- Pantin, H.M., Evans, C.D.R., 1984. The Quaternary history of the central and southwestern Celtic Sea. *Mar. Geol.* 57, 259–293.
- Patterson, D., 2015. Bounding containers [WWW Document]. URL  
<https://www.arcgis.com/home/item.html?id=564e2949763943e3b9fb4240bab0ca2f>
- Patton, H., Hubbard, A., Andreassen, K., Auriac, A., Whitehouse, P.L., Stroeve, A.P., Shackleton, C., Winsborrow, M., Heyman, J., Hall, A.M., 2017. Deglaciation of the Eurasian ice sheet complex. *Quat. Sci. Rev.* 169, 148–172. <https://doi.org/10.1016/j.quascirev.2017.05.019>
- Peck, V.L., Hall, I.R., Zahn, R., Grousset, F., Hemming, S.R., Scourse, J.D., 2007. The relationship of Heinrich events and their European precursors over the past 60 ka BP: a multi-proxy ice-rafted debris provenance study in the North East Atlantic. *Quat. Sci. Rev.* 26, 862–875.  
<https://doi.org/10.1016/j.quascirev.2006.12.002>
- Peltier, W.R., Fairbanks, R.G., 2006. Global glacial ice volume and Last Glacial Maximum duration from an extended Barbados sea level record. *Quat. Sci. Rev.* 25, 3322–3337.  
<https://doi.org/10.1016/j.quascirev.2006.04.010>

- Peters, J.L., Benetti, S., Dunlop, P., Ó Cofaigh, C., 2015. Maximum extent and dynamic behaviour of the last British-Irish Ice Sheet west of Ireland. *Quat. Sci. Rev.* 128, 48–68. <https://doi.org/10.1016/j.quascirev.2015.09.015>
- Phillips, E., Everest, J., Diaz-Doce, D., 2010. Bedrock controls on subglacial landform distribution and geomorphological processes: evidence from the Late Devensian Irish Sea Ice Stream. *Sediment. Geol.* 232, 98–118. <https://doi.org/10.1016/j.sedgeo.2009.11.004>
- Plets, R.M.K., Callard, S.L., Cooper, J.A.G., Long, A.J., Quinn, R.J., Belknap, D.F., Edwards, R.J., Jackson, D.W.T., Kelley, J.T., Long, D., Milne, G.A., Monteys, X., 2015. Late Quaternary evolution and sea-level history of a glaciated marine embayment, Bantry Bay, SW Ireland. *Mar. Geol.* 369, 251–272. <https://doi.org/10.1016/j.margeo.2015.08.021>
- Praeg, D., McCarron, S., Dove, D., Ó Cofaigh, C., Monteys, X., Coxon, P., Accettella, D., Cova, A., Facchin, L., Romeo, R., Scott, G., 2015a. Submarine geomorphology of the Celtic Sea - new observations and hypotheses for the glaciation of a mid-latitude continental shelf. *Eur. Geosci. Union Conf. Poster*.
- Praeg, D., McCarron, S., Dove, D., Ó Cofaigh, C., Scott, G., Monteys, X., Facchin, L., Romeo, R., Coxon, P., 2015b. Ice sheet extension to the Celtic Sea shelf edge at the Last Glacial Maximum. *Quat. Sci. Rev.* 111, 107–112. <https://doi.org/10.1016/j.quascirev.2014.12.010>
- Preusser, F., Reitner, J.M., Schlüchter, C., 2010. Distribution, geometry, age and origin of overdeepened valleys and basins in the Alps and their foreland. *Swiss J. Geosci.* 103, 407–426. <https://doi.org/10.1007/s00015-010-0044-y>
- Rahmstorf, S., Box, J.E., Feulner, G., Mann, M.E., Robinson, A., Rutherford, S., Schaffernicht, E.J., 2015. Exceptional twentieth-century slowdown in Atlantic Ocean overturning circulation. *Nat. Clim. Chang.* 5, 475–480. <https://doi.org/10.1038/nclimate2554>
- Rasmussen, S.O., Bigler, M., Blockley, S.P., Blunier, T., Buchardt, S.L., Clausen, H.B., Cvijanovic, I., Dahl-Jensen, D., Johnsen, S.J., Fischer, H., Gkinis, V., Guillevic, M., Hoek, W.Z., Lowe, J.J., Pedro, J.B., Popp, T., Seierstad, I.K., Steffensen, J.P., Svensson, A.M., Vallelonga, P., Vinther, B.M., Walker, M.J.C., Wheatley, J.J., Winstrup, M., 2014. A stratigraphic framework for abrupt climatic changes during the Last Glacial period based on three synchronized Greenland ice-core records: refining and extending the INTIMATE event stratigraphy. *Quat. Sci. Rev.* 106, 14–28. <https://doi.org/10.1016/j.quascirev.2014.09.007>

- Reynaud, J.-Y., Tessier, B., Berné, S., Chamley, H., De Batist, M., 1999a. Tide and wave dynamics on a sand bank from the deep shelf of the Western Channel approaches. *Mar. Geol.* 161, 339–359. [https://doi.org/10.1016/S0025-3227\(99\)00033-X](https://doi.org/10.1016/S0025-3227(99)00033-X)
- Reynaud, J.-Y., Tessier, B., Proust, J.-N., Dalrymple, R., Marsset, T., De Batist, M., Bourillet, J.-F., Lericolais, G., 1999b. Eustatic and hydrodynamic controls on the architecture of a deep shelf sand bank (Celtic Sea). *Sedimentology* 46, 703–721. <https://doi.org/10.1046/j.1365-3091.1999.00244.x>
- Ritz, C., Edwards, T.L., Durand, G., Payne, A.J., Peyaud, V., Hindmarsh, R.C.A., 2015. Potential sea-level rise from Antarctic ice-sheet instability constrained by observations. *Nature* 528, 115–118. <https://doi.org/10.1038/nature16147>
- Roberts, D.H., Dackombe, R. V, Thomas, G.S.P., 2007. Palaeo-ice streaming in the central sector of the British-Irish Ice Sheet during the Last Glacial Maximum: evidence from the northern Irish Sea Basin. *Boreas* 36, 115–129. <https://doi.org/10.1080/03009480600991219>
- Roberts, D.H., Evans, D.J.A., Callard, S.L., Clark, C.D., Bateman, M.D., Medialdea, A., Dove, D., Cotterill, C.J., Saher, M., Cofaigh, C., Chiverrell, R.C., Moreton, S.G., Fabel, D., Bradwell, T., 2018. Ice marginal dynamics of the last British-Irish Ice Sheet in the southern North Sea: ice limits, timing and the influence of the Dogger Bank. *Quat. Sci. Rev.* 198, 181–207. <https://doi.org/10.1016/j.quascirev.2018.08.010>
- Rust, B.R., Romanelli, R., 1975. Late Quaternary subaqueous outwash deposits near Ottawa, Canada, in: Jopling, A.V., McDonald, B.C. (Eds.), *Glaciofluvial and Glaciolacustrine Sedimentation*. SPEM Special Publication 23, pp. 177–192.
- Rydningen, T.A., Vorren, T.O., Laberg, J.S., Kolstad, V., 2013. The marine-based NW Fennoscandian ice sheet: glacial and deglacial dynamics as reconstructed from submarine landforms. *Quat. Sci. Rev.* 68, 126–141. <https://doi.org/10.1016/j.quascirev.2013.02.013>
- Schoof, C., 2010. Ice-sheet acceleration driven by melt supply variability. *Nature* 468, 803–806. <https://doi.org/10.1038/nature09618>
- Schoof, C., 2007. Ice sheet grounding line dynamics: steady states, stability, and hysteresis. *J. Geophys. Res. Earth Surf.* 112, 1–19. <https://doi.org/10.1029/2006JF000664>

- Scourse, J., Haapaniemi, A.I., Colmenero-Hidalgo, E., Peck, V.L., Hall, I.R., Austin, W.E.N., Knutz, P.C., Zahn, R., 2009a. Growth, dynamics and deglaciation of the last British-Irish ice sheet: the deep-sea ice-rafted detritus record. *Quat. Sci. Rev.* 28, 3066–3084.  
<https://doi.org/10.1016/j.quascirev.2009.08.009>
- Scourse, J., Uehara, K., Wainwright, A., 2009b. Celtic Sea linear tidal sand ridges, the Irish Sea Ice Stream and the Fleuve Manche: palaeotidal modelling of a transitional passive margin depositional system. *Mar. Geol.* 259, 102–111. <https://doi.org/10.1016/j.margeo.2008.12.010>
- Scourse, J.D., 1991. Late Pleistocene stratigraphy and palaeobotany of the Isles of Scilly. *Philos. Trans. R. Soc.* 334, 405–448.
- Scourse, J.D., Austin, W.E.N., Bateman, R.M., Catt, J.A., Evans, C.D.R., Robinson, J.E., Young, J.R., 1990. Sedimentology and micropalaeontology of glaciomarine sediments from the Central and Southwestern Celtic Sea. *Geol. Soc. London, Spec. Publ.* 53, 329–347.  
<https://doi.org/10.1144/GSL.SP.1990.053.01.19>
- Scourse, J.D., Austin, W.E.N., Long, B.T., Assinder, D.J., Huws, D., 2002. Holocene evolution of seasonal stratification in the Celtic Sea: refined age model, mixing depths and foraminiferal stratigraphy. *Mar. Geol.* 191, 119–145. [https://doi.org/10.1016/S0025-3227\(02\)00528-5](https://doi.org/10.1016/S0025-3227(02)00528-5)
- Scourse, J.D., Furze, M.F.A., 2001. A critical review of the glaciomarine model for Irish sea deglaciation: evidence from southern Britain, the Celtic shelf and adjacent continental slope. *J. Quat. Sci.* 16, 419–434. <https://doi.org/10.1002/jqs.629>
- Scourse, J.D., Saher, M., Van Landeghem, K.J.J., Lockhart, E.A., Purcell, C., Callard, L., Roseby, Z., Allinson, B., Pieńkowski, A.J., Ó Cofaigh, C., Praeg, D., Ward, S., Chiverrell, R.C., Moreton, S., Fabel, D., Clark, C.D., 2019. Advance and retreat of the marine-terminating Irish Sea Ice Stream into the Celtic Sea during the Last Glacial: timing and maximum extent. *Mar. Geol.* 412, 53–68.
- Scourse, J.D., Ward, S.L., Wainwright, A., Bradley, S.L., Uehara, K., 2018. The role of megatides and relative sea level in controlling the deglaciation of the British-Irish and Fennoscandian ice sheets. *J. Quat. Sci.* 1–11. <https://doi.org/10.1002/jqs.3011>
- Sejrup, H.P., Hjelstuen, B.O., Dahlgren, K.I.T., Hafliðason, H., Kuijpers, A., Nygård, A., Praeg, D., Stoker, M.S., Vorren, T.O., 2005. Pleistocene glacial history of the NW European continental margin. *Mar. Pet. Geol.* 22, 1111–1129. <https://doi.org/10.1016/j.marpetgeo.2004.09.007>

- Seo, K.-W., Waliser, D.E., Lee, C.-K., Tian, B., Scambos, T., Kim, B.-M., van Angelen, J.H., van den Broeke, M.R., 2015. Accelerated mass loss from Greenland ice sheet: links to atmospheric circulation in the North Atlantic. *Glob. Planet. Change* 128, 61–71.  
<https://doi.org/10.1016/j.gloplacha.2015.02.006>
- Shaw, J., 2003. Submarine moraines in Newfoundland coastal waters: implications for the deglaciation of Newfoundland and adjacent areas. *Quat. Int.* 99–100, 115–134.  
[https://doi.org/10.1016/S1040-6182\(02\)00125-8](https://doi.org/10.1016/S1040-6182(02)00125-8)
- Shumskiy, P.A., 1960. Density of glacier ice. *J. Glaciol.* 3, 568–573.
- Small, D., Smedley, R.K., Chiverrell, R.C., Scourse, J.D., Ó Cofaigh, C., Duller, G.A.T., McCarron, S., Burke, M.J., Evans, D.J.A., Fabel, D., Gheorghiu, D.M., Thomas, G.S.P., Xu, S., Clark, C.D., 2018. Trough geometry was a greater influence than climate-ocean forcing in regulating retreat of the marine-based Irish-Sea Ice Stream. *Geol. Soc. Am. Bull.* 130, 1981–1999.  
<https://doi.org/10.1130/B31852.1>
- Smedley, R.K., Scourse, J.D., Small, D., Hiemstra, J.F., Duller, G.A.T., Bateman, M.D., Burke, M.J., Chiverrell, R.C., Clark, C.D., Davies, S.M., Fabel, D., Gheorghiu, D.M., McCarroll, D., Medialdea, A., Xu, S., 2017. New age constraints for the limit of the British-Irish Ice Sheet on the Isles of Scilly. *J. Quat. Sci.* 32, 48–62. <https://doi.org/10.1002/jqs.2922>
- Smith, M.J., Clark, C.D., 2005. Methods for the visualization of digital elevation models for landform mapping. *Earth Surf. Process. Landforms* 30, 885–900. <https://doi.org/10.1002/esp.1210>
- Stokes, C.R., Clark, C.D., 1999. Geomorphological criteria for identifying Pleistocene ice streams. *Ann. Glaciol.* 28, 67–74. <https://doi.org/10.3189/172756499781821625>
- Stokes, C.R., Clark, C.D., Lian, O.B., Tulaczyk, S., 2007. Ice stream sticky spots: a review of their identification and influence beneath contemporary and palaeo-ice streams. *Earth-Science Rev.* 81, 217–249. <https://doi.org/10.1016/j.earscirev.2007.01.002>
- Stokes, C.R., Tarasov, L., Blomdin, R., Cronin, T.M., Fisher, T.G., Gyllencreutz, R., Hättestrand, C., Heyman, J., Hindmarsh, R.C.A., Hughes, A.L.C., Jakobsson, M., Kirchner, N., Livingstone, S.J., Margold, M., Murton, J.B., Noormets, R., Peltier, W.R., Peteet, D.M., Piper, D.J.W., Preusser, F., Renssen, H., Roberts, D.H., Roche, D.M., Saint-Ange, F., Stroeve, A.P., Teller, J.T., 2015. On the reconstruction of palaeo-ice sheets: recent advances and future challenges. *Quat. Sci. Rev.* 125, 15–49. <https://doi.org/10.1016/j.quascirev.2015.07.016>

- Storrar, R.D., Evans, D.J.A., Stokes, C.R., Ewertowski, M., 2015. Controls on the location, morphology and evolution of complex esker systems at decadal timescales, Breidamerkurjökull, southeast Iceland. *Earth Surf. Process. Landforms* 40, 1421–1438.  
<https://doi.org/10.1002/esp.3725>
- Storrar, R.D., Stokes, C.R., Evans, D.J.A., 2014. Morphometry and pattern of a large sample (>20,000) of Canadian eskers and implications for subglacial drainage beneath ice sheets. *Quat. Sci. Rev.* 105, 1–25. <https://doi.org/10.1016/j.quascirev.2014.09.013>
- Stride, A.H., 1963. North-east trending ridges of the Celtic Sea. *Proc. Ussher Soc.* 1, 62–63.
- Stride, A.H., Belderson, R.H., Kenyon, N.H., Johnson, M.A., 1982. Offshore tidal deposits: sand sheet and sand bank facies, in: Stride, A.H. (Ed.), *Offshore Tidal Sands: Processes and Deposits*. Chapman & Hall, New York, pp. 95–125.
- Syvitski, J.P.M., 1991. Towards an understanding of sediment deposition on glaciated continental shelves. *Cont. Shelf Res.* 11, 897–937.
- Syvitski, J.P.M., Praeg, D.B., 1989. Quaternary sedimentation in the St. Lawrence estuary and adjoining areas, Eastern Canada: an overview based on high-resolution seismo-stratigraphy. *Géographie Phys. Quat.* 43, 291–310. <https://doi.org/10.7202/032784ar>
- Tappin, D.R., Chadwick, R.A., Jackson, A.A., Wingfield, R.T.R., Smith, N.J.P., 1994. United Kingdom offshore regional report: the geology of Cardigan Bay and the Bristol Channel. British Geological Survey.
- Terzaghi, K., 1943. *Theoretical Soil Mechanics*. John Wiley & Sons, New York.
- Tóth, Z., Wheeler, A.J., McCarron, S.G., Monteys, X., 2016. Esker ridges and seismostratigraphic evidence for a southerly ice flow extending onto the present nearshore continental shelf of the Celtic Sea, SE Ireland. *Am. Geophys. Union Conf. Poster*.  
<https://doi.org/10.13140/RG.2.2.35266.99529>
- Trommelen, M.S., Ross, M., Ismail, A., 2014. Ribbed moraines in northern Manitoba, Canada: characteristics and preservation as part of a subglacial bed mosaic near the core regions of ice sheets. *Quat. Sci. Rev.* 87, 135–155. <https://doi.org/10.1016/j.quascirev.2014.01.010>
- Uehara, K., Scourse, J.D., Horsburgh, K.J., Lambeck, K., Purcell, A.P., 2006. Tidal evolution of the northwest European shelf seas from the Last Glacial Maximum to the present. *J. Geophys. Res.* 111, 1–15. <https://doi.org/10.1029/2006JC003531>

UKHO, n.d. Admiralty marine data portal [WWW Document]. URL  
<https://data.admiralty.co.uk/portal/home/>

Van Landeghem, K.J.J., Baas, J.H., Mitchell, N.C., Wilcockson, D., Wheeler, A.J., 2012. Reversed sediment wave migration in the Irish Sea, NW Europe: a reappraisal of the validity of geometry-based predictive modelling and assumptions. *Mar. Geol.* 295–298, 95–112.  
<https://doi.org/10.1016/j.margeo.2011.12.004>

Van Landeghem, K.J.J., Wheeler, A.J., Mitchell, N.C., 2009a. Seafloor evidence for palaeo-ice streaming and calving of the grounded Irish Sea Ice Stream: implications for the interpretation of its final deglaciation phase. *Boreas* 38, 119–131. <https://doi.org/10.1111/j.1502-3885.2008.00041.x>

Van Landeghem, K.J.J., Wheeler, A.J., Mitchell, N.C., Sutton, G., 2009b. Variations in sediment wave dimensions across the tidally dominated Irish Sea, NW Europe. *Mar. Geol.* 263, 108–119.  
<https://doi.org/10.1016/j.margeo.2009.04.003>

Veillette, J.J., 1986. Former southwesterly ice flows in the Abitibi-Timiskaming region: implications for the configuration of the late Wisconsinian ice sheet. *Can. J. Earth Sci.* 23, 1724–1741.

Wagner, T.J.W., Dell, R.W., Eisenman, I., Keeling, R.F., Padman, L., Severinghaus, J.P., 2018. Wave inhibition by sea ice enables trans-Atlantic ice rafting of debris during Heinrich events. *Earth Planet. Sci. Lett.* 495, 157–163. <https://doi.org/10.1016/j.epsl.2018.05.006>

Ward, S.L., Neill, S.P., Scourse, J.D., Bradley, S.L., Uehara, K., 2016. Sensitivity of palaeotidal models of the northwest European shelf seas to glacial isostatic adjustment since the Last Glacial Maximum. *Quat. Sci. Rev.* 151, 198–211.  
<https://doi.org/10.1016/j.quascirev.2016.08.034>

Ward, S.L., Neill, S.P., Van Landeghem, K.J.J., Scourse, J.D., 2015. Classifying seabed sediment type using simulated tidal-induced bed shear stress. *Mar. Geol.* 367, 94–104.  
<https://doi.org/10.1016/j.margeo.2015.05.010>

Westley, K., Quinn, R., Forsythe, W., Plets, R., Bell, T., Benetti, S., McGrath, F., Robinson, R., 2011. Mapping submerged landscapes using multibeam bathymetric data: a case study from the north coast of Ireland. *Int. J. Naut. Archaeol.* 40, 99–112. <https://doi.org/10.1111/j.1095-9270.2010.00272.x>



- Whitehouse, P.L., 2018. Glacial isostatic adjustment modelling: historical perspectives, recent advances, and future directions. *Earth Surf. Dyn.* 6, 401–429. <https://doi.org/10.5194/esurf-6-401-2018>
- Wilmes, S.-B., & Green, J.A.M. (2014). The evolution of tides and tidal dissipation over the past 21,000 years. *Journal of Geophysical Research: Oceans*, 119, 4083–4100. <https://doi.org/10.1002/2013JC009605>
- Wilson, L.J., Austin, W.E.N., Jansen, E., 2002. The last British Ice Sheet: growth, maximum extent and deglaciation. *Polar Res.* 21, 243–250.
- Winsborrow, M.C.M., Clark, C.D., Stokes, C.R., 2010. What controls the location of ice streams? *Earth-Science Rev.* 103, 45–59. <https://doi.org/10.1016/j.earscirev.2010.07.003>
- Wöelfl, A.-C., Snaith, H., Amirebrahimi, S., Devey, C.W., Dorschel, B., Ferrini, V., Huvenne, V.A., Jakobsson, M., Jencks, J., Johnston, G., Lamarche, G., Mayer, L., Millar, D., Pedersen, T.H., Picard, K., Reitz, A., Schmitt, T., Visbeck, M., Weatherall, P., Wigley, R., 2019. Seafloor mapping - the challenge of a truly global ocean bathymetry. *Front. Mar. Sci.* 6, 1–16. <https://doi.org/10.3389/fmars.2019.00283>